Changes in silicon and nitrogen cycling off Peru during the past 20,000 years

Kristin Doering

2016

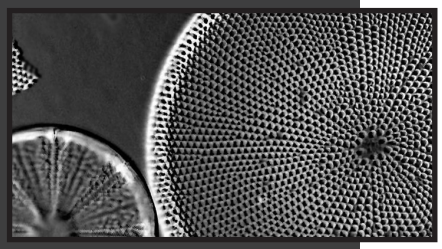

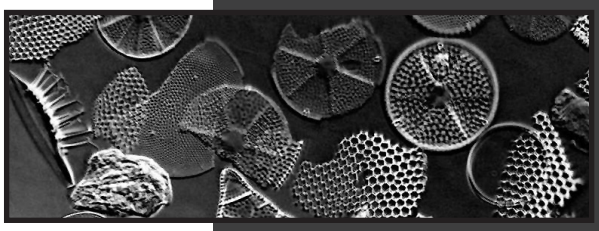

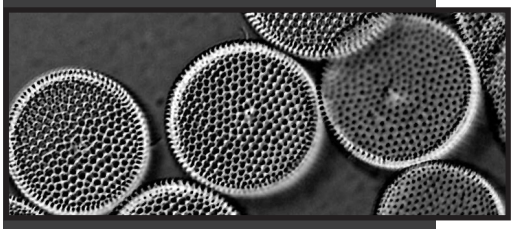

Dissertation

Cover:

Light-microscopic pictures of diatoms taken during this thesis.
From top to bottom: *Coscinodiscus concinnus* and *Actinoptychus* spp.; mixed diatom sample including *Chaetoceros diadema* (spore), *Biddulphia alternans* and *Actinoptychus senarius*; several specimen of *Thalassiosira* spp.; *Chaetoceros didymus* and *Actinoptychus senarius*.

Changes in silicon and nitrogen cycling off Peru during the past 20,000 years

Veränderungen im Silizium- und Stickstoff-Kreislauf vor Peru während der vergangenen 20.000 Jahre

Dissertation
Zur Erlangung des akademischen Grades
Dr. rer. nat.

Der Mathematisch-Naturwissenschaftlichen Fakultät
Der Christian-Albrechts-Universität zu Kiel

vorgelegt von
Kristin Doering
Kiel, 2016

1. Gutachter und Betreuer:	Prof. Dr. Ralph Schneider
2. Gutachter:	Prof. Dr. Martin Frank
Tag der Disputation:	20. Juni 2016
Zum Druck genehmigt:	20. Juni 2016

gez. Prof. Dr. Wolfgang J. Duschl, Dekan

Erklärung

Hiermit erkläre ich gemäß § 8, dass ich die vorliegende Abhandlung, abgesehen von der Beratung durch meinen Betreuer, nach Inhalt und Form selbstständig erarbeitet habe und keine anderen, als die von mir aufgeführten, Quellen und Hilfsmittel verwendet wurden. Diese Arbeit ist unter Einhaltung der Regeln guter wissenschaftlicher Praxis der Deutschen Forschungsgemeinschaft entstanden und wurde weder in Auszügen noch in ganzer Form an einer anderen Stelle im Rahmen eines Prüfungsverfahrens eingereicht.
Teile dieser Arbeit sind bereits in Fachzeitschriften veröffentlicht, wurden zur Veröffentlichung eingereicht oder sind in Vorbereitung eingereicht zu werden.

Kiel, den 17.05.2016

Kristin Doering

Contents

Summary

The Peruvian coastal upwelling region is characterized by very high surface water primary productivity. Enhanced oxygen consumption during the degradation of organic matter and sluggish ventilation lead to suboxic to anoxic conditions in subsurface waters resulting in one of the largest Oxygen Minimum Zones (OMZs) globally, which causes enhanced N-loss processes in the water column and shelf sediments. The strength and spatial extent of these processes in the past have been regulated by changes in oceanic and atmospheric circulation, which have in turn been controlled by global and regional climatic changes.

Reconstructions of surface water dissolved silicic acid ($Si(OH)_4$) and nitrate (NO_3^-) utilization as a function of primary productivity and the strength of pelagic denitrification in the oxygen-depleted subsurface waters supplying the upwelling have shown to be recorded by stable silicon isotope composition ($\delta^{30}Si$) of diatom and bulk sediment nitrogen isotope compositions. However, species-specific Si isotope enrichment factors for some marine diatoms species have shown to potentially affect past $\delta^{30}Si$ records of diatoms due to past shifts in the dominance of particular diatom species. To account for potential biases due to the prevalence of different diatom species off Peru surface sediment $\delta^{30}Si$ of small mixed (11-32µm; $\delta^{30}Si_{bSi}$) and of large handpicked (*Coscinodiscus*; >150µm; $\delta^{30}Si_{coscino}$) diatom species were investigated and compared to the diatom assemblages. The results show that the $\delta^{30}Si_{Coscino}$ values generally record near-complete Si utilisation during stratified conditions towards the end of the growth season. In contrast, lower $\delta^{30}Si_{bSi}$ signatures of the small mixed diatom fraction have been related to weak upwelling intensity, when low $Si(OH)_4$ concentrations do not permit intense blooms, and small diatom species record low initial silicate isotope utilisation. Whereas, highest $\delta^{30}Si_{bSi}$ values record a gradual increase of $Si(OH)_4$ utilisation within the seasonal diatom succession during intense bloom events. The calculated offset between $\delta^{30}Si_{Coscino}$ and $\delta^{30}Si_{bSi}$ ($\Delta^{30}Si_{coscino-bSi}$) is suggested as a novel approach to estimate upwelling intensity, with low $\Delta^{30}Si$ values reflecting strong upwelling and high $\Delta^{30}Si$ values reflecting weak upwelling conditions. In addition the influence of the diatom assemblage on the $\delta^{30}Si_{bSi}$ record off Peru due to species-specific isotope fractionation is demonstrated to be minor.

Variations in diatom productivity and $Si(OH)_4$ utilization based on $\delta^{30}Si_{bSi}$ and $\delta^{30}Si_{Cosicno}$ signatures and of upwelling intensity inferred from the diatom assemblages and $\Delta^{30}Si$ values along the entire Peruvian shelf (5°S to 15°S) since the Last Glacial Maximum were used to reconstruct the influence of changes in ocean and atmosphere circulation on the Peruvian upwelling region. The records show a northward shift of the main upwelling cell from its modern position between 12°S and 15°S towards 9°S during the last deglaciation, due to

the more northerly position of Southern Westerly Winds and the South Pacific Subtropical High. Modern conditions with the main upwelling zone located between 10°S and 15°S were only established at the onset of the Holocene. Changes in $\delta^{30}Si_{bSi}$ are not only influenced by the degree of $Si(OH)_4$ utilization and upwelling intensity, but also by the preformed $\delta^{30}Si(OH)_4$ signature of upwelled subsurface waters. However, the reconstruction of the variability in the preformed $\delta^{30}Si(OH)_4$ signatures of subsurface waters reaching the Peruvian shelf during the deglaciation only showed a slight potential increase in the preformed $\delta^{30}Si(OH)_4$, which is currently not significantly outside of our long-term reproducibility for $\delta^{30}Si$ measurements.

In contrast to the relatively constant preformed $\delta^{30}Si(OH)_4$ signatures of subsurface waters along the Peruvian shelf, the $\delta^{15}N$ of NO_3^- increases within the southward flowing subsurface waters due to the ongoing denitrification in the suboxic waters along the Peruvian margin. This increase in $\delta^{15}N_{NO3-}$ of subsurface waters is also recorded in the $\delta^{15}N_{bulk}$ values of surface sediments. To differentiate between the influence of denitrification and the degree of NO_3^- utilization in the past records the $\delta^{15}N_{bulk}$ values were compared to $\delta^{30}Si_{bSi}$, records, which only reflect the degree of $Si(OH)_4$ utilization. The correlation of $\delta^{30}Si_{bSi}$ and $\delta^{15}N_{bulk}$ values within a compilation of several records of along the Peruvian shelf covering the past 600 years showed that variations at single core sites were mainly influenced by variability in nutrient utilization. However, the correlation of $\delta^{15}N_{bulk}$ and $\delta^{30}Si_{bSi}$ for the Current Warm Period (CWP; 150 years BP to present) characterized by high surface productivity and upwelling intensity showed that values of $\delta^{15}N_{bulk}$ records increased continuously southwards following increasing denitrification similar to the present day situation. Further reconstructions of the correlation of $\delta^{15}N_{bulk}$ and $\delta^{30}Si_{bSi}$ values along the shelf from 9°S to 15°S covering the last 20,000 years, showed similar results with a dominant control of NO_3^- and $Si(OH)_4$ utilization at each core site. The latitudinal comparison of $\delta^{30}Si_{bSi}$ and $\delta^{15}N_{bulk}$ signatures for different time periods has shown a consistent southward increase in $\delta^{15}N_{bulk}$ from North to South, most likely reflecting ongoing denitrification. However, the records did not point to enhanced denitrification during the deglaciation as previously suggested. Instead, the records either reflect a higher preformed $\delta^{15}N_{NO3-}$ values of subsurface waters reaching the Peruvian shelf or reduced N_2 fixation, which further decreased the N inventory.

Given that $\delta^{15}N_{bulk}$ can be affected by alteration during early diagenesis, the $\delta^{15}N$ of diatom-bound organic matter, which is thought to be physically protected from early diagenesis, was also investigated. The direct comparison of $\delta^{15}N_{bulk}$ and $\delta^{15}N_{db}$ showed that $\delta^{15}N_{db}$ values were constantly higher than $\delta^{15}N_{bulk}$ values. Most likely these higher $\delta^{15}N_{db}$ values results from the uptake of higher subsurface $\delta^{15}N_{NO3-}$ signatures of upwelled waters by diatoms, while $\delta^{15}N_{bulk}$ values also incorporate organic matter from other organisms which was a consequence of lighter $\delta^{15}N$ signatures during more stratified conditions.

Zusammenfassung

Das peruanische Auftriebsgebiet ist gekennzeichnet durch eine sehr hohe Primärproduktivität im Oberflächenwasser. Die Zersetzung von organischem Material und eine relativ langsame Wassermaschenmischung führen zu starker Sauerstoffnutzung und starken sub-oxischen bis an-oxischen Bedingungen und eine der global größten Sauerstoffminimumzonen (OMZs), in der es zum Abbau von Nitrat in der Wassersäule und in Schelfsedimenten kommt. Die Stärke und das Ausmaß dieser Prozesse in der Vergangenheit sind direkt abhängig von der ozeanischen und atmosphärischen Zirkulation, die durch globale und regionale Klimaveränderungen beeinflusst wurden.

Zur Rekonstruktion der Oberflächenwassernutzung von der gelöster Kieselsäure ($Si(OH)_4$) und des Nitrats (NO_3^-) während der Primärproduktivität, sowie der Intensität von der Denitrifizierung in der Wassersäule haben sich die Verhältnisse von stabilen Silizium-Isotopen in Diatomeen ($\delta^{30}Si$) und von sedimentären Stickstoff Isotopen ($\delta^{15}N_{bulk}$) als Hilfsmittel bewährt. Allerdings, haben artenabhängige Si-Isotopen Fraktionierungsfaktoren verschiedener Diatomeenarten gezeigt, dass Veränderungen in der Dominanz der Arten einen starken Einfluss auf die Aufzeichnung vergangener $\delta^{30}Si$- Schwankungen haben können. Um die Auswirkungen der veränderlichen Häufigkeit verschiedener Diatomeenarten auf die $\delta^{30}Si$-Signaturen in den Sedimentarchiven des peruanischen Schelfs zu bestimmen, wurden hier deshalb zum Einen $\delta^{30}Si$ Werte von kleinen gemischten Diatomeenarten (11-32µm; $\delta^{30}Si_{bSi}$) und zum anderen von großen handgepickten Diatomeen (*Coscinodiscus*; >150µm) aus den Oberflächensedimenten untersucht und mit der Diatomeen Vergesellschaftung verglichen. Die Ergebnisse zeigen, dass die $\delta^{30}Si_{coscino}$ Werte generell eine nahezu vollständige $Si(OH)_4$-Nutzung unter stratifizierten Bedingungen am Ende des Wachstumszyklus im peruanischen Auftrieb aufzeichnen. Im Gegensatz dazu, entsprechen niedrigere $\delta^{30}Si_{bSi}$ Werte einem schwächerem Auftrieb entsprechen, während dem niedrige $Si(OH)_4$ Konzentrationen keine starken Diatomeenblüten zulassen und die kleinen Diatomeenarten niedrige Nährstoffnutzung am Anfang einer Blüte aufzeichnen. Dagegen zeichnen die höchsten $\delta^{30}Si_{bSi}$ Werte eine graduelle Zunahme der Nährstoffnutzung durch die saisonale Diatomeen-Abfolge während starker Diatomeenblüten auf. Der Unterschied zwischen den $\delta^{30}Si_{coscino}$ und $\delta^{30}Si_{bSi}$ Werten ($\Delta^{30}Si_{coscino\text{-}bSi}$) stellt einen ein neuartigen Ansatz zur Bestimmung der Auftriebsstärke dar, da niedrige $\Delta^{30}Si$ Werte starken Auftrieb und hohe $\Delta^{30}Si$ schwachen Auftrieb reflektieren. Insgesamt, hat die Abschätzung eines potentiellen Einflusses der Diatomeenvergesellschaftungen auf die $\delta^{30}Si_{bSi}$ Werte gezeigt, dass artenabhängige Isotopenfraktionierung nur einen geringen Effekt auf die $\delta^{30}Si_{bSi}$ Werte vor Peru hatte.

Die Rekonstruktion von Primärproduktion, Nährstoffnutzung basierend auf $\delta^{30}Si_{bSi}$- und $\delta^{30}Si_{coscino}$-Signaturen und der Auftriebsintensität anhand der Diatomeen-vergesellschaftung sowie der $\Delta^{30}Si$ Werte anhand von Sedimentarchiven entlang gesamten Schelfbereich (5°S bis 15°S) seit dem letzten Glazialen Maximum, wurde genutzt, um den Einfluss von Veränderungen in ozeanischer und atmosphärischer Zirkulation auf das peruanische Auftriebsgebiet zu untersuchen. Die Rekonstruktionen zeigen eine Verlagerung des Hauptauftriebsgebiets von seiner heutigen Position zwischen 12°S und 15°S nach 9°S während des Deglazials, bedingt durch eine nördlichere Position der südlichen Westwindzone und des Südpazifischen Hochdruckgebiets. Die heutigen Bedingungen der Hauptauftriebszone zwischen 10°S und 15°S haben sich erst zu Beginn des Holozäns etabliert. Veränderungen in den $\delta^{30}Si_{bSi}$ Werten werden nicht nur von der Nährstoffnutzung und Auftriebsstärke sondern auch von der $\delta^{30}Si(OH)_4$ Signatur der aufgetriebenen Wassermassen bestimmt. Die Berechnung einer Änderung der Wassermassen–$\delta^{30}Si(OH)_4$-Signatur, die das Peruanische Schelf während des Deglazials erreicht haben, ergab nur eine geringe Zunahme in den $\delta^{30}Si(OH)_4$ Werten, die momentan in Paläo-Rekonstruktionen nicht aufgelöst werden kann.

Im Gegensatz zu der $\delta^{30}Si(OH)_4$-Signatur wird der heutige $\delta^{15}N$ Wert von NO_3^- innerhalb der südwärts fließenden Wassermassen durch anhaltende Denitrifizierung unter suboxischen Bedingungen kontinuierlich schwerer. Diese Zunahme im $\delta^{15}N_{NO3-}$ Wert von aufgetriebenen Wassermassen wird auch in den $\delta^{15}N_{bulk}$ Werte im Oberflächensediment wider gespiegelt. Um in Paläo-Rekonstruktionen von $\delta^{15}N_{bulk}$ Werten zwischen Nährstoffnutzung und dem Einfluss von Denitrifizierung zu unterscheiden, wurden hier die $\delta^{15}N_{bulk}$ und $\delta^{30}Si_{bSi}$ Werte korreliert, da $\delta^{30}Si_{bSi}$ im Gegensatz zu $\delta^{15}N_{bulk}$ hauptsächlich vom Grad der Nährstoffnutzung beeinflusst werden. Die Korrelation von $\delta^{30}Si_{bSi}$ und $\delta^{15}N_{bulk}$ Werten anhand von mehreren Sedimentkernen entlang des Schelfs während der letzten 600 Jahre zeigt, das Änderungen in den Isotopenverhältnissen an den einzelnen Kernlokationen hauptsächlich durch veränderte Nährstoffnutzung verursacht wurden. Allerdings zeigt der Vergleich von $\delta^{30}Si_{bSi}$ und $\delta^{15}N_{bulk}$ Verhältnissen während starker Produktivität und Auftrieb, dass die $\delta^{15}N_{bulk}$ Werte kontinuierlich nach Süden zunehmen, was auf verstärkte Denitrifizierung hinweist und ähnlich zu heutigen Beobachtungen ist. Weitere Rekonstruktionen basierend auf dem Vergleich von $\delta^{15}N_{bulk}$ und $\delta^{30}Si_{bSi}$ entlang des Schelfs während der letzten 20.000 Jahre haben eine ähnliche Abhängigkeit der Isotopenwerte von Nährstoffnutzung gezeigt. Der Vergleich der $\delta^{30}Si_{bSi}$ und $\delta^{15}N$ Werte aller Sedimentkerne für verschiedene Zeitabschnitte hat außerdem gezeigt, dass die $\delta^{15}N_{bulk}$ Werte von Nord nach Süd kontinuierlich um 1.5‰ schwerer wurden, ein Anzeichen für anhaltende Denitrifizierung. Allerdings, deuten die Verhältnisse zwischen den $\delta^{15}N_{bulk}$ Werten entlang des Schelfs nicht auf einen verstärkten Einfluss von Denitrifizierung während des Deglazials hin, wie allgemein angenommen. Stattdessen, deuten die Ergebnisse

hier entweder auf einen schwereren $\delta^{15}N_{NO3-}$ Wert der aufgetriebenen Wassermassen oder auf eine Reduktion von N_2 Fixierung hin.

Da $\delta^{15}N_{bulk}$ Werte während der Frühdiagenese im Sediment verändert werden können wurde zum Vergleich der $\delta^{15}N$ Wert von organischem Material in den Diatomeen gemessen, von dem angenommen wird, dass er gegen bakterielle Zersetzung geschützt ist. Der direkte Vergleich von $\delta^{15}N_{bulk}$ und $\delta^{15}N_{db}$ Werten basierend auf einem Sedimentkerns von 15°S vor Peru zeigt, das die $\delta^{15}N_{db}$ Werte im Vergleich kontinuierlich höher sind. Wahrscheinlich werden diese höheren $\delta^{15}N_{db}$ Werte dadurch verursacht, das Diatomeen die hohen $\delta^{15}N_{NO3-}$ Werte des aufgetriebenen Wassers aufnehmen, während die $\delta^{15}N_{bulk}$ Werte auch organisches Material anderer Organismen enthalten die leichtere $\delta^{15}N$ Signaturen enthalten können.

Abbreviations

AR	Accumulation rate
AAIW	Antarctic Intermediate Water
BP	Before present
bSi	biogenic opal
C	Carbon
CO_2	Carbon dioxide
EEP	Eastern Equatorial Pacific
EF	Equatorial Front
ETP	Equatorial Tropical Pacific
ETNP	Equatorial Tropical North Pacific
ETSP	Equatorial Tropical South Pacific
EUC	Equatorial Undercurrent
HS1	Heinrich Stadial 1
HNLC	High-Nitrate-Low-Chlorophyll
IRMM	Standard
ITCZ	Intertropical Convergence Zone
ka	kilo year
LGM	Last Glacial Maximum
MC-ICPMS	Multi collector Ion induced Plasma Masspectrometer
N	Nitrogen
N_2	dinitrogen gas
NH_4^+	Ammonium
N_2O	nitrous oxide
NO_2-	Nitrite
NO_3-	Nitrate
O_2	Oxygen
OM	Organic matter
OMZ	Oxygen Minimum Zone
PCCC	Peru Chile Counter Current
PCUC	Peru Chile Undercurrent
PO_4^{3-}	Phosphate
PP	Primary productivity
PUE	Peruvian Upwelling Ecosystem
R^2	correlation coefficient
rpm	rounds per minute
SAMW	Subantarctic Mode Water
SFB	Sonderfoschungsbereich

Si	Silicon
$Si(OH)_4$	Silicic acid
SSCC	Subsurface Counter current
SST	Sea Surface Temperature
YD	Younger Dryas
$\delta^{30}Si$	stable silicon isotope signatures
$\delta^{30}Si_{bSi}$	$\delta^{30}Si$ signatures of small mixed diatom species (11-32µm)
$\delta^{30}Si_{Coscino}$	$\delta^{30}Si$ signatures of large handpicked mono-generic diatoms (*Coscinodiscus* spp.; >125/150µm)
$\delta^{15}N$	nitrogen isotope signatures
$\delta^{15}N_{bulk}$	bulk sedimentary $\delta^{15}N$ signatures
$\delta^{15}N_{db}$	diatom-bound $\delta^{15}N$ signatures
Δ or $\Delta^{30}{}_{SiCoscino\text{-}bSi}$	The diffrrence between $\delta^{30}Si_{Coscino}$ and $\delta^{30}Si_{bSi}$

I. Introduction

The main objective of this thesis is an improved understanding of past silicon and nitrogen cycling and their connection to climatically driven changes in the expansion of the oxygen minimum zone off Peru associated with climate change from the last Glacial to the Holocene. As the low oxygen concentrations are associated with high primary productivity dominated by diatoms, silicon isotope and nitrogen isotope compositions from diatoms as well as the nitrogen isotopes of bulk sediment from hemipelagic muds are used as proxies for past silicic acid and nitrate utilization in surface waters and potential recorders of N-loss processes induced by changes in OMZ intensity.

1.1 The Marine Silicon and Nitrogen Cycle

In the world ocean silicon (Si; Fig. 1.1) occurs mostly (~95%) in the form of undissociated monomeric silicic acid ($Si(OH)_4$) with an average concentration of about 70 µM. In seawater, $Si(OH)_4$ is one of the major nutrients for phytoplankton growth (Ragueneau et al., 2000). The $Si(OH)_4$ is almost exclusively used by diatoms, which build biogenic opal ($bSiO_2$) frustules. The main process removing $Si(OH)_4$ from seawater is the biological precipitation of opal by marine organisms such as diatoms, silicoflagellates and radiolarians (Nelson et al., 1995; De La Rocha et al., 1998), transporting silica to the seafloor, thus initiating the biological cycle of Si (Nelson et al., 1995; Tréguer et al., 1995; Ragueneau et al., 2000).

The main pathways that serve as external sources of $Si(OH)_4$ to the ocean are all ultimately derived from the weathering of the Earth's crust. Accordingly, silicon sourced from weathering of siliceous rocks enters the ocean in dissolved form via rivers, via atmospheric dust deposition and subsequent dissolution or via low temperature alteration of seafloor basalts (Tréguer et al., 1995; Tréguer and De La Rocha, 2013). During transport from the weathering sites, until ultimately ending in the ocean, Si is involved in various biogeochemical processes, such growth of freshwater diatoms and precipitation of secondary clay minerals (Georg et al., 2009). Dissolved Si has a residence time in the ocean of about 10,000 years (Tréguer and De La Rocha, 2013) and, in total, a global ocean content of about 97,000 T mol dissolved Si (Tréguer et al., 1995; Tréguer and De La Rocha, 2013). As a consequence of utilization and ocean circulation $Si(OH)_4$ is fractionated between the different oceanic basins (Ragueneau et al., 2000) ranging from less than 1 µM in the low latitude surface waters to more than 170 µM in the intermediate North Pacific. Overall the $Si(OH)_4$

concentrations remain relatively low throughout the upper 1,000 m in the water column, except for the equatorial and northern Pacific and the Southern Ocean.

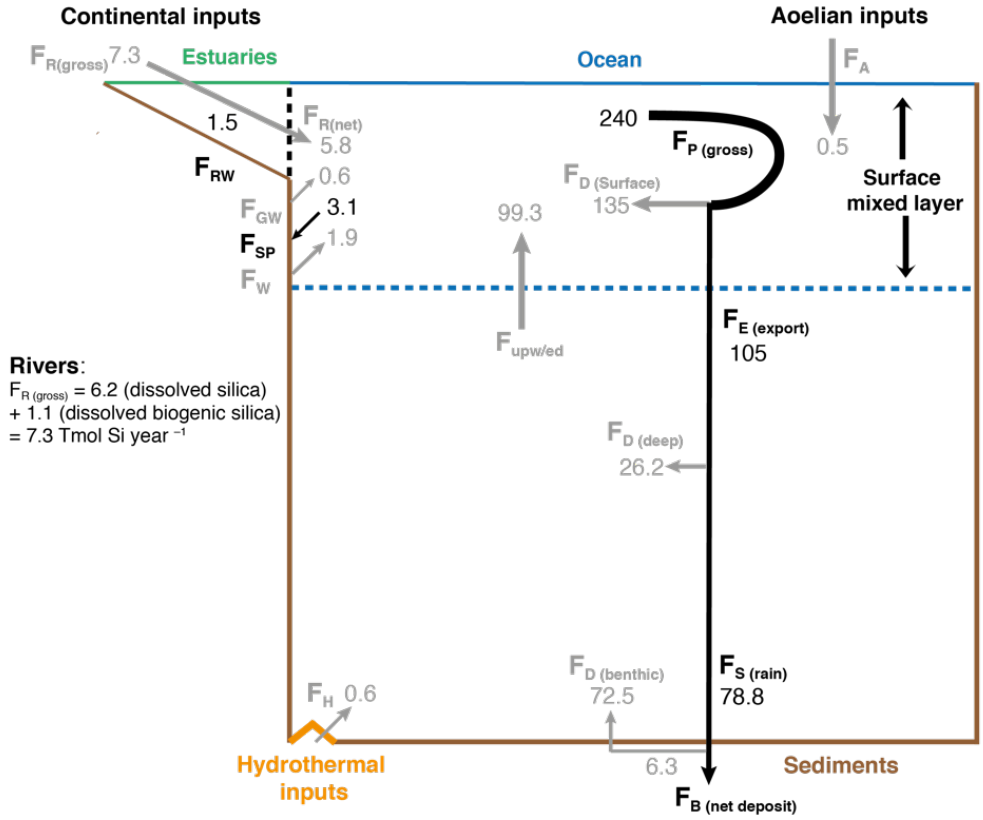

Figure 1.1: Biogeochemical cycle of silicon in the world ocean at steady state: a possible balance that is in reasonable agreement with the individual range of each flux (F). Modified from (Tréguer, 2013).

Nitrogen (N) is a major element in organic structures such as amino acids, porphyrins and amino sugars and has a fundamental role in biogeochemical cycles (Brandes et al., 2007). Most of the nitrogen in the oceans is present in five forms: dinitrogen gas (N_2); nitrate (NO_3^-), the dominant form biologically used in oxic environments); nitrite (NO_2^-); ammonium (NH_4^+), most dominant form in anoxic environments; particulate N and dissolved organic N (Brandes et al., 2007).

The marine nitrogen cycle (Fig. 1.2) is characterized by N_2 fixation, riverine inputs, atmospheric fallout, burial of organic matter in the sediments, and water column and sedimentary denitrification (conversion of fixed N to N_2; (Codispoti et al., 2001). Bioavailable N includes NO_3^-, NO_2^- and NH_4^+, whereas N_2 is only accessible for N_2 fixing bacteria that are able to reduce N_2 to ammonium. The main processes that remove fixed N again from the ocean are the anaerobic ammonium oxidation (anammox), which converts NH_4^+ with NO_2^- into N_2; and denitrification, which reduces NO_3^- back to N_2 (Gruber and Sarmiento, 1997). Anammox is a chemolithoautotrophic process that fixes inorganic carbon with energy from N_2 production (Lam et al., 2009). Denitrification is defined as the sequential reduction from NO_3^- to N_2 (NO_3^-

$\rightarrow NO_2^- \rightarrow N_2O \rightarrow N_2$) and is coupled to the oxidation of organic matter by bacteria and archaea. Both denitrification and anammox occur when water column O_2 concentrations are below 2-10 µmol L^{-1} (Lam et al., 2009), leading to loss of bio-available nitrogen (Gruber and Sarmiento, 1997). The balance between N_2 fixation, denitrification and anammox, in combination with the other N pathways (Fig. 1.2), defines the oceanic N budget (Gruber and Sarmiento, 1997). In the conventional paradigm of oceanic nitrogen cycling gaseous N_2 becomes bioavailable via N_2 fixation and is lost to the atmosphere when facultative anaerobic microorganisms respire NO_3^- in the absence of oxygen and produce N_2, which is performed via heterotrophic denitrification. Accordingly, the N inventory depends mostly on the balance between losses via denitrification (Codispoti et al., 2001) and anammox (Dalsgaard et al., 2003) on the one hand and gains through N_2 fixation on the other.

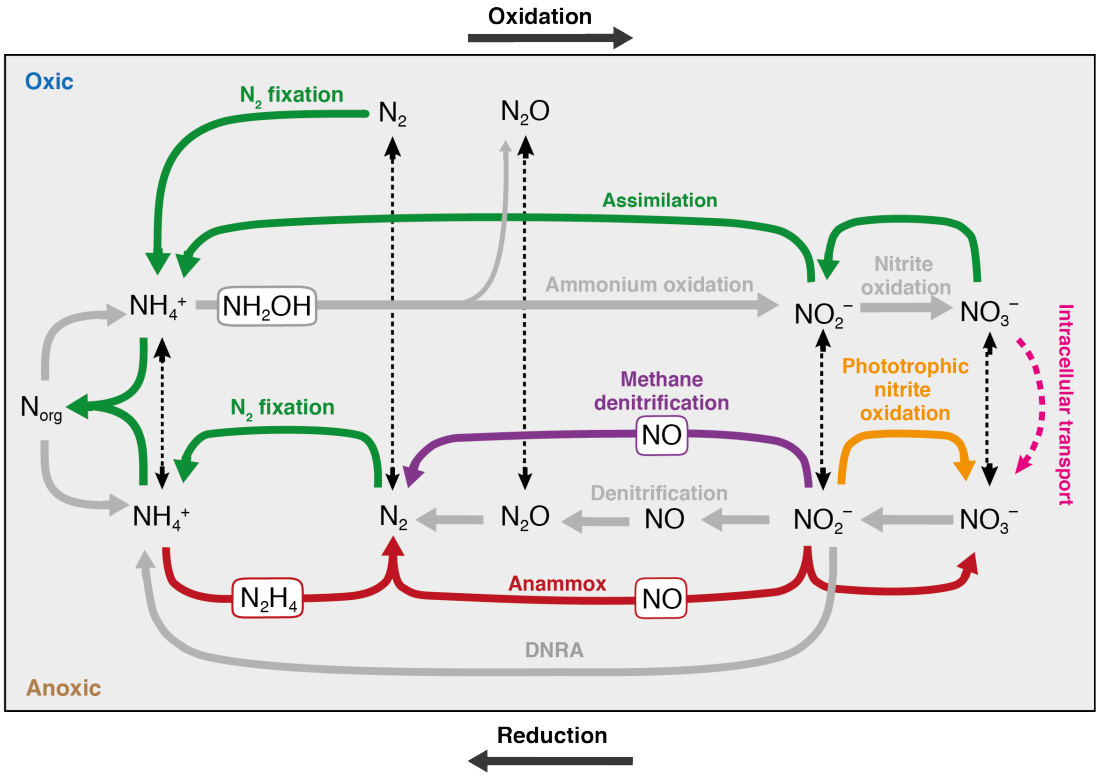

Figure 1.2: Schematic representation of the nitrogen cycle. Metabolic transformations are shown as thick arrows. Also shown are the classical processes of assimilation (green) and dissimilation (gray) as well as recently discovered metabolisms (colored). The upper part of the figure shows aerobic and lower part anaerobic processes. The dashed vertical arrows indicate interactions between oxic and anoxic environments. The relative sizes of arrowheads indicate the dominant direction of transport. Modified from Thamdrup, (2012).

1.2 Stable Silicon and Nitrogen Isotopes

1.2.1 Silicon Isotopes

There are three naturally occurring stable isotopes of silicon, ^{28}Si (92%), ^{29}Si (5%) and ^{30}Si (3%). The silicon isotope composition of a material is denoted by δ^{30}Si, where:

$$(1)\quad \delta^{30}\mathrm{Si} = [(^{30}\mathrm{Si}/^{28}\mathrm{Si})_{\mathrm{samples}} / (^{30}\mathrm{Si}/^{28}\mathrm{Si})_{\mathrm{standard-NBS28}} - 1]\times 1000.$$

When diatoms take up dissolved silicic acid for mineralization of opaline frustules (Tréguer et al., 1995) they preferentially incorporate the lighter isotopes (^{28}Si) leaving the residual $Si(OH)_4$ in surface water enriched in heavier isotopes (^{30}Si) and thus progressively increasing silicon isotope ratios in the surface water reflect a progressive $Si(OH)_4$ depletion (Varela et al., 2004; Cardinal et al., 2005; Reynolds et al., 2006; Beucher et al., 2008). Accordingly, changes in the marine silicon cycle and diatom paleo-productivity can be assessed via stable silicon isotope compositions (De La Rocha et al., 1998; Reynolds et al., 2006).

Based on culture experiments (De La Rocha et al., 1997) the fractionation for silicon between seawater and the diatom silica was found to follow a fractionation factor α of ~0.998 corresponding to the production of diatom silica with an enrichment factor (ε) for δ^{30}Si of -1.1 ‰. This factor was supported by several observational studies and model experiments (De La Rocha et al., 1997; Milligan et al., 2004; Varela et al., 2004; Beucher et al., 2008). Recent new culture experiments for different diatom species report varying enrichment factors between -0.5‰ to -2‰ (Sutton et al., 2013). Additionally to culture experiments on the same species as the original studies (*Thalassiosira weissflogii and Thalassiosira pseudonana*, De La Rocha et al., 1997; Milligan et al., 2004) some Southern Ocean species were studied (i.e. *Porosira glacilis*, *Thalassiosira antarctica*, *Thalassiosira nordenskioeldii*, *Fragilariopsis kerguelensis*, *Chaeotceros brevis*). Of these species the two polar species had significantly different enrichment factors with a ε value of -0.54‰ for *F. kerguelensis* and a ε value of -2.09‰ for *C. brevis* (Sutton et al., 2013). It is still unclear if these culture experiments represent the same range of fractionation as diatoms in the natural environment and if interspecific variation ε represented by the extreme values for *C. brevis* and *F. kerguelensis*, are also detectable in nature.

One further key question is whether the opal δ^{30}Si signal from diatoms produced in surface waters is preserved with fidelity in the sediments. Until now

core top calibrations (Egan et al., 2012; Ehlert et al., 2012) found a good correspondence between the core top diatom $\delta^{30}Si$ values and the $Si(OH)_4$ in the overlying surface waters, which should reflect the extent of $Si(OH)_4$ depletion. These results suggest that the sedimentary signal reflects the cumulative seasonal drawdown of $Si(OH)_4$ and that species composition does not impact the $\delta^{30}Si$ (Egan et al., 2012).

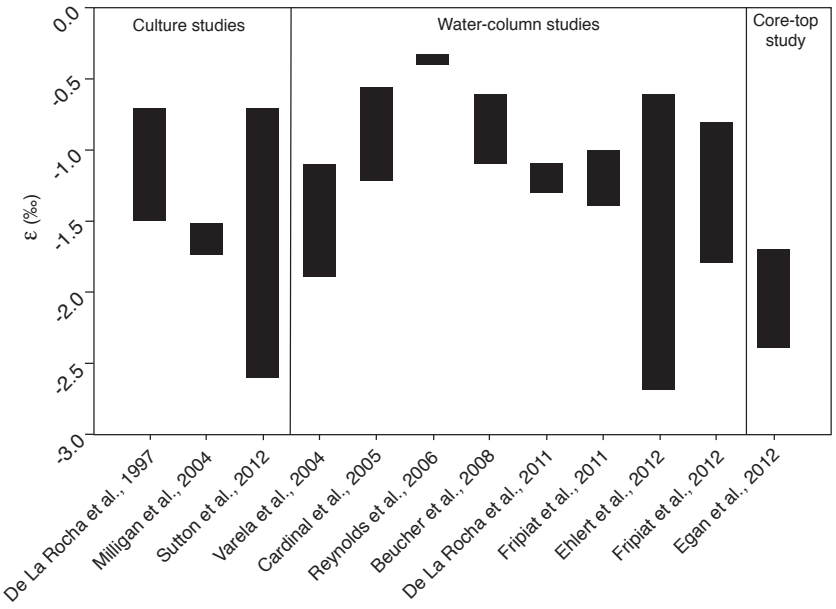

Figure 1.3: Apparent fractionation factors estimated from a number of culture, water column and sediment core top studies (De La Rocha et al., 1997; Milligan et al., 2004; Varela et al., 2004; Cardinal et al., 2005; Reynolds et al., 2006; Beucher et al., 2008; Fripiat et al., 2011; De La Rocha et al., 2011; Fripiat et al., 2012; Egan et al., 2012; Ehlert et al., 2012; Sutton et al., 2013). Modified from Hendry and Brzezinski, (2014).

The biological utilization of Si by diatoms only occurs in the surface waters as the algae require light for photosynthesis, hence all marine Si isotope variations are ultimately derived from surface water productivity (Reynolds et al., 2006). At depth remineralization releases $Si(OH)_4$ with lower $\delta^{30}Si$ compared to surface $Si(OH)_4$. Nutrient and isotope profiles can be used to estimate isotope fractionation using either an open system model (continuous delivery of Si into the euphotic zone) or a closed system model (assuming one isolated pulse of Si delivered into the euphotic zone followed by closed system dynamics) depending on the nature of the vertical nutrient supply (De La Rocha et al., 1997; Beucher et al., 2007). These models are described by the following equations:

$$\text{Open: } \delta^{30}\text{Si(OH)}_{4\,\text{observed}} = \delta^{30}\text{Si(OH)}_{4\text{initial}} - \varepsilon\times(1-f) \quad (2)$$

$$\text{Closed} = {}^{30}\text{Si(OH)}_{4\,\text{observed}} = \delta^{30}\text{Si(OH)}_{4\text{initial}} + \varepsilon\times\ln(f) \quad (3)$$

where $\delta^{30}Si(OH)_{4\ observed}$ is the measured $\delta^{30}Si(OH)_4$ in surface waters, $\delta^{30}Si(OH)_{4\ initial}$ is that of the water mass supplying Si to surface waters and f is the fraction of the supply that remains in surface waters. In both isotope models knowledge of

the $\delta^{30}Si(OH)_4$ of waters ventilating to the surface is required. Uncertainty in this value has led to considerable variations in estimates of ε (see Fig. 1.3) inspiring efforts to better understand $\delta^{30}Si(OH)_4$ distributions in subsurface waters (Reynolds et al., 2006).

1.2.2 Nitrogen Isotopes

There are two stable nitrogen isotopes, ^{14}N (99.63% of the N) and the rare ^{15}N. During the assimilation of NO_3^- phytoplankton preferentially incorporates NO_3^- with the lighter ^{14}N isotope (Waser et al., 1998) leaving the dissolved NO_3^- enriched in ^{15}N (Wada and Hattori, 1978; Waser et al., 1998; Sigman, Altabet, McCorkle, et al., 1999; Granger et al., 2004). Given that NO_3^- is the ultimate N source for phytoplankton, the progressive consumption of NO_3^- leads to an increase in $\delta^{15}N$ of phytoplankton produced in the surface ocean and is exported as sinking OM (Altabet and François, 2001; Lourey et al., 2003). Field and laboratory studies have demonstrated this link between NO_3^- utilization and the isotopic composition of particulate nitrogen in oceanic ecosystems (Wada and Hattori, 1978; Altabet et al., 1991; Altabet and François, 1994; Montoya and McCarthy, 1995; Wu et al., 1997; Waser et al., 1998; Sigman, Altabet, McCorkle, et al., 1999). Isotopic fractionation for nitrogen is influenced by several processes with characteristic differences in enrichment factors: N_2 fixation ~-1‰; sedimentary denitrification = 0‰; NO_3^- uptake ~5‰; water column denitrification ~20-30 ‰ (after (Sigman et al., 2001; Galbraith et al., 2004). In the eastern Pacific $\delta^{15}N$ of upwelled NO_3^- to the surface may be higher, due to exchange with zones of water column denitrification (Cline and Kaplan, 1975). This isotopically heavy NO_3^- is mixed upwards, incorporated into phytoplankton and transferred to the sediment which thereby records an elevated $\delta^{15}N$ signal.

In open ocean sediment the bulk sedimentary $\delta^{15}N$ signature was shown to potentially increase by 2-3‰ due to diagenetic alteration during incorporation into the sediment record (Altabet and François, 1994; Brzezinski, 2002; Robinson et al., 2012). As this process is likely to effect downcore records several studies started to focus on phytoplankton bound organic material or on sediments from continental slopes, which generally record the $\delta^{15}N$ with little 'diagenetic' isotopic alteration during sinking and sedimentation (Ganeshram et al., 2000; Freudenthal et al., 2001; Thunell and Kepple, 2004). It is generally thought that diagenetic alteration is more pronounced in oxic deep-sea sediments.

Diatom-bound N is thought to be physically protected from early bacterial diagenesis by the microfossil matrix of diatom frustules (Shemesh et al., 1993; Sigman, Altabet, François, et al., 1999). Shemesh et al., (1993) pioneered the use of diatom frustules to overcome the uncertainties arising from diagenesis

of bulk sediment carbon and nitrogen isotopic composition. The method to extract and measure the diatom-bound nitrogen isotope composition ($\delta^{15}N_{db}$) was significantly improved recently (Sigman, Altabet, François, et al., 1999; Robinson et al., 2004; Brunelle et al., 2007). These studies successfully proved that $\delta^{15}N_{db}$ also varies with NO_3^- utilization, similar to $\delta^{15}N_{bulk}$ signatures (Sigman, Altabet, McCorkle, et al., 1999). Based on the successful estimation of $\delta^{15}N_{db}$ as proxy for nitrate utilization several studies investigated the $\delta^{15}N$ of diatom intrinsic organic matter for paleo-reconstructions of NO_3^- utilization (Sigman, Altabet, François, et al., 1999; Crosta et al., 2002; Robinson et al., 2005; Brunelle et al., 2007; Jacot Des Combes et al., 2008; Brunelle et al., 2010; Studer et al., 2012). Another advantage of $\delta^{15}N_{db}$ is given by the possible comparison of $\delta^{15}N_{db}$ with $\delta^{30}Si$ of diatoms from the same sample material, which was for example applied to reconstruct past variations in the relative $Si(OH)_4$ and NO_3^- consumption in the Southern Ocean (Horn et al., 2011).

1.3 Marine diatoms

Diatoms are a group of microscopic, eukaryotic phytoplankton, which make up to 25% of the annual global photosynthesis (Nelson et al., 1995). They are the most diverse group of phytoplankton with more than 200,000 estimated different species, ranging in size from a few µm to several mm consisting of single cells or chains of connected cells (Armbrust, 2009). The cell walls of diatoms, so-called frustules, are mainly composed of amorphous hydrated SiO_2 ($SiO_2 \cdot H_2O$; Mortlock and Froelich, 1989) taken up from the surrounding seawater either as $Si(OH)_4$ or as $Si(OH)_3^-$. The frustules contain small proportions of proteins embedded within the walls that can precipitate silica: *silaffins*, highly modified phosphorus proteins; long-chain *polyamines*; and *silacidins*, acidic protein (Armbrust, 2009; Sumper and Kröger, 2004). By forming cell walls from dissolved silicic acid ($Si(OH)_4$) in sea water the diatoms control the biogenic cycling of silicon in the world's oceans (Tréguer et al., 1995; Armbrust, 2009). Accordingly, diatoms contribute up to 40% of global marine primary productivity (Nelson et al., 1995). Approximately half of the opal produced in the euphotic zone is exported to deep waters, of which about 3% of are preserved and buried in ocean floor sediments globally, while the remainder is either remineralized in the water column or at the sediment water interface (Tréguer et al., 1995; Brzezinski and Nelson, 1995; Tréguer and De La Rocha, 2013).

Diatoms are found worldwide, but they tend to dominate phytoplankton communities within well-mixed equatorial divergences (Dugdale and Wilkerson, 1998) and coastal upwelling regions (de Mendiola, 1981; Armbrust, 2009), where sufficient light, inorganic NO_3^-, phosphate (PO_4^{3-}), $Si(OH)_4$ and trace elements are available (Morel and Price, 2003), as found along the Peruvian margin.

Studies off Peru report that the diatom assemblages in surface sediments generally reflect the diversity and abundance of the modern biocoenotic species distribution in surface waters (De Vries and Schrader, 1981). Typical diatom groups preserved in sediments along the continental margin represent either (1) upwelling or (2) non-upwelling conditions, while the latter includes coastal planktonic, oceanic planktonic as well as coastal benthic diatom groups (Fig. 1.4; Schuette, 1980b; Schuette, 1980a; de Mendiola, 1981; De Vries and Schrader, 1981; Schuette and Schrader, 1981; Abrantes et al., 2007).

(1) **Coastal upwelling diatom groups** occurring in nutrient-rich, turbulent waters: *Chaetoceros* spp. and resting spores (RS), *Skeletonema costatum*, *Thalassionema nitzschioides* var. *nitzschioides*;

(2) **Non-upwelling diatom groups:**
Coastal planktonic (temperate, cosmopolitan) with high-to-moderate nutrient waters: *Actinocyclus* spp., *Actinoptychus* spp., *Asteromphalus* spp., and *Cyclotella* spp.;
Oceanic planktonic (warm, temperate) from nutrient-depleted waters such as *Nitzschia* spp., *Pseudo-Nitzschia* spp. and *Rhizosolenia* spp.,
Coastal benthic diatoms such as *Biddulphia* spp., *Cocconeis* spp., and *Delphineis karstenii*;

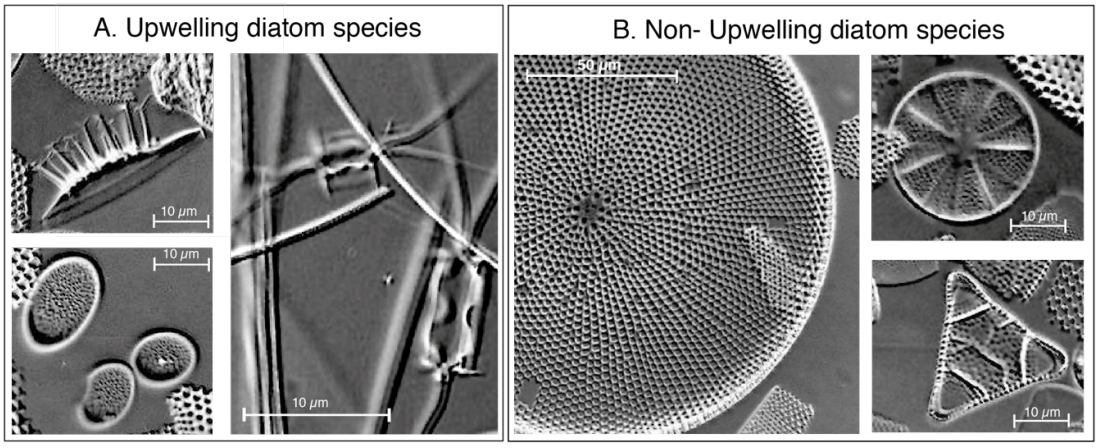

Figure 1.4: Light microscope images of A. Upwelling diatom species: *Chaetoceros diadema* (spore, left-side top), *C. affinis* (spore; left side bottom) and *C. didymus* (veg + spore); B. Non-Upwelling diatom species: *Coscinodiscus concinnus* (left side), *Actinoptycus vulgaris* (right side top) and *Biddulphia alternans* (right side bottom). All pictures are taken from samples prepared in this thesis.

1.4 Main features of the Peruvian coastal upwelling region

The Peruvian coastal upwelling is recognized as one of the most productive systems of the world oceans (indicated by the Chlorophyll *a* concentration, Fig. 1.5 A) . Upwelling is induced by trade winds and Ekman transport (Wyrtki, 1981) (indicated by the Sea Surface Temperature (°C) in Fig. 1.5 B) leading to high amounts of nutrients supplied to the water surface. The entire region is thus characterized by high primary production resulting in a high flux of organic material through the water column, which is decomposed under consumption of dissolved oxygen. The high oxygen demand in this region combines with sluggish ventilation to one of the globally most pronounced oxygen minimum zones (OMZs; Wyrtki, 1962), which are defined by an oxygen content of less than 20 µmol kg^{-1} (Fig. 1.5 A; Fuenzalida et al., 2009).

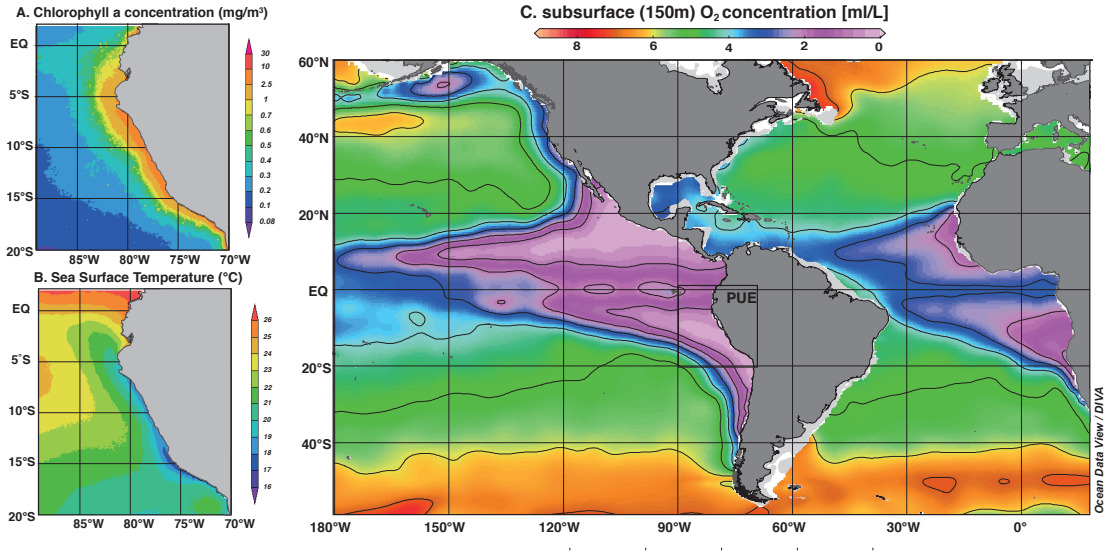

Figure 1.5: Maps of A. Chlorophyll a concentration (mg/m^2); B. Sea Surface Temperature (°C), averaged for the period between 1997 and 2015 (http://oceancolor.gsfc.nasa.gov/cgi/l3); C. Dissolved oxygen concentration (ml/L) at 150m water depth in the Eastern Pacific and the Atlantic; the area of the Peruvian Upwelling Ecosystem (PUE) is highlighted.

Tropical OMZs in the Eastern Tropical North Pacific (ETNP) and Eastern Tropical South Pacific (ETSP) constitute the most important regions of low oxygen in the present day ocean and the nutrient cycling in these regions affects the entire global ocean. The extent and intensity of OMZs are likely to increase in the future as global warming and nutrient enrichment deplete the ocean of oxygen. It has been predicted by model calculations that the ocean will progressively loose oxygen over the next 200 years (Bopp et al., 2002). Moreover a 50-year time series of dissolved oxygen concentrations revealed vertical

expansion of the intermediate depth OMZs in the eastern equatorial Atlantic and the equatorial Pacific during this timeframe (Stramma et al., 2008). On the one hand this is related to oceanic warming but the main reason is the decreased ocean ventilation due to circulation changes related to the anthropogenically induced climate change.

Furthermore, OMZs are important for the global carbon cycle as photosynthetic organisms bind atmospheric CO_2 near the water surface, which is then transferred into the deep via the flux of organic material (Berger and Herguera, 1989). Bioproductivity in these regions therefore has a substantial influence on the CO_2 concentrations in the atmosphere. On the other hand dissolved CO_2 is released from deeper water masses to the atmosphere via upwelling when the upwelled deeper water masses warm up reaching the water surface, which reduces the solubility of CO_2.

Oceanographic and atmospheric circulation

The zonal surface current system in the Eastern Tropical Pacific (ETP) consists of westward- and eastward-flowing currents (Fig. 1.6). Along the Peruvian margin the main westward currents are the is the South Equatorial Current (SEC; 3° N to 10° S) (Kessler, 2006). South-easterly trade winds drive surface waters northwards, thereby generating the Peru-Chile Coastal Current (PCCC) flowing along the shore and the Peru-Chile Current (PCC) further offshore (Fiedler and Talley, 2006 and references therein). The southward flowing subsurface Peru-Chile Undercurrent (PCUC) is the main source of the waters upwelling off Peru (Zuta and Guillén, 1970; Brink et al., 1983; Toggweiler et al., 1991). Approximately 30% of the PCUC waters originate from the eastward flowing Equatorial Undercurrent (EUC; 1.5°N-1.5°S), the primary Southern Subsurface Counter Current (pSSCC; 2°S-4.7°S) and the secondary Southern Subsurface Counter Current (sSSCC; 5.8-8.2°S) (Brink et al., 1983; Toggweiler et al., 1991; Montes et al., 2010). The remaining 70% of the PCUC waters originate from upwelling from below the PCUC (35%) and weak diffuse currents in the domain south of 9°S (35%) (Montes et al., 2010).
The oceanographic conditions in the ETP are a result of interactions of basin-scale atmospheric circulation with local processes occurring at the land sea interface (Strub et al., 1998). The South Pacific Subtropical High drives equator-ward winds along the western coast of South America. To the North the system is bordered by the Intertropical Convergence Zone, which constitutes the belt of converging northern and southern trade winds and is associated with intense convection and precipitation. The ITCZ reaches its northernmost extent in the month of August (~12° N) when southeast trade winds are stronger. In contrast, the ITCZ is located closest to the equator in April (~2°N) when northeast trade winds are stronger (Waliser and Gautier, 1993).

The strongest source of temporal variability in the ETP, superimposed on the annual variability, are El Niño events (Wang and Fiedler, 2006), which occur every 2-7 years (McPhaden et al., 2006) and are part of a coupled ocean atmosphere heat flux interaction of the El Niño-Southern Oscillation (ENSO) (Philander, 1990). During an El-Niño (EN) events the trade winds are weakened, while the surface layers in the eastern and central equatorial Pacific are warming (McPhaden et al., 2006). Additionally, the ITCZ is shifted southward causing a weakening of the eastward trade winds in the western Pacific, which reduces the east-west tilt of the thermocline depth and enhances the redistribution of warm surface water into the EEP causing significantly higher sea surface temperatures (Fiedler and Talley, 2006; Wang and Fiedler, 2006). Even in those regions where wind-driven upwelling continues the nutrient supply to the euphotic zone substantially decreases due to deepened thermocline (Huyer et al., 1987; Chavez and Barber, 1987). Furthermore, along with the thermocline the layer of oxygen depleted water deepens thereby oxygenating the shelf and altering levels of denitrification and the export flux of organic matter as well as the remineralization and supply of micronutrients such as Fe from the shelf sediments (Morales et al., 1999). In contrast to El Niño events, the opposite La Niña phases are characterized by strengthened trade winds, a shallower thermocline, and cooler sea surface temperatures causing the nutrient supply to strongly increase and to fuels primary productivity (Wang and Fiedler, 2006).

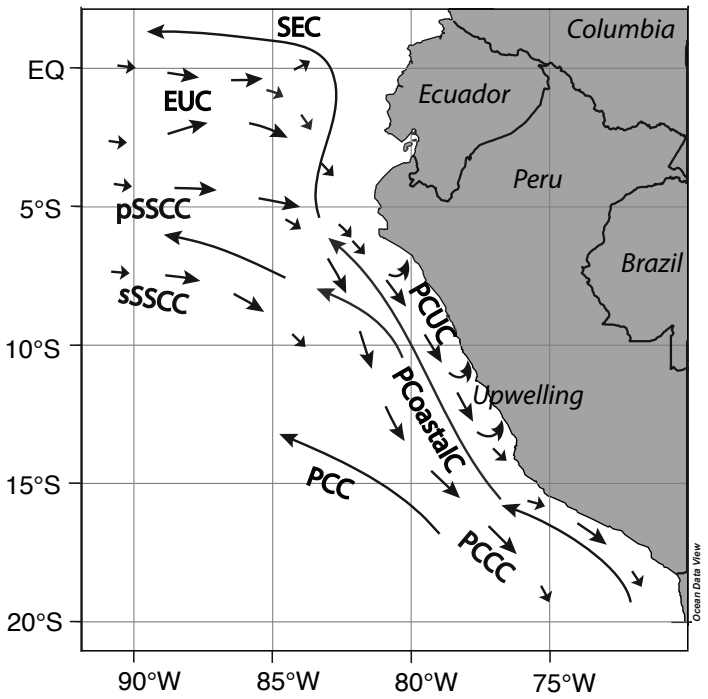

Figure 1.6: Map of surface (black arrows) and subsurface (dashed arrows) currents off Peru. Surface currents: SEC – South Equatorial Current; PCC – Peru-Chile-Current. PCcC – Peru Coastal Current; subsurface currents: EUC – Equatorial Undercurrent. pSSCC - primary Southern Subsurface Counter Current. sSSCC – secondary Subsurface Counter current. PCCC – Peru-Chile Counter Current. PCUC – Peru-Chile Undercurrent.

Nutrient Distribution and Primary Productivity

Coastal upwelling is driven by Ekman transport generated by southeast trade winds that blow along the west coast of South America (Wyrtki, 1981). Ekman transport moves surface waters offshore and replaces them with waters from below the thermocline. Seasonally, coastal upwelling is highest when the strongest southeast trade winds blow over this region in austral winter, and is reduced when southeast trade winds are relatively weak in austral summer (Wyrtki, 1975; Kessler, 2006). The coastal upwelling system is generally characterised by high rates of primary productivity of phytoplankton (as indicated by the chlorophyll *a* concentration in Fig. 1.1 B) (Chavez and Barber, 1987; Chavez, 1995; Fiedler, 2002; Fiedler and Talley, 2006). Accordingly, coastal waters off Peru are extremely rich in chlorophyll and this biomass production extends westwards for up to 1000 km offshore (Pennington et al., 2006). This high productivity can only occur due to thermocline shoaling and local wind-driven upwelling of subsurface waters (indicated by lowered SSTs(°C), Fig. 1.1 C), which provides nutrients to the euphotic zone.

Overall the rate of primary productivity is regulated by nutrient supply of nitrate (NO_3^-), silicate ($Si(OH)_4$) and phosphate (PO_4^{3-}) and iron (Fe), as well as by light and physical export of waters (offshore transport or subduction of water masses) (Messié and Chavez, 2015). The ultimate sources of the nutrients are the subsurface waters such as the EUC (Lukas, 1986) as well as vertical admixture of remineralized organic matter from shelf sediments (Franz et al., 2012; Ehlert et al., 2012). In the Peruvian upwelling region Fe is mainly supplied to the euphotic zone via remineralization from the shelf sediments, which occurs under O_2-depleted conditions in the bottom waters (Noffke et al., 2012). Along the shelf region off Peru local areas of extremely high productivity are associated with the shape of the coastline, i.e. capes and adjacent bay areas, found at 6°S, 9°S, 12S and 15°S (Rojas de Mendiola, 1981). Due to the observed regional differences in upwelling strength, nutrient supply and consumption, different zones of limitation occur. Subsurface NO_3^- reduction processes (denitrification, anammox) consume NO_3^- in the upwelling source waters, so that surface NO_3^- can become exhausted before PO_4^{3-} (Penningon et al., 2006). In the shelf area, however, nutrient concentrations of NO_3^-, PO_4^{3-} and partly Fe are generally very high and thus not limiting for diatoms (Bruland et al., 2005; Franz et al., 2012). Instead, $Si(OH)_4$ concentrations are assumed to be limiting diatom production during austral summer (Dugdale et al., 2002; Franz et al., 2012), while iron and light limitations were shown to prevail during austral winter (Hutchins et al., 2002; Bruland et al., 2005; Pennington et al., 2006; Echevin et al., 2008; Messié and Chavez, 2015). Offshore, and in particular in regions of the narrow continental shelves, phytoplankton productivity is also limited by the micronutrient iron (Fe) (Hutchins et al., 2002; Moore et al., 2004; Brzezinski et al., 2011). Given the overall high nutrient supply to the near-shore area of the Peruvian coastal upwelling region diatoms are generally the dominant

phytoplankton group (Blasco, 1971; Estrada and Blasco, 1985; DiTullio et al., 2005; Bruland et al., 2005; Abrantes et al., 2007).

1.5 Outline of the Thesis

The main goal of the DFG funded Collaborative Research Centre SFB 754 is to investigate changes in supply and consumption of oxygen in the oxygen-depleted tropical oceanic areas in past, present and future climates. Oxygen distribution in the global ocean is controlled by a close interplay of climate dynamics (e.g. atmospheric exchanges, oceanic ventilation) and oceanic biochemistry (e.g. PP and organic matter degradation due to bacterial activity). Along the Peruvian margin, changes in the surface hydrology originate from either local wind-driven upwelling or from the Pacific basin-scale circulation changes. The PP at the sea surface is directly linked to the upwelling-driven nutrient input.

The aim of this thesis is to improve the understanding of present and past $\delta^{30}Si$ compositions of diatoms by the measurements of $\delta^{30}Si$ of different size fractions of diatoms. Additionally, the influence of the recent observations of species-dependent isotope fractionation on present and past $\delta^{30}Si$ signatures off Peru is investigated by determination of the associated diatom assemblages. The main goal is to apply $\delta^{30}Si$ as means of $Si(OH)_4$ utilization reconstructions for sediments along the Peruvian margin in order to improve our understanding of the coupling of the local silicon cycle to larger scale variations in the biogeochemical properties of the Eastern Equatorial South Pacific since the Last Glacial Maximum.

Furthermore, diatom-bound nitrogen isotope compositions are measured to verify the fidelity of bulk sediment nitrogen isotope records at the Peruvian margin. Given that $\delta^{30}Si$ and $\delta^{15}N_{db}$ measurements can be conducted on the same sample material, the latter is also applied to provide a better a better understanding of the coupling of the silicon and nitrogen cycling within the Peruvian coastal upwelling area of the past 20,000 years.

The following chapters are providing the main methods, results and discussion of the thesis. Chapters I, II, III and IV are presented in the form of separate articles, either published, in review or in preparation for submission.

Chapter I presents a combined surface sediment and downcore study, that aims to disentangle observed stable silicon isotope compositions of different diatom size fractions in terms of upwelling intensity and nutrient utilization. This study is a continuation and extension of a study from (SFB 754 B7, phase 1) aiming to answer open questions and providing additional information of the connection between diatom silicon isotope signatures and diatom assemblages.

Chapter II provides a compilation of biogenic opal concentrations and of stable silicon isotope records of different size fractions compared to the diatom assemblages of four sediment cores covering the entire Peruvian Margin and the main productivity and oxygen gradients between 5°S and 15°S. The major objective of this manuscript is the reconstruction of past export productivity, nutrient utilization and upwelling intensity in response to regional and global variability in oceanographic and atmospheric circulation over the last 20,000 years.

Chapter III contains a comparison of stable silicon isotope compositions of diatoms versus bulk sedimentary nitrogen isotope compositions presented for three short cores covering the Peruvian shelf between 11°S and 15°S over the last 600 years. Based on the premise that $\delta^{30}Si$ is controlled mainly by the degree of $Si(OH)_4$ utilization, while the $\delta^{15}N$ is influenced by both nitrate utilization and subsurface denitrification, the correlation of $\delta^{30}Si$ versus $\delta^{15}N$ is suggested to enable the quantification of relative effects of both nutrient utilization and denitrification on the $\delta^{15}N$ record.

Chapter IV investigates the fidelity of past bulk sediment nitrogen isotope records based on analysis of preservation of organic matter via C/N ratios and by comparison with diatom-bound nitrogen isotope compositions, which are thought to be unaffected by alteration during early diagenesis. Furthermore, following the approach of Chapter III, a direct comparison between $\delta^{15}N_{db}$ and $\delta^{30}Si$ of diatom is used to infer variations in nutrient utilization and denitrification along the Peruvian shelf between 9°S and 15°S over the past 20,000 years.

II. Publications and manuscripts

Declaration of my contribution to the following chapters

Chapter I:

Publication: Doering, K., C. Ehlert, P. Grasse, X. Crosta, S. Fleury, M. Frank, and R. Schneider (2016), Differences between mono-generic and mixed diatom silicon isotope compositions trace present and past nutrient utilisation off Peru, *Geochimica et Cosmochimica Acta*, *177*(C), 30–47, doi:10.1016/j.gca.2015.12.029.

Statement:
All measurements were done by myself. I analyzed the data and wrote the manuscript. Xavier Crosta counted the diatom abundances. Both Xavier Crosta and Sophie Fleury helped defining the diatom assemblage groups. All co-authors helped to improve and revise the manuscript.

Chapter II:

Publication: Doering, K., Erdem Z., Ehlert, C., Fleury S., Frank M. and Schneider R., (in review with *Paleoceanography*) Changes in diatom productivity and upwelling intensity off Peru since the Last Glacial Maximum: local response to basin-scale atmospheric and oceanic forcing.

Statement:
All measurements were performed by myself. I analyzed the data and wrote the manuscript. The age models of sediment core M77/2-052-2 and 029-3 were developed by Zeynep Erdem and Sophie Fleury. All co-authors helped to improve and revise the manuscript.

Chapter III:

Manuscript: Doering, K., Fleury S., Ehlert C., Martinez P., Frank M. and Schneider R., Latitudinal variations of $\delta^{30}Si$ and $\delta^{15}N$ along the Peruvian shelf: quantifying nutrient utilization versus denitrification over the past 600 years

Statement:
All measurements were performed by myself. I analyzed the data and wrote the manuscript. All co-authors helped to improve and revise the manuscript.

Chapter IV:

Manuscript: Doering, K., Robinson R. S., Martinez P., Ehlert C. Frank M. and Schneider R., Disentangling deglacial biogeochemical cycling of nutrients off Peru based on bulk sediment and diatom-bound $\delta^{15}N$ records

Statement:
All measurements were performed by myself. The diatom-bound $\delta^{15}N$ data of core M77/2-003-2 was measured together with Rebecca Robinson at her laboratory at the University of Rhode Island. The bulk sediment $\delta^{15}N$ and total N concentrations for all cores were measured at the University of Bordeaux in the laboratory of Philippe Martinez. I analysed the data and wrote the manuscript. All co-authors helped to improve and revise the manuscript.

Chapter I. Differences between mono-generic and mixed diatom silicon isotope compositions trace present and past nutrient utilisation off Peru

Kristin Doering[1,2*], Claudia Ehlert[3], Patricia Grasse[2], Xavier Crosta[4], Sophie Fleury[5], Martin Frank[2] and Ralph Schneider[1]

[1]Institute of Geosciences, University of Kiel
[2]GEOMAR Helmholtz Centre for Ocean Research Kiel, Germany
[3]Max Planck Research Group - Marine Isotope Geochemistry Carl von Ossietzky University (ICBM), Oldenburg, Germany
[4]Université de Bordeaux, UMR CNRS 5805 EPOC, France
[5]Department of Marine Science and Convergence Technology, Hanyang University ERICA campus, 55 Hanyangdaehak-ro, Sangnok-gu, Ansan-si, Gyeonggi-do 426-791, South Korea

Published in March 2016 in Geochimica et Cosmochimica Acta **177**, 30-47

Abstract

In this study we combine for the first time silicon (Si) isotope compositions of small mixed diatom species ($\delta^{30}Si_{bSiO2}$) and of large handpicked mono-generic (i.e. genus = *Coscinodiscus*) diatom samples ($\delta^{30}Si_{Coscino}$) with diatom assemblages extracted from marine sediments in the Peruvian upwelling region in order to constrain present and past silicate utilisation.

The extension of a previous core-top data set from the Peruvian shelf demonstrates that $\delta^{30}Si_{Coscino}$ values record near-complete Si utilisation, as these are similar to the isotopic composition of the subsurface source waters feeding the upwelling. In contrast, the $\delta^{30}Si_{bSiO2}$ of small mixed diatom species increase southward along the shelf as well as towards the shore. We attribute highest $\delta^{30}Si_{bSiO2}$ values partly to transient iron limitation but primarily to the gradual increase of Si isotope fractionation within the seasonal diatom succession, which are mainly recorded by small diatom species during intense bloom events. In contrast, lower $\delta^{30}Si_{bSiO2}$ values are related to initial Si isotope utilisation during periods of weak upwelling, when low $Si(OH)_4$ concentrations do not permit intense blooms and small diatom species record substantially lower $\delta^{30}Si$ signatures. As such, we propose that the intensity of the upwelling can be

deduced from the offset between $\delta^{30}Si_{bSiO2}$ and $\delta^{30}Si_{Coscino}$ (Δ), which is low for strong upwelling conditions and high for prevailing weak upwelling.

We apply the information extracted from surface sediments to generate a record of the present-day main upwelling region covering the past 17,700 years and find that this location has also been characterized by a persistent offset (Δ). By comparison with the diatom assemblages we show that the coastal upwelling system changed markedly between weak and strong upwelling conditions. In addition, our model calculations to quantify species-specific Si isotope fractionation effects based on the diatom assemblages indicate an overall minor influence that cannot explain the high amplitude in the measured $\delta^{30}Si_{bSiO2}$ record.

1. Introduction

The silicon (Si) isotope composition ($\delta^{30}Si$) of diatom frustules is used to reconstruct silicic acid ($Si(OH)_4$) utilisation in ocean surface waters in order to better understand the biogeochemical cycling of nutrients and their relationship to the extent of primary productivity (PP). In regions dominated by diatoms, e.g. the Southern Ocean, the North Pacific and coastal upwelling areas, PP is ultimately regulated by $Si(OH)_4$ availability (e.g. Lisitzin, 1971). Given that diatoms preferentially incorporate the lighter isotopes (^{28}Si and ^{29}Si relative to ^{30}Si) when utilising $Si(OH)_4$ for mineralization of their opaline frustules (De La Rocha et al., 1997), both the residual $Si(OH)_4$ in surface waters and the diatom opal produced from these waters become progressively enriched in the heavier isotopes with increasing $Si(OH)_4$ utilisation (Douthitt, 1982; De La Rocha et al., 1997).

Studies of the modern ocean have contributed to the understanding of the relationship between $\delta^{30}Si$ of biogenic opal ($bSiO_2$) and $Si(OH)_4$ in the context of utilisation, remineralization and dissolution (Varela et al., 2004; Cardinal et al., 2005; 2007; Beucher et al., 2008; Fripiat et al., 2011; Egan et al., 2012; Ehlert et al., 2012). These studies are the basis for the use of silicon isotopes from biogenic opal in sediments to reconstruct past changes in $Si(OH)_4$ utilisation (De La Rocha et al., 1998; Beucher et al., 2007; Reynolds et al., 2008; Pichevin et al., 2009; Ellwood et al., 2010; Maier et al., 2013; Ehlert et al., 2013). Core-top calibrations of diatom $\delta^{30}Si$ show that the sedimentary signal reflects the cumulative seasonal drawdown of $Si(OH)_4$ but can be significantly biased by siliceous components other than diatoms (Egan et al., 2012; Ehlert et al., 2012). Moreover, Sutton et al. (2013) reported species-specific Si isotope enrichment factors for several marine diatoms species, which had previously been assumed to be species independent (De La Rocha et al., 1997). Therefore, changes in the dominance of different diatom species on seasonal to geological timescales may substantially influence the reconstructed Si isotope composition of diatom opal

Published in Geochimica Cosmochimica Acta 177 (2016), 30-47

in the paleo record and thus the reconstruction of $Si(OH)_4$ utilisation. The potential effects of diatom species-dependent Si isotope fractionation thus require a comparison of the $\delta^{30}Si$ signal with shifts in the diatom assemblages in the sedimentary record, in addition to more detailed analyses of modern seasonal variations of the $\delta^{30}Si$ of $Si(OH)_4$ in the surface waters and particulate (diatom) opal in the water column (e.g. Cao et al., 2012).

For the present-day Southern Ocean water column Cardinal et al. (2007) reported Si isotopic signatures of diatoms to be unrelated to particle size (i.e. >0.4µm, 20-70µm and >70µm). This has so far ben supported by records of past $\delta^{30}Si$ signatures from the North Pacific (Maier et al., 2013) and Eastern Equatorial Pacific (Ehlert et al., 2013). However, in a case study of the Peruvian coastal upwelling area Ehlert et al. (2012) compared the present-day Si isotope compositions of dissolved $Si(OH)_4$ in the water column ($\delta^{30}Si_{SiOH4}$) with that of diatoms in the underlying surface sediments of the shelf. Their first comparison of Si isotope compositions of mixed diatom species ($\delta^{30}Si_{bSiO2}$; 11-32µm) and handpicked mono-generic diatoms ($\delta^{30}Si_{Coscino}$; >125µm; previously reported as $\delta^{30}Si_{diatom}$) revealed $\delta^{30}Si_{bSiO2}$ values being generally lighter than the $\delta^{30}Si_{Coscino}$ values. These lighter $\delta^{30}Si_{bSiO2}$ values may represent low Si utilisation due to continuous upwelling-induced nutrient supply, while $\delta^{30}Si_{Coscino}$ signatures record high Si utilisation during non-upwelling or summer conditions.

1.1 Regional setting and present-day upwelling and nutrient conditions off Peru

In the Eastern Equatorial Pacific (EEP) year-round upwelling of high nutrient waters off Peru leads to extremely high PP (Pennington et al., 2006). The main source for the upwelled high nutrient waters is the subsurface Peru-Chile Undercurrent (PCUC), which flows southward between 4 and 14°S at a depth between 50 and 150m along the shelf (Fig.1) (Zuta and Guillén, 1970; Brink et al., 1983; Toggweiler et al. 1991). The PCUC is partly fed by eastward flowing subsurface waters of the Equatorial Undercurrent (EUC), the primary Southern Subsurface Counter Current (pSSCC) and secondary Southern Subsurface Counter Current (sSSCC).

In general, the PP is controlled by the flux of nutrients to the euphotic zone (Barber and Chávez, 1991). The high PP associated with high export productivity and remineralisation of organic matter induces an intense Oxygen Minimum Zones (OMZ) (Fuenzalida et al., 2009). The ultimate sources of the nutrients are Subantarctic Mode Waters, feeding the EUC (Lukas, 1986) as well as vertical admixture of remineralised organic matter from shelf sediments (Franz et al., 2012; Ehlert et al., 2012). Overall the rate of PP is regulated by nutrient supply (macronutrients: nitrate (NO_3^-), silicate ($Si(OH)_4$) and phosphate (PO_4); micronutrients: iron (Fe), cadmium), light and physical export (offshore

transport or subduction of water masses; Messié and Chavez, 2014). Nutrient concentrations of NO_3^-, PO_4 and partly Fe are very high and thus not limiting for diatoms off Peru (Bruland et al., 2005; Franz et al., 2012). Instead, $Si(OH)_4$ concentrations are assumed to be limiting diatom production during austral summer (Dugdale et al., 2002; Franz et al., 2012), while iron and light limitation

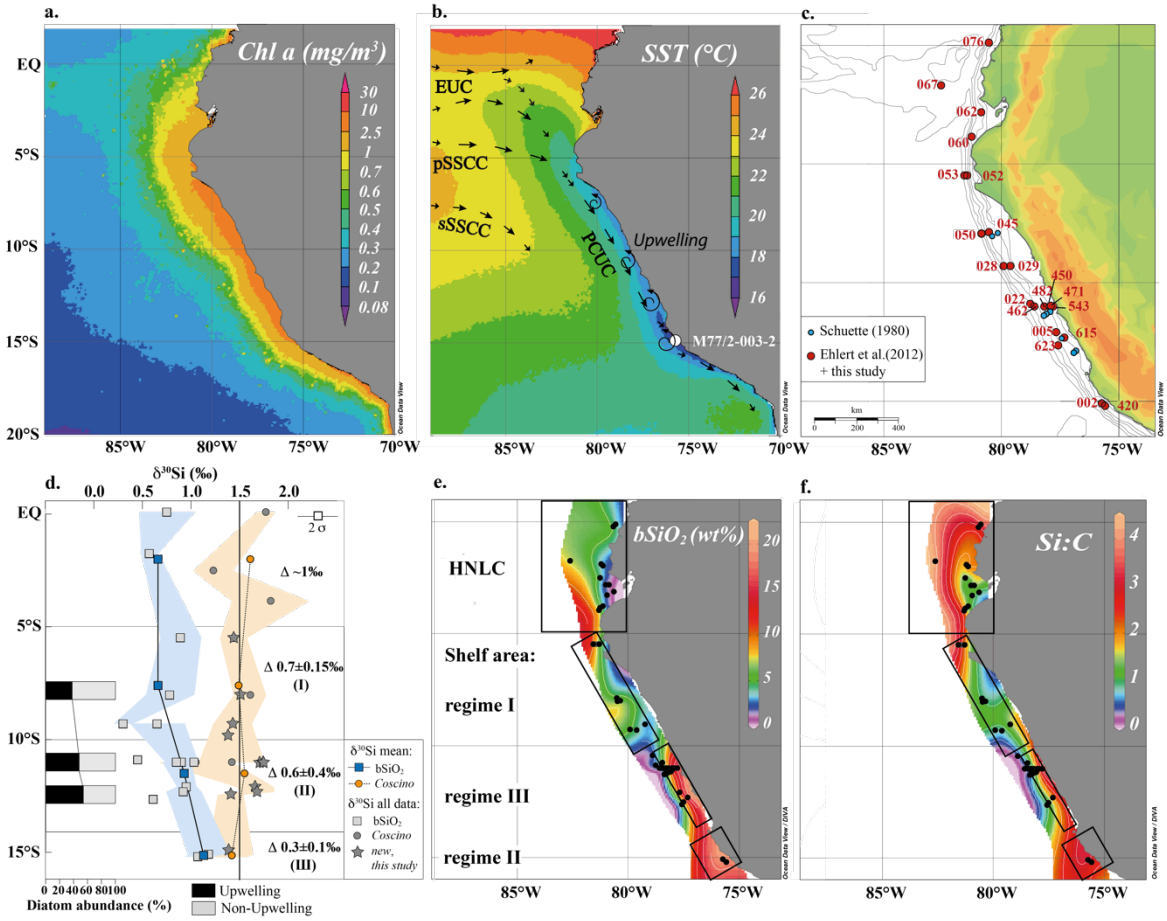

Figure 1: Maps showing a) chlorophyll *a* concentration and b) sea surface temperature averaged for the period between 1997 and 2015 (http://oceancolor.gsfc.nasa.gov/cgi/l3), with generalized circulation pattern of the currents in the near-shore area (modified after Ayón et al., 2008; Montes et al., 2010; Czeschel et al., 2011). EUC Equatorial Undercurrent, pSSCC primary Southern Subsurface Counter Current, sSSCC secondary Subsurface Counter current, PCUC Peru-Chile Undercurrent; The curved arrows near the coast indicate the upwelling of subsurface waters; The location of piston core M77/2-003-2 is given as white circle. c.) Location of surface sediment stations from this study (red circles and labels) and from Schuette (1980) (blue circles); the bathymetry is given for 0 to 5000 m water depth in 100 m increments; d.) Latitudinal distribution of the surface sediment mean $\delta^{30}Si$ (‰) of $bSiO_2$ (blue squares) and handpicked diatoms (*Coscinodiscus*; orange squares). The $\delta^{30}Si_{bSiO2}$ and $\delta^{30}Si_{Coscino}$ are given as mean values for 0-5°S, 5-10°S, 10-14°S and 15°S (Table 1). The black vertical line at +1.5‰ represents the $\delta^{30}Si_{Si(OH)4}$ value of the source water (PCUC); blue and red shaded areas represent the 2σ error of repeated sample measurements; relative diatom abundances (%) (after Schuette, 1980) for surface sediment indicated by blue circles for the area 5-15°S. The diatom assemblages are classified as upwelling-related (black bars) and non-upwelling diatoms (grey bars); e.) surface sediment $bSiO_2$ concentrations (wt%); f) surface sediment Si:C ratios; The black rectangles highlight the Northern area and different shelf areas (i.e. regime I, II and III) distinguished accordingly by Chl *a*, SST, $bSiO_2$ and Si:C values (see text for details).

Published in Geochimica Cosmochimica Acta 177 (2016), 30-47

is shown to prevail during austral winter (Hutchins et al., 2002; Bruland et al., 2005; Pennington et al., 2006; Echevin et al., 2008; Messié and Chavez, 2014). Potential iron limitation during winter when upwelling is most intense off Peru is in agreement with recent suggestions that iron limitation can arise in the course of intense upwelling if Fe is deficient relative to other macronutrients (Pichevin et a., 2014). However, due to the overall high nutrient supply to the near-shore area of the Peruvian coastal upwelling region diatoms are generally the dominant phytoplankton group (Blasco, 1971; Estrada and Blasco, 1985; DiTullio et al., 2005; Bruland et al., 2005; Abrantes et al., 2007).

Diatom assemblages are reliable indicators of the successional stages of PP and record the maturation of upwelling cells in marine sediments (Schuette and Schrader, 1981; MacIsaac et al., 1985; Schrader, 1992; Romero and Hebbeln, 2003). The PP successional stages generally follow four steps (Jones et al., 1983; MacIsaac et al., 1985; Hansen et al., 2014): (1) upwelling of cold, nutrient-rich waters with little biomass and low growth rates (2) water column stabilisation leads to increase in growth rates and nutrient consumption and diatoms to dominate the phytoplankton (3) Due to rapid consumption, nutrient concentrations decrease and higher growth rates result in intense diatom production (4) With the onset of nutrient depletion and limitation, growth rates and nutrient uptake diminish. The initial diatom assemblage that occurs during step (2) is composed of small diatoms with high production rates (early diatom succession stage), while the post-upwelling stage (3) is dominated by larger-sized diatoms species (Garrison, 1979; Tarazona et al., 2003). The final stage of nutrient depletion and limitation (4) is usually associated with dinoflagellates and large centric diatoms (Garrison, 1979; Tarazona and Arntz, 2001). Generally the whole cycle is completed in a couple of weeks, but can be interrupted by freshly upwelled water parcels. The change in dominant species is closely related to the transition from turbulent to more stable conditions in upwelled waters (Margalef, 1978; Blasco et al., 1981). Consequently, on an annual basis diatom assemblages follow the same principle of succession and thus vary depending on the different seasonal environmental conditions (Rojas de Mendiola, 1981; Kemp et al., 2000).

To better understand the relationship between $\delta^{30}Si_{bSiO2}$ and $\delta^{30}Si_{Coscino}$, we extended the core-top data set of $\delta^{30}Si_{Coscino}$ from Ehlert et al. (2012) in the main upwelling area off Peru and correlate the isotopic signatures to the diatom assemblages to evaluate the effect of seasonal and environmental variations, such as upwelling intensity and nutrient availability. The findings from surface sediments are then applied to the $\delta^{30}Si_{bSiO2}$ and $\delta^{30}Si_{Coscino}$ signals as well as the diatom assemblages from a sediment core from the Peruvian upwelling at 15°S covering the last 17,700 years. Additionally, changes in the diatom assemblage will be used to evaluate the influence of species-specific Si isotope fractionation on the Si isotope record.

2. Material and Methods

The data presented in this study were obtained from surface sediments from along the Peruvian shelf and upper slope between 0°N and 15°S (Fig.1; Table1) and from latest Pleistocene sediments of piston core M77/2-003-2 (003-2) recovered from 271 m water depth at 15°06'S, 75°41'W (Figs.1 and 2, Tables 1 and 2). Sediments were retrieved during the German R/V Meteor cruises M77/1 and M77/2 in 2008 in the framework of the Collaborative Research Centre (Sonderforschungsbereich/SFB) 754 funded by the German Science Foundation (DFG). Surface sediment samples were collected with a multicorer (MUC) and only the uppermost cm was used for sample preparation. Particulate organic carbon (C_{org}) and biogenic opal ($bSiO_2$) concentrations of the surface sediments were published previously by Mollier-Vogel et al. (2012) and Ehlert et al., (2012) (Supplementary material Table S1 and Fig. S1).

Core 003-2 consists of dark olive grey sediments, intercalated with dark greyish to pale yellow laminated intervals. Although smaller slumps and indications of bioturbation can be observed, the sediment record covers the past 17,700 years without major disturbances or hiatuses. The downcore C_{org} concentrations were measured by Mollier-Vogel (2012). The age model, previously established by Mollier-Vogel (2012) was improved by six additional AMS ^{14}C dates measured on the organic fraction soluble in weak sulphuric acid. All measurements were performed at the Leibniz Laboratory for Isotope Research and Dating at the University of Kiel. The 17 AMS ^{14}C results were converted into calendar years using the program CLAM2.2 (Blaauw, 2010), the Marine13 calibration curve (Reimer and Bard, 2013) and applying a reservoir age of 511±278 years following (Ortlieb et al., 2011) (supplementary material, Table S2). The program CLAM2.2 (Blaauw, 2010) is based on a Bayesian method and was used in order to provide the best fit between radiocarbon ages. The resulting age model is displayed in figure S2 of the supplementary material.

2.1 Diatom assemblages

Sediment treatment and slide preparation for the analyses of diatom assemblages from Core 003-2 followed the technique described by Rathburn et al. (1997). Diatom counting followed the procedures described by (Crosta and Koç, 2007). An average of 350 diatom valves were counted per sample at x1000 magnification and the total number of diatom valves per gram of dry sediment was calculated as follows:

$$Valves/g = ((N/n)\times(S/s)\times(V/v))/W,$$

where N is the number of valves counted and n the number of fields of view, S is the area of the evaporation tray, s the area of one field of view, V the volume of solution in the beaker, v the volume of solution put in the evaporation tray and W the weight of the sample. Total diatom numbers are presented in units of 10^6

Published in Geochimica Cosmochimica Acta 177 (2016), 30-47

valves per gram dry sediment (supplementary material, Table S3; after Schrader and Gersonde, 1978). Additionally, to provide an estimate of the composition of the 11-32µm fraction, smear-slides were prepared and counted at 400x magnification.

The abundances of two groups of diatom species representing upwelling and non-upwelling conditions were identified according to earlier studies off Peru (Schuette, 1980; De Vries and Schrader, 1981; Rojas de Mendiola, 1981; Schuette and Schrader, 1981; Abrantes et al., 2007).

(1) Coastal upwelling - nutrient-rich, turbulent waters (initial diatom succession stage, step 2): Chaetoceros spp. and resting spores (RS), Skeletonema costatum, Thalassionema nitzschioides var. nitzschioides;

Chaetoceros spp. is the most dominant species and forms of resting spores (RS) when nutrients are nearly exhausted in the euphotic zone (Schuette, 1980). *Thalassionema nitzschioides* and *Skeletonema costatum* are mainly associated with high nutrient conditions or freshly upwelled waters (Blasco, 1971; Margalef, 1978).

(2) Non-upwelling diatom species:

Coastal planktonic (temperate, cosmopolitan) - high-to-moderate nutrient waters (PP cycle, step 3): Actinocylcus spp., Actinoptychus spp., Asteromphalus spp., Coscinodiscus spp.;

Coastal planktonic species are generally found in the water and sediments close to the coast, their the spatial distribution pattern resembles that of upwelling group (1) (Schuette, 1980; Romero and Hebbeln, 2003) but they are associated with high to moderate surface water productivity and non turbulent conditions (Blasco, 1971; Rojas de Mendiola, 1981; Romero et al., 2003; Romero and Hebbeln, 2003).

Oceanic planktonic (warm, temperate) in nutrient-poor waters (PP cycle, step 4): Azpeitia spp., Nitzschia spp., Rhizosolenia spp., Thalassiosira spp.

Oceanic planktonic diatoms are often referred to as the tropical/subtropical group associated with low- to mid-latitude pelagic warm waters (Romero and Hebbeln, 2003).

Other diatom species: Cyclotella spp., (mainly C. striata and C. stylorum), Biddulphia spp. (mainly alternans), Cocconeis spp., Delphineis karstenii;

For simplification species overall accounting for less than 2% are not shown here but a complete overview is given in the supplementary material (Table S3). Handpicked diatoms were identified at 200-1000x magnification at irregular intervals and belong mainly to *Coscinodiscus asteromphalus*, *C. radiatus* and *C. concinnus* as part of group 2 (coastal planktonic diatoms).

2.2 Biogenic opal and silicon isotope analyses

The $bSiO_2$ concentration of the sediments, which represents the relative contribution of opal producing organisms (mainly diatoms, but also radiolarians

and sponge spicules), was quantified according to an automated leaching method using sodium hydroxide (DeMaster, 1981; Müller and Schneider, 1993) at a precision of 1-2% (1σ) (Table 1 and 2). For the downcore record of core 003-2 the $bSiO_2$ accumulation rates (AR_{bSiO2} g cm^{-2} ka^{-1}; Table 2) were calculated using the dry bulk density (g/cm^3) and the sedimentation rates (cm/ka) obtained based on the age model.

Diatoms were extracted from the sediment for the silicon isotope measurements in two different ways. For the $\delta^{30}Si_{bSiO2}$ measurements the size fraction 11-32µm was separated using chemical and physical cleaning techniques (sieving and heavy liquid separation) as described by Morley (2004). Following Morley et al. (2004) the 11µm grain size was used as lower size limit to completely remove clay minerals, while the 32µm size fraction was selected as the upper grain size limit to remove the generally larger radiolarians, as well as sponge spicules. All samples were scanned via light microscopy to verify their purity with respect to the detrital (clay) fraction and other opal phases prior to dissolution until pure (>95%) diatom samples were obtained. According to smear slide counts radiolarian and sponge spicules accounted for less than 1% and 5%, respectively (supplementary material, Fig. S3). In an additional procedure 200-500 large centric diatoms (*Coscinodiscus* spp.) were handpicked from the 125/150-250 µm size fraction to analyse the $\delta^{30}Si_{Coscino}$ signatures (after Ehlert et al., 2012).

From all samples an aliquot (~ 75 µl) was transferred into Teflon vials and dissolved in 1 mL 0.1 M NaOH at 130°C over 12h. Residual material was separated via centrifugation and remaining organic matter was removed by adding 200 µL concentrated H_2O_2 (Suprapur). Sample solutions were diluted with 4 mL MQ water and neutralised with 0.1 mL 1 M HCl (Reynolds et al., 2008). Al/Si ratios were measured on aliquots of the dissolved $bSiO_2$ samples using an *Agilent 7500 Series* quadrupole ICPMS at GEOMAR, Kiel to check for potential remaining contamination by clays (Table 2) and ranged between 2 and 210 mmol/mol (for the evaluation see supplementary material S3). Silicate concentrations of all sample solutions were measured colourimetrically using a photospectrometer (Grasshoff et al., 1999) and chromatographically purified on columns containing 1 mL pre-cleaned AG50W-X8 cation exchange resin (BioRad, mesh 200-400) following the method described by Georg et al. (2006) and modified by de Souza et al. (2012).

Silicon isotope ratios were determined on a *NuPlasma HR* Multi Collector-ICPMS at GEOMAR applying a standard-sample bracketing method (Albarède et al., 2004). Sample solutions were diluted to a Si concentration of 0.6 ppm and introduced into the MC-ICPMS via a Cetac Aridus II desolvating nebulizer system equipped with a PFA nebulizer with a 60-80 µL/min uptake rate. Silicon isotope compositions are reported in the δ-notation against the reference standard NBS28 in parts per thousand ($\delta^{30}Si = ((R_{sample}/R_{standard}) - 1) * 1000$), where R is the measured

$^{30}Si/^{28}Si$ ratio of the sample and the NBS28 standard, respectively. All samples were measured on at least three different days and at least 4-5 times per session, which resulted in uncertainties between 0.06‰ and 0.31‰. This external reproducibility is given as 2σ standard deviations of the mean $\delta^{30}Si$ value (Tab. 1 and 2). Long-term repeated measurements of the reference materials NBS28, IRMM018, and Big Batch gave average $\delta^{30}Si$ values of 0.00±0.23‰ (2σ), −1.51±0.18‰ (2σ) and −10.74±0.20‰ (2σ), respectively, which agree well with reported literature values (Reynolds et al., 2007). Overall, external reproducibility was within the long-term precision of ±0.23‰ (2σ). The latter is indicated as error bar on all figures, while the external reproducibility of the samples is indicated by coloured areas.

3. Results

3.1 Surface sediment stable silicon isotope compositions, Si:C and diatom assemblages

The surface sediment data set in this paper comprises the previous study of Ehlert et al., (2012) and eleven new Si isotope measurements of handpicked diatoms ($\delta^{30}Si_{Coscino}$) from the main upwelling area (see Table 1; Fig. 1d). The $\delta^{30}Si_{bSiO2}$ signatures are highly variable and increases from +0.6‰ to +1.1‰ in the South and decreases from the coast (+1‰) to lower values further offshore (+0.3‰; Table 1). In contrast, the $\delta^{30}Si_{Coscino}$ values are usually higher and exhibit little variability (+1.5±0.3‰) with one exception at 11°S where a low value of +1±0.38‰ was found. However, even this low $\delta^{30}Si_{Coscino}$ value is still within the uncertainty of the mean value. The offset between $\delta^{30}Si_{Coscino}$ and $\delta^{30}Si_{bSiO2}$ signatures ($\Delta = \delta^{30}Si_{Coscino} - \delta^{30}Si_{bSiO2}$) is highest in the North (0 – 5°S; Δ= 1‰) and considerably lower within the main upwelling area (5-10°S: $\Delta^{30}Si_{coscino\text{-}bSiO2}$ = 0.7±0.15‰; 10-14°S: $\Delta^{30}Si_{coscino\text{-}bSiO2}$ = 0.6±0.4‰; 15°S: $\Delta^{30}Si_{coscino\text{-}bSiO2}$ = 0.3±0.1‰)(All $\Delta^{30}Si_{coscino\text{-}bSiO2}$ values reported are positive for better distinction from $\delta^{30}Si$ signatures we omit a prefix; Table 1; Fig. 1d). Additionally, at 11°S and 12°S $\delta^{30}Si_{bSiO2}$ values decrease from the coast to the shelf-break indicating the influence of dynamic coastal processes. To focus on the high productivity near-shore process the regionally averaged Δ value (0.6±0.4‰) between 10°S and 14°S (regime II) was calculated only for the samples from depths shallower than 500m (i.e. excluding station 22 and 623; Supplementary Material Fig. S4).The differences in the $bSiO_2$ and C_{org} distributions (previously presented by Ehlert et al., 2012 and Mollier-Vogel et al., 2012) result in higher Si:C ratios (>3) at offshore locations in the North (0-5°S) and close to the coast in the South (10-15°S), while on the central shelf (5-10°S) the Si:C ratios remain close to 1 (Fig. 1f).

Due to lack of counts of the diatom assemblage from the core-top material presented here, assemblage data are used from Schuette et al. (1980) (Fig. 1 c and d). The diatom assemblages on the shelf show a slight increase in the contributions of upwelling-related over non-upwelling species from North (38% upwell. /62% non-upwell.) to South (54% upwell./46% non-upwell.; Table 1 and Fig. 1d).

Table 1: $bSiO_2$ concentrations and $\delta^{30}Si$ data for mixed diatom species ($\delta^{30}Si_{bSiO2}$) and mono-generic diatoms ($\delta^{30}Si_{Coscino}$) extracted from surface sediments on the Peruvian shelf (modified from Ehlert et al., 2012). 2σ represents the external reproducibility of repeated sample measurements. $\Delta^{30}Si$ corresponds to the difference between $\delta^{30}Si_{Coscino}$ and $\delta^{30}Si_{bSiO2}$. Samples marked in italics are new data presented in this study. The main upwelling area between 5 and 15°S is divided into three characteristic regimes (I =5-10°S; II = 10-14°S and III = ~15°S; see text for details) and averaged for $bSiO_2$ concentration, $\delta^{30}Si_{bSiO2}$, $\delta^{30}Si_{diatom}$ and $\Delta^{30}Si$, as marked in bold. Surface sediment diatom assemblage data are from Schuette (1980). The mean diatom percentages are given for open ocean station and shelf stations (Fig. 1b, blue circles) at 8°S, 11.5°S and 12.5°S. Total Upwell. = cumulative abundance off all upwelling related diatom species in % (*Chaetoceros* spp + *Skeletonema costatum*.+ *Thalassionema nitzschioides*); Total non-upwell. = 100 – total upwell.).

Station no.	Latitude (N)	Longitude (E)	Depth (m)	$bSiO_2$ (wt%)	$\delta^{30}Si$ $bSiO_2$	2σ	$\delta^{30}Si$ Coscino	2σ	$\Delta^{30}Si$	1σ
M77/2-076	0.09	-80.56	290	2.8	0.75	0.29	1.77	0.10	1.02	
M77/2-067	-1.75	-82.63	2075	7.1	0.57	0.09	-	-	-	
M77/2-062	-2.5	-81.25	1678	5.1	-	-	1.23	0.21	-	
M77/2-060	-3.85	-81.26	701	4.28			1.82	0.40		
Mean	**0 to -5**		**290-2075**	**4.8**	**0.62**	**0.19**	**1.61**	**0.24**	**1.02**	**-**
M77/2-052	-5.48	-81.45	1252	8.58	-	-	1.44	0.14	-	
M77/2-053	-5.48	-81.57	2607	11.5	0.89	0.21	*1.44*	*0.14*	0.55	
M77/2-	-8	-80.34	359	7.2	-	-	*1.51*	*0.12*	-	
M77/2-050	-8.02	-80.5	1013	7.4	0.78	0.25	1.61	0.17	0.83	
M77/2-028	-9.3	-79.9	1105	5.0	0.30	0.10	-	-	-	
M77/2-029	-9.3	-79.62	437	4.6	0.65	0.28	*1.43*	*0.20*	0.78	
Regime I	**-5 to -10**		**350-2500**	**5 - 10**	**0.66**	**0.21**	**1.49**	**0.16**	**0.72**	**0.15**
Diatoms groups:		**Upw**	**38%**	**Non-Upw**	**62%**					
M77/2-022	-10.89	-78.77	1923	4.7	0.45	0.25	-	-	-	
M77/1-462	-11	-78.75	2020	5.0	-	-	1.42	0.34	-	
M771-482	-11	-78.24	375	-	-	-	*1.74*	*0.18*	-	
M77/1-450	-11	-78.17	319	13.9	0.90	0.17	*1.74*	*0.12*	0.84	
M771-471	-11	-78.17	316	13.9	-	-	*1.71*	*0.21*	-	
M77/1-469	-11	-77.94	145	17.6	1.03	0.15	1.05	0.38	0.02	
M77/1-543	-11	-77.79	77	12.9	0.85	0.15	-	-	-	
Diatoms groups:		**Upw**	**48%**	**Non-Upw**	**52%**					
M77/1-623	-12.64	-77.58	1085	5.9	0.61	0.13	-	-	-	
M77/1-615	-12.43	-77.41	290	-	-	-	*1.41*	*0.14*	-	
M77/2-005	-12.09	-77.67	214	10.9	0.95	0.10	*1.66*	*0.19*	0.71	
M77/1-620	-12.31	-77.32	150	17.7	0.92	0.18	*1.68*	*0.18*	0.76	
Diatoms groups:		**Upw**	**54%**	**Non-Upw**	**46%**					
Regime II	**-11 to -14**		**50-400**	**10 - 15**	**0.93**	**0.15**	**1.55**	**0.22**	**0.58**	**0.38**
M77/2-002	-15.08	-75.73	290	20.6	1.18	0.22	*1.41*	*0.24*	0.24	
M77/1-420	-15.19	-75.58	516	17.3	1.07	0.13	*1.42*	*0.16*	0.34	
Regime III	**-15**		**290-516**	**17 - 20**	**1.1**	**0.18**	**1.4**	**0.20**	**0.29**	**0.07**

Published in Geochimica Cosmochimica Acta 177 (2016), 30-47

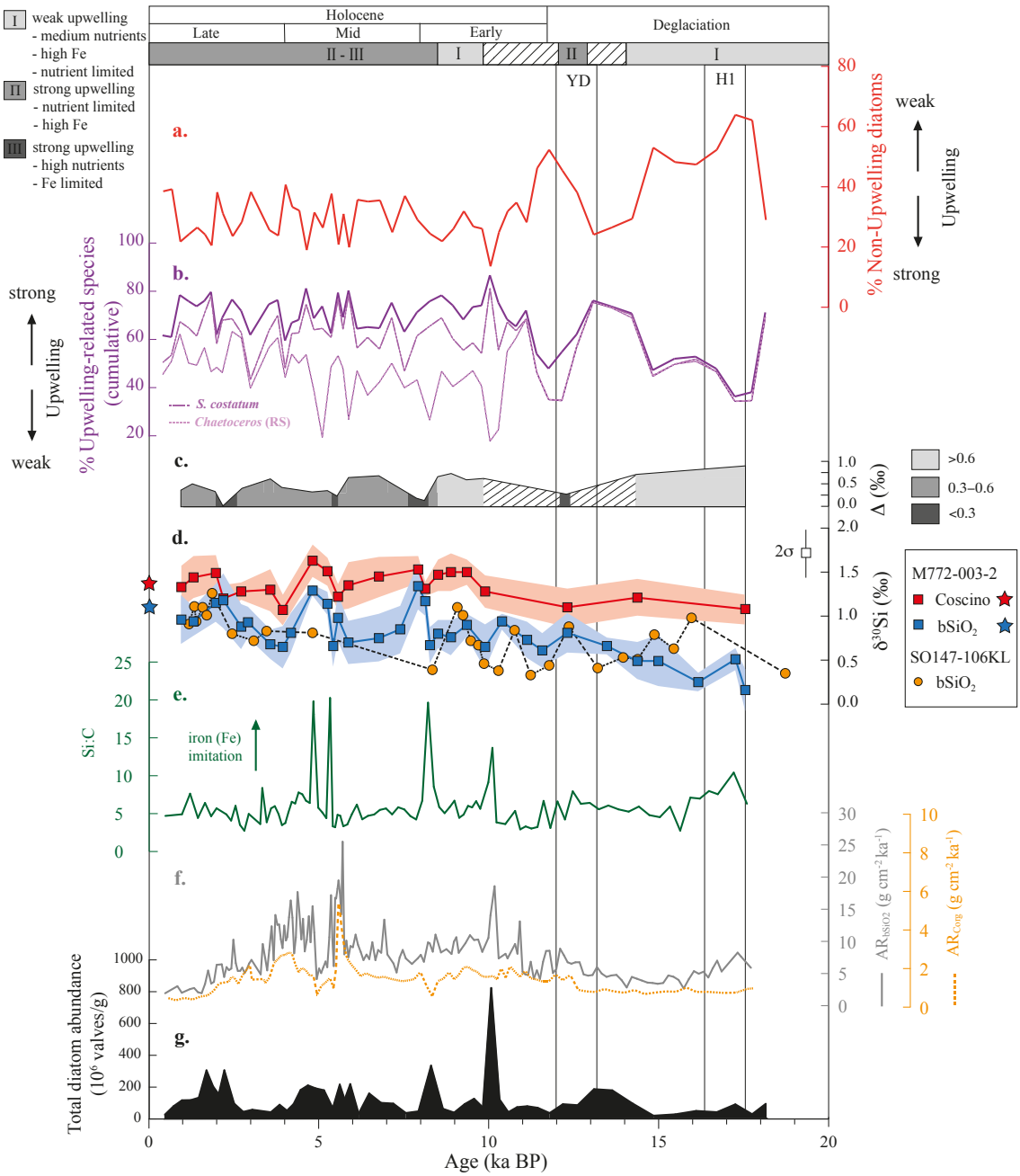

Figure 2: Downcore records from core M77/2-003-2; Percentages of (a) non-upwelling-related diatom species (red line) and (b) upwelling-related diatom species (purple line), within (b) cumulative contribution of *Chaetoceros* (RS; light purple dotted line) and *S. costatum* (purple dashed line) are shown; (c) Δ ($\Delta^{30}Si_{coscino-bSiO2}$) (grey shadings indicate the different regimes, see legend); (d) $\delta^{30}Si_{bSiO2}$ (blue squares) and $\delta^{30}Si_{Coscino}$ (red squares) as well as the $\delta^{30}Si_{bSiO2}$ record of core SO147-106KL from 12°S (orange circles; Ehlert et al., 2013); blue and red shaded areas represent 2σ error of repeated sample measurements; the blue and red stars mark the core-top values of both fractions of core M77/2-002 (Ehlert et al., 2012). (e) Si:C ratios; (f) AR_{bSiO2} (g cm^{-2} ka^{-1}; solid grey line) and AR_{Corg} (g cm^{-2} ka^{-1}; orange dotted line); (g) total diatom abundance of core (# 10^6 valves/g of dry sediment; black area); Time periods are classified as: (I) weak upwelling based on lowest diatom valve abundance (<50 x10^6 valves/g) and decreased percentages of upwelling-related diatom species (<70%) but higher Si:C ratios of 5-10 indicative of increased iron limitation (II) stronger upwelling based on elevate diatom abundance between 50 and 200 x10^6 valves/g, a high percentage of upwelling-related species (>70%) but lower Si:C ratios (~5) indicating reduced iron limitation; (III) strong upwelling based on highest diatom abundance (>200 x10^6 valves/g), diatom assemblages dominated by upwelling-species (>70%) and high Si:C (5-20) indicating iron limitation.

3.2 Downcore diatom assemblages, silicon isotope compositions and accumulation rates of $bSiO_2$ and C_{org}

The diatom assemblage record of core 003-2 shows variations in the amount of upwelling-related and non-upwelling diatom groups from the deglaciation to the Holocene (Table 3;Fig. 2a and b), while the total diatom abundance (Fig. 2g) closely follows the maximum percentages of upwelling-related diatom species. However, based on estimates of smear-slides performed on core 003-2 the 11-32µm size fraction samples did not contain diatom species smaller than 11 µm such as *S. costatum*, *T. nitzschioides* or vegetative cells of *Chaetoceros* spp. due to the sample processing (e.g. sieving and gentle ultrasonication) This results in overall lower abundances of upwelling species (*Chaetoceros* RS) between 5% and 25% with only 5-10% during the deglaciation and up to 25% during the Holocene at 11ka, 6ka and 2 ka BP (supplementary material Fig. S5). The total diatom abundance remains generally low (20-100 x 10^6 valves/g) during the deglaciation but shows a broad peak centred around 13 ka (~200 x 10^6 valves/g). During the Early (11.7 to 8.2 ka BP) and Mid Holocene (8.2 to 4 ka BP) non-upwelling species were less abundant, accounting for less than 40% of the overall diatom assemblage, while the contribution of the upwelling-related species increased (60-80%). Overall four periods of highest contributions of upwelling-related diatoms and total diatom abundances occurred during the Holocene at 9.7 ka, 7.9 ka, 5.7-4.3 ka and 2-1.3 ka (Fig. 2b). During the deglaciation (17.7-11.7 ka BP) the AR_{bSiO2} and AR_{Corg} are around 5±1.5 and 0.9±0.3 g cm^{-2} ka^{-1}, while the Si:C ratios are on average as high as 6±1.7. The low mean $\delta^{30}Si_{bSiO2}$ (+0.5±0.4‰) and $\delta^{30}Si_{Coscino}$ (+1.1±0.15‰) signatures during the deglaciation result in high Δ values around 0.8±0.1‰, with the exception of a low signature of 0.3‰ during the Younger Dryas (YD; 12.8-11.7 ka BP) (Fig. 2c; Table 2).

During the Holocene the AR_{bSiO2} increased to 9±4 (g cm^{-2} ka^{-1}) with maximum values at 10 ka, 5.3 ka and 4.8 ka BP. Similarly, AR_{Corg} values increase to 1.7± 0.8 g cm^{-2} ka^{-1} and maximum values of 5 g cm^{-2} ka^{-1} at 5.5 ka and 3 at 4 ka BP. The Si:C ratios are on average at 6±3.6 but exhibits distinct maxima of up to 20 at 10 ka, 8.2 ka, 5.3 ka and 4.8 ka BP. During the Holocene $\delta^{30}Si_{bSiO2}$ and $\delta^{30}Si_{Coscino}$ signatures increase to overall higher mean values (+0.9±0.4‰ and +1.4±0.3‰). The $\delta^{30}Si_{bSiO2}$ record shows little variability between 11 ka and 8 ka BP (+0.8±0.1‰), followed by a peak of +1.3‰ that slightly lags behind the maximum observed in $AR_{bSiO2,}$ Si:C and diatom abundance. The $\delta^{30}Si_{Coscino}$ signatures increase to +1.4±0.1‰ between 10 ka and 6 ka BP with only a slight decrease at 8 ka BP. Accordingly, the Δ values remain high at 0.7±0.1‰ until 8.2 ka and decrease considerably afterwards to +0.2±0.03‰ at the transition from the Early to the Mid Holocene (8 ka BP) while remaining above 0.6‰ during the Mid and Late (4 to 0 ka BP) Holocene. During the Mid and Late Holocene

(8-6 ka BP and 4.2-2.2 ka BP) both $\delta^{30}Si_{bSiO2}$ and $\delta^{30}Si_{Coscino}$ decrease to +0.8±0.21‰ and +1.3±0.16‰, interrupted by maximum values of +1.2±0.1‰ and +1.5±0.1‰, at 8 ka, 5.3-4.2 ka and 2.2-1.8 ka BP, respectively. Correspondingly, the Δ values are low (0.25±0.15‰) during prevailing maximum $\delta^{30}Si_{bSiO2}$ signatures (+1.2±0.1‰), but higher (0.5±0.19‰) during periods when $\delta^{30}Si_{bSiO2}$ decreases (+0.8±0.21‰).

Table 2: Downcore records for AR_{bSiO2} values (g cm^{-2} ka^{-1}), Si:C ratios, $\delta^{30}Si$ (mixed species and handpicked diatoms) and Al/Si elemental ratios obtained from core M77/2-003-2 and resulting $\Delta^{30}Si$ values; 2σ represents the external reproducibility of repeated sample measurements.

Age (ka)	AR_{bSiO2} ($g/cm^3/ka$)	Si:C	$\delta^{30}Si$ (‰) $bSiO_2$	2 σ	Al/Si (mmol/mol)	$\delta^{30}Si$ (‰) Coscino	2 σ	$\Delta^{30}Si$	Regime (I, II or III)
0.95	2.01	4.91	0.96	0.27	30	1.33	0.24	0.37	III
1.31	2.75	-	0.94	0.16	6	1.44	0.23	0.40	III
1.97	6.35	5.70	1.15	0.21	20	1.49	0.20	0.34	III
2.19	4.47	-	1.18	0.31	2	1.20	0.16	0.02	III
2.72	5.91	-	0.88	0.25	36	1.28	0.09	0.41	II
2.92	6.55	4.96	0.93	0.17	6	-	-		II
3.58	12.34	5.70	0.68	0.16	8	1.30	0.24	0.62	II
3.95	12.46	-	0.65	0.24	12	1.07	0.17	0.43	II
4.19	13.68	6.56	0.81	0.22	29	-	-		III
4.83	11.38	19.81	1.29	0.06	7	1.63	0.18	0.33	III
5.27	10.64	-	1.14	0.13	15	1.51	0.15	0.36	III
5.44	16.77	-	0.66	0.23	23	-	-		II
5.58	17.58	-	0.98	0.26	7	1.22	0.15	0.24	III
5.89	9.27	-	0.70	0.24	27	1.35	0.26	0.62	II
6.79	8.23	5.49	0.75	0.26	6	1.45	0.22	0.70	II
7.42	8.67	-	0.85	0.27	12	-	-		II
7.95	7.91	-	1.34	0.26		1.53	0.15	0.19	III
8.16	9.84	-	1.17	0.16	4	1.31	0. 08	0.14	III
8.30	8.40	-	0.67	0.20	8	-	-		II
8.54	8.28	5.86	0.80	0.15	35	1.47	0.18		II
8.92	9.96	-	0.76	0.20	6	1.50	0.21	0.47	II
9.39	10.96	6.02	0.90	0.12	18	1.50	0.14	0.60	II
9.93	10.55	-	0.65	0.25	55	1.28	0.18	0.75	II
10.43	8.07	-	0.94	0.08	9	-	-		II
11.17	6.83	-	0.73	0.20		-	-		I
11.62	8.51	6.68	0.61	0.19	22	-	-	-	I
12.36	6.52	-	0.81	0.22	12	1.10	0.21	0.28	III
13.53	4.70	6.07	0.66	0.09	-	-	-		I
14.43	3.90	5.93	0.49	0.21	81	1.21	0.20	0.72	I
15.05	3.53	4.53	0.49	0.28	17	-	-		I
16.23	5.28	6.98	0.25	0.10		-	-		I
17.33	7.63	-	0.51	0.12	28	-	-		I
17.62	5.89	6.30	0.16	0.23	209	1.08	0.16	0.91	I

4. Discussion

4.1 Differences in biogeochemical regimes along the modern shelf

The characteristic year-round upwelling and high PP off Peru (Pennington et a., 2006) are generally contrasted by low PP at open-ocean areas further offshore and in the equatorial upwelling region in the North. The latter regions receive significantly less nutrients from subsurface waters due to absent or weak upwelling of subsurface waters are generally limited in Fe due to low contributions from atmospheric dust. As such, the open ocean and the equatorial upwelling systems are described as High-Nitrate-Low-Chlorophyll (HNLC) areas, where PP is thought to be co-limited by $Si(OH)_4$ and iron supply (Dugdale et al., 1995; Hutchins et al., 2002). Overall, the differences in upwelling intensity and PP between the shelf and these HNLC areas is indicated by the distribution of annually averaged Chlorophyll a concentrations and Sea Surface Temperatures (Fig.1 a and b). Furthermore, along the shelf upwelling intensity increases from North to South (SST decreases, respectively) and PP is highest within 100km from the coast (highest Chl a). At the shelf PP is generally not limited by Fe, which is released under oxygen-deficient bottom-water conditions from upper shelf sediments (<600m; Hutchins and Bruland, 1998; Johnson et al., 1999; Bruland et al., 2005; Noffke et al., 2012) and upwelled waters become enriched in iron through interaction with bottom sediments. Therefore, the shelf width has a major influence on iron supply with higher Fe concentrations supplied from a wider shelf and low concentrations where the shelf is narrow (Johnson et al., 1999; Hutchins et al., 2001; Bruland et al., 2005). However, it has to be noted that sulphidic conditions at the shallow shelf can lead to a retention of iron in the sediments (Scholz et al., 2014).

Overall, we assume that Fe supply is high at the wide northern and central Peruvian shelf (5-14°S), but low at the narrow shelf area south of 15°S and in partly at the shallow shelf between 10 and 14°S (sulphidic conditions) following previous observations and model studies (Bruland et al., 2005; Franz et al., 2012; Scholz et al., 2014; Messié and Chavez, 2014). Accordingly, we can distinguish between the HNLC area (offshore and North) and the high PP shelf area, which can be further divided into: regime I – 5-10°S, moderate upwelling of nutrients and high Fe supply from the wide shelf; regime II – 10-14°S, strong upwelling and PP, high Fe from the wide shelf, but potentially effected by sulphidic conditions; regime III – 15°S, strong upwelling but low Fe supply from the narrow shelf.

The subdivision into HNLC, regime I, II and III is clearly reflected by the distribution of surface sediment $bSiO_2$ values and Si:C ratios, with <10%

Published in Geochimica Cosmochimica Acta 177 (2016), 30-47

$bSiO_2$ and Si:C = 1 in regime I, >10% $bSiO_2$ and variable Si:C of 1-3 in regime II and 15-20% $bSiO_2$ and Si:C = 3 in regime III. Based on this subdivision we will discuss the implications of the distribution of the different proxies within the surface sediment in the following sections.

4.1.1 Relationship between $\delta^{30}Si_{bSiO2}$ and $\delta^{30}Si_{Coscino}$ in core-top sediments

The HNLC condition in the northern area should be reflected by relatively high $Si(OH)_4$ utilisation and consequently high $\delta^{30}Si$ values, but only $\delta^{30}Si_{Coscino}$ signatures are observed to be high (mean: +1.6‰) while $\delta^{30}Si_{bSiO2}$ are low (mean: +0.6‰) (Fig.1d). Towards the South along the shelf the $\delta^{30}Si_{Coscino}$ signatures remain high while the $\delta^{30}Si_{bSiO2}$ signatures increase from +0.7‰ to +1.1‰. Consequently, the Δ values decrease from 0.7‰ to 0.3‰ (averaged values; Fig.1d; Table 1), which suggests increased Si utilisation concomitant with an intensification of upwelling conditions. However, with increasing upwelling intensity one would generally expect lower $\delta^{30}Si_{bSiO2}$ values and less complete Si utilisation in the southern part of the upwelling area, due to the continuous re-supply of unfractionated subsurface nutrients to surface waters. Conversely, $\delta^{30}Si_{Coscino}$ signatures show little variations and are all close to +1.5‰, reflecting near-complete Si utilisation (i.e. the diatom isotopic composition is close to that of the subsurface water/PCUC or source water value of +1.5‰ assuming steady-state/open system conditions; Fig. 1d; Table 1). In agreement with Ehlert et al., (2012), we suggest that the seasonal changes and succession of the diatom assemblages may have a major influence on the $\delta^{30}Si_{bSiO2}$ values.

Comparison of our $\delta^{30}Si$ signatures and Δ values with previously reported surface sediment diatom assemblages (Schuette, 1980) shows that the near-shore area between 10 and 15°S, where high $\delta^{30}Si_{bSiO2}$ (up to +1.1‰) prevail, is dominated by Chaetoceros RS and T. nitzschioides (upwelling-related species), associated with low abundances of non-upwelling species. In contrast, between 5 and 10°S, further away from the coast, moderate $\delta^{30}Si_{bSiO2}$ values (+0.7‰) are linked to increased percentages of non-upwelling species over upwelling-related species. Thus, the southward decrease in Δ coincides with a shift in diatom assemblages from low percentages of upwelling-related diatoms (regime I= high Δ), via moderate percentages (regime II= moderate Δ), to high percentages of upwelling-related diatoms associated with decreased contribution of non-upwelling diatoms (regime III= low Δ).

Changes in hydrography can lead to significant seasonal variations of both dissolved $\delta^{30}Si_{Si(OH)4}$ and particulate $\delta^{30}Si_{bSiO2}$ signatures, as observed for example in the South China Sea (Cao et al., 2012). Thus, the changes in Δ concomitant with a shift in the diatom assemblage are likely caused by seasonality and environmental conditions (i.e. upwelling strength, nutrient availability) within the three regimes (I, II and III). To better understand this linkage we will have a

Table 3: Downcore abundance of diatom species and groups over time for core M77/2-003-2 as well as the calculated values for e_{ass} (see text for details). *Chaet.* = *Chaetoceros* spp.; *Skel.* = *Skeletonema costatum*; *O-C*= *Others* (%) - *Chaetoceros* spp. (%); Total upwell. = The cumulative abundance off all upwelling related diatom species in %.; Non-Upwelling = 100% - Total Upwell. (%).

Age (ka)	Abundance Valves x 10^6	*Chaet* (%)	*Skel.* (%)	O - C (%)	ε_{ass}	Upwell. (%)	Non-Upwell. (%)
0.38	24	45	5	55	**-1.55**	**61**	**39**
0.63	77	51	3	49	**-1.60**	**61**	**39**
0.87	114	62	5	38	**-1.71**	**78**	**22**
1.12	115	50	15	50	**-1.59**	**76**	**24**
1.35	131	49	12	51	**-1.59**	**74**	**26**
1.57	303	56	14	44	**-1.66**	**76**	**24**
1.76	201	46	31	54	**-1.56**	**80**	**20**
1.92	152	48	10	52	**-1.58**	**62**	**38**
2.08	303	46	22	54	**-1.56**	**69**	**31**
2.36	94	63	5	37	**-1.72**	**76**	**24**
2.62	42	60	2	40	**-1.70**	**72**	**28**
2.88	55	40	4	60	**-1.49**	**62**	**38**
3.41	39	56	7	44	**-1.66**	**74**	**26**
3.66	86	60	9	40	**-1.70**	**76**	**24**
3.87	49	44	4	56	**-1.54**	**59**	**41**
4.06	91	54	9	46	**-1.63**	**67**	**33**
4.26	179	50	13	50	**-1.59**	**68**	**32**
4.47	208	53	21	47	**-1.63**	**81**	**19**
4.69	189	38	25	62	**-1.48**	**69**	**31**
4.93	177	19	45	81	**-1.29**	**74**	**26**
5.18	65	48	12	52	**-1.58**	**62**	**38**
5.38	213	53	24	47	**-1.62**	**79**	**21**
5.52	119	48	16	52	**-1.57**	**69**	**31**
5.68	216	27	52	73	**-1.36**	**80**	**20**
5.92	30	47	9	53	**-1.56**	**64**	**36**
6.22	157	37	24	63	**-1.46**	**65**	**35**
6.56	98	42	14	58	**-1.52**	**64**	**36**
6.91	94	50	19	50	**-1.59**	**75**	**25**
7.27	34	40	7	60	**-1.49**	**63**	**37**
7.63	45	43	18	57	**-1.53**	**71**	**29**
7.99	332	26	39	74	**-1.36**	**76**	**24**
8.33	61	47	22	53	**-1.56**	**78**	**22**
8.65	37	40	20	60	**-1.50**	**74**	**26**
8.95	90	43	12	57	**-1.53**	**68**	**32**
9.22	124	47	12	53	**-1.56**	**73**	**27**
9.47	70	40	14	60	**-1.50**	**74**	**26**
9.71	821	18	64	82	**-1.27**	**86**	**14**
9.95	119	22	33	78	**-1.32**	**75**	**25**
10.20	40	55	12	45	**-1.64**	**68**	**32**
10.45	71	60	3	40	**-1.70**	**65**	**35**
10.74	77	68	0	32	**-1.78**	**72**	**28**
11.04	67	46	0	54	**-1.56**	**54**	**46**
11.38	34	35	0	65	**-1.44**	**48**	**52**
11.76	90	34	0.3	66	**-1.44**	**55**	**45**
12.18	83	56	0.7	44	**-1.66**	**62**	**38**
12.65	184	75	0.0	25	**-1.84**	**76**	**24**
13.17	177	73	0.3	27	**-1.82**	**73**	**27**
13.75	94	69	1	31	**-1.78**	**71**	**29**
14.35	17	44	0.4	56	**-1.54**	**47**	**53**
14.97	26	50	0	50	**-1.59**	**52**	**48**
15.57	47	51	1	49	**-1.60**	**53**	**47**
16.16	40	46	0	54	**-1.56**	**48**	**52**
16.69	89	34	0	66	**-1.44**	**36**	**64**
17.17	27	34	0	66	**-1.44**	**38**	**62**
17.56	92	69	0	31	**-1.79**	**71**	**29**

Published in Geochimica Cosmochimica Acta 177 (2016), 30-47

more detailed look at the seasonal diatom succession stages under present-day upwelling and non-upwelling conditions in the following section.

4.1.2 The seasonal effect on diatom assemblages and consequences for the $\delta^{30}Si$ signal

During seasonally weaker upwelling of nutrients, upwelling-related diatom species are reduced to low contributions of *T. nitzschioides* and *Chaetoceros* spp. (Rojas de Mendiola, 1981), whereas coastal planktonic species dominate, reflecting non-upwelling (more stratified) conditions and an advanced succession stage. In contrast, the enhanced upwelling of nutrients during spring and fall causes intense blooms of *Chaetoceros* spp., *S. costatum* or *T. nitzschioides* (Rojas de Mendiola, 1981), small opportunistic diatom species (i.e. upwelling-related diatoms). As on-going nutrient consumption occurs during phases of relaxation, even under strong upwelling conditions, the initial bloom of upwelling-related diatoms will be followed by the emergence of coastal planktonic diatom species, as well as the formation of resting spores (RS). Overall, aged surface waters depleted in nutrients favour large centric diatom species (coastal planktonic species; *Coscinodiscus* spp.) with low growth rates. As these large centric diatoms represent a later succession stage in the evolution of blooms and already more stratified waters (Tarazona et al., 2003) they are representative of weaker upwelling, higher nutrient utilisation and thus reveal higher $\delta^{30}Si$ values.

The question arises, if and how the $\delta^{30}Si_{bSiO2}$ surface sediment record reflects these seasonal differences in PP upwelling intensity and diatom assemblages. The water column $\delta^{30}Si_{Si(OH)4}$ during summer presented by Ehlert et al., (2012) indicated high PP but low $Si(OH)_4$ utilisation between 10°S and 15°S, where active upwelling and re-supply of nutrients occurred. However, the corresponding $\delta^{30}Si_{bSiO2}$ in surface sediments from this area are highest (+1.1‰) indicating higher than the observed Si utilisation in the present-day water column. Therefore, either the available water column data only reflect a snapshot of the seasonal upwelling variability and $\delta^{30}Si_{bSiO2}$ signatures may increase further with proceeding diatom productivity, or the $\delta^{30}Si_{bSiO2}$ is biased by the diatom assemblage within the 11-32 µm fraction. *T. nitzschioides* and *Chaetoceros* spp. (and *S. costatum*) are preferentially removed from the samples measured for $\delta^{30}Si_{bSiO2}$ during sample preparation (see *2.2 Methods* and *Results 3.2*). Hence, this small fraction mainly consists of *Chaetoceros* RS and small coastal planktonic diatoms. The resulting $\delta^{30}Si_{bSiO2}$ signatures may lack a significant part of the diatom assemblage containing low isotopic values belonging to the early succession stage (initial upwelling) and rather reflect higher $\delta^{30}Si_{bSiO2}$ signatures from small coastal planktonic species included in more advanced stages of the succession (Fig. 3b and c). Furthermore, the formation of RS with progressive nutrient depletion, which should hence record higher $\delta^{30}Si_{bSiO2}$ values, and subsequent re-seeding by upwelling, could also

increase the initial $\delta^{30}Si_{bSiO2}$ signal. Overall, this strong upwelling scenario best explains the conditions at 10-15°S (regime II and III; Fig 3b and c), which is characterised by most intense upwelling conditions consistent with the observed diatom assemblages in the underlying sediments.

In contrast, at the wide shelf area between 5°S and 10°S, moderate mean $\delta^{30}Si_{bSiO2}$ values (+0.7‰) relate to increased percentages of non-upwelling diatom species and reduced contribution of upwelling-related species. As these samples are outside the influence of near-shore coastal upwelling and thus do not comprise intense blooms of upwelling-related species, they should reflect overall weaker upwelling or summer conditions. Low contributions of *Chaetoceros* spp. and *T. nitzschioides* mark a minor initial diatom succession/bloom prior to the appearance of small coastal planktonic diatoms. Thus, nutrient utilisation and Si isotope fractionation are lower when these small coastal planktonic diatoms bloom. This results in the observed lower $\delta^{30}Si_{bSiO2}$ values of the small diatom fraction in comparison to upwelling induced blooms and in a higher difference (Δ) between small and large centric (coastal) diatoms (Fig. 3a).

Accordingly, we propose that (1): The $\delta^{30}Si_{bSiO2}$ values are highest between 10 and 15°S because the upwelling of nutrient-rich waters results in more pronounced blooming events and re-seeding of RS (low Δ; regime II and III); (2): Where weak upwelling prevails (seasonal or regional) $\delta^{30}Si_{bSiO2}$ values are lower because the lack of intense bloom events lowers the Si fractionation of the small diatom fraction (high Δ; regime I); (3): The $\delta^{30}Si_{Coscino}$ signatures record high Si utilisation either during summer or under stratified conditions of the advanced succession stage of upwelling blooms. Unfortunately, there is to date no further seasonally resolved dissolved $\delta^{30}Si_{Si(OH)4}$ or diatom ($\delta^{30}Si_{Coscino}$ and $\delta^{30}Si_{bSiO2}$) data allowing the investigation of an entire production cycle to test the hypothetical scenarios 1, 2 and 3 described above. Nevertheless, to reconstruct past conditions off Peru we will apply the observed three scenarios (1,2 and 3, respectively) for determining upwelling strength and nutrient availability from the downcore record at 15°S, covering the last 17,700 years in the following section.

Although the observed relationship of strong upwelling and high nutrient supply with highest $\delta^{30}Si_{bSiO2}$ values that indicate high utilisation is generally counterintuitive a similar relationship has been reported previously in the Gulf of California Coastal Upwelling system (GoC; Pichevin et al., 2014). In contrast to the Peruvian Coastal Upwelling system upwelling conditions and relaxation at the GoC show a strong seasonality and large diatoms such as *Coscinodiscus* spp. are reported to adapt to more stratified condition often thriving in a deep chlorophyll maximum. Although such conditions should also lead to high Si utilisation and high $\delta^{30}Si_{Coscino}$ values isotopic signatures will ultimately be influenced by the source water signatures ($\delta^{30}Si_{SiOH4}$). Therefore, we suggest that Δ values in other regions may differ from our observation. However as long as $\delta^{30}Si_{bSiO2}$ mirrors upwelling conditions and $\delta^{30}Si_{Coscino}$ relaxation as well as near

complete $Si(OH)_4$ utilisation, Δ values should still reflect variations in upwelling conditions.

4.1.3 Effects of upwelling intensity and nutrient limitation on the surface sediment $\delta^{30}Si_{bSiO2}$ record

The availability of nutrients in the surface waters ultimately regulates PP ultimately influencing nutrient utilisation and the diatom species assemblages. NO_3^- or PO_4 limitation is generally not observed off Peru, instead $Si(OH)_4$ limitation has been widely suggested to limit PP off Peru (Dugdale et al., 2002; Franz et a., 2012). A possible mechanism that leads to preferential $Si(OH)_4$ uptake over NO_3^- (and carbon (C)) is iron limitation leading to increased Si:N (and Si:C) ratios (Hutchins and Bruland, 1998; Takeda, 1998; De La Rocha et al., 2000; Hutchins et al., 2002; Sarthou et al., 2005). Thus, under Fe deficient conditions diatoms increase frustule thickness leading to higher gravitational export but decrease the internal organic matter content. However, species effects can also lead to less silicified and organic-rich diatom frustules.

The reduced Fe availability concomitant with intense upwelling conditions support the observations of Pichevin et al., (2014) that with ongoing PP and nutrient consumption during upwelling blooms Fe becomes limiting leading to a high uptake of Si relative to nitrate and carbon thereby enhancing the Si burial due to frustule thickening. Accordingly, global Si:C ratios of settling particles between 1 and 10 are found in areas of high Si fluxes (Southern Ocean, North Pacific and equatorial Pacific; after Pichevin et al., 2014). Therefore, we conclude that the high Si:C ratios in the surface sediments of Northern Peru and at the southern shelf close to the coast between 10 and 15°S indicate iron limitation in these areas. However, while the HNLC is generally characterised by co-limitation of Si and Fe, the shelf area rather indicates transient Fe deficiency during enhanced upwelling. This means that initial macro- and micronutrient conditions are ideal for diatom blooms, but with on-going nutrient consumption Fe stress leads to frustule thickness and high Si:C ratios. This observation adds to our conclusions that $\delta^{30}Si_{bSiO2}$ signatures are higher where upwelling is most intense. Accordingly, the high $\delta^{30}Si_{bSiO2}$ values observed in regime II and III could in part be induced by the transient Fe limitation increasing the $Si(OH)_4$ utilisation via frustule thickening towards the end of upwelling blooms. However, so far a detailed study comparing nutrient ratios in surface waters with that of particulate organic matter is missing off Peru. Therefore, we suggest that Fe stress might influence $\delta^{30}Si_{bSiO2}$ but is not the major mechanism to explain our observations.

4.2 Reconstruction of past conditions

4.2.1 Combining silicic acid utilisation and diatom assemblages

As shown above the present-day shelf region off Peru is characterized by variations in the timing and duration of blooming events induced by the upwelling of nutrient-rich waters. We now want to apply the changes in diatom assemblages and Si isotope compositions, which are directly related to these different environmental conditions to reconstruct nutrient utilisation and upwelling intensity on longer timescales. We find that downcore AR_{bSiO2}, Si:C ratios, $\delta^{30}Si_{bSiO2}$ and $\delta^{30}Si_{Coscino}$ isotope data as well as diatom assemblages exhibit a pronounced shift between the deglaciation and the Holocene and that the isotopic offset (Δ) has been a persistent feature off Peru, at least during the past 17,700 years (Table 2).

During the deglaciation the low AR_{bSiO2} and total diatom abundances reflect decreased PP. According to low $\delta^{30}Si_{bSiO2}$ and Si:C this indicates enhanced iron deficiency with concomitant reduced Si utilisation. Similar low $\delta^{30}Si_{bSiO2}$ values were also measured in core SO147-106KL from 12°S (Fig. 2d; Ehlert et al., 2013). The diatom assemblages from our core 003-2 indicate a modest contribution of upwelling-related diatoms (Mean: 50±20 %), while relative abundances of coastal planktonic (non-upwelling species) are elevated (Mean: 20±10%; Fig.2 a, b), further confirming diminished upwelling intensity. Hence, weaker upwelling likely caused low diatom PP due to decreased nutrient supply to the photic zone, similar to present-day conditions between 5°S and 10°S. This is confirmed by high Δ values of +0.8±0.1‰ close to the offset reported for regime I (Δ=0.8‰). However, the deglacial $\delta^{30}Si_{Coscino}$ signatures remained considerably lower than modern values at +1.1‰, although Si:C are increased indicating iron limitation. As observed within modern surface sediments when iron is limiting either PP is low associated with low $\delta^{30}Si_{bSiO2}$ and high $\delta^{30}Si_{Coscino}$ values (HNLC area), or PP is intense with high $\delta^{30}Si_{bSiO2}$ and prolonged iron limitation associated with coastal upwelling blooms. At least for parts of the deglaciation reduced iron export was reported from 11°S due to poorer oxygenations (Scholz et al., 2014). The simultaneously low $\delta^{30}Si_{Coscino}$ values which should increase under both iron limitation and low silicate availability indicate either a change towards an isotopically lighter signal from the source waters, or a limitation of nutrients other than $Si(OH)_4$, such as NO_3^-, causing less complete $Si(OH)_4$ utilisation of source waters. The latter is supported by increased $\delta^{15}N$ values reported for the deglaciation off Peru due to increased denitrification under less oxygenated conditions, as well as more complete NO_3^- utilisation (Higginson, 2004; Scholz et al., 2014). Furthermore, RS formation of *Chaetoceros* spp. seems to be especially linked to nitrate limitation (Garrison, 1981; Oku and Kamatani, 1997). Thus, the high abundance of RS during the deglaciation could have been promoted by NO_3^- limitation.

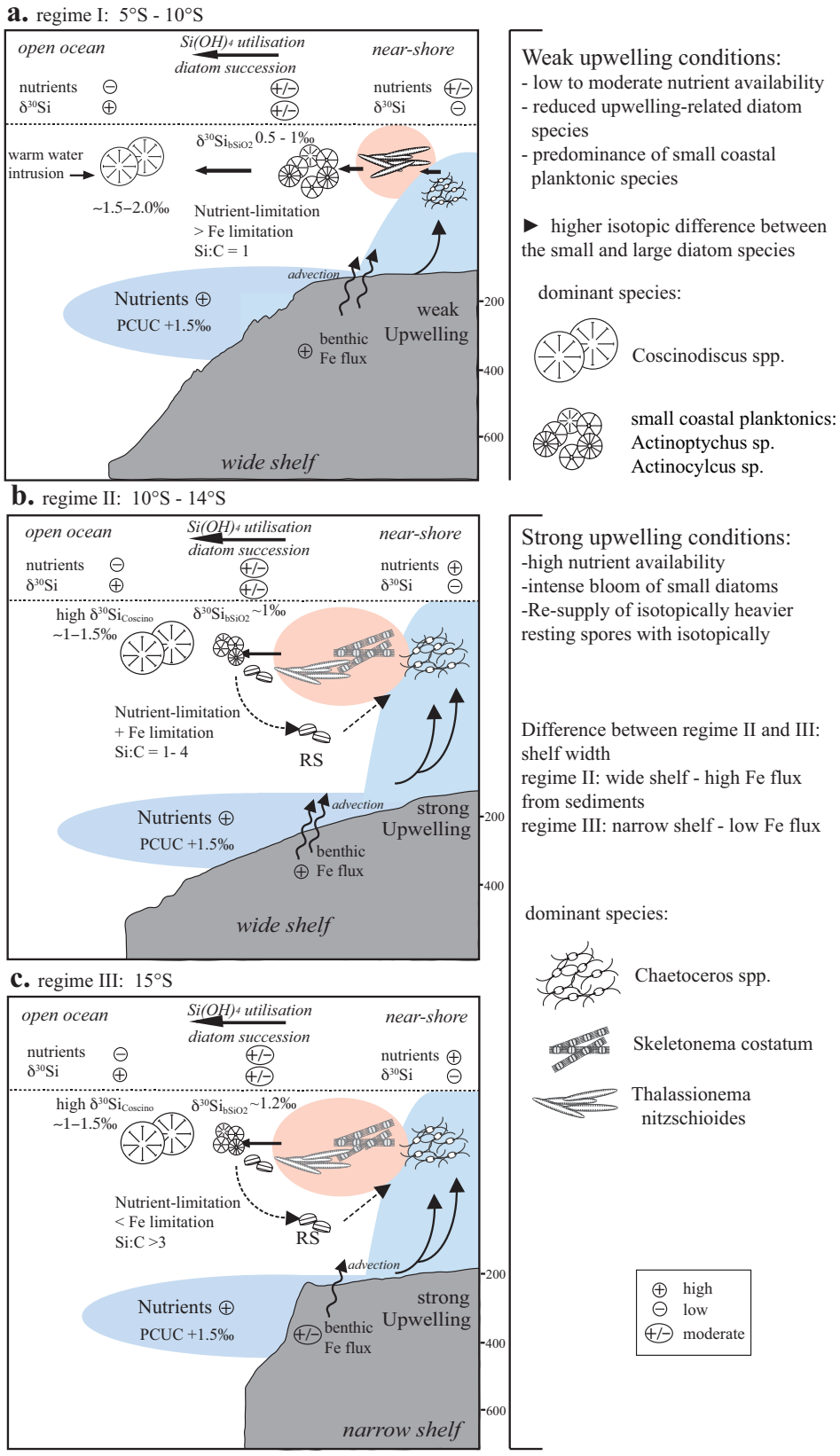

Figure 3: Schematic model showing seasonal or interannual diatom productivity for: a. regime I (5-10°S): weak upwelling conditions nutrient > iron limitation; b. regime II (10-14°S): strong upwelling conditions with nutrient > iron limitation; c. regime III (15°S): strong upwelling conditions with iron > nutrient limitation

At the transition from the deglaciation to the Early Holocene (11 to 8 ka BP) higher AR_{bSiO2} values and total diatom abundance are linked to a marked increase in the relative abundance of upwelling-related diatom species indicating greater upwelling intensity compared to the deglaciation. Interestingly, the $\delta^{30}Si_{bSiO2}$ record remained stable at moderate values (+0.8‰) while the $\delta^{30}Si_{Coscino}$ signature increased to +1.4‰, resulting in Δ values >0.6‰. In contrast, the record of SO147-106KL shows higher variability and shifts between high (+1.1‰) and low (+0.4‰) $\delta^{30}Si_{bSiO2}$ values (Fig. 2d). Thus, core 003-2 generally demonstrates a shift towards stronger upwelling conditions (regime II), but most likely the pronounced upwelling intensification at 10 ka BP is missing in the $\delta^{30}Si_{bSiO2}$ record as no sample was taken exactly for this time. In contrast, core SO147-106KL further to the North shows high variability with shifts between conditions of weakened (regime I) and periodically higher upwelling intensity and Si utilisation (regime II). These highly dynamic changes may have been induced by alternation of enhanced La Niña and El Niño-like conditions (Ehlert et al., 2013).

During the Mid to Late Holocene the variability of $\delta^{30}Si$, AR_{Corg} and diatom abundances are higher, reflecting periods of enhanced PP and $Si(OH)_4$ utilisation. This is especially true for three periods of enhanced AR_{Corg} values at 8.2-7.9 ka and 5.2-4.1 ka BP with peak values of Si:C and $\delta^{30}Si_{bSiO2}$. Simultaneously, the amount of *Chaetoceros* (RS) shows a marked decrease, while *S. costatum* often dominated the diatom assemblage (Fig.2 b). Such a dominance of *S. costatum* over *Chaetoceros* spp. within the diatom assemblage is commonly observed today at our study site during fall (Rojas de Mendiola, 1981) indicating a shift to intensified fall diatom blooms. This *S. costatum* dominance is linked to low Δ values (<0.3‰), thus supporting strong upwelling conditions and intense PP (regime III). In between the peak PP values, AR_{Corg} and diatom abundances indicate reduced PP in combination with weaker upwelling as shown by lower $\delta^{30}Si_{bSiO2}$ (+0.8‰) and higher Δ values (+0.3‰ to +0.6‰). Thus, the Holocene was characterised by generally intensified upwelling conditions in comparison to the deglaciation at our core location, Mid to Late Holocene conditions varied between moderate and high nutrient concentrations similar to those measured in the present-day centre of the upwelling area (regimes II and III; 10-15°S).

Overall the shift we observe in the $\delta^{30}Si_{bSiO2}$ and $\delta^{30}Si_{Cosino}$ records between the deglaciation and the Holocene highlights the transition from low to intensified $Si(OH)_4$ utilisation, as well as the intensification of upwelling conditions. This shift was associated with diatom assemblages that reflect a short upwelling season (deglaciation) to an assemblage indicative of a prolonged blooming season and more intense upwelling (Holocene). Thus, our findings from core-top sediments, showing that a smaller Δ is associated with more intense upwelling and stronger Si utilisation as well as iron limitation can be applied to the paleo record, demonstrating that the observed switch from high Δ

during the deglaciation to low Δ values during the Holocene is consistent with a shift from weak to enhanced upwelling conditions.

4.3 The influence of varying diatom assemblages on the $\delta^{30}Si$ record

Environmental conditions, such as upwelling intensity and nutrient availability, alter the amount of Si utilisation and thus the Si isotope composition of diatoms by regulating the diatom succession, the duration of blooming events, and the initiation of nutrient depletion. However, a bias on the Si isotope composition in biogenic silica may arise by the species-specific Si isotope fractionation factors of different diatom species. A crucial assumption for the paleo reconstructions of nutrient utilisation and PP based on $\delta^{30}Si$ has so far been that the isotopic enrichment factor during the incorporation of silicon in diatoms is species independent (De La Rocha et al., 1997). The recent study by Sutton et al., (2013) suggested species-dependent fractionation factors between -0.5 to -2.1‰, thus highlighting that changes in diatom assemblages could cause significant variability in $\delta^{30}Si$ records without changes in nutrient utilisation. Therefore, we will follow the approach of Sutton et al., (2013) and estimate the influence of the taxonomic composition on past $\delta^{30}Si$ records that considers the relative diatom species abundance as well as their specific isotope enrichment factor $^{30}\varepsilon$.

So far mainly polar or sub-polar diatom species have been studied regarding their fractionation factors, but isotope fractionation factors obtained from culturing studies can be found for Chaetoceros brevis, S. costatum and for various subgenera of Thalassiosira, roughly matching the species prevailing off Peru (De La Rocha et al., 1997; Sutton et al., 2013). Although, the $^{30}\varepsilon$ factors reported for S. costatum and Thalassiosira sp. range from -0.4 to -1.2‰ and from -0.4 to -1.8‰, respectively, the corresponding mean values of -1.1‰ are similar to the mean enrichment factor previously assumed for all diatom species (De La Rocha et al., 1997). Only for Chaetoceros brevis a significantly larger enrichment factor of $^{30}\varepsilon$ = -2.09‰ was reported. Thus, we test the potential influence of the different enrichment factors on our downcore record of core 003-2 by applying the model calculation adapted from Sutton et al., (2013). To calculate the variability in $^{30}\varepsilon$ caused by changes in the diatom assemblage (ε_{ass}, hereafter), we used the following equation:

$$\varepsilon_{ass} = \left((C/100 \times (-2.09\,‰)\right) + ((O/100 \times (-1.1‰)) \quad (1)$$

where *C* and *O* are the abundances of *Chaetoceros* spp. (RS) and *other* diatom species, respectively (Table 3, columns 3 and 4). For *Chaetoceros* spp. we applied a $^{30}\varepsilon$ value of -2.09‰ from *Chaetoceros brevis* (Sutton et al., 2013) and -1.1‰ (De La Rocha et al., 1997) was used as a mean value for the *other* diatom species. Like Sutton et al. (2013) we assume that the *Chaetoceros* spp. (RS) have the same enrichment factor as vegetative cells due to the lack of isotopic measurements of the RS themselves. So far little is known what controls the Si isotope fractionation within diatoms, but growth and uptake rates are generally

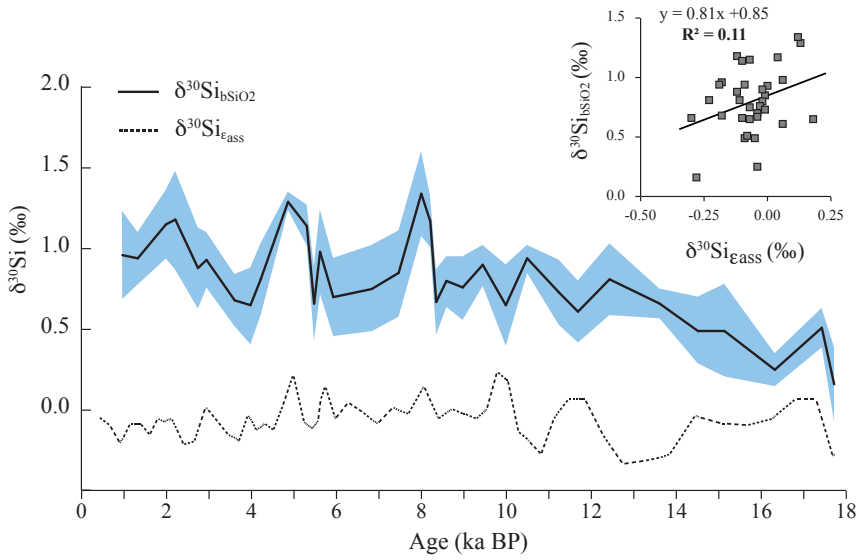

Figure 4: Comparison of $\delta^{30}Si_{bSiO2}$ (‰) record (thin black line with uncertainties indicated by blue shaded area) with model estimations for $\delta^{30}Si_{\varepsilon ass}$ (black dotted line). Left: steady state model assumptions with ε_{ass} based on Chaetoceros RS abundance (black thick line). Right: $\delta^{30}Si_{\varepsilon ass}$ versus $\delta^{30}Si_{bSiO2}$ (R^2 = 0.11, negative correlation). (For interpretation of the references to colour in this figure legend, the reader is referred to the web version of this article.)

associated with $Si(OH)_4$ availability (Sarthou et al., 2005). Thus, Hendry et al., (2010) speculated that, based on a similar observation for sponge spicule formation, if the fractionation process occurs at the site of Si uptake a higher uptake rate may lead to higher fractionation. Although RS are formed under nutrient deplete conditions growth rates are reported to be similar to the ones of the vegetative cells (Oku and Kamatani, 1997), potentially resulting in a similar isotope fractionation.

Based on equation (1) ε_{ass} will have values between -1.1‰ and -2.09‰. High values close to -1.1‰ relate to low amounts of RS and ε_{ass} will decrease towards -2.09‰ when RS amounts increase. The calculated ε_{ass} values range between -1.27‰ and -1.84‰ for the entire core (Tab. 3, column 6). To assess the effect on the $\delta^{30}Si_{bSiO2}$ signature in the core we applied the calculated ε_{ass} using following equation (Fry, 2006; Sutton et al., 2013):

$$\delta^{30}Si_{\varepsilon ass} = \delta^{30}Si_{Si(OH)4\ source} + {}^{30}\varepsilon_{ass} \quad (2)$$

where $\delta^{30}Si_{\varepsilon ass}$ is the isotopic composition of accumulated biogenic silica (mixed small diatoms) and $\delta^{30}Si_{Si(OH)4\ source}$ reflects the source water. The $\delta^{30}Si_{Si(OH)4\ source}$ was set to +1.5‰, ($\delta^{30}Si_{SiOH4}$ of the PCUC; Ehlert et al., 2012). In contrast to Sutton et al. (2013) we did not use a mixed layer value for $\delta^{30}Si_{Si(OH)4\ source}$, as we want to evaluate the potential species-specific effect independent from any influence of utilisation (the mean ($\delta^{30}Si_{SiOH4}$ mixed layer value would be +2‰). Obviously by neglecting the amount of utilisation the estimated $\delta^{30}Si_{\varepsilon ass}$ signatures are lower than the equivalent $\delta^{30}Si_{bSiO2}$ values.

Published in Geochimica Cosmochimica Acta 177 (2016), 30-47

The resulting values for $\delta^{30}Si_{\varepsilon_{ass}}$ are shown in comparison to measured $\delta^{30}Si_{bSiO2}$ values (Fig. 5). These results show that the amount of RS cannot explain the high variability observed in the measured $\delta^{30}Si_{bSiO2}$ record, as there is essentially no correlation between modelled $\delta^{30}Si_{\varepsilon_{ass}}$ and measured $\delta^{30}Si_{bSiO2}$ (R^2= 0.11). As we only included the specific $^{30}\varepsilon$ for *Chaetoceros brevis* (for *S. costatum* and *Thalassiosira* sp. mean value is = -1.1 ‰ included in *O*, respectively; De La Rocha et al., 1997) in our calculation, the knowledge of additional enrichment factors of other diatom species may help to deconvolve the effect of species composition observed in this study. It would be especially interesting to see if growth rates and $Si(OH)_4$ availability control the isotope fractionation, as the observed high $\delta^{30}Si_{bSiO2}$ values associated with high growth rates and $Si(OH)_4$ concentrations during intense upwelling could be further influenced by higher isotope fractionation. The minor impact of a species-dependent fractionation on $\delta^{30}Si_{bSiO2}$ suggests that the variability of $Si(OH)_4$ utilisation in the surface waters controlled by to environmental changes has the strongest effect on both the dissolved and particulate $\delta^{30}Si$ signal.

5. Conclusions

In this study we combine for the first time surface sediment mixed-species $\delta^{30}Si_{bSiO2}$ and mono-generic $\delta^{30}Si_{Coscino}$ (i.e. *Coscinodiscus* spp.) signatures with diatom assemblages to determine present and past silicate utilisation and upwelling intensity in the Peruvian upwelling region. We find a pronounced environmental control by upwelling intensity and nutrient availability on all applied proxies. Changes in the abundance of upwelling-related diatom species versus non-upwelling diatom species reflect the strength of near-shore upwelling, whereas $\delta^{30}Si_{bSiO2}$ signatures represented the small diatom fraction change in relation to Si utilisation, iron limitation and diatom succession stages.

Based on our results the modern Peruvian shelf can be subdivided into distinct regimes: Regime II and III denote strong upwelling reflected by intense blooms of small rapidly growing diatom species followed by the production of larger centric diatoms and the formation of resting spores (RS) as nutrient and iron depletion in surface waters proceeds. Due to the fractional loss of the smaller diatoms, the measured 11-32 µm fraction ($\delta^{30}Si_{bSiO2}$) lacks the initial diatom succession stage but concentrates isotopically heavier small coastal planktonic diatom species as well as RS, resulting in overall high $\delta^{30}Si_{bSiO2}$ values (+1.1‰) and a low offset between $\delta^{30}Si_{Coscino}$ and $\delta^{30}Si_{bSiO2}$ (Δ); In contrast regime I is characterised by weak upwelling conditions and by moderate nutrient and high iron availability accompanied by prolonged surface water stratification. This results in reduced contributions of upwelling-related diatom species but promote the dominance of coastal planktonic diatom species. After the initial diatom succession stage and intense blooming events are terminated Si

utilisation and isotope fractionation remain low until small coastal planktonic diatoms record the lower $\delta^{30}Si_{bSiO2}$ signal resulting in a higher Δ.

Downcore reconstructions of Core M77/2-003-2 show for the first time a persistent offset (Δ) combined with a marked shift from weak Deglacial to strong Holocene upwelling conditions. The comparison of the Si isotopic compositions with the reported diatom assemblage shows that the major shift in past Δ values was linked to an increase of upwelling-related diatom species during the Holocene. Consequently, variations in the past upwelling intensity and nutrient availability have been closely linked with the different regimes (I, II and II) observed today within the Peruvian upwelling area.

We conclude that during the vast interannual and seasonal changes in the intensity of the upwelling off Peru, the degree of silicate utilisation and the associated diatom assemblages have exerted the most important control on the $\delta^{30}Si$ record of the diatoms, whereas variable isotope enrichment factors of different diatom species have only had minor influence. Consequently, the combined use of diatom assemblages and $\delta^{30}Si$ signatures of different size fractions allows the reliable reconstruction of past silicate utilisation and upwelling intensity. Further improvements can be achieved by extended seasonal information from present day water column given that the $\delta^{30}Si_{bSiO2}$ may be biased by the fractional loss of important species.

Acknowledgements

This work is a contribution of the Collaborative Research Project 754 “Climate-Biogeochemistry interactions in the Tropical Ocean” (www.sfb754.de), which is supported by the Deutsche Forschungsgemeinschaft (DFG).

Appendix A. Supplementary data

Supplementary data associated with this article can be found, in the online version, at http://dx.doi.org/10.1016/ j.gca.2015.12.029.

Chapter II. Changes in diatom productivity and upwelling intensity off Peru since the Last Glacial Maximum: Response to basin-scale atmospheric and oceanic forcing

Kristin Doering[1,2*], Zeynep Erdem[2], Claudia Ehlert[3], Sophie Fleury[4], Martin Frank[2] and Ralph Schneider[1]

[1]Institute of Geosciences, University of Kiel, Ludewig-Meyn-Str. 10, 24118 Kiel, Germany
[2]GEOMAR Helmholtz Centre for Ocean Research Kiel, Wischhofstr. 1-3, 24148 Kiel, Germany
[3]Max Planck Research Group - Marine Isotope Geochemistry, Carl von Ossietzky University (ICBM), Carl-von Ossietzky-Str. 9-11, 26129 Oldenburg, Germany
[4]Department of Marine Science and Convergence Technology, Hanyang University ERICA campus, 55 Hanyangdaehak-ro, Sangnok-gu, Ansan-si, Gyeonggi-do 426-791, South Korea

under review with *Paleoceanography*

Key Points:

- Combined silicon isotope signatures and diatom assemblages trace export productivity and upwelling intensity
- Latitudinal shifts of Peruvian upwelling center mainly responded to movements of the SWW and ITCZ
- Compositions of upwelled subsurface waters off Peru not significantly influenced by changes in preformed nutrients

Abstract

We present new records of past accumulation rates of biogenic opal (AR_{bSi}), organic carbon (AR_{Corg}) and stable silicon isotope signatures ($\delta^{30}Si$) from the central (9°S) and northern (5°S) Peruvian margin covering the past 20,000 years. A new approach was used to reconstruct past upwelling intensity based on the difference between the $\delta^{30}Si$ signatures of small (11-32µm) and large (>150µm) diatom fractions ($\Delta^{30}Si_{coscino\text{-}bSi}$), in combination with the variance in diatom assemblages.

The combination of our records with two previously published records from the southern upwelling area (12-15°S) shows a general decoupling of the

environmental conditions on the central and southern shelf. A northward shift of the main upwelling cell from its modern position between 12°S and 15°S towards 9°S occurred during Termination 1. At this time only moderate upwelling and export productivity between 9°S and 12°S, due to the more northerly position of Southern Westerly Winds and the South Pacific Subtropical High. Furthermore, a marked decrease in export productivity between 12°S and 15°S during Heinrich Stadial 1 coincided with enhanced biogenic opal production in the Eastern Equatorial Pacific induced by a southward shift of the Intertropical Convergence zone and enhanced northeasterly trade winds. Modern conditions, with the main upwelling center and highest productivity between 12°S and 15°S were only established with the onset of the Holocene. Further estimation of the influence of past changes in preformed silica concentrations and $\delta^{30}Si$ signatures of subsurface waters reaching the Peruvian Upwelling System were shown to not strongly affect the $\delta^{30}Si$ records.

1. Introduction

The Eastern Equatorial Pacific (EEP) region hosts areas of pronounced biological productivity, the variability of which has been closely coupled with global climate and the carbon cycle [*Chavez and Barber*, 1987]. Highest productivity levels prevail within the Peru coastal upwelling system [*Berger and Herguera*, 1989; *Pennington et al.*, 2006], which is driven by year-round alongshore winds generating upwelling of nutrient-rich subsurface waters [e.g. *Chávez and Messié*, 2009]. Ultimately, the high productivity is regulated by the efficiency of wind-induced upwelling, which increases the nutrient flux to surface waters, the amount of nutrient utilization via iron fertilization originating from the shelf, nutrient concentrations in the subsurface waters and the depth of the thermocline [*Loubere*, 1999]. Modern and past variability of the system on seasonal and interannual timescales has been shown to be controlled by oceanographic and atmospheric circulation (e.g. the meridional shifts of the Intertropical Convergence Zone (ITCZ), the Walker and Hadley Circulation as well as El Niño-Southern Oscillation (ENSO) [*Barber and Chávez*, 1983; *Fiedler and Talley*, 2006; *Pennington et al.*, 2006]. Superimposed on this seasonal ocean-atmospheric cycle, interannual variability is generated by the ENSO [*Cane*, 2005], which is characterized by SST anomalies affecting the seasonal shifts of the ITCZ, whereby a southward shift of the ITCZ accompanies periods of increased SSTs in the eastern tropical Pacific, i.e. El Niño events [*Garreaud et al.*, 2009].

Paleoceanographic studies of the EEP system have suggested that millennial to glacial-interglacial scale variations were triggered by ocean-atmosphere interaction and orbital parameters controlling the position of the ITCZ as well

as by changes in the intensity of the Atlantic Meridional Overturning Circulation (AMOC), all of them affecting the atmospheric circulation in the EEP [*Timmermann et al.*, 2007; *Sifeddine et al.*, 2008; *Gutiérrez et al.*, 2009; *Kienast et al.*, 2013; *Dubois et al.*, 2014; *Salvatteci et al.*, 2014b]. Accordingly, at multi-centennial scales Northern Hemisphere cold periods (e.g. the Little Ice Age (LIA); 1400-1850 AD) the Peruvian Upwelling Ecosystem (PUE) was characterized by strongly diminished biological productivity and nutrient utilization associated with a deeper thermocline. This was paralleled by a weakened Walker Circulation and associated Trade Winds [*Sifeddine et al.*, 2008; *Gutiérrez et al.*, 2009; *Ehlert et al.*, 2015] as well as by higher precipitation caused by a southward shift of the ITCZ [*Gutiérrez et al.*, 2009; *Sachs et al.*, 2009]. In contrast, during warm periods (e.g. the Medieval Climate Anomaly; 900-1350 AD) productivity markedly increased, which was caused by enhanced Walker Circulation, more intense Trade Winds and a shallower thermocline in conjunction with a northerly position of the ITCZ and a strengthened South Pacific Subtropical High (SPSH) [*Gutiérrez et al.*, 2009; *Salvatteci et al.*, 2014b; *Ehlert et al.*, 2015].

The above factors are, however, difficult to distinguish and to reconstruct on longer millennial to orbital timescales and different reconstructions sometimes provide ambiguous results. Reconstructions of sea surface and subsurface temperatures (SST) from the equatorial Pacific have been applied to estimate the Walker circulation strength [*Kienast et al.*, 2013] and foraminifera-based stable isotope records ($\delta^{18}O$, $\delta^{13}C$; [*Spero et al.*, 2002; *Pena et al.*, 2008]) have been used to evaluate changes in subsurface water supply via 'ocean-tunneling' between the Southern Ocean and low-latitudes since the Last Glacial Maximum (LGM; 23-19 ka BP). These studies showed that during Heinrich Stadial 1 (HS1; 18-15 ka BP) the ITCZ moved southward in response to NH cooling and AMOC reduction causing enhanced regional upwelling in the EEP due to intensification of the Central American gap wind system (e.g. northeasterly trade winds; [*Timmermann et al.*, 2007; *Kienast et al.*, 2013; *Dubois et al.*, 2014]). At the same time there was an increase in the contribution of Southern Ocean sourced subsurface waters to the low latitudes (including the EEP) delivering higher amounts of dissolved silica ($Si(OH)_4$) and iron (Fe), which induced overall increased opal fluxes [*Kienast et al.*, 2006b; *Anderson et al.*, 2009; *Hendry and Brzezinski*, 2014]. There is, however, a conflicting interpretation for Termination 1 of a northward shift of the position of the ITCZ based on equatorial eolian dust analyses [*Xie and Marcantonio*, 2012; *bin Shaari et al.*, 2013], which have been suggested to result in the dominance of a La Niña–like mean state [*Pena et al.*, 2008; *Makou et al.*, 2010].

The changes described above should be directly reflected in marked variations in past upwelling intensity, diatom productivity and thus nutrient utilization off Peru but there are not many detailed records available [*De Vries and Schrader*, 1981; *Schrader and Sorknes*, 1991; *Schrader*, 1992]. This hampers

the understanding of the response of the PUE to changes in atmospheric and ocean circulation during the transition from the last glacial to the Holocene. Today, the high nutrient availability in the coastal area off Peru promotes a phytoplankton community that is dominated by diatoms [*Blasco*, 1971; *Estrada and Blasco*, 1985; *Bruland et al.*, 2005; *DiTullio et al.*, 2005], which further leads to high export rates of biogenic opal via episodic diatom bloom events recorded in laminated sediments of the essentially oxygen free bottom waters beneath the upwelling centers on the Peruvian shelf [*Brodie and Kemp*, 1994; *Salvatteci et al.*, 2014a; *Fleury et al.*, 2015; *Schönfeld et al.*, 2015]. Variations in past export productivity as well as changes in the diatom community were shown to indicate shifts between the proposed El Niño- or La Niña-like mean states that reflect larger scale oceanographic and climatic changes [*Fleury et al.*, 2015]. Furthermore, in recent years the application of stable silicon isotope ($\delta^{30}Si$) compositions of sedimentary diatoms has been successfully established as an indicator for past $Si(OH)_4$ utilization in surface waters. Several studies investigated the modern [*Beucher et al.*, 2008; 2011; *Ehlert et al.*, 2012; *Grasse et al.*, 2013] and past Si cycle in the EEP [*Pichevin et al.*, 2009] and PUE [*Ehlert et al.*, 2013] to gain improved insights into nutrient delivery and consumption.

In this study we aim to resolve the regional response of the PUE to basin-scale atmospheric and oceanographic variability during the last transition from a glacial into an interglacial. We combine the reconstruction of the amount of past export productivity with those of nutrient utilization and upwelling intensity. Past export productivity derived from accumulation rates of biogenic opal (bSi) and particulate organic carbon (C_{org}), whereas nutrient utilization is reconstructed from the $\delta^{30}Si$ signatures of different diatom fractions (11-32µm mixed diatom species: $\delta^{30}Si_{bSi}$; and >150µm handpicked mono-generic diatoms *Coscinodiscus* spp.: $\delta^{30}Si_{Coscino}$). Upwelling intensity is determined based on a new approach using the offset ($\Delta^{30}Si$) between $\delta^{30}Si_{Coscino}$ and $\delta^{30}Si_{bSi}$ signatures ($\delta^{30}Si_{Coscino}$-$\delta^{30}Si_{bSi}$) determined on the same sediment samples, as well as the diatom assemblage within the small diatom fraction (11-32µm). This approach is based on the finding that the larger diatom species reflect stratified conditions and near-complete nutrient utilization indicated by high $\delta^{30}Si_{Coscino}$ values [*Ehlert et al.*, 2012; *Doering et al.*, 2016]. In contrast, the $\delta^{30}Si_{bSi}$ signatures of small diatom species record the gradual increase in seawater $\delta^{30}Si(OH)_4$ as a result of progressive $Si(OH)_4$ utilisation during intense bloom events in direct response to the strength of upwelling [*Doering et al.*, 2016]. Hence, variable degrees of upwelling intensity and silicate utilization along the modern shelf result in lower $\delta^{30}Si_{bSi}$ signatures when upwelling was weak and vice versa, whereas $\delta^{30}Si_{Coscino}$ signatures show continuously high values reflecting the prevailing silicate limitation along the shelf during stratified conditions. Accordingly, $\Delta^{30}Si$ values are lowest in areas of most intense upwelling conditions and highest where weak upwelling and low $Si(OH)_4$ concentrations do not permit intense blooms [*Doering et al.*, 2016]. We use these relationships in our new own records in

combination with previous studies from the equatorial Pacific, PUE and the Chilean coast to better understand the factors that have driven past regional biogeochemical variations in the context of large-scale atmospheric and oceanographic changes in the EEP for the last 20,000 years BP.

2. Regional setting

The climatic and oceanographic conditions in the EEP are a result of interactions of basin-scale atmospheric circulation with local effects occurring at the land sea interface [*Strub et al.*, 1998]. The SPSH drives equator-ward winds along the western coast of South America (Fig. 1). To the North the system is bordered by the ITCZ, which constitutes the belt of converging northern and southern trade winds and is associated with intense convection and precipitation. Today, the ITCZ migrates between 3°N in austral summer (Feb–Mar; Fig 1 A) and 10°N, in austral winter (Aug–Sep; Fig 1 B), respectively [*Wyrtki*, 1975; *Kessler*, 2006]. During austral winter, strong cross-equatorial southeast trade winds drive enhanced upwelling along northern South America causing surface cooling and an enhanced cross-equatorial SST gradient (Fig. 1B; [*Wyrtki*, 1981]). In contrast, during austral summer trade winds and upwelling weakens, which results in higher SSTs in the EEP and thus in a weaker cross-equatorial SST gradient (Fig. 1 A; [*Chelton et al.*, 2001]).

Within the PUE along the Peruvian margin between 1°N to 18°S (Fig. 1A) south-easterly trade winds drive surface waters northwards, thereby generating the Peru-Chile Coastal Current (PCCC) flowing along the shore and the Peru-Chile Current (PCC) further offshore (Fig. 1B) [*Fiedler and Talley*, 2006 and references therein]. The southward flowing subsurface Peru-Chile Undercurrent (PCUC) is the main source of the waters upwelling off Peru [*Zuta and Guillén*, 1970; *Brink et al.*, 1983; *Toggweiler et al.*, 1991]. Approximately 30% of the PCUC waters originate from three subsurface currents [*Montes et al.*, 2010]: the eastward flowing subsurface waters of the Equatorial Undercurrent (EUC; 1.5°N-1.5°S), the primary Southern Subsurface Counter Current (pSSCC; 2°S-4.7°S) and the secondary Southern Subsurface Counter Current (sSSCC; 5.8-8.2°S) (Fig. 1C) [*Brink et al.*, 1983; *Toggweiler et al.*, 1991]. The remaining 70% of the PCUC waters originate from upwelling from below the PCUC (35%) and weak diffuse currents in the domain south of 9°S (35%) [*Montes et al.*, 2010]. The PCUC reaches its maximum velocity between 6°S and 10°S, leading to decreased deposition of sediments and reworking of bottom sediments [*Suess et al.*, 1987]. Further south the velocity of the subsurface current decreases allowing enhanced sediment deposition and high sedimentation rates along the upper continental slope, which is indicated by an organic-rich facies (>5wt% C_{org}; 11°S to 15°S at 50-500m water depth) also referred to as Peruvian mud-belt [*Krissek et al.*, 1980; *Suess et al.*, 1987]. The northern boundary of the

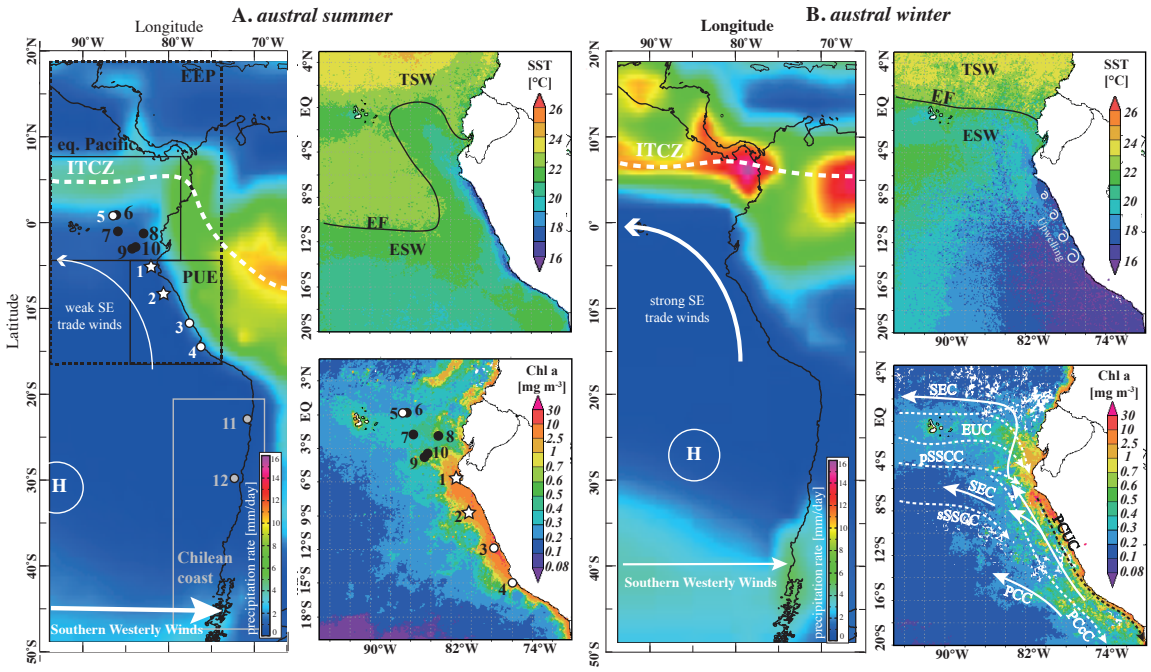

Figure 1: Comparison of environmental parameters controlling present day austral summer and winter conditions off Peru: A. Austral summer; Left: Mean precipitation rate (mm/day; Jun-Aug). The position of the ITCZ is indicated by white dotted lines and the approximate position of the Subtropical High is marked (H). The black (EEP) and grey (Chilean coast) circles indicate core sites used for comparison of opal fluxes, white circles indicate cores sites used for stable silicon isotope comparison, white stars indicate the two new cores presented in this study (see Table 2); Right top: Mean Sea Surface Temperatures (SST). The black lines show the position of the Equatorial Front (EF), TSW – Tropical Surface Water; ESW – Equatorial Surface Waters [*Fiedler and Talley*, 2006; *Kessler*, 2006]; Right bottom: Chlorophyll *a* concentration. B. Austral winter; Left: Mean precipitation rate (mm/day; Dec-Feb); Right top: Mean Sea Surface Temperatures (SST); Right bottom: Chlorophyll a concentration; Solid white arrows indicate surface currents: SEC – South Equatorial Current; PCC – Peru-Chile-Current. PCcC – Peru Coastal Current; Dashed arrows show subsurface currents: EUC – Equatorial Undercurrent. pSSCC - primary Southern Subsurface Counter Current. sSSCC – secondary Subsurface Counter current. PCCC – Peru-Chile Counter Current. PCUC – Peru-Chile Undercurrent. Precipitation rates were averaged over the last 30 years (1980-2010) from NASA GPCP (http://iridl.ldeo.columbia.edu; *Adler et al.*, 2003; *Hoffman et al.*, 2009). SST and Chl *a* are given for 2008 and were generated via http://oceancolor.gsfc.nasa.gov/cgi/. A list of the detailed locations and water depths of the cores displayed on fig. 1A is given in Table 1.

PUE is on average located between 4-5°S but varies seasonally and interannually [*Strub et al.*, 1998]. The shape of the coastline has led to the development of several main upwelling centers located today at 4-6°S, 7-9°S, 11-13°S and 14-16°S [*Zuta and Guillén*, 1970; *de Mendiola*, 1981].

Primary productivity (PP) off Peru is controlled by the supply of macro- and micro-nutrients (e.g. nitrate, $Si(OH)_4$, phosphate, Fe and cadmium), light and physical export (offshore transport or subduction of water masses; see *Messié and Chavez*, [2015]). The phytoplankton community is generally composed of early successional stages dominated by small diatoms (5-30 µm) with high reproduction rates, while later successional stages are characterized by larger sized species [*MacIsaac et al.*, 1985; *Tarazona et al.*, 2003; *Doering et al.*, 2016]. This change in species assemblages is closely related to the transition from

vertically mixed to more stratified conditions. In oceanic waters, which occur further offshore, the phytoplankton community is dominated by dinoflagellates and large diatoms with low reproduction and assimilation rates [*Ochoa and Gomez*, 1981; *Sanchez et al.*, 2000; *Ochoa et al.*, 2010].

On interannual timescales the ENSO cycle, a fluctuation between unusually warm (El Niño) and cold (La Niña) conditions in the eastern tropical Pacific is the main forcing mechanism of climatic variability superimposed on seasonality. El Niño events are characterized by warmer SSTs in the eastern and central tropical Pacific a deepening of the thermocline and the weakening of the trade winds in the eastern and central tropical Pacific. Although the source depth of upwelling water remains the same during El Niño events (i.e., 50-100 m) upwelling delivers only warm, nutrient-poor waters to the surface due to a deepened thermocline [*Huyer et al.*, 1987]. At the same time tropical and equatorial surface waters reach the coast off Peru [*Sanchez et al.*, 2000] and PP is reduced by about 50%, while the phytoplankton community is dominated by oceanic and equatorial dinoflagellates and large diatom species [*Barber and Chávez*, 1983; *Chavez*, 1989]. In contrast, La Niña events are associated with a stronger Walker (west–east or zonal) Circulation and a steep thermocline leading to an intensification of the coastal cold tongue.

Table 1: Location and Water Depth of the Cores used for comparison of opal fluxes.

No.	Core	Latitude	Longitude	Water depth	Reference
7	RC11-238[a]	-1.517	-85.817	2573	*Bradtmiller et al.*, [2006]
9	V19-30[a]	-3.383	-83.517	3091	*Bradtmiller et al.*, [2006]
10	TR163-31P[a]	-3.619	-83.971	3205	*Kienast et al.*, [2006b]
6	ME0005-24JC[a]	0.022	-86.463	2941	*Kienast et al.*, [2006b]
8	ME0005-27JC[a]	-1.853	-82.787	2203	*Dubois et al.*, [2010]
5	ODP202-1240A[a]	0.022	-86.463	2922	*Pichevin et al.*, [2009]
1	M77/2-052[b]	-5.483	-81.45	1249	*this study*, *Schönfeld et al.*, [2015]
2	M77/2-029[b]	-9.283	-79.617	444	*this study*, *Schönfeld et al.*, [2015]
3	SO147-106KL[b]	-12.05	-77.667	184	*Ehlert et al.*, [2013]
4	M77/2-003[b]	-15.1	-75.683	271	*Doering et al.*, [2016]
11	GeoB 7112-5	-24.033	-70.823	2507	*Mohtadi et al.*, [2004]
12	GeoB 7139-2	-30.2	-71.983	3267	*Mohtadi et al.*, [2004]

[a]opal fluxes were calculated via ^{230}Th normalization.

[b]opal fluxes were calculated without ^{230}Th normalization.

Intense upwelling and productivity associated with stronger utilization of surface water $Si(OH)_4$ by diatoms is commonly observed in upwelling regions, which leads to overall high $\delta^{30}Si$ signatures of diatom frustules preserved in the underlying sediments [*Ehlert et al.*, 2013; *Pichevin et al.*, 2014; *Ehlert et al.*, 2015]. It was also shown that the differentiation between $\delta^{30}Si$ signatures of small diatom species, representing upwelling blooms in spring, and large handpicked diatom species, which occur at the end of blooms or during summer conditions

is important to distinguish between $Si(OH)_4$ consumption during initial upwelling and late upwelling accompanied by more stratified conditions [*Doering et al.*, 2016].

3. Material and Methods

This study presents new records of two piston cores in combination with two previously published records, which together for the first time enable a reconstruction of upwelling intensity and utilization due to biogeochemical and oceanographic changes of the past 20,000 years along the entire Peruvian Margin (Fig. 1). New records of $\delta^{30}Si$ signatures of both, small-mixed diatoms (11-32µm; $\delta^{30}Si_{bSi}$) and larger handpicked diatoms (125/150-200µm *Coscinodiscus* spp.; $\delta^{30}Si_{Coscino}$), accumulation rates of bSi (g cm^{-2} ka^{-1}), as well as diatom assemblage analyses were generated for cores M77/2-029-3 (029; 9°17'S, 79°37'W, 444 m water depth) and M772-052-2 (052; 5°29'S, 81°27'W, 1249 m water depth), which were both retrieved during the German R/V Meteor cruise M77/2 in 2008 [*Pfannkuche et al.*, 2011], within the framework of the Collaborative Research Centre 754 (Sonderforschungsbereich/SFB 754) funded by the Deutsche Forschungsgemeinschaft (DFG). These new records are interpreted together with previously published records of cores M77/2-003-2 (003; 15°06'S, 75°41'W, 271 m water depth at; [*Doering et al.*, 2016]) and SO147-106KL (106KL; 12°03'S, 77°40'W, 184 m water depth [*Ehlert et al.*, 2013]), the latter of which was extended by seven new $\delta^{30}Si_{Coscino}$ measurements for this study.

3.1 Age models

The age model of core 052 [*Erdem et al.*, 2016], is based on five Accelerator Mass Spectrometer (AMS) ^{14}C datings of the planktonic foraminifera species *N. dutertrei* in combination with orbital tuning of $\delta^{18}O$ values of nearby core M77/2-059 [*Mollier-Vogel et al.*, 2013] and supported by correlation to the $\delta^{18}O$ of the EPICA ice core [*EPICA Community Members*, 2006]. The conventional radiocarbon dates were calibrated using the software Calib 7.0 and applying the marine calibration set Marine13 [*Reimer and Bard*, 2013]. The age model of core 029 originally based on 11 AMS ^{14}C datings [*Mollier-Vogel*, 2012] was improved by six additional AMS ^{14}C measurements (see supplements Tab. S1). All measurements were performed at the Leibniz Laboratory for Isotope Research and Dating at the University of Kiel. All ^{14}C ages were corrected by applying a reservoir age of 511±278 years following [*Ortlieb et al.*, 2011]. The resulting ages were converted into calendar years using the program CLAM2.2 [*Blaauw*, 2010] and the Marine13 calibration curve (see supplements Tab. S2; [*Reimer and Bard*, 2013]). CLAM2.2 was further used to provide a best fit between radiocarbon

ages using a 'smooth spline' age model (supplements Fig. S1). For cores 106KL and 003 published age model based on AMS ^{14}C ages were used: [*Rein*, 2004] for core 106KL and *Doering et al.*, [2016] for core 003. All ages are given in 1000 calendar years before 1950 AD (abbreviated as ka BP).

3.2 Biogenic opal, particulate carbon and Silicon isotope analyses

The bSi and organic carbon (C_{org}) concentrations for core 029 were part of the PhD Thesis of *Mollier-Vogel* [2012] (Tab. 2; for all data see supplements Table S3). Prior to geochemical analyses the freeze-dried sediments were ground in an agate mortar. The amount of bSi in the sediments was measured according to an automated leaching method using sodium hydroxide as described by [*DeMaster*, 1981; *Müller and Schneider*, 1993] with a precision of 1-2% (1σ). The total C content was determined by combustion of the sediment samples using a Carlo–Erba element analyzer (NA 1500). Accumulation rates (AR) were calculated using dry bulk density (g/cm^3) and sedimentation rates (SR; cm/ka) obtained based on the age models.

$\delta^{30}Si$ records were produced for cores 052 and 029. For the silicon isotope measurements diatoms were extracted from the sediment by chemical (HCl and H_2O_2) and physical cleaning (11 and 32µm sieve; heavy liquid separation with a sodium polytungstate solution set at 2.15 mg/l) as described in detail in *Ehlert et al.* [2012; 2013] and *Doering et al.* [2016]. For all samples the purity of the small diatom fraction was evaluated via light microscopy prior to dissolution and only pure (>95%) diatom samples were treated further. In addition large diatoms were hand-picked from the 125/150-250 µm size fraction following *Ehlert et al.*, [2012]. An important observation is the high abundance of sponge spicules (up to 10%) in the Holocene section of core 029 (see supplements Table S4). During this time period $\delta^{30}Si_{bSi}$ signatures are lighter than +0.5‰ and may have been altered by contributions of lighter sponge spicule $\delta^{30}Si_{bSi}$ which can be as low as -4‰ [*Hendry et al.*, 2010]. Hence, we evaluated the potential maximum contamination effect for the three samples of core 029 with sponge spicule content above 5% applying -4‰ value given that no specific $\delta^{30}Si$ signatures are available for sponges from the area off Peru. Applying these estimates the corrected signatures reach values of +0.4‰ and +0.6‰, which is well within the range of modern values at the core site and demonstrates that the measured $\delta^{30}Si_{bSi}$ signatures are reasonable.

All samples were dissolved in 1 mL 0.1 M NaOH and treated with 200 µL concentrated H_2O_2 (Suprapur). Sample solutions were diluted with 4 mL MQ water and neutralized with 0.1 mL 1 M HCl [*Reynolds et al.*, 2008], followed by a chromatographic purification with 1 mL pre-cleaned AG50W-X8 cation exchange resin (BioRad, mesh 200-400) [*de Souza et al.*, 2012b]. The Si isotope ratios were determined in 0.6 ppm sample solutions on a *NuPlasma HR* MC-ICPMS at GEOMAR via a standard-sample bracketing method [*Albarède et al.*,

2004]. Silicon isotope compositions are reported in the δ-notation relative to the reference standard NBS28 in parts per thousand ($\delta^{30}Si = ((R_{sample}/R_{standard}) - 1) * 1000$), where R_{sample} is the $^{30}Si/^{28}Si$ ratio of the sample and $R_{standard}$ is the $^{30}Si/^{28}Si$ ratio of the NBS28. Long-term repeated measurements of the reference materials NBS28, IRMM018, and Big Batch gave average $\delta^{30}Si$ values of 0.00±0.23‰ (2σ), –1.51±0.18‰ (2σ) and –10.74±0.20‰ (2σ), respectively. All $\delta^{30}Si$ measurements were run at least in triplicates resulting in an external reproducibility better than ±0.23‰ (2σ, Table 2).

Table 2: Downcore records of $\delta^{30}Si_{bSi}$, $\delta^{30}Si_{Coscino}$ and bSi of core M77/2-052, M77/2-029 and SO147-106KL. The bSi (wt%) data of core 029 were taken from Mollier-Vogel et al., [2012]. The data of core SO147-106KL were taken from *Ehlert et al.*, [2013] and new measurements of this core are marked in bold italic. The 2σ error represents the external reproducibility based on replicates.

M772-052						**M772-029**						**SO147-106KL**		
Age [ka BP]	bSi [wt%]	$\delta^{30}Si_{bSi}$ [‰]	2 σ	$\delta^{30}Si_{Coscino}$ [‰]	2 σ	Age [ka BP]	bSi [wt%]	$\delta^{30}Si_{bSi}$ [‰]	2 σ	$\delta^{30}Si_{Coscino}$ [‰]	2 σ	Age [ka BP]	$\delta^{30}Si_{Coscino}$ [‰]	2 σ
0.37	10.29	1.06	0.20	1.39	0.26	2.94	3.23	0.28	0.09	-	-	1.17	1.38	0.11
1.11	6.80	1.58	0.13	1.48	0.18	4.71	5.92	0.10	0.22	1.00	0.25	1.34	***1.41***	***0.13***
1.86	7.87	1.60	0.21	1.60	0.12	8.13	4.61	0.15	0.25	0.78	0.24	1.39	***1.37***	***0.14***
3.34	7.61	0.96	0.17	-	-	9.51	6.43	0.36	0.18	0.96	0.18	1.56	0.89	0.17
5.20	6.38	-	-	1.43	0.19	10.63	8.28	0.11	0.16	0.96	0.11	1.86	***1.51***	***0.18***
5.57	7.77	1.42	0.25	-	-	11.51	12.74	0.81	0.09	0.94	0.18	2.45	***1.47***	***0.16***
7.06	5.62	0.95	0.25	-	-	12.64	17.84	0.13	0.24	1.31	0.14	3.13	0.83	0.10
10.77	5.57	1.20	0.11	-	-	12.99	26.32	0.87	0.13	-	-	3.42	0.51	0.13
11.51	4.25	1.25	0.22	-	-	13.26	16.93	0.45	0.32	-	-	3.80	0.62	0.07
11.88	4.30	-	-	0.84	0.17	13.67	17.94	0.77	0.13	-	-	5.94	0.42	0.22
12.63	6.44	-	-	1.32	0.12	14.00	15.43	1.08	0.15	-	-	8.93	1.15	0.21
13.00	6.78	1.67	0.16	-	-	14.15	22.83	1.19	0.23	1.53	0.19	9.11	***1.5***	***0.27***
13.74	4.19	0.65	0.21	1.61	0.14	14.32	19.04	1.25	0.12	-	-	9.26	1.22	0.16
14.71	4.35	-	-	1.65	0.11	15.04	32.12	1.25	0.25	-	-	10.21	1.30	0.08
15.68	5.69	1.82	0.19	-	-	15.16	20.44	1.07	0.28	-	-	10.32	***1.4***	***0.19***
16.65	5.67	-	-	1.48	0.15	15.57	-	1.27	0.16	1.43	0.11	12.02	1.30	0.08
18.59	9.30	1.41	0.23	-	-	15.71	23.79	0.99	0.15	-	-	13.26	***1.51***	***0.15***
19.07	5.63	-	-	1.65	0.32	15.79	-	1.35	0.15	-	-	13.79	0.83	0.09
						15.97	27.03	0.91	0.18	-	-	14.16	0.58	0.16
						16.10	36.24	1.02	0.13	-	-	16.03	0.98	0.19
						16.15	37.09	1.15	0.17	-	-			
						16.33	20.61	1.18	0.12	-	-			
						16.37	39.29	0.90	0.24	-	-			
						16.47	14.51	1.10	0.15	1.31	0.13			
						16.77	-	1.28	0.15	-	-			
						16.84	26.73	1.20	0.16	-	-			
						16.96	42.55	1.11	0.13	-	-			
						17.16	21.23	1.04	0.14	-	-			
						17.25	15.15	1.18	0.23	-	-			
						17.40	34.20	1.08	0.11	-	-			
						17.46	15.61	1.24	0.18	1.40	0.09			
						17.57	27.31	1.08	0.25	-	-			
						17.74	21.55	1.11	0.31	-	-			
						18.03	18.14	1.25	0.24	-	-			
						18.09	25.30	1.26	0.12	1.47	0.33			
						18.15	25.82	1.02	0.21	-	-			
						18.27	-	1.13	0.19	-	-			

3.3 Diatom assemblage data

The diatom assemblages were determined on the separated and cleaned 11-32µm fractions by light microscopic analysis (at 200-400 x magnification; Fig 3B; supplements Table S4). Smear-slides were prepared of every second sample and when the amount of the sample permitted, three transects of 300 specimens were counted. With the exception of fragments of *Coscinodiscus* spp. diatom species counts were only performed on those frustules of which at least two-thirds of the frustule were preserved [*Crosta and Koç*, 2007]. The fragments of the large species were, however, all counted to estimate the contribution of the generally higher silicon isotope composition of this species on the mixed signatures of the small-sized fraction. The abundances of three groups of diatom species representing particular environmental conditions were identified according to earlier studies off Peru [*Schuette*, 1980; *de Mendiola*, 1981; *De Vries and Schrader*, 1981; *Schuette and Schrader*, 1981; *Abrantes et al.*, 2007]:

(1) Coastal upwelling with nutrient-rich, turbulent waters: *Chaetoceros* spp. and resting spores (RS), *Skeletonema costatum*, *Thalassionema nitzschioides* var. *nitzschioides*;

(2) Coastal planktonic (temperate, cosmopolitan) with high-to-moderate nutrient waters: *Actinocyclus* spp., *Actinoptychus* spp., *Asteromphalus* spp., And *Cyclotella* spp.;

(3) Other diatom species: oceanic planktonic (warm, temperate) from nutrient-depleted waters such as *Nitzschia* spp., and *Rhizosolenia* spp., and benthic diatoms such as *Biddulphia* spp., *Cocconeis* spp., and *Delphineis karstenii*;

The determination of the diatom assemblages in the 11-32µm fraction is only a simplified approach compared to the bulk sediment assemblage analyses given that the specific size range excludes smaller and larger diatom species. However, it was shown that this size range closely reflects the main assemblage composition [*Ehlert et al.*, 2012; 2013] and is suitable to contribute to the interpretation of the corresponding $\delta^{30}Si_{bSi}$ signatures.

4. Results and Discussion

The records of cores 052 and 029 complement those already existing for opal and organic carbon fluxes (AR_{bSi} and AR_{Corg}), $\delta^{30}Si_{bSi}$ and $\delta^{30}Si_{Coscino}$ records obtained from cores 106KL and 003 at the Peruvian margin (see Tab.1, Figs. 2 and 3). We combine the four records to comprehensively evaluate latitudinal shifts and changes in the degree of nutrient utilization (based on $\delta^{30}Si_{bSi}$ and $\delta^{30}Si_{Coscino}$) together with changes in export production and upwelling intensity (based on AR_{bSi} and AR_{Corg} and diatom assemblages; Fig. 2, 4). Hereby we focus on the comparison of the present-day conditions to changes during the

Holocene and Termination 1 for the coastal upwelling area off Peru between 5°S and 15°S during.

The dataset demonstrates that large and systematic variations in export production, nutrient utilization and upwelling intensity occurred over time at all four sites (i.e. temporal variations). It also documents pronounced spatial differences between the different locations along the Peruvian margin. All data indicate a correspondence of increased PP (AR_{bSi}) and intensified upwelling conditions (diatom assemblage and $\Delta^{30}Si_{Coscino\text{-}bSi}$) with elevated $\delta^{30}Si$ signatures as previously suggested for Coastal Upwelling Systems [*Ehlert et al.*, 2013; *Pichevin et al.*, 2014; *Ehlert et al.*, 2015; *Doering et al.*, 2016]. However, we do not observe synchronous changes in productivity and upwelling intensity between Termination 1 and the Holocene at the different core locations along the margin. Such temporal and spatial environmental variability along the Peruvian shelf is broadly consistent with previous investigations and comparisons in the region based on diatom assemblages [*De Vries and Schrader*, 1981] and is probably controlled by local differences in the response to large-scale atmospheric circulation changes (i.e. shift of the ITCZ, SPSH and ENSO frequency).

4.1.1 Regional changes in export productivity

Changes in past export productivity can be investigated by using the AR of bSi and C_{org}. In general, AR_{bSi} and AR_{Corg} co-vary in the records from the PUE, with the exception of core 052, for which a major difference between AR_{bSi} and AR_{Corg} can be observed (Fig. 2, 5°S). This core is located in the northern part of the margin below the shelf break at 1000 m water depth, characterized by very low sedimentation rates (20 to 27 cm/ka) resulting in the lowest AR_{bSi} and AR_{Corg} values of our Peruvian margin section (Fig. 2). We exclude potential dissolution effects given that for the low AR_{bSi} values bulk sedimentation rates are also low. The AR_{Corg} is highest shortly after the transition from the early Holocene (11.7 ka to 8.2 ka BP) to the mid Holocene (8.2 ka to 4 ka BP; up to 0.45 g cm^{-2} ka^{-1} at 8 ka BP), while the AR_{bSi} show a minimum at that time (0.6 g cm^{-2} ka^{-1}; Fig. 2, 5°S). The most likely explanation for the diverging AR_{bSi} and AR_{Corg} is higher productivity of non-siliceous phytoplankton at this time, which was either induced by a low $Si(OH)_4$ availability or enhanced water column stratification.
The other three more southerly records show co-varying SR, AR_{bSi} and AR_{Corg}. Core 029 from 9°S at 400 m water depth is located within an area where at present only small amounts of sediment are deposited due to high energy hydrographic conditions, such as peak velocities of the PCUC (for details see Erdem et al., [2016]). Hence, both, the modern and Holocene SRs (11-20 cm/ka) and ARs (mean AR_{bSi} value = 1.1 g cm^{-2} ka^{-1}) were relatively low (Fig. 2). In marked contrast, during Termination 1 bottom currents were obviously less effective and not erosive, which is documented by sedimentation rates of up to

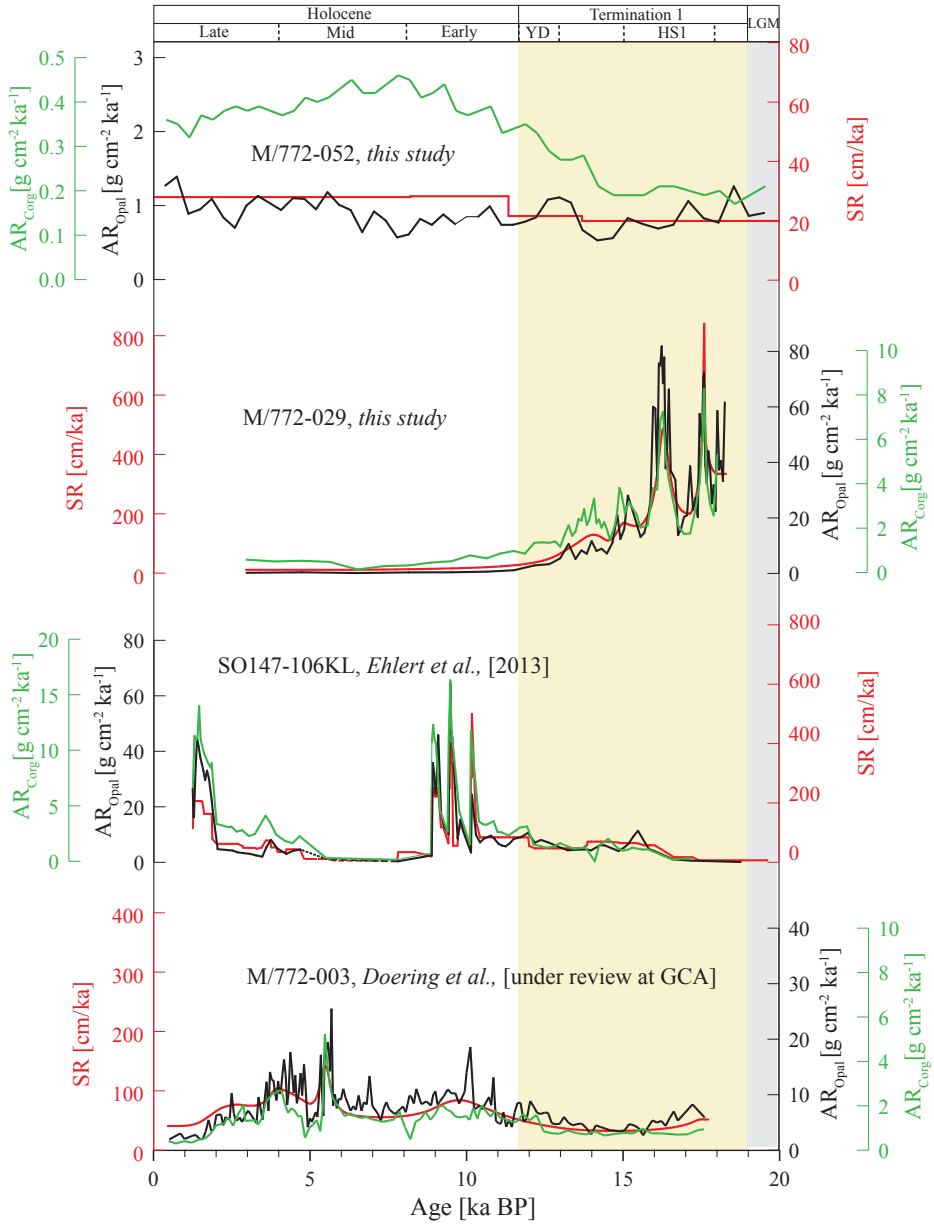

Figure 2: Time series of sedimentation rates [red lines; cm ka^{-1}], accumulation rates of biogenic opal (black lines) and organic carbon (green lines) [g cm^{-2} ka^{-1}] of cores M77/2-52, M77/2-29, SO147-106KL and M77/2-003. Note the different scales of the records of each core.

800 cm ka^{-1} at this location. The records from the southern shelf (12°S to 15°S) show substantially lower AR_{bSi} values during Termination 1 (mean AR_{bSi} = 5.6 g cm^{-2} ka^{-1} in 106KL and 5.4 g cm^{-2} ka^{-1} in 003), whereas much higher export productivity prevailed at both sites during the early Holocene (max AR_{bSi} = 64 g cm^{-2} ka^{-1} for 106KL and 19 g cm^{-2} ka^{-1} for 003). At 12°S highest export productivity (AR_{bSi} 40 to 64 g cm^{-2} ka^{-1}) occurred around 10-11 ka BP and around 2 ka BP. Core 003 shows a different evolution of export productivity (AR_{bSi}) with highest values at 10 ka BP (19 g cm^{-2} ka^{-1}), 5.7 ka BP (27 g cm^{-2} ka^{-1}) and between 4.5-5 ka BP (19 g cm^{-2} ka^{-1}), a period unfortunately not covered by core 106KL, due to a hiatus between 4.5 and 8 ka BP. Interestingly, ARbSi decreased after 2 ka BP in core 003 (2 g cm^{-2} ka^{-1}) when a marked increase (42 g

cm^{-2} ka^{-1}) was recorded in core 106KL. Overall, the variability in core 003 compares well with a bSi concentration record from 15°S covering the Holocene [Chazen et al., 2009], which confirms that core 003 provides an essentially undisturbed sediment record for the entire period considered.

4.1.2 Changes in nutrient utilization and upwelling intensity

In previous studies it was found that different diatom fractions represent different succession stages of blooming events, and therefore, are characterized by different $\delta^{30}Si$ representing variations in Si utilization [*Ehlert et al.*, 2013; *Doering et al.*, 2016]. Our new records also indicate that $\delta^{30}Si_{Coscino}$ values in general are higher than $\delta^{30}Si_{bSi}$ values of the same sample (Fig. 3). The surface $\delta^{30}Si_{bSi}$ and $\delta^{30}Si_{Coscino}$ signatures of cores 029, 106KL and 003 are generally in good agreement with distribution patterns in surface sediments [*Doering et al.*, 2016] characterized by heavier $\delta^{30}Si_{bSi}$ signatures (~+1‰) and lower $\Delta^{30}Si$ (= $\delta^{30}Si_{Coscino}$ - $\delta^{30}Si_{bSi}$) values (+0.3 to +0.6‰) denoting increased export productivity (AR_{bSi}) and upwelling intensity (high abundance of upwelling-related diatoms; Fig. 4B top). Hence, the difference in $\delta^{30}Si$ signatures between both size fractions ($\Delta^{30}Si$) was shown to correlate with upwelling intensity, with lowest $\Delta^{30}Si$ values (<+0.3‰) where upwelling is strongest and vice versa. In a complementary approach the upwelling intensity was determined based on the diatom assemblage of the 11-32 µm fraction, which was previously shown to reflect the main diatom assemblage of the bulk sediment [*Doering et al.*, 2016]. Accordingly, intense upwelling conditions are reflected by high abundances of upwelling-related species between 10 and 60% (Fig. 4 and Fig. 5C).

The central and the southern shelf (9°S to 15°S) during Termination

Following these previous observations as a prerequisite, the high $\delta^{30}Si_{bSi}$ signatures (+1.05±0.25‰), low $\Delta^{30}Si$ values (mean value = 0.3‰; Fig. 3 and 5B) and increased abundance of upwelling–related diatoms (up to 15%; Fig. 4 and 5C) at 9°S during Termination 1, associated with highest AR_{bSi} (up to 80 g cm^{-2} ka^{-1}), indicate conditions of high productivity and upwelling intensity very similar to those observed today at the southern shelf (between 12°S and 15°S). Conversely, lower AR_{bSi} values indicative of less intense export productivity during Termination 1 at 12°S and 15°S are associated with low $\delta^{30}Si_{bSi}$ values (+0.69±0.28‰ 106KL; +0.48±0.22‰ core 003) and higher $\Delta^{30}Si$ values of +0.83 and +0.64, the latter indicating a significantly weakened upwelling cell at that time. Please note that mean $\Delta^{30}Si$ and $\delta^{30}Si_{Coscino}$ values of core 106KL were calculated based on new $\delta^{30}Si_{Coscino}$ data produced in this study, given that the previously published $\delta^{30}Si_{Coscino}$ signatures of that core [*Ehlert et al.*, 2013] were not measured at the same sample depths as the $\delta^{30}Si_{bSi}$ signatures. The $\delta^{30}Si_{Coscino}$ of core 106KL [*Ehlert et al.*, 2013] show a much lower mean value of

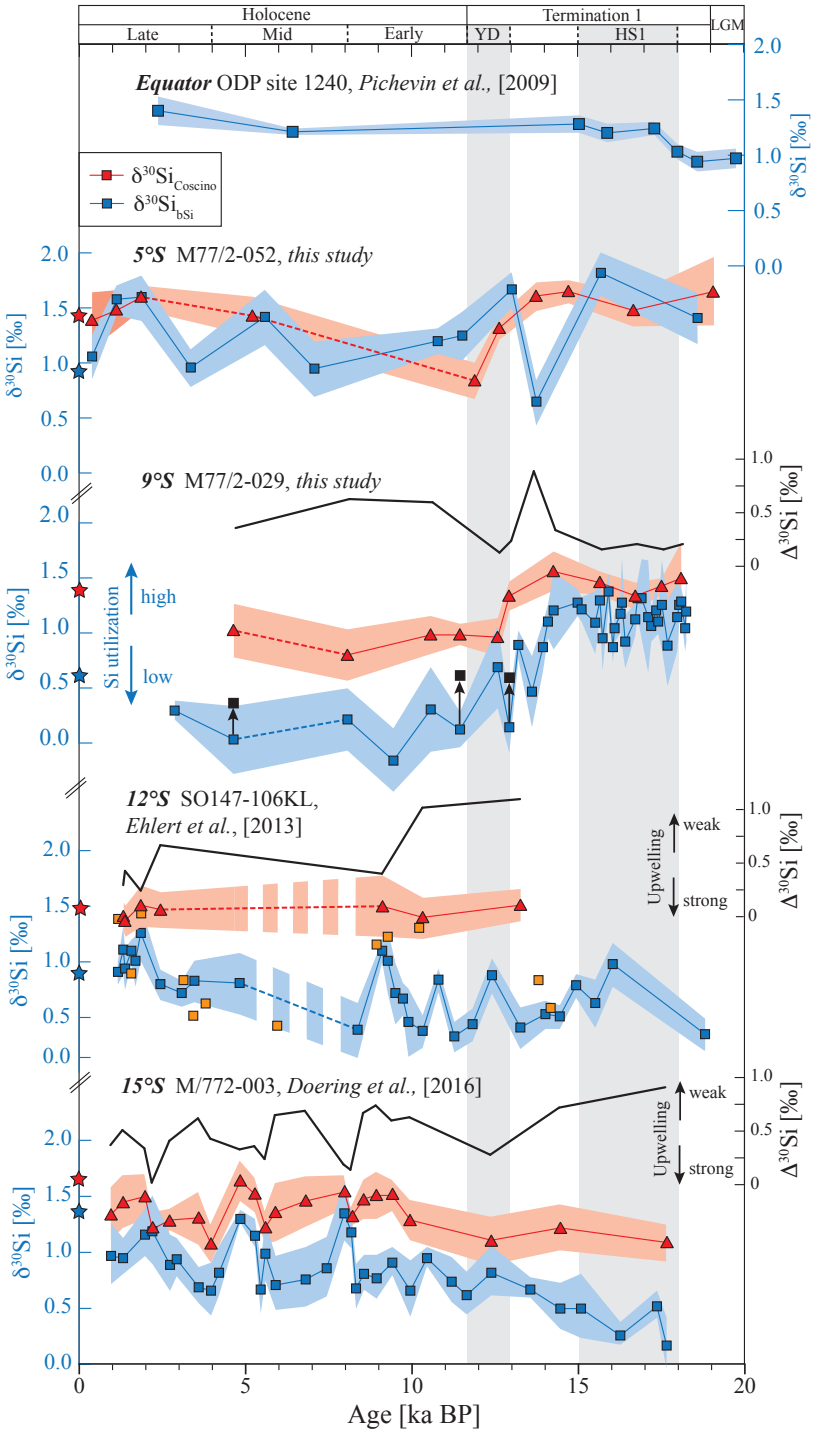

Figure 3: Downcore $\delta^{30}Si_{bSi}$ (blue squares and line) and $\delta^{30}Si_{Coscino}$ (red triangles and line) signatures of cores M77/2-052, M77/2-029, M77/2-003, SO147-106KL and ODP Site 1240. The corresponding offset $\Delta^{30}Si_{Coscino\text{-}bSi}$ (Δ) is given as black line for cores M77/2-029, M77/2-003 and SO147-106KL. The previously reported $\delta^{30}Si_{Coscino}$ signatures of core S0147-106KL [*Ehlert et al.*, 2013] are marked as orange squares. Black squares for core 029 indicate $\delta^{30}Si_{bSi}$ signatures corrected for sponge $\delta^{30}Si$ (see text for details). Areas marked with dashed lines indicate gaps in the $\delta^{30}Si$ record due to low sedimentation rates (M77/2-029) and/or very low bSi content (M77/2-029, M77/2-52). The hiatus in the sedimentary record of core 106KL between ~4.5 and 8 ka BP is marked as striped areas for $\delta^{30}Si_{bSi}$ and $\delta^{30}Si_{Coscino}$. The red and blue stars mark the $\delta^{30}Si_{bSi}$ and $\delta^{30}Si_{Coscino}$ signatures of the corresponding core-top samples. Grey shadings highlight Heinrich Stadial 1 and the Younger Dryas.

+0.88±0.34‰ in comparison to the signatures of the other Peruvian cores, which are close to +1.5‰. Similarly, the range of variation in $\delta^{30}Si_{bSi}$ signatures (+0.7±0.3‰) is much higher than in the other cores. It is striking that this high variability is observed at 12°S, located between the areas dominated by high PP (AR_{bSi} > 10 g cm^{-2} ka^{-1}) and high utilization ($\delta^{30}Si_{bSi}$ = +1.1‰) further North (9°S) and low PP (AR_{bSi} < 10 g cm^{-2} ka^{-1}) and lower utilization ($\delta^{30}Si_{bSi}$ = +0.5‰) further South (15°S) during Termination 1. However, high $\delta^{30}Si_{bSi}$ values (+1‰) are associated with high (>20%) abundances of upwelling-related diatoms, although the AR_{bSi} values remained stable at a low level (<10 g cm^{-2} ka^{-1}). Consequently, at 12°S a short-term occurrence of enhanced upwelling conditions with $\delta^{30}Si_{bSi}$ values close to +1‰ and upwelling-related diatoms >20% is not reflected by higher opal accumulation rates to the sediment during this time interval. This may indicate that the core site was more strongly affected by local variability of the environmental forcing factors.

The central and the southern shelf (9°S to 15°S) during the Holocene

During the Holocene AR_{bSi}, $\delta^{30}Si_{bSi}$ and $\delta^{30}Si_{Coscino}$ signatures, as well as $\Delta^{30}Si$ values shifted to their respective present day conditions at each location with intense upwelling conditions (AR_{bSi} >10 g cm^{-2} ka^{-1} , $\delta^{30}Si_{bSi}$= +0.8 to +0.9‰ and $\Delta^{30}Si$ = 0.3 to 0.5 ‰) at the Southern Shelf (between 12°S and 15°S) and weaker upwelling conditions (AR_{bSi} < 10 g cm^{-2} ka^{-1}, $\delta^{30}Si_{bSi}$ = +0.3‰ and $\Delta^{30}Si$ = 0.7 ‰) towards the North at 9°S. The above evidence is supported by a shift from laminated to non-laminated sediments in the northern cores, hence from high productivity and oxygen free bottom waters to low productivity and higher bottom water oxygenation [*Brodie and Kemp*, 1994; *Salvatteci et al.*, 2014a; *Fleury et al.*, 2015; *Schönfeld et al.*, 2015]. This is in agreement with a shift in the distribution of different sediment facies types [*Suess et al.*, [1987].

The northern Peruvian shelf (equator to 5°S)

Unlike all other $\delta^{30}Si_{Coscino}$ records of this study, which are generally substantially heavier than the $\delta^{30}Si_{bSi}$ signatures, the $\delta^{30}Si_{bSi}$ and $\delta^{30}Si_{Coscino}$ signatures of core 052 overlap, which is accompanied by highly abundant *Coscinodiscus* spp. fragments (>60%) within the 11-32 µm fraction (Figs. 3, 4). In contrast, the $\delta^{30}Si_{bSi}$ signature extracted from the modern surface sediments of core 052 follows the general pattern of all other locations and is significantly lower than that of $\delta^{30}Si_{Coscino}$ ($\Delta^{30}Si$= 0.5‰), which is accompanied by a diatom assemblage revealing a higher amount of upwelling-indicating species (10%) and less *Coscinodiscus* spp. fragments (50%) in comparison to the down-core record (Figs. 3, 4). Although it was not possible to measure $\delta^{30}Si_{bSi}$ and $\delta^{30}Si_{Coscino}$ values for the same sampling interval throughout the whole core due to extremely low bSi concentrations of ~5wt% in some core sections mainly during the early and

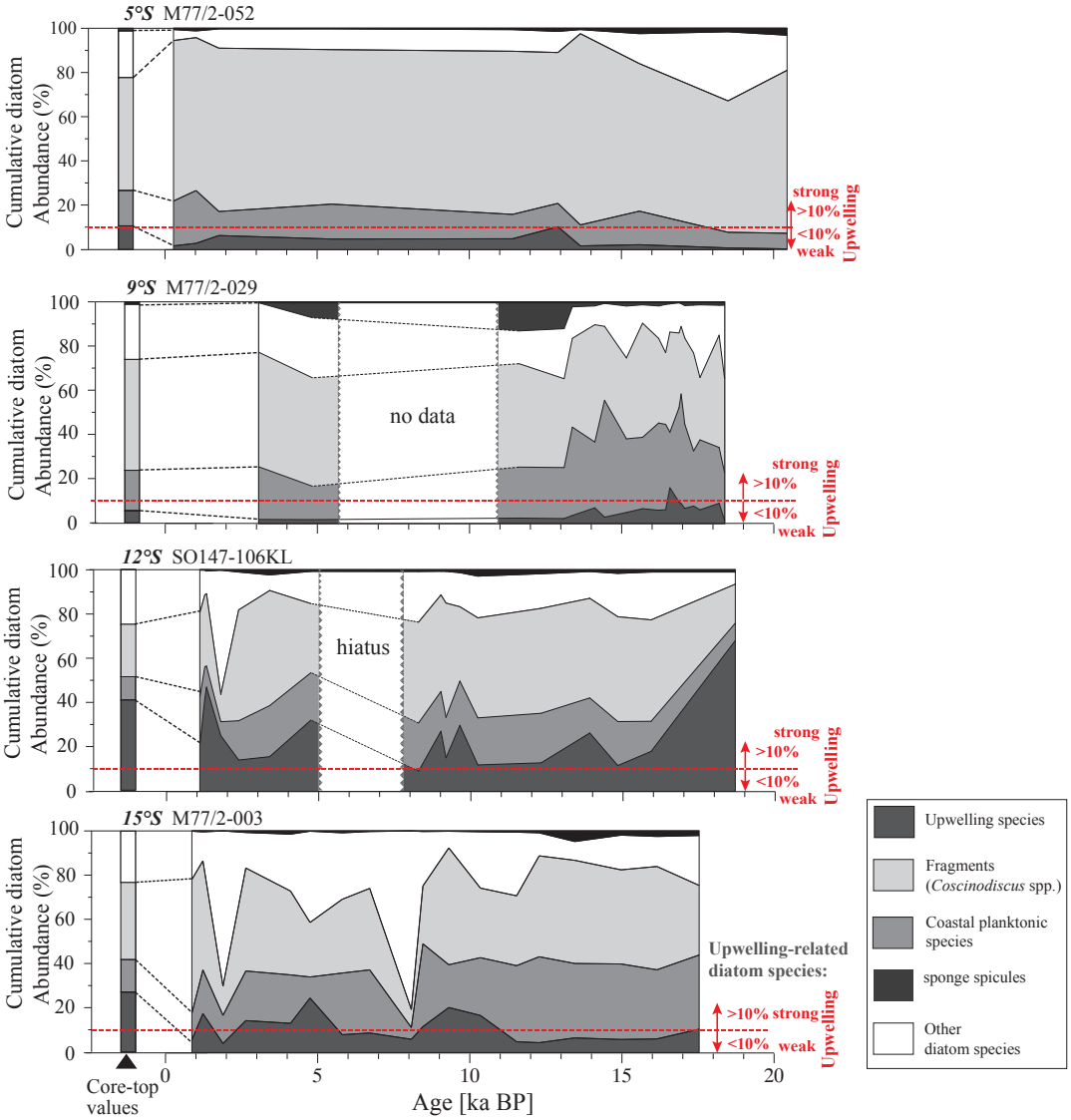

Figure 4: Cumulative diatom assemblages of cores M77/2-052, M77/2-029, M77/2-003, SO147-106KL; core top values are given as bar plot on the left hand side; sponge spicules – black; *other* diatom species – white; *Coscinodiscus* spp. fragments - light grey; coastal planktonic species –grey; upwelling-related species – dark grey. The horizontal red dashed lines on the four records marks the 10% abundance of upwelling related species.

beginning of the mid Holocene both fractions exhibit signatures close to +1.5‰ along the whole record (mean $\delta^{30}Si_{bSi}$ = +1.3 ± 0.35‰ and $\delta^{30}Si_{Coscino}$ = +1.44 ± 0.2‰). This value corresponds to the present day signatures carried by the PCUC, which supplies the upwelling cells off Peru [*Ehlert et al.*, 2012]. The lowest values occurred during the early and mid Holocene ($\delta^{30}Si_{bSi}$ = +1.13±0.16‰; $\delta^{30}Si_{Coscino}$= +0.84±0.17‰). The overlap of the $\delta^{30}Si_{bSi}$ and $\delta^{30}Si_{Coscino}$ signatures is most likely caused by the low abundance of small diatom species leading to relatively high amounts of *Coscinodiscus* fragments in the 11-32µm fraction which are generally associated with higher δ^{30}Si values [*Ehlert et al.*, 2012, 2013; *Doering et al.*, 2016]. Furthermore, the δ^{30}Si records of core 052 agree well with the record of ODP site 1240, located in the equatorial High-Nitrate-Low-Chlorophyll (HNLC) area of the EEP (Fig. 3 and 5A top; [*Pichevin*

et al., 2009; *Arellano-Torres et al.*, 2011]). Accordingly, we suggest that near-complete $Si(OH)_4$ utilization and thus Si-limited conditions have prevailed in the surface waters at these two sites since HS1.

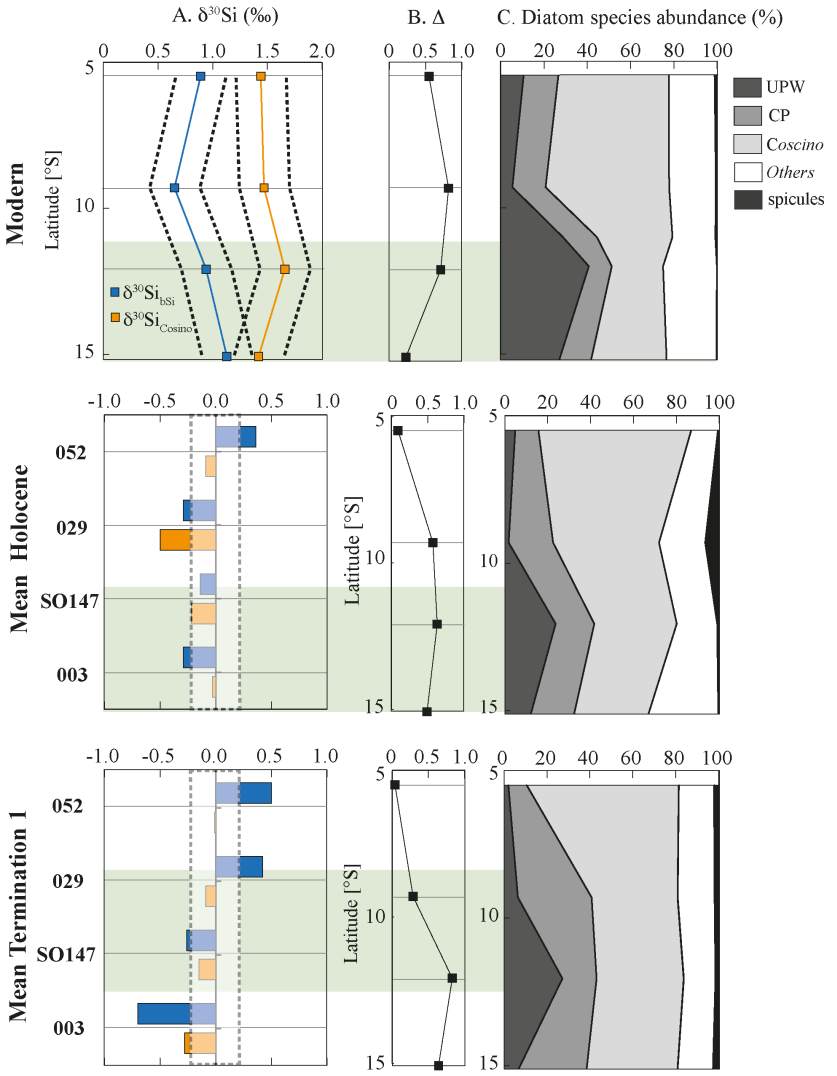

Figure 5: **Latitudinal distribution of A. mean $\delta^{30}Si_{bSi}$ and $\delta^{30}Si_{Coscino}$ signatures; B. estimated $\Delta^{30}Si_{Coscino\text{-}bSi}$ (Δ) values over latitude ($\Delta = \delta^{30}Si_{Coscino} - \delta^{30}Si_{bSi}$); C. cumulative diatom abundance of different diatom species groups. The top panel denotes the distribution of modern data at 5.5°S, 9°S, 12°S and 15°S the middle panel shows the mean Holocene, and the bottom panel displays the mean Termination 1 data. The $d^{30}Si_{bSi}$ and $d^{30}Si_{Coscino}$ signatures for the Holocene and Termination 1 in A. are given as deviations from the modern mean values. Dashed lines indicate measurement uncertainties. UPW – Upwelling-related species (*Chaetoceros* RS); CP- Coastal planktonic diatoms; Coscino – Fragments of *Coscinodiscus* spp.; *Others* – Unclassified diatom groups (i.e. oceanic, benthic or brackish species); spicules – sponge spicules; The areas highlighted in green indicate the areas of strongest upwelling conditions during the respective time periods.**

4.1.3 Summarizing past latitudinal differences in export productivity and upwelling

The combination of the four proxy records (Fig. 5, top and middle), allows a reconstruction of the past variability of the silicate system along the Peruvian margin. Both $\delta^{30}Si_{bSi}$ and $\delta^{30}Si_{Coscino}$ records show that upwelling intensity and diatom productivity were highest in the northern part of the PUE (052 and ODP Site 1240 i.e. $\delta^{30}Si_{bSi}$) during Termination 1 and low in the southern part (cores 29, 106KL and 003) during that period of time. During the Younger Dryas (YD) the records of core 029, 003 and 106KL started to converge, before upwelling intensity and diatom productivity at the southern sites started to increase pronouncedly during the early Holocene while both upwelling and PP remained low at site 029 ($\delta^{30}Si_{bSi}$ ~0.5‰). This switch in the spatial distribution of upwelling intensity is also reflected in the record of Δ^{30}Si values, which were previously shown to decrease with the intensity of the upwelling [*Doering et al.*, 2016]. Accordingly, the Δ^{30}Si values were generally low during HS1 and the YD (+0.25‰) and high during the Holocene (+0.65‰), while the Δ^{30}Si values of core 003 decreased from Termination 1 to the Holocene, indicating an overall northward shift of the upwelling center during the Holocene (Fig. 5B). Furthermore, the comparison of the mean values ($\delta^{30}Si_{bSi}$, $\delta^{30}Si_{Coscino}$, Δ^{30}Si and diatom species composition) during Termination 1 and the Holocene (given as difference from modern values; Fig. 5) indicates that (1) Holocene values were generally similar to modern conditions, (2) although δ^{30}Si signatures were markedly heavier and Δ^{30}Si values were lower in core 029 during Termination 1 this was only accompanied by an increase of the relative abundance of upwelling-related diatoms to ~ 10%, (3) during Termination 1 the overall upwelling strength (see Δ^{30}Si values; Fig. 5B) off Peru decreased and the most intense upwelling occurred from 9°S to 12°S instead of 12°S to 15°S at present, and (4) during reduced upwelling conditions indicated by high Δ^{30}Si and >10% upwelling-related diatoms, as observed during Termination 1 at 15°S and during the Holocene at 9°S, both $\delta^{30}Si_{bSi}$ and $\delta^{30}Si_{Coscino}$ (+1 to +1.2‰) decrease, although the latter should be also high during more stratified conditions given that the values reflect near-complete nutrient utilization at the northern shelf (core 052).

4.2 Mechanisms driving past PP variability and upwelling intensity

Variations in productivity off Peru have mainly been driven by changes in nutrient and Fe fluxes to surface waters, which vary due to upwelling strength variations induced by the trade winds as well as variable nutrient concentrations in the subsurface waters and the depth of the thermocline [*Loubere*, 1999]. Those variations in upwelling strength and thermocline depth are expected to have

been closely coupled to ocean-atmospheric circulation, which determine the position and strength of the SPSH linked to Walker Circulation strength as well as to the position of the ITCZ and the Southern Westerly Winds (SWW) (Fig. 1; [*Barber and Chávez*, 1983; *Strub et al.*, 1998]). Variations during the late Holocene have previously been suggested to follow northern hemisphere warm and cold periods, with increased upwelling intensity and PP (La Niña-like mean state) occurring during warm periods and reduced upwelling and PP conditions (El Niño-like mean state) during colder periods [*Sifeddine et al.*, 2008; *Gutiérrez et al.*, 2009; *Salvatteci et al.*, 2014b; *Ehlert et al.*, 2015]. However, the regional differences in the evolution of productivity, nutrient utilization and upwelling conditions on the Peruvian shelf between 5°S and 15°S presented here indicates that the variations observed between the LGM and today were much more complex and likely influenced by local differences between the core sites as well as differences in the response of ocean-atmospheric along the margin.

4.2.1 Response of Peruvian Upwelling to past forcing by the ocean-atmospheric circulation

During Termination 1 export production and upwelling intensity at 15°S decreased as, reflected by low AR_{bSi} and $\delta^{30}Si_{bSi}$ and high $\Delta^{30}Si$ (Fig. 2 and Fig. 3). These conditions are similar to previous reconstructions for the LIA (1400 - 1850 AD; *Ehlert et al.*, [2015]), where low surface productivity and upwelling intensity have been suggested to be driven by a more southerly position of the ITCZ and a weak/contracted SPSH inducing El Niño-like conditions [*Sifeddine et al.*, 2008; *Gutiérrez et al.*, 2009; *Sachs et al.*, 2009; *Ehlert et al.*, 2015]. This is consistent with interpretations based on eastern equatorial records for HS1 during Termination 1 (Fig. 7B; [*Dubois et al.*, 2011; *Kienast et al.*, 2013]). In contrast, at the same time at 12°S productivity (AR_{bSi}; Fig. 2) and upwelling intensity ($\Delta^{30}Si$ and diatom assemblages; Fig. 3) were highly variable and do not seem to follow any specific driving mechanism (such as ITCZ movement or SPSH strength). Upwelling strength and productivity are highly dependent on the coastline and shelf depth. Accordingly, as the sea-level was 120 meters below the present level [*Fairbanks*, 1989] prior to 10 ka BP, the shape of the coastline was different and thus potentially shifting the upwelling centers to different locations. Furthermore, core 106KL (12°S), which was accordingly located in water depths as shallow as 60 m during Termination 1 and turbulence in this near-shore area may periodically have been too intense to allow high surface productivity [*Margalef*, 1978]. Moreover, the particular shape of the shoreline at 15°S to 16°S today also promotes strong coastal eddy formation leading to high near-shore productivity [*Altabet et al.*, 2012; *Stramma et al.*, 2013], which might have been absent during Termination 1. Hence sea-level driven variations of the coastline at this location in the past may have significantly affected our record,

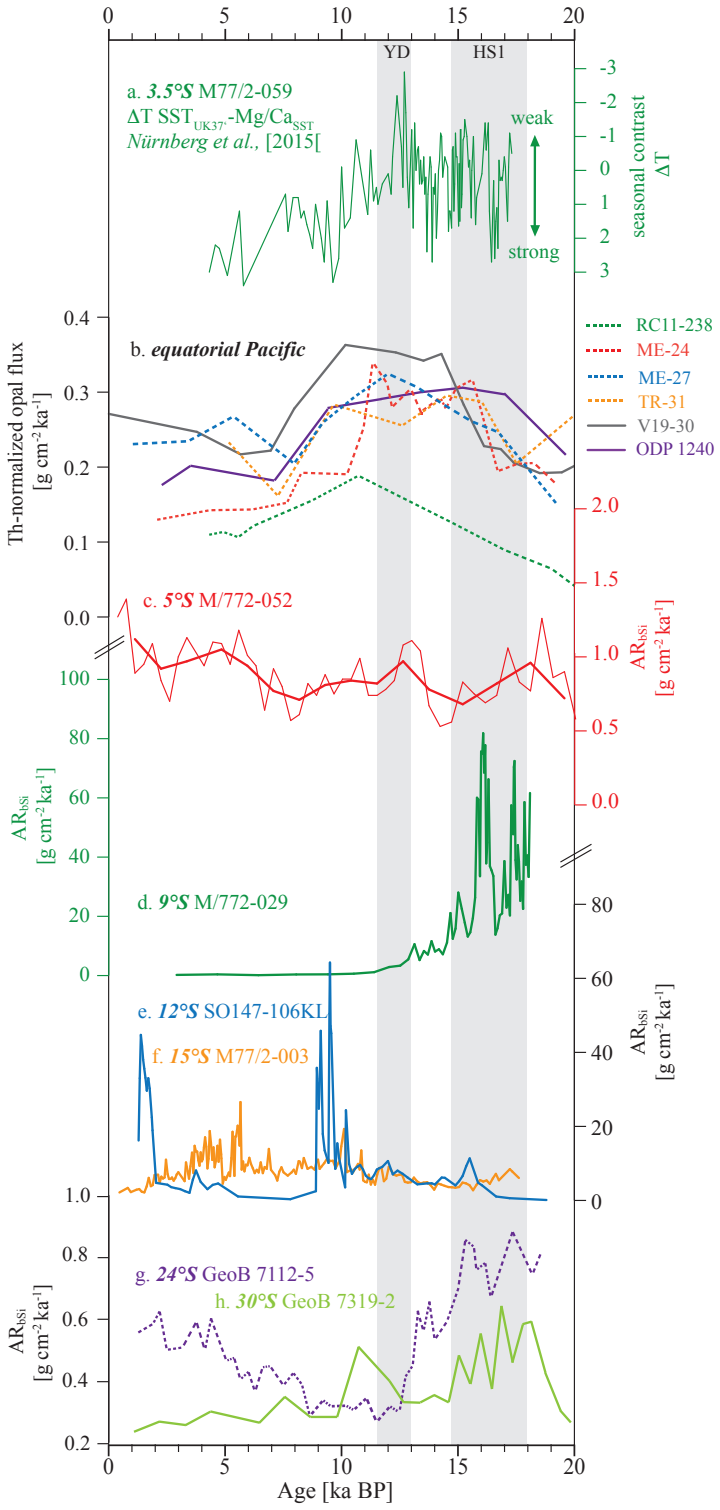

Figure 6: **Downcore comparison of a. Difference between UK'$_{37}$ and Mg/Ca SSTs given as ΔT SST$_{UK'37-Mg/Ca}$ of core M77/2-059 [Nürnberg et al., 2015];, biogenic opal fluxes from the EEP (b.; [Bradtmiller et al., 2006, Kienast et al., 2006b; Pichevin et al., 2009; Dubois et al., 2010]) the Peruvian Upwelling System (c-f; this study [Ehlert et al., 2013; Schönfeld et al., 2015; Doering et al., 2016]) and the Chilean Coast (g and h ; [Mohtadi, 2004]) over the past 20,000 years. Accumulation rates for the EEP and the Southern Chilean Coast (PC1 and PC3) are given as ^{230}Th-normalized opal fluxes, while the records from the Peruvian Upwelling System and Northern Chilean Coast (GeoB 7112 and 7319) were calculated without ^{230}Th-normalization and were calculated from opal content, sedimentation rates and dry bulk densities. All values are given in g cm^{-2} ka^{-1}.**

which, however, remains to be verified through a dedicated modelling study, which is beyond the scope of this study.

Altogether, during Termination 1, the moderate to high $\delta^{30}Si_{bSi}$ signatures at 9°S and 12°S as well as low $\Delta^{30}Si$ values and diatom assemblages with a considerable (>10%) amount of upwelling-related species clearly indicate that at least moderate to strong upwelling conditions were maintained in this area of the Peruvian margin all the time. Similar observations were made previously based on diatom assemblages records [*De Vries and Schrader*, 1981] and molecular organic geochemical proxies [*Makou et al.*, 2010] at 11°S, both indicating continuously strong upwelling or at least moderate upwelling conditions during Termination 1. Nevertheless, upwelling intensity and diatom productivity was substantially lower at 15°S (core 003-2) at the same time, suggesting a spatial shift in the main upwelling center from a modern location between 12°S and 15°S to 9°S and 12°S during the Termination. However, such a spatial shift in the main upwelling center is neither in agreement with a La Niña-like mean state, which should be accompanied by intense SE trade winds promoting upwelling along the whole margin, nor with an El Niño-like mean state which should cause low productivity along the whole area.

Prevailing high productivity and intense upwelling at 9°S after the LGM and at the onset of HS1 correlates with high opal fluxes in the Southern Ocean (e.g. SO: *Anderson et al.*, [2009]; eq. Pacific: Fig. 5 b, [*Bradtmiller et al.*, 2006; *Kienast et al.*, 2006a; *Dubois et al.*, 2010; *Hayes et al.*, 2011]) and at the Chilean Coast between 10 ka and 15 ka BP. The high productivity at the Chilean coast was suggested to be caused by a northerly position of the SWW and the Antarctic Circumpolar Current (ACC) during the LGM (Fig. 6 g, h 24-30°S; [*Mohtadi*, 2004]), which also induced enhanced vertical mixing in the Southern Ocean leading to an increase in opal production south of the Antarctic Polar Front during Antarctic warming between approximately 10 ka to 15 ka BP (concomitant with Heinrich Stadials, Fig. 7B; [*Toggweiler et al.*, 2006; *Anderson et al.*, 2009; *Hendry and Brzezinski*, 2014]). These records are consistent with a shift of the main upwelling center to 9°S off Peru (Fig. 5, bottom, green shading) which likely occurred in response to the northward shift of the SWW and SPSH during the LGM followed by a transient southward shift during Termination 1.

Based on the increased ventilation and enhanced surface productivity accompanied by a decreasing dust transport to the Southern Ocean, it was proposed that the formation of intermediate waters in the Southern Ocean increased promoting an enhanced export of $Si(OH)_4$ to the low latitudes between 10 ka and 15 ka BP [*Anderson et al.*, 2009; *Hayes et al.*, 2011; *Pena et al.*, 2013; *Hendry and Brzezinski*, 2014], which may also potentially have stimulated diatom opal PP in these regions. This is supported by records from the equatorial Pacific indicating high (^{230}Th-normalised) opal fluxes during Termination 1, which strongly increase at the onset of HS1 (Fig. 6 b; [*Bradtmiller et al.*, 2006; *Kienast et al.*, 2006a; *Dubois et al.*, 2010; *Hayes et al.*, 2011]). In addition to the

increased nutrient supply to the EEP, which may have lifted the co-limitation of surface productivity by $Si(OH)_4$ and Fe an increase of equatorial upwelling intensity was previously invoked to explain the doubling of export production in the equatorial Pacific during Termination 1 [*Hayes et al.*, 2011]. Based on alkenone paleothermometry *Dubois et al.*, [2011] and *Kienast et al.*, [2013] proposed an increase of equatorial upwelling intensity north of the equator due to an enhancement of the north-easterly trade winds as a consequence of a reduction in AMOC strength and hence intensification of the Central American gap wind system associated with the more southerly position of the ITCZ during HS1. However, other studies favour a strengthened upwelling, thermocline shoaling and increased equatorial productivity due to a La Niña-like mean state accompanied by an increase in south-easterly trade winds as the main causes for the changes observed [*Pena et al.*, 2008; *bin Shaari et al.*, 2013]. In comparison to this evolution in opal productivity at the equatorial Pacific during HS1 we do not observe an increase in productivity at the northern shelf edge (5°S) during Termination 1 but rather a decrease in upwelling intensity. Given that this location (5°S) is generally unaffected by the influence of strong coastal upwelling, regardless of the position of the upwelling cell, we can exclude a strong impact of changing nutrient supply for example via the EUC to the PUE based on this record. This is in agreement with a nearby record at 3.5°S, where enhanced influence of upwelled waters from the South is also not observed prior to 4 ka BP [*Nürnberg et al.*, 2015]. Moreover, the high sedimentation rates and laminations observed at the central shelf (9°S) indicate a substantial decrease in current velocities and a shift in the hydrographic system at the onset of Termination 1. Such a change may either have been established by enhanced La Niña-like conditions [*Montes et al.*, 2011] or could be explained by a weaker seasonal SST contrast and inferred decrease in EUC velocities during the Termination [*Nürnberg et al.*, 2015].

Overall, the combined records of opal accumulation rates, $\delta^{30}Si_{bSi}$ values and diatom assemblages suggest that the onset of Termination 1 was characterized by moderate upwelling and export productivity between 9°S and 12°S, which was markedly different from modern conditions due to the more northern position of SWW and the SPSH. Southeasterly trade winds do not seem to have intensified as the coastal cold tongue did not expand further north, which is in agreement with reports of a potentially weaker ITCZ during the LGM [*McGee et al.*, 2014]. With the onset of HS1 a southward shift in the mean position of the ITCZ the associated strengthening of the NE trade winds causing a regional increase in equatorial upwelling [*Dubois et al.*, 2011; *Kienast et al.*, 2013], is consistent with the continuous decrease in upwelling intensity, export productivity and nutrient utilization at 9°S as well as with prevailing low productivity and upwelling intensity at 15°S. Accordingly, the southward movement of the ITCZ is in accordance with reconstructions of enhanced river run-off from northern Peru at this time period [*Mollier-Vogel et al.*, 2013].

Modern conditions characterized by increased productivity and upwelling along the southern shelf were thus only established during the early Holocene after the YD. Ultimately, our reconstructions and comparison of past diatom productivity and upwelling conditions off Peru do not indicate shifts simply following El Niño- or La Niña-like mean states as neither the seasonal (Fig. 1) nor interannual (i.e. ENSO) modern variations can explain the observed changes, but rather support a connection to shifts in the position of the ITCZ and SWW, affecting the SPSH. However, while changes in atmospheric and oceanographic circulation control the amount of productivity and upwelling intensity, nutrient concentration and isotopic compositions of subsurface waters might be independently controlled by preformed $\delta^{30}Si(OH)_4$ signatures and $Si(OH)_4$ concentrations delivered to the PCUC linked to changes in Southern Ocean ventilation and productivity.

4.3 Potential changes in nutrient concentrations and isotopic signatures of source waters of the upwelling

Along the Peruvian margin the dissolved seawater $\delta^{30}Si$ signal, apart from utilization, is influenced by the mixing of water masses [*Reynolds et al.*, 2008; *Fripiat et al.*, 2011] and the remineralization of the diatom opal in subsurface waters [*Grasse et al.*, 2013]. The subsurface $\delta^{30}Si$ distribution was shown to record a combination of preformed seawater $\delta^{30}Si$ signal and addition of a lower $\delta^{30}Si$ signal originating from remineralization [*de Souza et al.*, 2012a]. Accordingly, the observed variations in the past $\delta^{30}Si_{bSi}$ and $\delta^{30}Si_{Coscino}$ should also reflect possible changes in the preformed $\delta^{30}Si(OH)_4$.

4.3.1 Modern source water contributions and compositions along the Peruvian shelf

The upwelling of the nutrient-rich PCUC along the Peruvian margin induces high productivity in surface waters. These nutrients are delivered to the PCUC via the EUC, sSSCC, pSSCC and by remineralized $Si(OH)_4$ along the Peruvian margin, which is visible as a tongue of high surface silicate concentrations extending westwards from the Peruvian coast [*de Souza et al.*, 2012a; *Grasse et al.*, 2013]. The modern EUC is composed of southern- (SAMW) and northern-sourced (NPIW) water masses, whereby the southern source supplies about 30% and the northern one contributes 70% of the dissolved silica [*Dugdale et al.*, 2002]. Consistent with this observation it has previously been shown that the SAMW is characterized by high dissolved $\delta^{30}Si$ signature of +1.8‰ and $Si(OH)_4$ concentrations of 10-15 µM (Fig. 7A; Table 3) [*Cardinal et al.*, 2005; 2007; *Hendry et al.*, 2010; *de Souza et al.*, 2012a]. The NPIW is characterized by higher silicate concentrations around 30 µM [*Dugdale et al.*, 2002] and a lower $\delta^{30}Si$

signature of +1.3‰ [*Reynolds et al.*, 2006]. Calculations of conservative mixing between these two sources leads to a dissolved silica concentration of 24 µM and a $\delta^{30}Si$ signature of +1.45‰ for the EUC (Table 3). This is in agreement with the observed $\delta^{30}Si(OH)_4$ signatures for the EUC of +1.5±0.2‰ [*Grasse et al.*, 2013].

During HS1, still elevated Fe supply to the Southern Ocean, mixing in the Subantarctic [*Bostock et al.*, 2004] accompanied by a breakdown of the glacial stratification and increased upwelling around Antarctica [*Anderson et al.*, 2009] led to an efficient ventilation of intermediate and deep waters. Such an increase in upwelling is thought to result in an increase in both Si and Fe supply to surface waters and formation of Southern Ocean Intermediate Waters (SAMW) with higher silicate concentrations (Silicic Acid Ventilation Hypothesis (SAVH) [*Hendry and Brzezinski*, 2014]), which was then advected to low latitudes where it potentially controlled productivity in the equatorial Pacific as well as along the Peruvian margin via ocean tunneling.

Table 3: Parameters used for Water Mass Mixing Calculations of Northern and Southern Source Waters contributing to the EUC.

	Modern			Termination 1		
	f [Si flux]	$Si(OH)_4$ µmol/kg	$\delta^{30}Si$ [‰]	f [Si flux]	$Si(OH)_4$ µmol/kg	$\delta^{30}Si$ [‰]
NPIW	0.69 [a]	29.8[a]	+1.3	0.58	29.8 [a]	+1.3
SAMW	0.31 [a]	11.5 [a]	+1.8	0.42	19	+2.5
calculated EUC		24.3	**+1.45**		25.5	**+1.8**

[a] values from [*Dugdale et al.*, 2002]

4.3.2 Estimation of the influence due to variations in past source water $Si(OH)_4$ and $\delta^{30}Si$

The available opal-based evidence from the Southern Ocean indicates that there were major ecological changes on glacial-interglacial timescales, which have led to a change in the composition of southern sourced intermediate waters (for simplification we will refer only to SAMW in the following) (Fig. 7 B). Burial rates of bSi, upwelling intensity and thus the supply of dissolved silica to the surface were enhanced during Termination 1 in both the Southern Ocean and equatorial Pacific [*Spero*, 2002; *Bradtmiller et al.*, 2006; *Anderson et al.*, 2009; *Calvo et al.*, 2011; *Hayes et al.*, 2011; *Pena et al.*, 2013]. In a recent study *Robinson et al.*, [2014] estimated much higher $\delta^{30}Si$ values of dissolved silica of approximately +2.5‰ and increased concentrations of 18-20µM for SAMW during HS1 (see also *Rousseau et al.*, [2016]). We estimate for this time period that the contribution of SAMW to the subsurface/intermediate waters in the equatorial Pacific increased to ca. 40% (Fig. 7B, Table 3), which is consistent

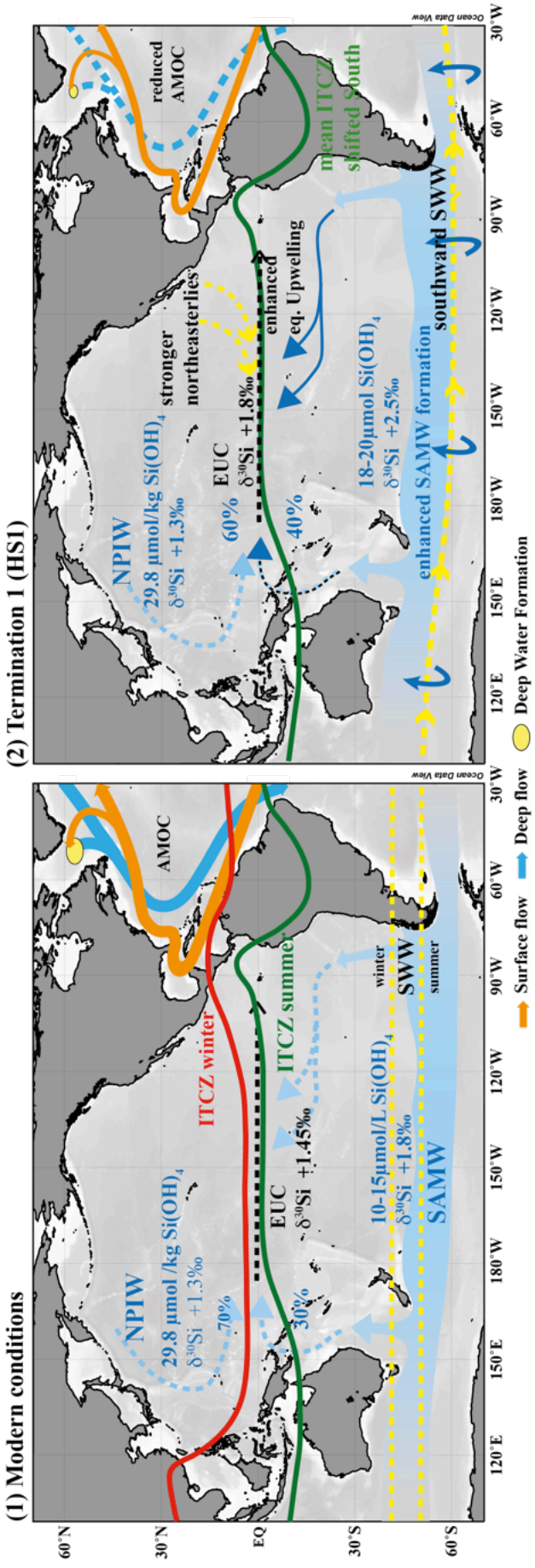

Figure 7: Schematic illustration of oceanic and atmospheric conditions prevailing (1) modern conditions and (2) during Termination 1 (HS1) (modified from *Dubois et al.*, [2011]). Modern silicon isotope signatures and dissolved silicate concentrations for NPIW and SAMW were taken from *de Souza et al.*, [2012]; (2) the data for the SAMW during HS1 were taken from *Robinson et al.*, [2014].

with observations based on $\delta^{13}C$ and ε_{Nd} records from the EEP during this time interval [*Spero*, 2002; *Pena et al.*, 2008; *Hayes et al.*, 2011; *Pena et al.*, 2013].
Although a quantitative estimation of the relative contributions of southern versus northern Pacific source waters during Termination 1 is not possible based on our data, these indicate an increase in supply from the South. To evaluate the potential influence via a change in the preformed $\delta^{30}Si(OH)_4$ we used $Si(OH)_4$ concentrations, flow and fluxes of the EUC as reported previously by *Dugdale et al.*, [2002]. Following the approach of *Hayes et al.*, [2011] we assumed North Pacific Intermediate Water (NPIW) as the only northern source and SAMW as the only southern source of nutrients to the EUC (Table 3). During HS1 the estimated change in $Si(OH)_4$ flux results in an increase to 42% from SAMW and reduces the contribution of NPIW to 58% (Fig. 6B; Table 4). At the same time the dissolved silica concentration of the EUC would increase by only 1.2 µmol/kg (Table 3; difference between modern and calculated $Si(OH)_4$ concentration). Furthermore, due to the proposed increase in the $\delta^{30}Si(OH)_4$ signature of SAMW to +2.5‰ our calculation gives a $\delta^{30}Si(OH)_4$ signature of the HS1-EUC of +1.8‰, which is 0.35‰ higher than the calculated modern value (+1.45‰, Table 3). As the EUC (and the SSCCs) contributes about 30% of the volume transported to the PCUC, the $\delta^{30}Si(OH)_4$ signature of the latter would have increased by as much as 0.17‰ based on our calculation. This small potential alteration of the past $\delta^{30}Si(OH)_4$ signature is in agreement with our $\delta^{30}Si_{Coscino}$ records of core 052 and 029, which are still within the range of the modern +1.5‰ signature. Moreover, a small increase in the $\delta^{30}Si(OH)_4$ signature of the PCUC by approximately 0.2‰ is consistent with the data given that the $\delta^{30}Si_{Coscino}$ values of core 052 during Termination 1 are similar to those of the late Holocene, which indicates near-compete Si utilization, despite that weaker upwelling (lower amount of *Chaetoceros* spp.) is observed. Similarly, in core 029 the $\delta^{30}Si_{bSi}$ signatures reach comparable to modern values (+1‰) and Holocene values on the southern shelf (+1‰), but do not indicate a correspondingly strong increase in upwelling-related diatoms.

5. Conclusions

In this study we present two new records of opal fluxes, $\delta^{30}Si$ signatures and diatom assemblages. We combine these new records with two previously reported records to reconstruct the variations of PP and nutrient utilization along the entire Peruvian margin for the past 20,000 years, which have responded to changes in atmospheric and oceanographic circulation since the LGM.

At the transition between the LGM and Termination 1, productivity and utilization were markedly higher on the central shelf between 9°S and 12°S, indicating a slower PCUC and more intense upwelling conditions. At the same

time, the southern shelf was characterized by low sedimentation rates, productivity and upwelling intensity, most likely indicating a shift of the main upwelling center as a consequence of a northward shift of the ITCZ and the SWW belt. Although shifts in the past PUE could be coupled to general variations in ocean-atmosphere circulation (such as ITCZ and SWW position) reported for the Pacific during the last glacial-interglacial, changes observed during Termination 1 do not strictly coincide with alternating El Niño- or La Niña-like mean states, but are also affected by local factors along the coast such as coastline morphology and sea level change. In contrast, Holocene productivity generally ranged between moderate and high values at the southern shelf, while low or interrupted sedimentation at the central shelf and near-complete $Si(OH)_4$ utilization and more stratified conditions characterized the northern region, similar to modern conditions. Based on our data we were also able to estimate the influence in past variations in preformed silicate supply and accompanying $\delta^{30}Si(OH)_4$ on the $\delta^{30}Si$ signatures. The results suggest an only slight maximum increase in $\delta^{30}Si(OH)_4$ of the PCUC by as much as 0.17‰, which is currently not resolvable in paleo records. Such a small alteration of past $\delta^{30}Si(OH)_4$ signature is in agreement with our $\delta^{30}Si_{Coscino}$ records, which do not indicate a strong increase in $\delta^{30}Si$. However, the contribution of a slightly increased preformed $\delta^{30}Si(OH)_4$ signature of the dissolved silicate supplied to the PCUC during Termination 1 may still have contributed to the pronounced zonal difference observed in our $\delta^{30}Si_{bSi}$ records along the Peruvian margin.

Acknowledgments and Data

This work is a contribution of the Collaborative Research Project 754 “Climate-Biogeochemistry interactions in the Tropical Ocean” (www.sfb754.de), which is supported by the Deutsche Forschungsgemeinschaft (DFG).

Chapter III. Latitudinal variations of $\delta^{30}Si$ and $\delta^{15}N$ along the Peruvian shelf: quantifying nutrient utilization versus denitrification over the past 600 years

Kristin Doering [1,2*], Sophie Fleury[3], Claudia Ehlert[4], Philippe Martinez[5], Martin Frank[2] and Ralph Schneider[1]

[1]Institute of Geosciences, University of Kiel, Ludewig-Meyn-Str. 10, 24118 Kiel, Germany
[2]GEOMAR Helmholtz Centre for Ocean Research Kiel, Wischhofstr. 1-3, 24148 Kiel, Germany
[3]Department of Marine Science and Convergence Technology, Hanyang University ERICA campus, 55 Hanyangdaehak-ro, Sangnok-gu, Ansan-si, Gyeonggi-do 426-791, South Korea
[4]Max Planck Research Group - Marine Isotope Geochemistry, Carl von Ossietzky University (ICBM), Carl-von Ossietzky-Str. 9-11, 26129 Oldenburg, Germany
[5]EPOC, UMR CNRS 5805, Université de Bordeaux 1, Allée Geoffroy Saint Hilaire, 33615 Pessac Cedex, France

Manuscript in preparation

Abstract

The sedimentary stable nitrogen isotope compositions ($\delta^{15}N$) and silicon isotope composition of diatoms ($\delta^{30}Si$) generally reflect the degree of nutrient utilization by past primary producers. However, in ocean areas where suboxic conditions prevail, the $\delta^{15}N$ records are further influenced by water column denitrification causing an increase in subsurface $\delta^{15}N$ signature of dissolved nitrate (NO_3^-), which is ultimately recorded within the sediments. Past reconstructions from the Peruvian Margin have shown that increased upwelling intensity, productivity, and N-loss processes occurred simultaneously during global warm periods, while all these processes weakened during cold periods. High sedimentary $\delta^{15}N$ values are generally explained by enhanced denitrification, while the effects of NO_3^- utilization are neglected.

Given that both $\delta^{30}Si$ and $\delta^{15}N$ are controlled by the degree of nutrient utilization, but only $\delta^{15}N$ is influenced by denitrification, it should be possible to disentangle past variations of these two processes. Based on the observation that subsurface $\delta^{15}N_{NO3-}$ increases today from North to South along the Peruvian shelf, due to ongoing denitrification within the pole-ward flowing subsurface waters, we present a latitudinal approach to reconstruct the factors controlling $\delta^{30}Si$ and $\delta^{15}N$ off Peru over the past 600 years. Three new records between 11°S

and 15°S are presented and compared to previously published records. These results show that variations at single core sites were mainly influenced by variability in nutrient utilization rather than subsurface N-loss processes, as was suggested previously. However, based on the latitudinal distribution of the records we demonstrate that during the Current Warm Period $d^{15}N$ records increase towards the South following increasing denitrification similar to the present day situation.

1. Introduction

Investigations of the isotopic compositions of nutrients, such as silicic acid ($Si(OH)_4$) and nitrate (NO_3^-), have been used to infer changes of biogeochemical cycles of the past. The preferential incorporation of the lighter isotopes ^{14}N and ^{28}Si into organic matter and biogenic opal, respectively, during primary productivity in surface waters leads to an increase in the $\delta^{15}N$ and $\delta^{30}Si$ in the remaining dissolved nutrients as a results of progressive consumption of the nutrient pools [*Wada and Hattori*, 1978; *Altabet et al.*, 1991; *De La Rocha et al.*, 1997]. Accordingly, the relative degree of utilization of NO_3^- and $Si(OH)_4$ is recorded in the $\delta^{15}N$ and $\delta^{30}Si$ of the resulting organic matter and biogenic opal, respectively. In combination with tracers such as organic carbon, opal or biogenic barium accumulation rates, both $\delta^{15}N$ and $\delta^{30}Si$ can be generally employed as tracers contributing to the evaluation of past productivity and corresponding nutrient utilization [*Pichevin et al.*, 2009; *Horn et al.*, 2011a].

However, in coastal upwelling areas where upwelling of nutrient-rich subsurface waters causes high surface productivity, subsequent degradation of the high organic matter (OM) flux leads to extensive oxygen consumption in the water column [*Zuta and Guillén*, 1970; *Pennington et al.*, 2006]. Under the resulting low oxygen concentrations nitrate (NO_3^-) is used as an oxidant during OM degradation and is transferred to N_2 leading to a net loss of bio-available nitrogen (e.g., denitrification and anammox; [*Codispoti*, 2006; *Lam et al.*, 2009]). Due to the high isotope fractionation factor (~20‰) occurring during denitrification, the $\delta^{15}N$ signatures of NO_3^- ($\delta^{15}N_{NO3-}$) in subsurface waters strongly increase imprinting a heavy $\delta^{15}N_{NO3-}$ signal to surface waters during upwelling [*Cline and Kaplan*, 1975]. These ^{15}N-enriched nitrates are incorporated by phytoplankton and ultimately deposited in marine sediments. Accordingly, although $\delta^{15}N$ values also vary in phase with productivity proxies, higher $\delta^{15}N$ values in productive and poorly ventilated regions, such as most of the upwelling areas, are generally interpreted as the consequence of stronger denitrification associated with more intense anoxic conditions [*Agnihotri et al.*, 2006; *De Pol-Holz et al.*, 2007; *Agnihotri et al.*, 2008; *Gutiérrez et al.*, 2009; *Mollier-Vogel et al.*, 2012; *Salvatteci et al.*, 2014; *Fleury et al.*, 2015]. However, as $\delta^{15}N$ records were

shown to be coupled to both nutrient utilization and water column oxygenation, both processes should influence the $\delta^{15}N$ recorded within the organic matter.

In contrast, the compositions of diatoms ($\delta^{30}Si_{bSi}$) are primarily controlled by surface water diatom productivity and $Si(OH)_4$ utilization [*De La Rocha et al.*, 1998; *Brzezinski*, 2002] closely coupled to the amount of productivity and upwelling strength in the study area [*Ehlert et al.*, 2012; 2013; *Grasse et al.*, 2013; *Ehlert et al.*, 2015; *Doering et al.*, 2016]. Thus, the combination of both $\delta^{30}Si_{bSi}$ and $\delta^{15}N_{bulk}$ compositions off Peru has been applied to provide a measure to disentangle past nutrient utilization and denitrification processes [*Ehlert et al.*, 2015]. First results for the past 600 years showed that both isotopic compositions were mainly influenced by nutrient utilization suggesting that denitrification was not the main control on past isotope variations [*Ehlert et al.*, 2015] somewhat contradicting previous interpretations of N-loss having been the main driver of changes in $\delta^{15}N_{bulk}$ records.

Today, $\delta^{15}N_{NO3-}$ increases southwards along the Peruvian Margin due to the continuous enrichment in ^{15}N by denitrification in pole-ward flowing subsurface waters. Here, we intent to verify whether this southward increase of $\delta^{15}N_{NO3-}$ due to denitrification were present for different time periods in the past, based on the correlation of $\delta^{30}Si_{bSi}$ and $\delta^{15}N_{bulk}$ signatures for different time periods to improve the detection of variations in $\delta^{15}N_{bulk}$ as a function of denitrification versus nutrient utilization. Therefore, we present three new records for $\delta^{30}Si_{bSi}$ and biogenic opal (bSi) concentrations from the Peruvian shelf between 11°S and 15°S covering the last 600 to 1000 years BP. These are compared to previously published $\delta^{15}N_{bulk}$ data obtained from the same cores [*Fleury et al.*, 2015] and $\delta^{30}Si_{bSi}$ versus $\delta^{15}N_{bulk}$ records from 14°S [*Ehlert et al.*, 2015].

1.2 Regional setting

Along the Peruvian margin the main source for the upwelled high nutrient waters is the subsurface Peru-Chile Undercurrent (PCUC), which flows southward between 4°S and 14°S at a depth between 50 and 150 m along the shelf [*Brink et al.*, 1983; *Toggweiler et al.*, 1991]. The PCUC is fed by eastward flowing subsurface waters of the Equatorial Undercurrent (EUC) and the subsurface jet – the Southern Subsurface Counter Current (SSCC; consisting of the primary and secondary SSCC) (see Fig. 1 in *Thesis Chapter. I*). These subsurface currents deliver silicic acid ($Si(OH)_4$) and nitrate (NO_3^-) with preformed source signatures with mean values of +1.5±0.2‰ for $\delta^{30}Si(OH)_4$ [*Beucher et al.*, 2011; *Ehlert et al.*, 2012; *Grasse et al.*, 2013] and mean $\delta^{15}N_{NO3-}$ values of 7.1±0.3‰ for the EUC and 5.5±0.3‰ for the SSCC [*Rafter et al.*, 2012].

The present day surface sediment $\delta^{15}N$ and $\delta^{30}Si$ compositions show that both nutrient signatures increase from North to South. However, only the dissolved present-day $\delta^{15}N_{NO3-}$ increases southward caused by denitrification, the dissolved $\delta^{30}Si(OH)_4$ remains close to the source value of +1.5‰ for PCUC [*Mollier-Vogel et al.*, 2012; *Ehlert et al.*, 2012]. Along the northern shelf between 1°N and 10°S, where O_2 concentrations [O_2] are >20µmol L^{-1} N-loss is not observed and the $\delta^{15}N_{bulk}$ values in the sediments range between +4‰ and +5‰ close to the source value of ~5‰ of $\delta^{15}N_{NO3-}$, indicating a high degree of NO_3^- utilization [*Mollier-Vogel et al.*, 2012]. In contrast, the $\delta^{30}Si_{bSi}$ signatures in that area are highly variable (between +0.25 and +0.89‰) reflecting an overall lower degree of utilization in comparison to $\delta^{15}N_{bulk}$ [*Ehlert et al.*, 2012; *Doering et al.*, 2016].

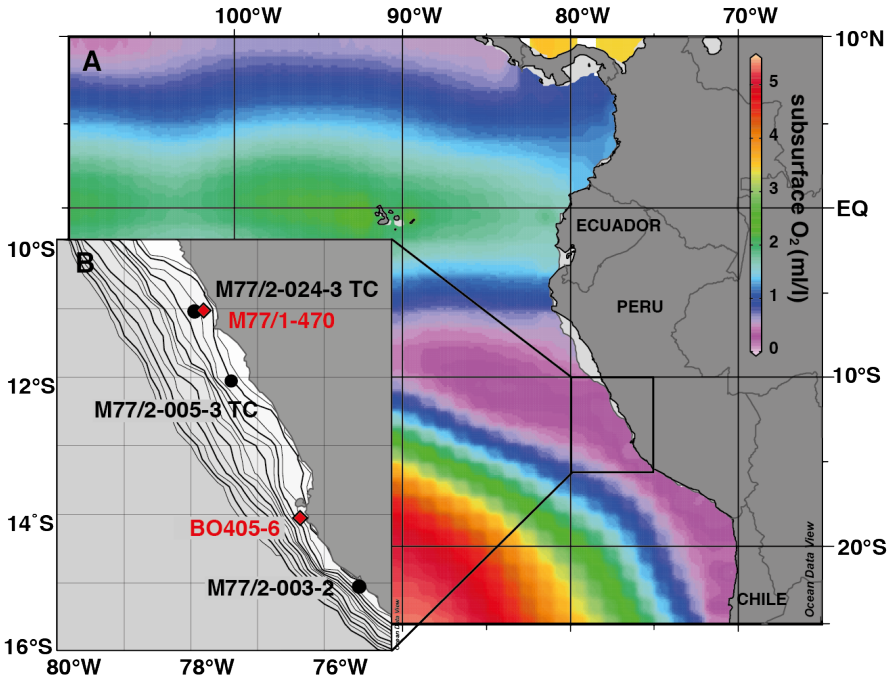

Figure 1: A. Subsurface (150m) oxygen concentration in the Equatorial Pacific. B. Inset map shows locations of cores M77/2-024-5, M77/2-005-3, M77/2-003-2TC and BO405-6 in more detail. The bathymetry is given for 0 to 1000 m water depth in 50 m increments.

Along the central Peruvian shelf (10-12°S) the subsurface $\delta^{15}N_{NO3-}$ values increase southward due to denitrification, resulting in a subsurface source value of +9‰ for the $\delta^{15}N_{NO3-}$ (after *Mollier-Vogel et al.*, [2012]). There, both $\delta^{30}Si_{bSi}$ and $\delta^{15}N_{bulk}$ reflect increasing nutrient utilization associated with increasing upwelling intensity and productivity, assuming source water mass values of +9‰ for $\delta^{15}N_{NO3-}$ and +1.5‰ for $\delta^{30}Si(OH)_4$, and a nutrient utilization of 1:1 of $Si(OH)_4$ and NO_3^-. At the southernmost shelf (12°S – 17°S) highest productivity and upwelling intensity prevail, leading to a further increase in the subsurface $\delta^{15}N$ signature up to +11.5 ‰ (averaged value for 13-16°S) [*Mollier-Vogel et al.*, 2012].

2. Material and Methods

2.1 Core locations and age models

All data in this study was measured on three short, fine-laminated Trigger cores retrieved from the main upwelling region off the Peruvian margin during the German R/V Meteor cruise M77/2 in 2008 as part of the Collaborative Research Center (SFB) 754. New records of $\delta^{30}Si_{bSi}$ and biogenic opal (bSi) concentrations were generated for core M77/2-024-5 TC (11°05'S, 78°00'W, 210 m water depth), M77/2-005-3 TC (2°05'S, 77°40'W, 214 m water depth) and core M77/2-003-2 TC (15°06'S, 75°41'W, 271 m water depth). The age models were taken from the previously published study of Fleury et al. [2015]. The age model of core M772-003-2 was established through the combination of ^{210}Pb and ^{14}C analysis and cores M772-005-3 and M772-024-5 were correlated to the reference core M77/2-003-2, which spans the longest time period.

2.2 Biogenic opal and Silicon isotope analyses

The amount of biogenic opal (bSi) in the sediments was measured following an automated leaching method using sodium hydroxide described by [*DeMaster*, 1981; *Müller and Schneider*, 1993] with a precision of 1-2% (1σ). The total C content was determined by combustion of the sediment samples using a Carlo–Erba element analyzer (NA 1500).

For the silicon isotope measurements diatoms were extracted from the sediment by (1) chemical and (2) physical cleaning (11 and 32µm sieve; heavy liquid separation with a sodium polytungstate solution set at 2.15 mg/l) as described in detail in *Ehlert et al.* [2012; 2013] and *Doering et al.* [2016]. For all samples the purity of the small diatom fraction was evaluated via light microscopy prior to dissolution and only pure (>95%) diatom samples were treated further. All samples were dissolved in 1 mL 0.1 M NaOH and treated with 200 µL concentrated H_2O_2 (Suprapur). Sample solutions were diluted with 4 mL MQ water and neutralized with 0.1 mL 1 M HCl [*Reynolds et al.*, 2008], followed by a chromatographic purification with 1 mL pre-cleaned AG50W-X8 cation exchange resin (BioRad, mesh 200-400) [*de Souza et al.*, 2012]. The Si isotope ratios were determined in 0.6 ppm sample solutions on a *NuPlasma HR* MC-ICPMS at GEOMAR applying a standard-sample bracketing method [*Albarède et al.*, 2004]. Silicon isotope compositions are reported in the δ-notation relative to the reference standard NBS28 in parts per thousand ($\delta^{30}Si = ((R_{sample}/R_{standard}) - 1) * 1000$), where R_{sample} is the $^{30}Si/^{28}Si$ ratio of the sample and $R_{standard}$ is the $^{30}Si/^{28}Si$ ratio of the NBS28. All $\delta^{30}Si$ measurements were run at least in triplicates, with uncertainties ranging between between 0.05‰ and 0.27‰ (2σ). Long-term repeated measurements of the reference materials NBS28, IRMM018, and Big Batch gave average $\delta^{30}Si$ values

of 0.00 ± 0.24‰ (2 σ), 1.40 ± 0.21‰ (2 σ) and 10.60 ± 0.25‰ (2 σ), respectively. Overall, the external reproducibility was within the long-term precision of ±0.23‰ (2 σ).

3. Results and discussion

The climate of the last millennium is generally divided into three climatic phases including the Current Warm Period (CWP; beginning around AD 1800-1850), the Little Ice Age (LIA; between AD 1450 and AD 1850) and the Medieval Warm Period (MWP; between AD 1100 and AD 1375). Off Peru, the CWP and MWP have been characterized by high upwelling, productivity and N-loss processes [*Sifeddine et al.*, 2008; *Gutiérrez et al.*, 2009; *Salvatteci et al.*, 2014; *Fleury et al.*, 2015], whereas, the Little Ice Age (LIA; ~200 to 400 years BP) has been shown to be characterized by low productivity and denitrification intensity for the present main upwelling area between 10°S and 15°S [*Sifeddine et al.*, 2008; *Díaz-Ochoa et al.*, 2009; *Gutiérrez et al.*, 2009; *Salvatteci et al.*, 2014]. Past reconstructions agree that latter conditions were a consequence of larger scale climatic changes induced by weakening of the Walker circulation, reduction of the South Pacific subtropical High and a southward shift of the mean position of the Intertropical Convergence Zone and the associated precipitation belt [*Sifeddine et al.*, 2008; *Gutiérrez et al.*, 2009; *Sachs et al.*, 2009; *Salvatteci et al.*, 2014; *Fleury et al.*, 2015]. These climate changes are thought to have caused a deepening of the nutricline and diminished surface productivity, and thus more oxygenated subsurface waters, accompanied by a decrease in surface productivity (bSi concentrations, this study, [*Ehlert et al.*, 2015]; Si/Fe [*Fleury et al.*, 2015]; TOC [*Gutiérrez et al.*, 2009]; bSi and TOC [*Salvatteci et al.*, 2014]) further matched by a strong reduction in sedimentary redox sensitive trace metals molybdenum (Mo) and rhenium (Re) in the sediments, which indicate increased bottom-water oxygenation during the LIA (Fig. 3. d; [*Sifeddine et al.*, 2008; *Salvatteci et al.*, 2014]).

All in all, the well-studied biogeochemical evolution of the Peruvian shelf over the last millennium and the significant differences in productivity and subsurface oxygenation between the CWP and the LIA are the basis to gain more insights into the relationship between nutrient utilization and denitrification via past $\delta^{30}Si_{bSi}$ and bulk sedimentary $\delta^{15}N$ records.

3.1 Latitudinal changes in biogenic opal production and silicate consumption over time

The data of the three sediment cores from the shelf area between 11°S and 15°S presented here show that diatom productivity, and $Si(OH)_4$ utilization, reconstructed via bSi concentrations and $\delta^{30}Si_{bSi}$ values, were generally lower

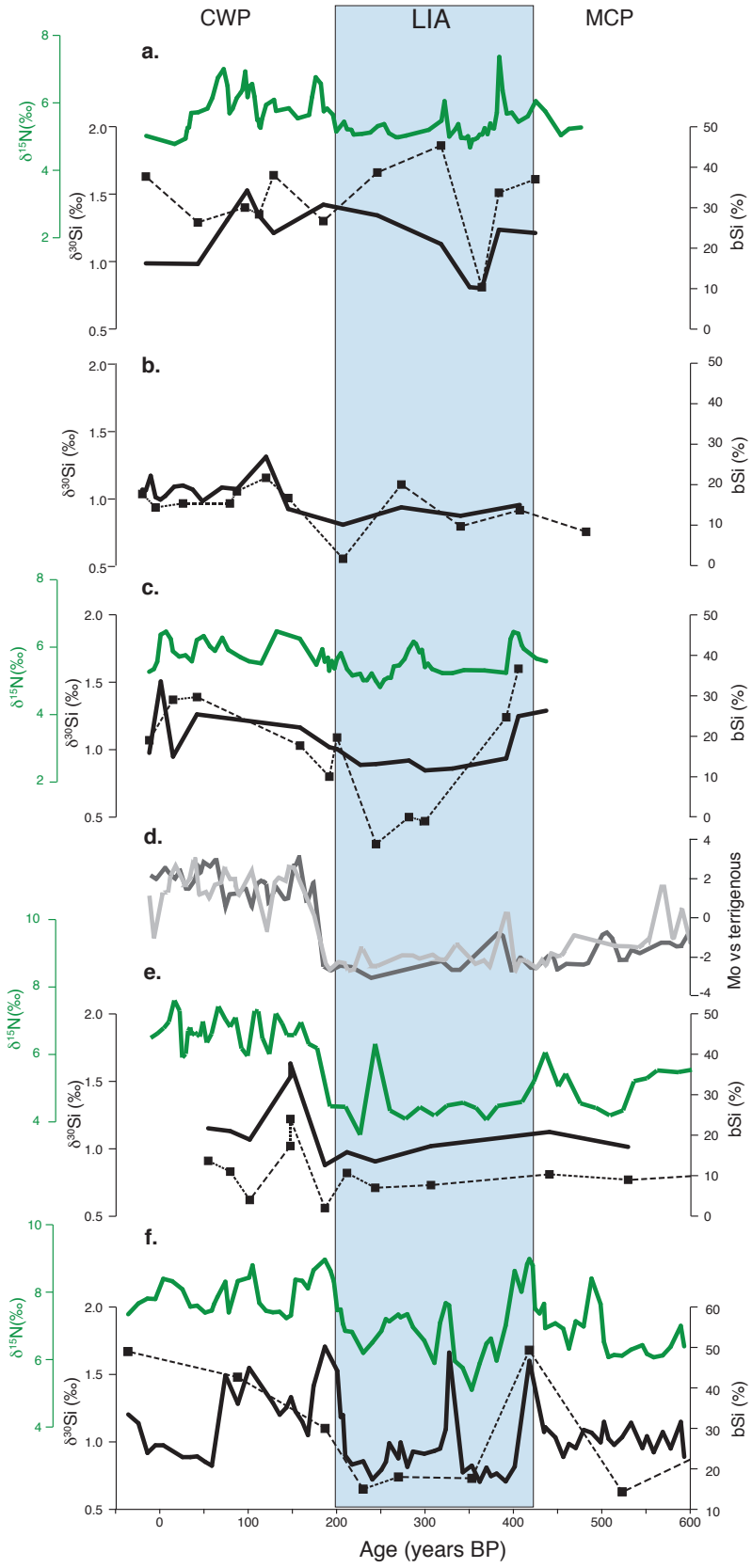

Figure 2: Downcore comparison for $\delta^{15}N$ (‰), bSi (%), $\delta^{30}Si$ (‰) and Mo vs terrigenous of cores: a.) M77/2-024-5TC, b.) M77/1-470 [*Ehlert et al.*, 2015], c.) M77/2-005-3TC, d.) BO405-13 and -6 [Sifeddine et a., 2008], e.) B0405-6 [*Ehlert et al.*, 2015; *Gutierrez et al.*, 2009] and f.) M77/2-003-2TC.

Table 1: Downcore record of core M77/2-024-5TC for $\delta^{30}Si$ (‰) and bSi content (wt%). 2σ represents the external reproducibilities of repeated sample measurements.

Age yrs BP	depth (mm)	bSi (wt %)	$\delta^{30}Si$ (‰)	2 σ
-39	0	16.2	1.63	0.21
-17	45	16.1	1.29	0.21
41	115	34.3	1.40	0.15
71	135	29.3	1.35	0.23
81	160	23.7	1.64	0.14
131	215	30.7	1.30	0.12
166	265	28.1	1.66	0.22
184	305	21.0	1.86	0.13
261	395	10.1	0.81	0.19
288	435	24.6	1.51	0.16
354	475	23.8	1.61	0.08

Table 2: Downcore record of core M77/2-005-3TC for $\delta^{30}Si$ (‰) and bSi content (wt%). 2σ represents the external reproducibilities of repeated sample measurements.

Age yrs BP	depth (mm)	bSi (wt %)	$\delta^{30}Si$ (‰)	2 σ
-19	0	15.9	1.15	0.17
21	40.00	15.0	1.37	0.11
51	70.00	25.4	1.39	0.18
106	125	18.8	1.03	0.18
146	165	17.3	0.80	0.22
171	190	15.1	1.09	0.16
226	245	13.1	0.30	0.21
276	295	14.0	0.50	0.15
306	325	11.6	0.47	0.20
351	370	14.5	1.24	0.24
371	390	25.0	1.60	0.19

Table 3: Downcore record of core M77/2-003-2TC for $\delta^{30}Si$ (‰) and bSi content (wt%). 2σ represents the external reproducibilities of repeated sample measurements.

Age yrs BP	depth (mm)	bSi (wt %)	$\delta^{30}Si$ (‰)	2 σ
-50	0	39.2	1.67	0.18
45	95	40.5	1.48	0.05
128	175	41.9	1.10	0.26
164	205	20.8	0.65	0.23
195	240	23.9	0.74	0.13
262	305	19.4	0.73	0.27
314	355	46.7	1.68	0.10
401	440	29.1	0.63	0.12
499	535	40.6	1.02	0.14
530	565	42.0	1.10	0.13
587	620	49.5	1.03	0.12
639	670	53.5	1.28	0.13
690	720	28.7	1.00	0.13
732	760	26.0	0.61	0.07

during the Little Ice Age (LIA; Fig 2; Tables 1-3) than during the Current Warm Period (CWP). The data shows an increase in bSi content from mean values of 19±7% at 11°S, 16±5% and 24±8% at 15°S during the LIA to values of up to 21±7%, 25±7% and 32±8% during the CWP, respectively. Similarly, the $\delta^{30}Si$ records follow a similar trend of lower $\delta^{30}Si$ mean values of +0.87±0.51‰ and +0.71±0.05‰ during the LIA, in contrast to mean values of +1.48±0.16‰,

+1.13±0.25‰ and +1.42±0.29‰ during the CWP, respectively. The bSi concentrations and $\delta^{30}Si$ records of cores M77/2-005-3TC at 12°S and 003-2TC at 15°S indicate lowest bSi and $\delta^{30}Si$ values during the LIA, similar to previously reported records of cores M77/1-470 at 11°S and B0405-6 at 14°S [*Ehlert et al.*, 2015]. Moreover, the bSi concentrations and $\delta^{30}Si$ values in these cores show overall positive relationships with R^2 =0.48 and R^2=0.47. However, there is no significant relationship between bSi and $\delta^{30}Si$ observed for core M77/2-024-5TC (R^2=0.18) at 11°S and the bSi and $\delta^{30}Si$ values are not substantially different between the LIA and CWP. Furthermore, the mean bSi of 20±7% and $d^{30}Si$ values of +1.48±0.16‰ during the LIA are significantly higher than the mean bSi of 13±2% and $d^{30}Si$ of +0.87±0.15‰ of the nearby core M77/1-470 (Fig. 2b; *Ehlert et al.*, [2015]). This might be explained by limited $Si(OH)_4$ supply at site M77/2-024-5 during the LIA resulting in an increased degree of silicate utilization without inducing enhanced productivity. However, due to the close proximity of core M77/1-470, it is unlikely that the $Si(OH)_4$ supply was significantly different at site M77/2-024-5. Furthermore, other productivity proxies such as the Si/Fe ratio and the total diatom abundance previously shown for core M772-024-5TC do not indicate similarly high biogenic opal production during the LIA [*Fleury et al.*, 2015]. However, the finely laminated sediments also indicate short periods of higher productivity during the LIA (for details see *Fleury et al.*, [2015]). Accordingly, the high mean bSi and $\delta^{30}Si$ values obtained from core M77/2-024-5TC could be an artifact of the low sample resolution.

As previously shown the $\delta^{15}N$ values of the three cores presented in this study were slightly lower with mean values of 5.2±0.35‰, 5.5±0.41‰ and 6.8±0.75‰ during the LIA, than the mean $\delta^{15}N$ values of 5.8±0.36‰, 5.9±0.56‰ and 7.9±0.50‰ during the CWP [*Fleury et al.*, 2015]. The observed trend in $\delta^{15}N$ reported for core M77/2-003-2TC is similar to the previously published $\delta^{15}N$ record of core BO405-6 located at 14°S (Fig. 3 e; *Gutiérrez et al.*, [2009]. Overall, productivity and nutrient utilization proxies (bSi and $\delta^{30}Si$) varied in phase with $\delta^{15}N$ (Fig. 2).

3.2 Respective imprints of nutrient utilization versus denitrification on the records

Along the Peruvian shelf the present-day surface sediment $\delta^{15}N$ values have shown increasing values from 4‰ to 10‰ from the equator to 17°S, reflecting a southward increase in subsurface source water NO_3^- isotopic compositions from 5‰ to 14.5‰ due to ongoing denitrification (Fig. 3a; *Mollier-Vogel et al.*, [2012]). Besides this southward increase in the influence of denitrification on subsurface waters, the $\delta^{15}N$ values where shown to reflect a high degree of NO_3^- utilization north of 10°S, where subsurface $\delta^{15}N$ still remains close to the preformed $\delta^{15}N_{NO3-}$ source of 5‰ delivered to the area, while further South (12°S – 17°S) lower NO_3^- utilization only records part of the observed increase

in subsurface $d^{15}N_{NO3-}$ of up to 14.5‰ via denitrification [*Mollier-Vogel et al.*, 2012]. In contrast, $\delta^{30}Si_{bSi}$ signatures of small mixed diatoms in surface sediments were previously shown to increase southwards associated with increased productivity and upwelling intensity [*Doering et al.*, 2016]. Accordingly, $\delta^{30}Si_{bSi}$ values reflect lowest $Si(OH)_4$ utilization north of 10°S, while the degree of utilization increases southwards with upwelling conditions and productivity [*Doering et al.*, 2016]. Overall, along the entire margin $\delta^{30}Si_{bSi}$ to $\delta^{15}N_{bulk}$ ratio are controlled by different degrees nutrient utilization, assuming $\delta^{30}Si(OH)_4$ source value of +1.5‰ as and increasing $\delta^{15}N_{NO3-}$ source water signatures equal to +5‰, +9‰ and +11.5‰ at 11, 12 and 15°S respectively, due to N-loss (Fig. 3a). Given that the records presented here (excluding bSi and $\delta^{30}Si_{bSi}$ data for core M77/2-24-5TC) and previously from the shelf area between 11°S and 15°S (Fig. 2 a-f) indicate significant changes in upwelling intensity, productivity and subsurface oxygenation between the CWP and the LIA, we present similar $\delta^{30}Si_{bSi}$ to $\delta^{15}N_{bulk}$ correlations for these time periods accordingly (Fig. 3 b, c).

Furthermore, we apply estimations of the degree of surface water nutrient utilization based on the stable isotope composition of Si. Generally, the degree of nutrient utilization can be described assuming either Rayleigh-type (single input followed by no additional nutrients newly supplied to a particular parcel of water followed by fractional loss as a function of production and export) or steady-state (continuous supply and partial consumption of nutrients causing a dynamic equilibrium of the dissolved nutrient concentration and the product) fractionation behavior [*Mariotti et al.*, 1981]. For means of simplification we will only provide the values derived from steady state fractionation, which was shown to better reflect upwelling conditions off Peru [*Ehlert et al.*, 2012]. For this calculation we apply fractionation factors of –1.1‰ ($\delta^{30}Si$) and –5‰ ($\delta^{15}N$) and assume a constant source water signature of +1.5‰ for $\delta^{30}Si(OH)_4$ (i.e. the mean $\delta^{30}Si(OH)_4$ of the PCUC).

3.2.1 The Current Warm Period

The correlation of $\delta^{30}Si_{bSi}$ to $\delta^{15}N_{bulk}$ for the CWP shows that the isotopic compositions of cores M77/2-005-3 and B0405-6 generally plot close to the utilization lines assuming +9‰ as $\delta^{15}N_{NO3-}$ source (present-day 10-12°S, respectively). Unlike present-day data, the correlation at 11°S (M77/2-024-5TC) shows highest $\delta^{30}Si_{bSi}$ and $\delta^{15}N_{bulk}$ values during the CWP, reflecting high nutrient utilization close to 100% for both nutrients. Furthermore, while mean $\delta^{15}N_{bulk}$ values clearly increase between 11°S to 14°S from +5.8‰ (M77/2-005-3) to +6.8‰ (B0405-6), the mean $\delta^{30}Si_{bSi}$ values decrease from +1.1±0.25‰ to +0.9±0.22‰. Accordingly, $Si(OH)_4$ utilization decreases from near complete utilization at 11°S, over 70% at 12°S, to 50% at 14°S. If we assume equivalent

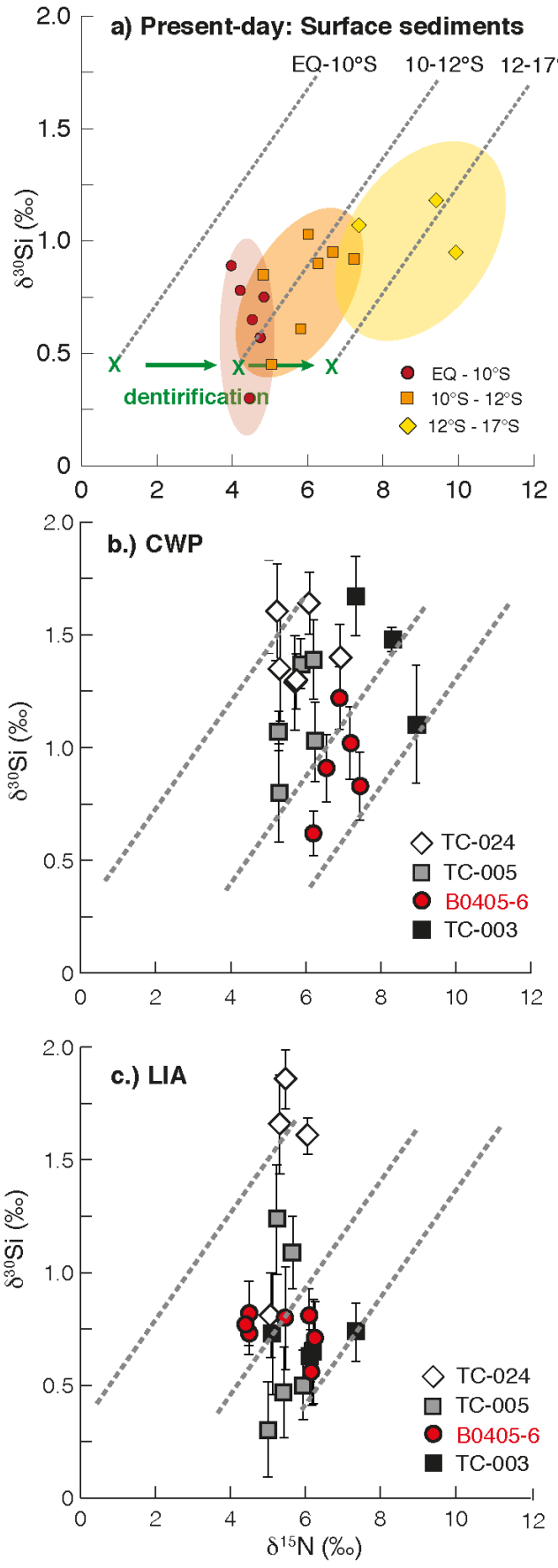

Figure 3: Correlation of $\delta^{30}Si$ (‰) versus $\delta^{15}N$ (‰) for a.) surface sediments (modified after Ehlert et al., 2015), and cores M77/2-024-5TC (white diamonds), 005-3TC (grey squares), 003-2TC (black squares) and BO405-6 (red circles; Ehlert et al., [2015]), over b.) the CWP and c.) the LIA. The grey dashed lines indicate 1:1 utilization of $Si(OH)_4$:NO_3^- for the area between the EQ and 10°S, 12°S to15°S and 15°S to 17°S. The green crosses and arrows indicate the present-day increase in subsurface $\delta^{15}N_{NO3-}$ due to denitrification. Data points that plot above the utilization curves reflect predominant $Si(OH)_4$ limitation, whereas data points below record stronger NO_3^- limitation.

utilization for both $Si(OH)_4$ and NO_3^- (i.e. 70% and 50%) the calculated source water signatures of $\delta^{15}N_{NO3-}$ increased from +5‰ at 11°S to +7.5‰ at 12°S and +9.5‰ at 14°S. In comparison to these estimations, the $\delta^{30}Si_{bSi}$ and $\delta^{15}N_{bulk}$ values at 15°S (M77/2-003-2TC) do not simply fall on a 1:1 utilization line for $Si(OH)_4$ and NO_3^- . For this core only three $\delta^{30}Si_{bSi}$ values were measured indicating a relatively high variability between values of +1.1±0.26‰ and +1.67±0.18‰. Accordingly, $Si(OH)_4$ utilization varies between 60% and ~100%, respectively. Despite this variability the $\delta^{15}N$ values are similar with a $\delta^{15}N_{mean}$ of +8±0.5‰. However, even though the $Si(OH)_4$ utilization does not indicate a clear trend during the CWP at 15°S, the $\delta^{15}N$ indicates that the increased subsurface $\delta^{15}N_{NO3-}$ of +9.5‰ calculated for 14°S also concerns the core location at 15°S.

On the whole, while $\delta^{30}Si_{bSi}$ seems to have been higher during the CWP in comparison to present-day surface sediment values, the $\delta^{15}N_{bulk}$ values and calculated subsurface $\delta^{15}N_{NO3-}$ source values indicate a similar southwards increase from +5‰ to +9.5‰ during the CWP. Thus, we suggest that the net increase in $\delta^{15}N_{bulk}$ from North to South resembles the modern increase caused by denitrification in subsurface waters.

3.2.2 The Little Ice Age

The correlation of $\delta^{30}Si_{bSi}$ and $\delta^{15}N_{bulk}$ during the LIA shows that the values at the different core locations also do not simply fall on the 1:1 utilization line. The range of $\delta^{15}N_{bulk}$ is much smaller centered at about 5‰, while that for $\delta^{30}Si_{bSi}$ varies at a much larger spread between +0.3‰ and +1.7‰ compared to the CWP. The $\delta^{30}Si_{bSi}$ to $\delta^{15}N_{bulk}$ values of core M77/2-024-5TC at 11°S indicate both high $Si(OH)_4$ and NO_3^- utilization similar to the conditions observed during the CWP. Accordingly, this would indicate near complete utilization of both nutrients assuming source signatures of +1.5‰ and +5‰, respectively. However, as discussed above, the $\delta^{30}Si_{bSi}$ and thus $Si(OH)_4$ utilization in core M77/1-470 was significantly lower, with a $\delta^{30}Si_{bSi}$ of +0.87‰ and approximate $Si(OH)_4$ utilization of 43%. Similarly, the values of core M772-005-3TC at 12°S indicate a high variability in $\delta^{30}Si_{bSi}$ between +0.3‰ and +1.2‰, while $\delta^{15}N_{bulk}$ remains between +4.8‰ and +6.5‰, which either reflects a high degree of NO_3^- utilization of a source water $\delta^{15}N_{NO3-}$ of roughly +5‰, or the low utilization of a higher $d^{15}N_{NO3-}$ source. As subsurface oxygenation was higher during the LIA (Fig. 2d, Mo record [*Sifeddine et al.*, 2008]), and productivity (bSi records) and upwelling (based on the diatom assemblage [*Fleury et al.*, 2015]) were both reported to be reduced during the LIA, an increase in $\delta^{15}N_{NO3-}$ source water value can be excluded. However, under prevailing El Niño-like conditions during the LIA atmospheric and oceanic circulation was different. A weak Walker circulation and weakened winds driving the upwelling, as a consequence of the SPSH contraction [*Salvatteci et al.*, 2014], caused a deepening of the

thermocline Although the source depth of upwelling water remained the same during recent El Niño events (i.e., 50-100 m) upwelling delivers only warm, nutrient-poor waters to the surface [*Huyer et al.*, 1987]. This may have changed the source water isotopic signatures and would therefore impact also the degree of nutrient utilization. Unfortunately, there are to date no $\delta^{15}N_{NO3-}$ values of the water column measured during El Niño events. Instead, if we assume a constant $\delta^{15}N_{NO3-}$ source values (+5‰) the steep correlation of $\delta^{30}Si_{bSi}$ to $\delta^{15}N_{bulk}$ observed for cores M77/2-024-5 and M77/2-005-3TC implies that the Peruvian upwelling system has rather been $Si(OH)_4$-limited during that time, which is similar to the present day north of 10°S.

Moreover, the comparison of the $\delta^{30}Si_{bSi}$ to $\delta^{15}N_{bulk}$ values of core M77/2-003-2TC indicates a similar trend as the previously published data of core B0405-6, with low $\delta^{30}Si_{bSi}$ values of +0.71±0.05‰ and +0.77±0.04‰, but strongly increasing $\delta^{15}N_{bulk}$ values from +5.1‰ to +8.6‰ and from +4.4‰ to +6.2‰ (Fig. 3 c). The most likely explanation is that NO_3^- limitation occurred at these locations during the LIA, given that an increase caused by denitrification is unlikely due to the higher subsurface oxygenation observed for the area [*Sifeddine et al.*, 2008; *Salvatteci et al.*, 2014].

Conclusions

We present a latitudinal comparison of $\delta^{30}Si_{bSi}$ and $\delta^{15}N$ records along the Peruvian shelf between 11°S and 15°S over the past 600 years. It was previously shown that during the last 600 years, upwelling intensity and productivity were overall weaker and subsurface oxygenation was higher during the Little Ice Age (200-400 years BP), while the opposite was the case during the CWP and MWP. While most reconstructions considered the nitrogen isotopic ratio as a tracer of denitrification, a recent study comparing $\delta^{30}Si_{bSi}$ and $\delta^{15}N_{bulk}$ compositions in surface sediments and downcore record off Peru pointed to nutrient utilization as the dominant process driving past $\delta^{15}N$ values. Therefore, the aim of this study was to successfully trace both nutrient utilization (under the from of NO_3^-) and denitrification and quantify their respective influence on the records along the Peruvian margin during the past 600 years.

As denitrification was shown to increase southward along the shelf today, we applied a latitudinal correlation between $\delta^{30}Si_{bSi}$ and $\delta^{15}N_{bulk}$ based on the compilation of three new records along with previously published archives. Our results indicate that during the LIA, when productivity was low and subsurface oxygenation was higher, both $\delta^{30}Si_{bSi}$ and $\delta^{15}N_{bulk}$ where controlled generally by either $Si(OH)_4$ or NO_3^- utilization, in agreement with previous findings. Based on the latitudinal comparison of $\delta^{30}Si_{bSi}$ and $\delta^{15}N_{bulk}$ during the CWP we show that the isotopic compositions of both nutrients have mainly been driven by the degree of nutrient consumption at each core location. In parallel, highest $\delta^{15}N_{bulk}$

values reaching up to 8‰ and larger are only measured in cores south of 14°S. This implies that the effect of denitrification on the source water signature of $\delta^{15}N_{NO3-}$ is clearly detectable only in records from this latitude. It may be further implied from this finding that the source water signature of $\delta^{15}N_{NO3-}$ increased from North to South due to denitrification, resulting in values of +5‰ to +9.5‰, in the past 600 years has been similar to modern observations.

Acknowledgement

This work is a contribution of the Collaborative Research Project 754 "Climate-Biogeochemistry interactions in the Tropical Ocean" (www.sfb754.de), which is supported by the Deutsche Forschungsgemeinschaft (DFG).

Chapter IV. Disentangling deglacial biogeochemical cycling of nutrients off Peru based on bulk sediment and diatom-bound $\delta^{15}N$ records

Kristin Doering [1,2*], Rebecca S. Robinson[3], Philippe Martinez[4], Claudia Ehlert[5], Martin Frank[2] and Ralph Schneider[1]

[1]Institute of Geosciences, University of Kiel, Ludewig-Meyn-Str. 10, 24118 Kiel, Germany
Phone: +49-431-600-2267
[2]GEOMAR Helmholtz Centre for Ocean Research Kiel, Wischhofstr. 1-3, 24148 Kiel, Germany
[3]Graduate School of Oceanography, University of Rhode Island, Narrangasett, RI, United States
[4]EPOC, UMR CNRS 5805 OASU, Université de Bordeaux, Allée Geoffroy Saint Hilaire, 33615 Pessac cedex, France
[5]Max Planck Research Group - Marine Isotope Geochemistry, Carl von Ossietzky University (ICBM), Carl-von Ossietzky-Str. 9-11, 26129 Oldenburg, Germany

Manuscript in preparation

Abstract

Bulk sedimentary nitrogen isotopes ($\delta^{15}N_{bulk}$) are a common tool to infer past changes of the marine N cycle. By direct comparison with diatom-bound nitrogen isotope compositions ($\delta^{15}N_{db}$) we investigate potential biases induced by diagenesis of the organic matter (OM) in order to reliably reconstruct past variations of the biogeochemical cycles in the upwelling area off Peru. Overall, no significant influence of OM quality on the $\delta^{15}N_{bulk}$ records was detectable, given that the $\delta^{15}N_{db}$ values were generally identical within 2‰ of the $\delta^{15}N_{bulk}$ values of the same samples. We suggest that the lower $\delta^{15}N_{bulk}$ values likely reflect a lower annual/mean signal, while diatom-bound records reflect a higher seasonal $\delta^{15}N$ signal of upwelled waters influenced by denitrification.

Supported by a very similar pattern of temporal variation in the $\delta^{15}N_{db}$ record we present a compilation of a new $\delta^{15}N_{bulk}$ record and two previously published ones covering the Peruvian shelf between 9°S and 15°S to investigate changes in the N cycle during the past 20,000 years. All three records support the previous observation of elevated $\delta^{15}N$ values during Termination1 (8 to 11‰) and much lower values during the end of the Glacial and the Holocene (4 to 7‰). Correlation of $\delta^{30}Si_{bSi}$ and $\delta^{15}N$ indicated that all records are generally

controlled by nutrient utilization. However, additionally denitrification consistently increases the subsurface source signature of $\delta^{15}N_{NO3-}$ by ~1.5‰, which is recorded during the complete time. Accordingly, we suggest that higher deglacial $\delta^{15}N$ are caused by higher preformed $\delta^{15}N_{NO3-}$ delivered to the Equatorial Pacific as well as by reduced N_2 fixation due to enhanced bottom-water oxygenation and reduced iron and phosphate release during Termination 1, rather than by enhanced denitrification as previously suggested.

Keywords: nitrogen isotopes; silicon isotopes; diatoms; denitrification; Peruvian Coastal Upwelling Ecosystem

1. Introduction

1.1 Reconstructing the marine N cycle based on nitrogen isotope measurements

The inventory of total fixed nitrogen (N) in the ocean and its availability in the surface waters are important controls on primary production (Dugdale and Goering, 1967). Variations of both the N inventory and primary productivity have significant implications for the modern and past global biogeochemical cycling (Galbraith and Jaccard, 2015; Moore et al., 2013).

During primary productivity phytoplankton preferentially take up the lighter isotope of nitrate ($^{14}NO_3^-$) from seawater into the newly formed organic matter (OM), leaving the residual dissolved nutrients enriched in the heavier isotopes (Altabet et al., 1991; Wada and Hattori, 1978). With increasing utilization rates the dissolved NO_3^- in surface water becomes consequently progressively enriched in ^{15}N, resulting in a parallel increase in the isotopic composition ($\delta^{15}N$) of the OM which is produced and exported to the sediments (Altabet and Francois, 2001; Lourey et al., 2003). In oligotrophic marine ecosystems bulk sediment $\delta^{15}N$ ($\delta^{15}N_{bulk}$) was shown to experience an early diagenetic increase of up to 2-5‰ (Altabet and Francois, 1994; Brzezinski et al., 2002; Freudenthal et al., 2001; Robinson et al., 2012; Sigman et al., 1999a). To avoid alteration of past $\delta^{15}N$ reconstructions several studies instead focused on productive continental margin environments (Altabet et al., 1999; Freudenthal et al., 2001a; Kienast et al., 2002; Thunell et al., 2004) or diatom-bound OM (Brunelle et al., 2007; Robinson et al., 2005; Sigman et al., 1999a). These approaches followed the premise that sediments on continental slopes record the $\delta^{15}N_{bulk}$ of exported marine OM with little diagenetic isotopic alteration due to faster particle sinking and OM burial (Ganeshram et al., 2000; Thunell and Kepple, 2004). Whereas, diatom-bound N is thought to be physically protected from early bacterial diagenesis (Shemesh et al., 1993; Sigman et al., 1999a) with the N being native to the OM within diatoms, mainly as amino acids (Ingalls et

al., 2004; Kröger et al., 2000; Poulsen et al., 2003). However, so far only few studies have investigated the modern isotope compositions of such diatom-specific organic N pools from continental margin areas (Kalansky et al., 2011), where seasonally or annually changing oxygen-deficient conditions can cause a dominant role for N-loss processes.

1.2 Nitrogen cycling and N isotope fractionation along the continental margin off Peru

The Peru Upwelling Ecosystem (PUE) is one of the most productive marine ecosystems in the world, which is caused by intense coastal upwelling (cf. Pennington et al., 2006; Zuta and Guillén, 1970). The high surface productivity and OM fluxes cause rapid oxygen consumption in subsurface waters, resulting in one of the globally largest oxygen minimum zones (OMZ). The low oxygen (O_2) levels (2–10 µmol L^{-1}) in the water column along the Peruvian coast cause NO_3^- to be used as an oxidant during OM degradation. This leads to its transformation into N_2 via denitrification and anammox and results in a net loss of bio-available N (Codispoti, 2006; Lam et al., 2009). These N-loss processes are accompanied by pronounced isotope fractionation of 20 ‰, producing isotopically lighter products (N_2 and N_2O), whereas the residual NO_3^- in subsurface waters is rendered isotopically heavy (Brandes et al., 2007; Cline and Kaplan, 1975; Granger et al., 2008; Liu and Kaplan, 1989; Sigman et al., 2009). The intense upwelling delivers the isotopically the heavy NO_3^- to the surface waters where it is taken up by phytoplankton leading to a marked enrichment of ^{15}N in the sinking particulate OM (Altabet, 2006; Altabet et al., 1995; Ganeshram et al., 1995). In addition to the N-loss processes the degree of denitrification recorded by $\delta^{15}N_{bulk}$ signatures in the surface sediments is strongly influenced by the degree of NO_3^- utilization along the shelf (Mollier-Vogel et al., 2012).

Overall, $\delta^{15}N_{bulk}$ records are influenced by the preformed $\delta^{15}N$ of the water mass as well as any process that adds or removes N, such as remineralization or water column denitrification, along its flow path in the subsurface. Thus the sedimentary $\delta^{15}N$ can reflect changes in ocean circulation, the biological pump, and large scale N cycling (Brandes and Devol, 2002; Deutsch et al., 2004; Galbraith et al., 2008; Robinson and Sigman, 2008; Sigman et al., 2009) and may be viewed as a paleoredox proxy for denitrification under suboxic conditions (Galbraith et al., 2004; Jaccard and Galbraith, 2011).

1.3 Past shifts in $\delta^{15}N$ along the Peruvian continental shelf

Sedimentary $\delta^{15}N_{bulk}$ records from the oxygen-depleted region off Peru have been interpreted to reflect past changes in the intensity of subsurface NO_3^- loss linked to the extent and strength of oxygen depletion (Agnihotri et al., 2008; De

Pol-Holz et al., 2007; Gutiérrez et al., 2009). Records from the eastern tropical Pacific (ETP) have shown consistently higher $\delta^{15}N_{bulk}$ values during the last deglacial, (Termination 1 (T1), than to today (De Pol-Holz et al., 2006; Emmer and Thunell, 2000; Ganeshram et al., 2000; Hendy and Pedersen, 2006; Higginson, 2004; Martinez et al., 2006; Pichevin et al., 2010; Salvatteci et al., 2016; Thunell and Kepple, 2004; Verleye et al., 2013). However, differences in the extent and timing of elevated $\delta^{15}N_{bulk}$ signatures have been observed between the eastern tropical North Pacific (ETNP) and South Pacific (ETSP) (Martinez et al., 2006). More precisely, ETNP records display a clear northern hemisphere forcing, whereas changes in the records from the ETSP were in phase with temperature variations in Antarctica (De Pol-Holz et al., 2007; Martinez et al., 2006; Pichevin et al., 2010; Robinson et al., 2007). Overall, the high deglacial $\delta^{15}N$ values were attributed to globally increased (benthic) denitrification linked to enhanced ocean de-oxygenation (Galbraith et al., 2013), although a significant influence by local processes such as enhanced water column stratification could not be ruled out (De Pol-Holz et al., 2006).

Changes in glacial to Holocene variations in the ETP N cycle have been closely linked to variations in the expansion of the eastern Pacific OMZ via transport of highly enriched $\delta^{15}N$ signatures originating from denitrification along the coasts via subsurface currents (Martinez et al., 2006). Although generally elevated $\delta^{15}N$ values off Peru have been reported for T1 in comparison to the Holocene, most likely reflecting enhanced denitrification, productivity was reported to be lower and bottom water oxygenation to be higher during this period of time (Salvatteci et al., 2016). While the latter can be explained by a stronger influence of well-oxygenated Antarctic Intermediate Water (AAIW) along the Peruvian shelf (Muratli et al., 2009; Salvatteci et al., 2016), the reduced local productivity off Peru is inconsistent with higher denitrification. Instead, during T1 the system could also have been shifted towards enhanced coccolithophorid over diatom productivity (Higginson, 2004), which may have been caused by a shift in the nutrient (silicic acid ($Si(OH)_4$) to NO_3^-) delivered from the Southern Ocean.

1.4 Past latitudinal shifts in $\delta^{15}N$ and comparison to past $\delta^{30}Si_{bSi}$ records

The main focus of this study is a comparison of the $\delta^{15}N$ records from three piston cores from 9°S to 15°S. To better evaluate potential diagenetic alteration of the $\delta^{15}N$ signal of the organic matter via winnowing and downslope transport or periodically better bottom-current oxygenation we present a record of diatom-bound $\delta^{15}N$ from the modern high productivity zone (15°S). The analyses of diatom-bound material also provide the possibility to directly compare past shifts in denitrification and nutrient utilization via comparison of $d^{15}N$ signatures with previously published $\delta^{30}Si_{bSi}$ values of diatoms obtained for

the same samples. In contrast to $\delta^{15}N$, the Si isotope composition of $Si(OH)_4$ in surface waters has mainly been controlled by the $Si(OH)_4$ utilization by diatoms, representing the most dominant phytoplankton group in upwelling areas (Brzezinski, 2002; Egan et al., 2012; De La Rocha et al., 1998). Accordingly, the comparison of $\delta^{15}N$ and $\delta^{30}Si_{bSi}$ has been applied previously to differentiate between past changes in nutrient utilization and denitrification of the Peruvian upwelling area (Ehlert et al., 2015).

2. Material and Methods

2.1 Core location and age model

All data presented in this study were obtained from two piston cores collected along the Peruvian Margin during RV Meteor cruise M77/2 conducted within the Collaborative Research Centre 754 - Climate-Biogeochemistry interactions in the Tropical Ocean (SFB 754) and one piston core retrieved during RV Sonne Cruise SO147: M77/2-029-3 (029-3) from 9°S, 444 m water depth; SO147-106KL (106KL) from 12°S, 184 m water depth; and M77/2-003-2 (003-2) from 15°S, 271 m water depth. Records of particulate organic carbon (C_{org}) and $\delta^{30}Si_{bSi}$ of all cores are discussed in Doering et al. (under review at *Paleoceanography*). The $\delta^{15}N_{bulk}$ records of core -029-3 and 003-2 were published previously in Mollier-Vogel (2012). The age models for core 106KL has been previously published by Rein et al, (2005) and for cores 029-3 and 003-2 by Doering et al. (2016).

2.2 Nitrogen isotope measurements of bulk sediments

The $\delta^{15}N_{bulk}$ and total N contents (N_{tot}) were measured at the University of Bordeaux 1 (EPOC, UMR CNRS 5805, France) on 5 to 60 mg of homogenized and freeze-dried bulk sediment. Samples were encapsulated in tin cups and then injected into a Carlo-Erba CN analyzer 2500 coupled directly to a Micromass-Isoprime mass spectrometer, using He as carrier gas. The isotopic ratio is expressed in the delta notation with N_2 of air as standard: $\delta^{15}N = [(^{5}N/^{14}N)_{sample} - (^{15}N/^{14}N)_{standard} / (^{15}N/^{14}N)_{standard}]* 1000$.
The precision of the isotope analyses determined by repeated measurements of selected sediment samples and of international and in-house standards is ±0.2‰.
Accumulation rates of N_{tot} were calculated using the previously determined sedimentation rates (cm ka^{-1}) and dry bulk densities (g cm^{-3}) (Doering et al., under review at *Paleoceanography*).

2.3 Diatom-bound nitrogen isotope measurements

To isolate diatom-bound N, we applied (1) physical separation steps to isolate the diatoms microfossil fraction from the bulk sediment and (2) chemical oxidation of the diatom microfossil fraction to remove labile organic on the exterior of the diatoms.

The physical separation method followed the methodss of Brunelle et al., (2007) and Sigman et al. (1999a): 1.5-4 g freeze-dried sediment was decarbonized with approximately 20 ml of 25% HCl (i.e. 3 parts H_2O and 1 part HCL). Afterwards samples were put into an ultrasonic bath for 10 minutes and then sieved through a 150µm sieve to remove bigger radiolarians. For removal of the clay fraction differential settling was performed (settling ~1.5 hours) and repeated up to 10 times. Finally detrital grains were removed via a heavy liquid separation step (~2.15 g/ml Sodium Poly Tungstate) and samples were filtered through 5 µm polycarbonate filters.

The separated diatom samples were chemically cleaned by a preliminary oxidation of the externally attached organic matter with ~5 ml of 18 M sulfuric acid, ~15 ml saturated potassium permanganate and ~15 ml saturated oxalic acid (Hasle and Fryxell, 1970). In a subsequent reductive cleaning step a heated sodium dithionite solution was used (80°C for 1 h) to remove adsorbed metals, followed by two final 1 h oxidation steps of organic matter using first a diluted (~35%) and then a concentrated (72%) solution of perchloric acid in a 100°C water bath (Horn et al., 2011b; Morales et al., 2013). Splits of the clean, dry diatom samples were dissolved and the organic N was oxidized to nitrate in a 0.22 M potassium persulfate and 1.5 M sodium hydroxide solution in an autoclave at 120°C for 20 min (Bronk et al., 2000; Robinson et al., 2004).

Nitrate concentrations of the persulfate-oxidized frustule N were measured by chemiluminescence after reduction to NO using a Teledyne Instruments (Model 200E) chemiluminescence NO/NO_X analyzer (Braman and Hendrix, 1989). The $\delta^{15}N_{db}$ values were measured by gas chromatography-isotope ratio mass spectrometry (GC-IRMS) on a Thermo Delta V Advantage IRMS at the University of Rhode Island. In total 20 nmol NO_3^- was converted to N_2O by the denitrifier method for introduction into the IRMS (Sigman et al., 2001). The potassium nitrate reference materials IAEA-N3, USGS 32, and USGS 34 (+4.7‰, +180‰, and -1.8‰, respectively) were used to standardize $\delta^{15}N$ results (Gonfiantini et al., 1995; Revesz et al., 1997). Precision was determined by multiple measurements of standards within each run and replicate measurements of samples. Approximately half of the $\delta^{15}N_{db}$ samples were run in duplicate or triplicate resulting in a precision of ±0.5‰.

3. Results

3.1 Accumulation rates of total nitrogen and C/N ratios

The accumulation rates of total nitrogen concentrations (AR_{Ntot}; g cm^{-2} ka^{-1}) in core 029-3 (P°S) range between 0.2 and 1.2 g cm^{-2} ka^{-1}, with highest values of 1.2 and 0.9 g cm^{-2} ka^{-1} early during T1 at 17.5 ka BP and 16.3 ka BP. The AR_{Ntot} decrease continuously from average values of 0.4±0.5 g cm^{-2} ka^{-1} during T1 to 0.1±0.1 g cm^{-2} ka^{-1} during the Holocene (Fig. 1a). In contrast, the AR_{Ntot} in sediment cores 106KL (12°S) and 003-2 (15°S) increase from 0 -0.25 g cm^{-2} ka^{-1} and 0.07-0.16 g cm^{-2} ka^{-1} during T1 to values of 0.16-2.00 g cm^{-2} ka^{-1} and 0-0.55 g cm^{-2} ka^{-1} during the Holocene. Overall, highest AR_{Ntot} values of 1.3 g cm^{-2} ka^{-1} and 2.0 g cm^{-2} ka^{-1} were reached during the late (1.1 to 1.9 ka BP) and the early Holocene (8.9 to 10.1 ka BP) in core 106KL. Instead in core 003-2 highest AR_{Ntot} values occurred during the mid Holocene (Fig. 1a).

The C/N ratios in all three cores presented here remain between 1 and 12.5. Core 003-2 exhibits C/N values in a narrow range between 8.8 and 10.5, with one outlier at 6.8. The C/N ratios of core 106KL range from 9.5 and 12.5. In contrast, highest variability in the C/N ratios is observed in core 029-3 with values continuously increasing from 6 to 11.3 at T1. The highest ratio of 11.3 was reached at 11 ka BP before slightly decreasing to 9.2 during the Holocene (Fig. 1b).

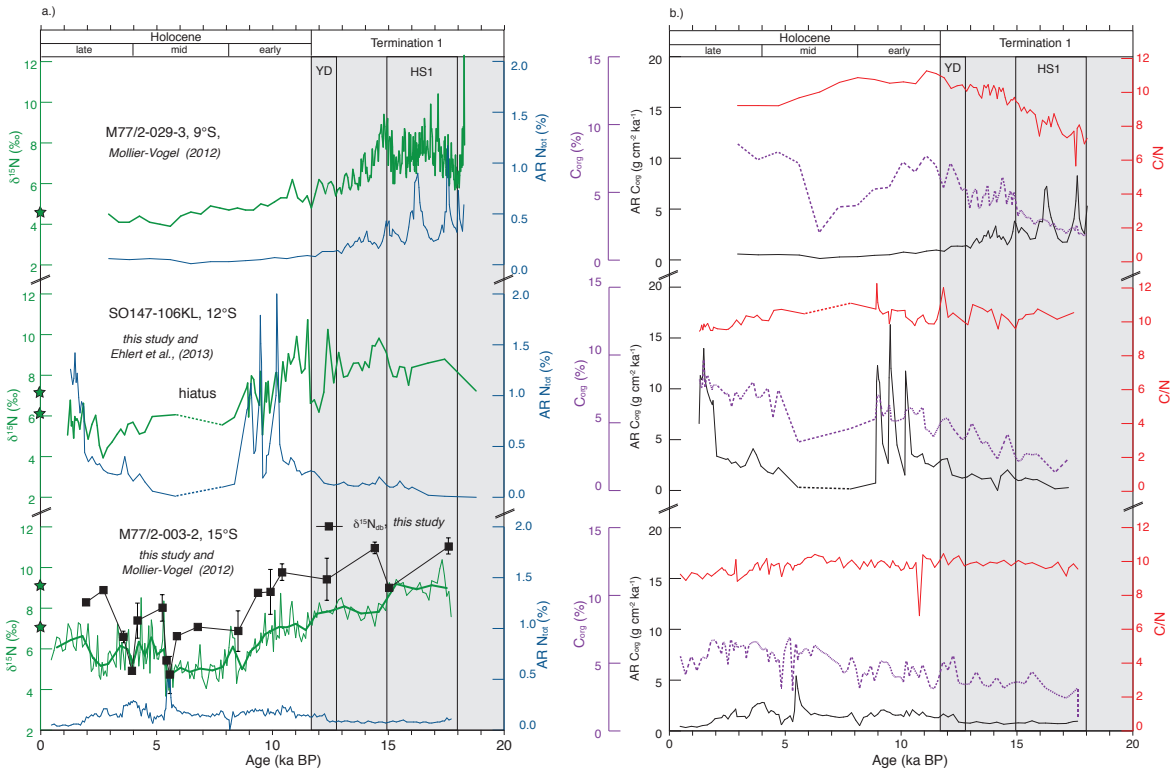

Figure 1: **Figure 1:** Downcore records of cores 029-3, 106KL and 003-2 over the last 20,000 years for a) AR_{Ntot} (blue), $\delta^{15}N_{bulk}$ (green) and $\delta^{15}N_{db}$ (black; only for core M77/2-003-2); and b.) C_{org} (dotted violet line), AR $_{org}$ (black) and the C/N ratio (red). Termination 1, Heinrich Stadial 1 (HS1) and the Younger Dryas (YD) are highlighted. Modern $\delta^{15}N$ of surface sediments are marked with stars. Error bars for $d^{15}N_{db}$ indicate the 1s error based on replicate measurements.

3.2 Nitrogen isotope compositions

The $\delta^{15}N_{bulk}$ values of core 029-3 (9°S) range between +3.9‰ and +12.3‰, with highest $\delta^{15}N$ values during the early T1 until 15 ka BP. At 15 ka BP $\delta^{15}N_{bulk}$ values as high as +9.4‰ are reached before continuously decreasing to +3.9‰ during the late Holocene (Fig. 1b). The $\delta^{15}N_{bulk}$ values of core 106KL (12°S) range between +3.9‰ and +10.7‰, with highest $\delta^{15}N_{bulk}$ signatures during T1. $\delta^{15}N_{bulk}$ values decrease to +6.6 ‰ during the Younger Dryas (YD; 11.7-12.8 ka BP) before increasing again to 10.7 ‰ at the onset of the Holocene. During the early Holocene the $\delta^{15}N_{bulk}$ signal continuously decreased to values of +5.5 ‰ with only small variations during the mid and late Holocene.
The $\delta^{15}N_{bulk}$ values of core 003-2 (15°S) varied between of +3.7 and +10.4‰, with highest $\delta^{15}N_{bulk}$ values during T1. During the early Holocene $\delta^{15}N_{bulk}$ signatures continuously decrease until reaching minimum values of +3.7‰ during the mid Holocene an increase again to during the Late Holocene. In addition to the $\delta^{15}N_{bulk}$ measurements, diatom-bound $\delta^{15}N$ ($\delta^{15}N_{db}$) analyses on samples, were performed on samples of core 003-2. The obtained $\delta^{15}N_{db}$ signatures range from +4.6 to 10.9 ‰ (Fig. 1a) overall following the same as $\delta^{15}N_{bulk}$ values with highest values during the T1 and lower values during the Holocene.

4. Discussion

In this study we discuss a compilation of records of three cores (029-3, 106KL and 003-2) for accumulation rates of C_{org} (Doering et al., under review), N_{tot} and $\delta^{15}N$ of bulk sediments (Mollier-Vogel, 2012 and this study) as well as the first diatom-bound $\delta^{15}N$ record of the PUE. The $\delta^{15}N_{bulk}$ records presented here compare well with existing records from the ETNP (Hendy and Pedersen, 2006; Thunell and Kepple, 2004) and the ETSP (southern Peruvian shelf: Ganeshram et al., 2000; Higginson, 2004; Salvatteci et al., 2016; and Chilean shelf: De Pol-Holz et al., 2006; Martinez et al., 2006) with a progressive increase during Termination 1 and subsequent decrease during the Holocene. However, in comparison to $\delta^{15}N_{bulk}$ records from Chile, which have revealed a decrease during the Antarctic Cold Reversal (Martinez et al., 2006), the records from the Peruvian shelf indicate overall little overlap with the temperature records from Antarctica. Most likely, in the absence of a direct connection with either Antarctic or Northern Hemisphere climate signals (i.e. YD and HS1) suggests a dominant influence of local changes in in the lateral supply of oxygen (ventilation) and in the oxidant demand resulting from local changes in upwelling intensity and associated productivity, or a combination of both.

Although the fidelity of $\delta^{15}N_{bulk}$ records from continental shelf is generally assumed as high sedimentation rates and anoxic conditions prevent diagenetic alteration, surface sediment investigations of the Peruvian shelf

indicate a small influence of winnowing and sporadic oxygenation on $\delta^{15}N$ compositions of the sediments (Arthur et al., 1998; Junium et al., 2015). Evidence for variations in the strength of surface and export productivity, as well as the bottom water oxygenation since the LGM was demonstrated by recent studies applying redox sensitive trace metals (Re/Mo; Salvatteci et al., 2016;) and accumulation rates of biogenic opal (Doering et al., under review). This shows the need for a more detailed evaluation of the past biogeochemical cycling of nutrients in context of global climate changes as well as local environmental variability. Accordingly, the following discussion is divided in two main parts with (1) a detailed evaluation of past C_{org}, N_{tot} and $\delta^{15}N_{bulk}$ records regarding potential OM alteration including a comparison of bulk sediment and diatom-bound $\delta^{15}N$ signatures and (2) a discussion of the $\delta^{15}N$ records based on a comparison with $\delta^{30}Si_{bSi}$ signatures to differentiate between nutrient utilization and variations in the N cycling concerning denitrification, N_2 fixation, NO_3^- utilization, and the total N inventory.

4.1 Evaluation of the preservation of $\delta^{15}N$ from bulk sediments

To assess the potential alteration of $\delta^{15}N_{bulk}$ within the sediments the variability in the C/N ratios is a useful indicator of differential preservation of the C and N pools (Freudenthal et al., 2001; Junium and Arthur, 2007) has been used to constrain the sources or of post-depositional alteration of the OM (Schubert and Calvert, 2001). Generally, low C/N ratios of 5-7 strongly point to OM of marine origin (Redfield, 1963), while terrestrial OM has higher C/N ratios of >20. The C/N records of 029-3, 106KL and 003-2 all range between 1 and 11 (Fig. 1 and Fig. 2), and thus point to a dominant marine source of the OM supporting previous observations from surface sediments (Arthur et al., 1998; Junium et al., 2015). However, while C/N ratios remain rather stable over time within the southern cores 106KL (12°S) and 003-2 (15°S; Fig.1a), the C/N ratios of core 029-3 continuously increase from values of 6 up to 11 throughout T1. This change may either be caused by a shift in the contribution of the OM from different sources or by the preferential degradation of N-enriched organic compounds (Macko and Estep, 1984; Schubert and Calvert, 2001).

Comparison of C/N ratios to the $\delta^{15}N_{bulk}$ records shows no significant correlations in cores 106KL and 003-2 (Fig. 2h-i), which suggests that modification of the $\delta^{15}N_{bulk}$ signal due to preferential N degradation seems insignificant (Kienast, 2000) as well as no contribution of N_{inorg} with a different $\delta^{15}N$ signatures. However, in core 029-3 a negative correlation between C/N and $\delta^{15}N_{bulk}$ (Fig. 2g) may point to diagenetic alteration. If we assume that the observed Holocene to glacial decrease in N_{tot} and C_{org} is caused by diagenesis, we would expect an elevated $d^{15}N$ composition concomitant with the slight increase observed in the C/N ratio towards the Holocene, which is not the case. The Holocene increase of the C/N ratios can in part be explained by selective

removal of labile, nitrogen-bearing compounds during early diagenesis and slow loss of ammonium diffusing from the sediment (Junium and Arthur, 2007). It is possible that diagenesis results in small shifts in bulk $\delta^{15}N$ values in organic matter-rich deposits but it appears more likely that the observed low $\delta^{15}N$ values reflect primary processes. Overall, as the linear relationship between C_{org} and N_{tot} results from mixing of two end members, organic-rich samples are expected to have significantly higher C/N ratios than samples with lower C_{org} contents (Calvert, 2004). Accordingly, variations in the C/N ratios based on shifts in the productivity can be assessed by a further comparison of C/N ratios to the amount of C_{org} for all records (Fig. 2 d-f). While the absence of a significant correlation between the C/N ratio and C_{org} for cores 106KL and 003-2 indicates a positive correlation (R^2=0.48) for core 029-3 most likely indicates a change in productivity between T1 and the Holocene. In summary, observations based on bulk sediment materials suggest no detectable alteration of the $\delta^{15}N_{bulk}$ signature.

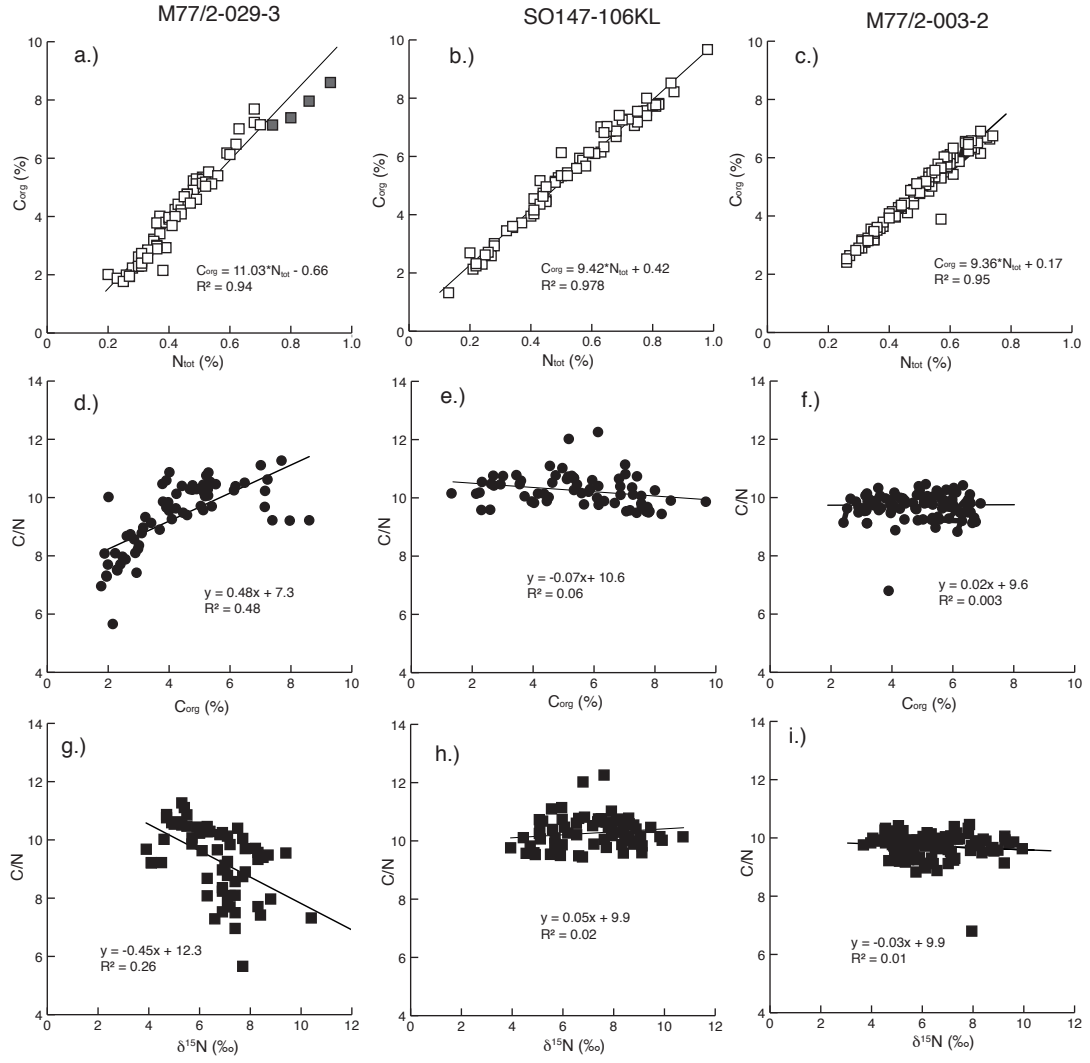

Figure 2: Correlation of C_{org} (%) versus N_{tot} (%), C/N versus C_{org}, and c.) C/N versus $\delta^{15}N$ in core M77/2-029-3, SO1547-106KL and M77/2-003-2.

4.2 Comparison of diatom-bound and bulk sediment $\delta^{15}N$: Do diatoms record the same signal as sediments?

Previously studies suggested that early diagenetic changes of bulk sediment N content and $\delta^{15}N$ do not affect diatom-bound N, which is thought to be physically protected by the microfossil matrix (Hayes et al., 1989; Sigman et al., 1999a). Diagenetically altered $\delta^{15}N_{bulk}$ signatures were found to be generally higher than the corresponding $\delta^{15}N_{b}$ values (Sigman et al., 1999).

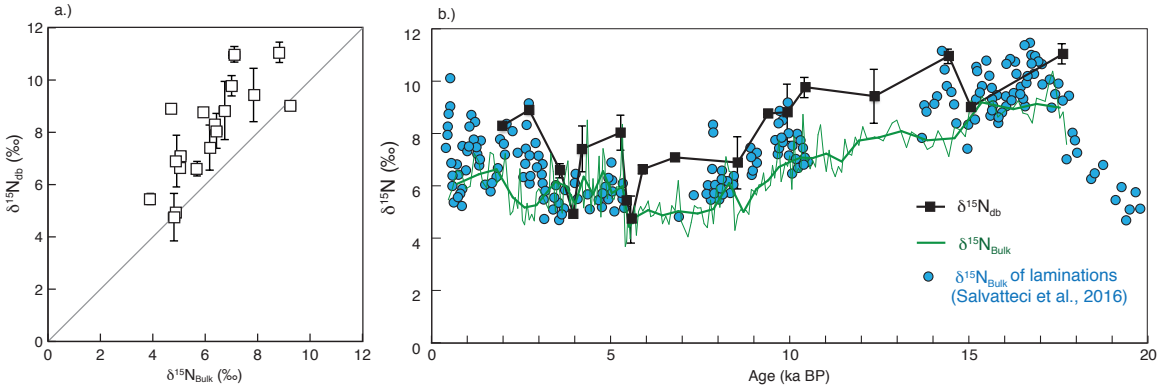

Figure 3: a.) Correlation of diatom-bound and bulk sediment $\delta^{15}N$ measurements of core 003-2. The grey line indicates the 1:1 ratio. Error bars denote the precision of $\delta^{15}N_{db}$ measurement; Error bars of the $\delta^{15}N_{bulk}$ measurements (0.2 σ) are smaller than symbol size. b). Downcore record of $\delta^{15}N$ of bulk sediments (green) and diatom-bound material (black) in comparison to bulk $\delta^{15}N$ values obtained from distinct laminations (Salvatteci et al., 2016).

In general $\delta^{15}N_{db}$ of core 003-2 (15°S) presented here show the same trend as $\delta^{15}N_{bulk}$ but are approximately 2‰ higher (Figs. 1 and 3). A similar correlation of higher $\delta^{15}N_{db}$ than $\delta^{15}N_{bulk}$ was also observed in the Northern Pacific (Brunelle et al., 2007), where, however, a the offset between bulk sediment and diatom-bound $\delta^{15}N$ changed in its extent between glacials and interglacials. This difference was attributed to a change in deep ocean oxygenation and thus the intensity of degradation and remineralization of organic matter. However, although diagenetic alteration of bulk sediments could also lower the $\delta^{15}N_{bulk}$ values, it is commonly rather assumed to increase the signatures thus rendering a diagenetic bias of the $\delta^{15}N_{bulk}$ of core 003-2 unlikely. The difference between $\delta^{15}N_{bulk}$ and $\delta^{15}N_{db}$ of this core 003-2 has remained relatively constant over time with only three overlapping values, one during the T1 and two during the Mid Holocene (Fig. 1 and 3b). A similar relationship was found in modern surface sediments at 13°S with lower $\delta^{15}N_{bulk}$ than compound-specific $\delta^{15}N$ values of chlorins (Junium et al., 2015). These authors suggested that OM was sourced from the shallow shelf and transported downslope, and that $\delta^{15}N_{bulk}$ values were altered during transport and reworking or reflect signals from multiple sources or more ancient OM. For a compilation of different cores close to our core location at 15°S Salvatteci et al., (2016) presented $\delta^{15}N_{bulk}$ values of single laminations ($\delta^{15}N_{bulk\ lamination}$), which allows a more detailed comparison of $\delta^{15}N_{bulk}$ and $\delta^{15}N_{db}$. The downcore comparison of these three records, i.e. $\delta^{15}N_{bulk}$,

$\delta^{15}N_{bulk\ laminations}$ and $\delta^{15}N_{db}$ (Fig. 3b) shows that $\delta^{15}N_{bulk\ laminations}$ has a high variability, whereas $\delta^{15}N_{db}$ values correspond to the highest and $\delta^{15}N_{bulk}$ to the lowest boundaries. Most likely, samples of laminations with values close to $d^{15}N_{db}$ are likely derived from layers consisting mainly of diatoms whereas samples of laminations with lower $\delta^{15}N$ values are closer to the $\delta^{15}N_{bulk}$, consisting of a mixture or different OM. Such an observation of high $\delta^{15}N$ signal derived from diatoms is not unexpected, as diatom blooms are associated with intense upwelling conditions and high PP. Thus, diatoms are expected to incorporate the higher $\delta^{15}N$ of NO_3^- of upwelled subsurface water labeled by N-loss processes. In summary, both $\delta^{15}N_{bulk}$ and $\delta^{15}N_{db}$ seem to reflect both the same trend so we will further use all three $\delta^{15}N_{bulk}$ records for paleo-interpretations.

4.3 Past changes in biological productivity and nutrient consumption

Along the Peruvian shelf the processes influencing the downcore $d^{15}N_{bulk}$ signal seem to be much more complex than this simple denitrification argument. Although the modern surface sediment $\delta^{15}N_{bulk}$ increases from 4‰ to 10‰ from the equator to 17°S, corresponding to southward increase of the $\delta^{15}N$ signal of dissolved NO_3^- in the subsurface source waters from 5‰ to 14.5‰ due ongoing denitrification (Mollier-Vogel et al., 2012), this cannot completely explain the lower amplitude in the shift of the $\delta^{15}N_{bulk}$ signal. Besides the southward increase in the denitrification in subsurface waters, the $\delta^{15}N_{bulk}$ values were shown to also reflect a higher degree of NO_3^- utilization north of 10°S, where subsurface $\delta^{15}N$ still remains close to 5‰. Further South (12°S – 17°S) incomplete NO_3^- utilization is probably responsible for a certain part of the increase in surface $\delta^{15}N$ of dissolved NO_3^- (Mollier-Vogel et al., 2012). Accordingly, the $\delta^{30}Si_{bSi}$ signatures of small diatoms in surface sediments were previously shown to constantly increase southwards, which is associated with increased primary productivity and upwelling conditions (Doering et al., 2016). The direct comparison of surface sediment $\delta^{30}Si_{bSi}$ to $\delta^{15}N$ shows that both are strongly influenced by surface water utilization, whereas subsurface denitrification only plays a minor role (Fig. 5 a) (Ehlert et al., 2015).

4.3.1 Evolution of denitrification, export productivity and nutrient utilization over the last 20,000 years

The combination of the $\delta^{15}N$ and $\delta^{30}Si_{bSi}$ records from sediments of Peru has been shown to track the changes in productivity, nutrient utilization and denitrification (Ehlert et al., 2015; Doering et al., 2016). The three cores covering the Peruvian shelf between 9°S and 15°S, presented here demonstrate higher $\delta^{15}N_{bulk}$ and $\delta^{15}N_{db}$ values of 6‰ to 11‰ during Termination 1 compared to modern values of 4‰ to 9.5‰ (Fig. 1b and Fig. 4) As the trends for both $\delta^{15}N_{bulk}$ and $\delta^{15}N_{db}$ are constantly the same over time, we will not

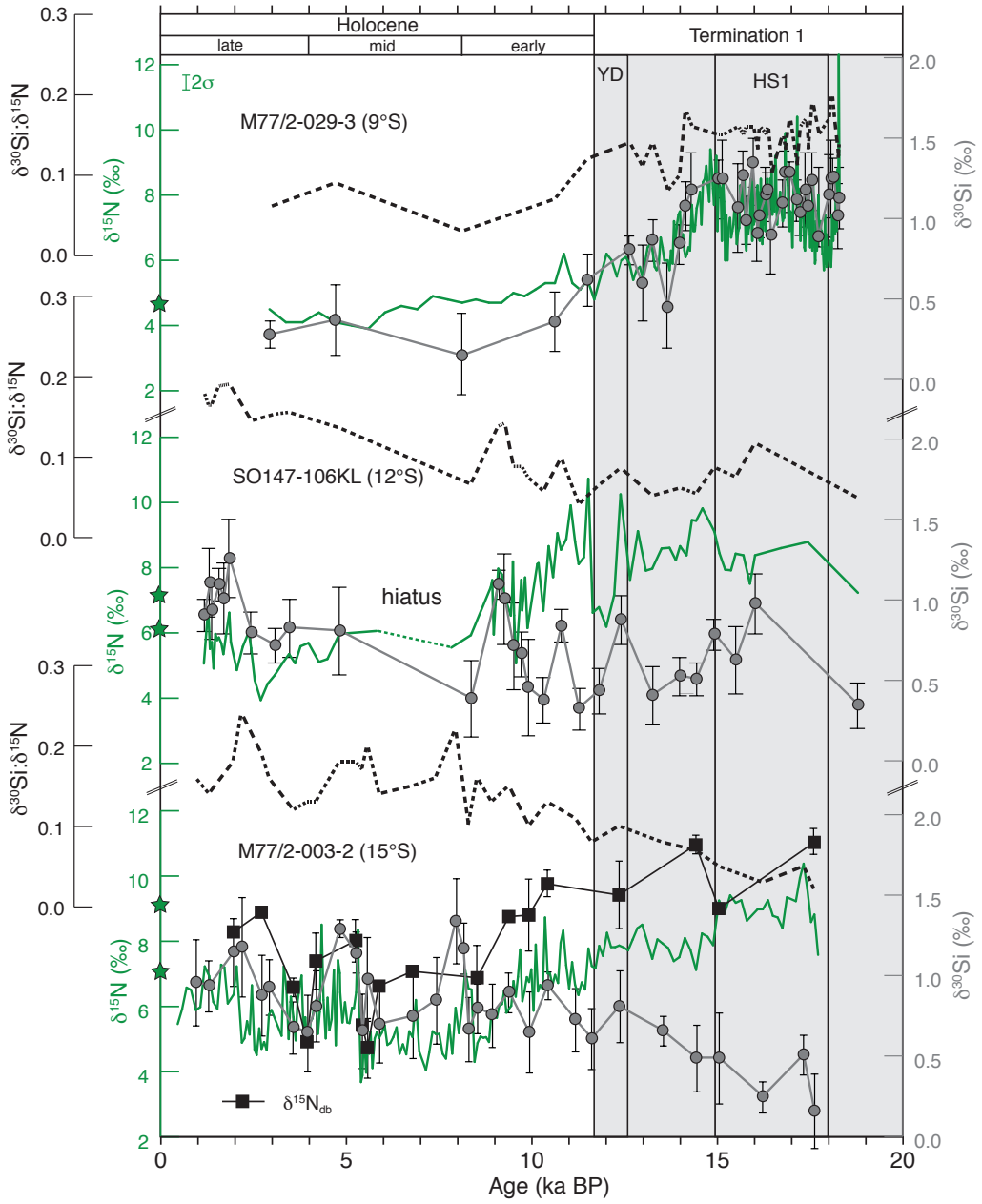

Figure 4: Downcore comparison of $\delta^{15}N_{bulk}$ (green), $\delta^{15}N_{db}$ (black squares), $\delta^{30}Si_{bSi}$ (grey circles) and $\delta^{30}Si_{bSi}$:$\delta^{15}N_{bulk}$ (dashed black line) over the last 20,000 years.

differentiate between the both in the following referring to only $\delta^{15}N$ records. While the $\delta^{15}N$ records from 12°S and 15°S are in close agreement with previous studies from the southern shelf area (Ganeshram et al., 2000; Higginson, 2004; Salvatteci et al., 2016), the 9°S record shows an earlier decrease in $\delta^{15}N$ starting already at 14 ka BP. Furthermore, at 9°S the higher deglacial $\delta^{15}N$ values show the same trend as the higher AR_{Corg} indicating higher productivity (Fig. 1a), and the same trend as higher $\delta^{30}Si_{bSi}$ indicating stronger surface water silicic acid ($Si(OH)_4$) utilization and upwelling conditions (Fig. 4; Doering et al., under review). In contrast, the $\delta^{15}N$ records of 12°S and 15°S indicate the opposite. High $\delta^{15}N$ values are associated with lower AR_{Corg} and AR_{Ntot} indicating lower productivity (Fig.1 a, b), (Doering et al., 2016; Ehlert et al., 2013) and lower

$\delta^{30}Si_{bSi}$ values reflecting lower $Si(OH)_4$ utilization and weaker upwelling conditions (Doering et al., under review). This is in agreement with previous studies reporting lower deglacial productivity at 15°S based on Ba/Al ratio (Ganeshram et al., 2000) and Ni concentrations (Salvatteci et al., 2016).

$\delta^{30}Si_{bSi}$ to $\delta^{15}N_{bulk}$ of core 029-3 (9°S) show a positive correlation between both proxies given that both $d^{15}N_{bulk}$ and $d^{30}Si_{bSi}$ show a trend from higher deglacial (average +1.1‰ and 7.2‰) to lower Holocene values (on average +0.4‰ and 4.8‰). Accordingly, the higher isotope ratios in both $\delta^{15}N$ and $\delta^{30}Si_{bSi}$ could indicate higher nutrient utilization during T1, while the lower isotope ratios could indicate lower nutrient utilization during the Holocene. However, $\delta^{15}N$ values from the T 1 as high as 7.2±1.9‰ require an increase in the $\delta^{15}N$ of NO_3^- of source waters. Modern $\delta^{15}N_{NO3-}$ values of source water at the same location only reach values of maximum 6‰. Hence, for deglacial $\delta^{15}N$ at the core site to reach values of 7.2±1.9‰ an increase in $\delta^{15}N_{NO3-}$ of at least 1.5‰ is needed, which could be either achieved by an increase the preformed source water $\delta^{15}N_{NO3-}$ value or by denitrification at the shelf.

In contrast, $\delta^{15}N$ and $\delta^{30}Si_{bSi}$ from 12°S and 15°S behave differently throughout the entire records (Fig. 4), mainly between the Holocene and T1. However, the differentiation between specific time periods of the records of both locations results in positive correlation of $\delta^{15}N$ and $\delta^{30}Si_{bSi}$ (Fig. 4). Core 106KL (12°S) indicates mainly a difference between moderate (+0.65 ± 0.3‰) $\delta^{30}Si_{bSi}$ and high (8.4 ± 0.9‰) $\delta^{15}N$ during T1-Early Holocene (10 ka to 19 ka BP) and high (+0.9 ± 0.25‰) $\delta^{30}Si_{bSi}$ and moderate (6.2 ± 1.1‰) $\delta^{15}N$ values during the Mid-Late Holocene (0 to 10 ka BP). In contrast, the variations observed in the $\delta^{30}Si_{bSi}$ versus $\delta^{15}N$ record of core 003-2 (15°S) seem to be more variable. Here, a stepwise decrease in $\delta^{15}N$ and increase in $\delta^{30}Si_{bSi}$ divides the correlation between the early T1 (14-18 ka BP; mean $\delta^{15}N$ = 8.8 ± 0.75‰ and $\delta^{30}Si_{bSi}$ = 0.4 ± 0.15‰) and late T1 (11.7-14 ka BP; mean $\delta^{15}N$ = 7.8 ± 0.3‰ and $\delta^{30}Si_{bSi}$ = +0.74 ± 0.1‰). The Holocene is divided into the early Holocene (8-11.7 ka BP) with high mean $\delta^{15}N$ of +6.5 ± 0.9‰ and moderate mean $\delta^{30}Si_{bSi}$ of +0.8±0.2‰ and the Mid-Late Holocene (0 to 8 ka BP) with moderate mean $\delta^{15}N$ (+5.6±0.9‰) and high mean $\delta^{30}Si_{bSi}$ (+0.93 ± 0.2‰).

Overall, a positive relationship between $\delta^{30}Si_{bSi}$ and $\delta^{15}N$ observed for all records over the different time periods (i.e. T1 and Holocene) indicates that both proxies are mainly driven by nutrient utilization, which is in agreement with previous observations (Ehlert et al., 2015). However, as denitrification has a higher fractionation factor (~20‰) than nitrate utilization (5‰) the slope of the observed regression lines are expected to be smaller the higher the influence of denitrification is. Accordingly, the negative correlation between $\delta^{30}Si_{bSi}$ and $\delta^{15}N$ observed during the early Holocene at 15°S (003-2; Fig. 5.c) may indicate a stronger influence of enhanced subsurface denitrification. Another explanation for the observed increase in $\delta^{15}N$ associated with constant $\delta^{30}Si_{bSi}$ values at the time could be enhanced utilization of NO_3^- over $Si(OH)_4$ and/or NO_3^-

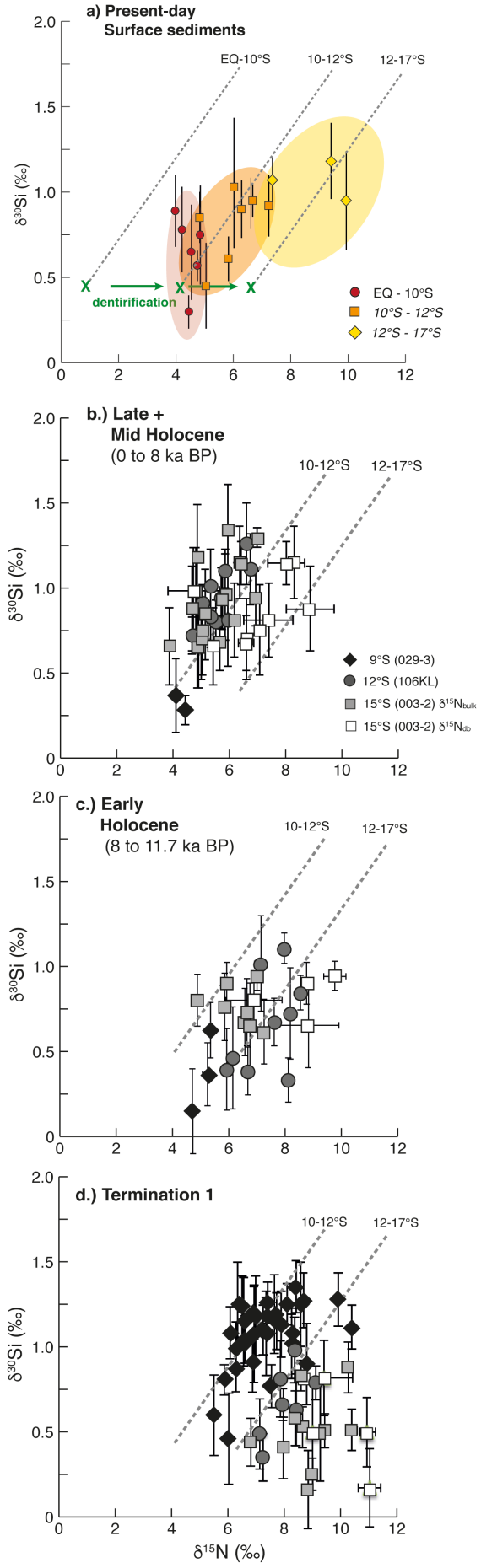

Figure 5: a.) present-day surface sediment $\delta^{15}N_{bulk}$ versus $\delta^{30}Si_{bSi}$: red circles = EQ-10°S; orange squares = 10°S-15°S; yellow diamonds = 15°S - 17°S. Dashed lines indicate a relationship between $\delta^{30}Si_{bSi}$ and $\delta^{15}N_{bulk}$ predominantly influenced by surface water utilization. Green crosses mark the $\delta^{15}N$ of NO_3^- of subsurface source waters, which increases southwards due to intensifying denitrification (modified after Ehlert et al., 2015). b-d) Downcore $\delta^{15}N$ versus $\delta^{30}Si_{bSi}$ for the time periods Late and Mid Holocene, Early Holocene and Termination 1. The different cores are marked as black diamonds (029-3), grey dots (106KL), grey squares (003-2 $\delta^{15}N_{bulk}$) and white squares (003-2 $\delta^{15}N_{db}$).

limitation. For instance, the lower $\delta^{30}Si_{bSi}/\delta^{15}N$ ratio (Fig. 4), often employed to estimate shifts in consumption between NO_3^- and $Si(OH)_4$ (Horn et al., 2011a; Robinson et al., 2014), further indicates enhanced NO_3^- over $Si(OH)_4$ consumption at the southern shelf during T1. However, along the continental margin potential changes in source water isotopic compositions as well as overprinting via denitrification complicate the quantification of nutrient utilization.

In order to further track the extent of nutrient utilization versus denitrification in the past we followed the approach from previously published surface sediments to produce a latitudinal comparison of $\delta^{30}Si_{bSi}$ versus $\delta^{15}N$ over three distinct time periods evident in all three cores, respectively: Termination 1, the early Holocene, and the mid to late Holocene (Fig 5, b-d). Based on surface sediment distributions $\delta^{15}N$ and $\delta^{30}Si_{bSi}$ are expected to fall on 1:1 utilization lines (Fig. 5, dashed lines), which were calculated based on a fractionation factor of -1.1‰ for $\delta^{30}Si_{bSi}$ and +5‰ for $\delta^{15}N$ relative to subsurface source water along the Peruvian shelf, which varies for $\delta^{15}N$ but not for $\delta^{30}Si_{bSi}$ (Ehlert et al., 2012,15; Mollier-Vogel et al., 2012). Limitation by either NO_3^- or $Si(OH)_4$ would result in either a flatter or steeper relation of the data, respectively. In addition, denitrification could also result in flatter pattern of the $\delta^{15}N$ versus $\delta^{30}Si$ data. Denitrification occurs in subsurface waters prior to upwelling an uptake of nutrients by phytoplankton. Due to its high fractionation factor of 20‰, denitrification presents an increase in the source value for $\delta^{15}N$, thus increasing from 5‰ to 11.5‰ from the equator to 17°S (Fig. 5a). The comparison of $\delta^{30}Si_{bSi}$ versus $\delta^{15}N_{bulk}$ (including $\delta^{15}N_{db}$ for core 003), indicates that all data for the record during all three time periods are generally the result of fractionation during utilization and not denitrification. The increase of $\delta^{15}N$ from North to South observed in surface sediments, is similar in the downcore record during all three time periods and remains quite stable at ~1.3‰. This observation indicates a stable level of denitrification, at least along the shelf between 9°S and 15°S, during the past 20 ka BP. Nevertheless, the $\delta^{15}N$ source value at 9°S was clearly higher during T1 (See discussion above).

4.3.2 Implications for variations in the past biogeochemical cycle off Peru

Within the Peruvian OMZ the major mechanism acting on the sedimentary $\delta^{15}N$ record include the amount of surface productivity, subsequent OM degradation, water column ventilation, the amount of oxygen delivered to the region, as well as nutrient concentrations and isotope signatures of source waters (Galbraith 2013). Considering the N inventory, variations in denitrification and N_2 fixation are supposed to have the main effect (Galbraith 2013). Previous studies often suggested that the observed high deglacial $\delta^{15}N$ were induced by enhanced water column or benthic denitrification due to the growing

continental shelves (Deutsch et al., 2004; Galbraith et al., 2013; Ganeshram et al., 2000). However, enhanced N-loss processes would also lead to a decrease in the N inventory and higher NO_3^- consumption (Deutsch et al., 2004). Thus less of the highly fractionated NO_3^- could be transported to proximate areas close to the ETSP OMZ. Therefore, enhanced denitrification during T1 as the only cause for the higher sedimentary $\delta^{15}N$ values is unlikely to explain similarly high $\delta^{15}N$ values in areas generally unaffected by denitrification like the Chilean coastal area.

Other mechanisms controlling the variations in the $\delta^{15}N$ records off Peru could be either the preformed $\delta^{15}N$ of NO_3^- or the amount of NO_3^- reaching Peruvian subsurface waters acts as another strong influence on variations in the past $\delta^{15}N$ records. Today, the Peru-Chile Undercurrent (PCUC) is the main subsurface water source upwelled along the Peruvian shelf. The PCUC itself is fed by the poleward flowing Equatorial Undercurrent (EUC; $\delta^{15}N_{NO3-}$ = 7.1±0.3‰) and the eastward flwoing subsurface jets the Northern and Southern Subsurface Counter Currents (NSCC and SSCC) with $\delta^{15}N_{NO3-}$ signatures 6.8±0.4‰ and 5.5±0.3‰, respectively (Rafter et al., 2012). Overall, intermediate waters originating from the Southern Ocean, namely Subantarctic mode water (SAMW), constitute an important source of nutrients to the ETP (Sarmiento et al., 2004; Toggweiler et al., 1991). After formation in the Subantarctic zone, SAMW flows northward along the South American coast causing the $\delta^{15}N$ of NO_3^- to continuously increase due to water column denitrification and NO_3^- consumption, before missing with PCUC at ~25°S. Furthermore, SAMW is transferred to the ETP via the subtropical gyre ventilating the equatorial Pacific intermediate waters as EqPac (SAMW). The mean $\delta^{15}N_{NO3}$- of SAMW in the SE Pacific is 6.3±0.2‰ (Sigman et al., 2000; 1999b) (Rafter et al., 2012), while EqPac (SAMW) equivalent shows an increase to $\delta^{15}N_{NO3}$- values of 7.1‰ (Rafter et al., 2012). During the T 1, (mainly HS1) the $\delta^{15}N_{NO3-}$ value of SAMW has been shown to significantly increase to about 9‰ (Robinson et al., 2014) due to enhanced ventilation and productivity in the Southern Ocean. Accordingly, this higher $\delta^{15}N_{NO3-}$ source values as well as more nitrate was transferred during the Termination, could have increased the preformed $\delta^{15}N_{NO3-}$ source value reaching the ETP by about 1‰.

An additional explanation for higher deglacial sedimentary $\delta^{15}N$ values in the ETSP could be varying degrees of denitrification and N_2 fixation influencing the N inventory. Previous studies assumed that N_2 fixation mainly occurs in surface waters of the oligotrophic ocean (Deutsch et al., 2007). However, recent field observations in the OMZ off Peru have demonstrated that N_2 fixation performed by heterotrophic diazotrophs in the ETSP occurs concurrently with N-loss processes (Dekaezemacker et al., 2013; Löscher et al., 2014; Löscher et al., 2015). These studies demonstrate that N_2 fixation performed by heterotrophic diazotrophs occurs in the OMZ off Peru fueled by high primary production and the elevated iron and phosphate concentrations across the shelf

region. Moreover, heterotrophic N_2 fixation seems to be directly linked to anammox and other N-turnover processes, thus in principle confirming the model of Deutsch et al. (2007), which suggest a close spatial coupling of N-loss and N_2 fixation processes, with the highest rates in shelf waters with high organic matter load and high iron availability (Löscher et al., 2014). Accordingly, within the modern ETSP-OMZ the low oxygen concentrations in subsurface waters favors N-loss processes, P release and increased iron bioavailability are favorable for N_2 fixation (Deutsch et al., 2001; Deutsch et al., 2007). It was, however, shown previously that oxygen concentrations were higher during T1 due to enhanced northward flow of intermediate waters transporting higher oxygen concentrations to the bottom-waters along the shelf (Muratli et al., 2009; Salvatteci et al., 2016). These higher bottom-water oxygen concentrations likely caused diminished iron and phosphate release from the sediments (Doering et al., 2016; Scholz et al., 2014) as well as lower anammox rates, thus could have reduced the deglacial N_2 fixation in comparison to today or during the Holocene. This is in agreement with a recent model study (Eugster et al., 2013), which shows that the a global decrease in the N inventory during the deglaciation could have caused by a strong reduction in the rate of N_2 fixation at the beginning of the deglaciation. Accordingly, reduced deglacial N_2 fixation, commonly associated with low $\delta^{15}N$ values, and a constant denitrification rate that further reduced the local N inventory could likely have caused a further increase in the $\delta^{15}N$ signal as observed in Peruvian $d^{15}N$ records.

Summary and Conclusions

The reconstruction of past N cycling along continental shelves using $\delta^{15}N_{bulk}$ has often been inferred to be unbiased by diagenetic alteration of OM due to the high local sedimentation rates. However, given that also in these environments the OM in past sediments may be potentially altered due to lateral and downslope material transport or periodic oxidation of bottom sediments, we try to estimate potential shifts in past $\delta^{15}N_{bulk}$ off Peru based on combined analysis of C/N ratios, $\delta^{15}N_{bulk}$ and more resistant diatom-bound $\delta^{15}N$ values. Overall, the C/N ratios show that OM in the records is predominantly of marine origin and do not reflect significant alteration of $\delta^{15}N_{bulk}$. The comparison of $\delta^{15}N_{bulk}$ with diatom-bound $\delta^{15}N$, which is physically protected from early diagenesis, further confirms insignificant diagenetic alteration of $\delta^{15}N_{bulk}$ as both $\delta^{15}N_{bulk}$ and $\delta^{15}N_{db}$ revealed overall similar isotope compositions and trends throughout the record. However, $\delta^{15}N_{db}$ values were constantly up to 2‰ higher than $\delta^{15}N_{bulk}$ values. We suggest that this results because diatoms incorporate the higher subsurface $\delta^{15}N_{NO3-}$ signatures caused by denitrification. In contrast, the $\delta^{15}N_{bulk}$ signatures predominantly reflect an annual composition including other forms of organic matter produced by phytoplankton that occurs during more stratified conditions,

thus potentially recording lighter $\delta^{15}N$ signatures unaffected by N-loss processes.

The presented $\delta^{15}N_{bulk}$ records covering the Peruvian shelf between 9°S and 15°S confirm previous observation of high deglacial $\delta^{15}N$ values (8 to 11‰) and decreasing moderate values during the Holocene (4 to 7‰). However, only the $\delta^{15}N$ record at 9°S is positively correlated with increased export productivity (AR_{Corg} and AR_{Ntot}), while the records at 12°S and 15°S indicate a negative relationship with high $\delta^{15}N$ associated with decreasing export productivity and upwelling during Termination 1. Based on comparison of $\delta^{15}N_{bulk}$ and $\delta^{30}Si_{bSi}$ showed that both isotope systems were positively correlated for different time periods we can show that each record is ultimately controlled by both NO_3^- to $Si(OH)_4$ utilization. However, in addition there is a consistent southward increase in $\delta^{15}N_{NO3-}$ of source waters by about 1.5‰ from 9°S to 15°S is found, most likely reflecting ongoing denitrification. Although, we constantly found indicators of denitrification during the last ~19,000 years, the records do not indicate enhanced denitrification during the deglacial as previously suggested. Instead, our findings support that the hypothesis that equatorial subsurface currents transmitted a ~1‰ higher pre-formed deglacial (H1) $\delta^{15}N_{NO3-}$ signature. Furthermore, the previously suggested northward shift observed at the centers of high productivity and upwelling conditions during Termination 1 did not only coincide with a similar northward movement of denitrification, but was also coupled to enhanced inflow of oxygen-rich Southern Ocean intermediate waters (SAMW and AAIW). The higher bottom-water oxygenation likely caused a decrease of iron and phosphate release from shelf sediments reduced the influence of low $\delta^{15}N_{NO3-}$ values generated by heterotrophic N_2 fixation on the deglacial N cycle off Peru.

Acknowledgements

This work is a contribution of the Collaborative Research Project 754 “Climate-Biogeochemistry interactions in the Tropical Ocean” (www.sfb754.de), which is supported by the Deutsche Forschungsgemeinschaft.

III. Conclusions and Outlook

Conclusions

The main goal of this study was to reconstruct of external factors controlling the extension and strength of the oxygen minimum zone, along the Peruvian shelf region during the past 20,000 years by tracing primary production, silicate and nitrate utilization, upwelling intensity and N-loss processes. The Peruvian upwelling area is a high productivity region that results in one of the globally largest OMZs. Upwelling intensity and remineralization of nutrients are directly driving the primary productivity above the OMZ. Therefore it is of great interest to better understand the factors controlling the nutrient cycling as a whole.

To improve the application of $\delta^{30}Si$ as a tracer for silicon cycling in records of the past in **Chapter 1** of this study the $\delta^{30}Si$ from different diatom size fractions, i.e. of small mixed diatoms (11-32µm; $\delta^{30}Si_{bSi}$) and of large hand-picked mono-generic diatoms (*Coscinodiscus* spp.; >150µm; $\delta^{30}Si_{coscino}$), and their relationship with the diatom assemblages in surface sediments off Peru were investigated. The results showed that the $\delta^{30}Si_{coscino}$ of the surface sediments showed nearly constant values close to +1.5‰ indicating near-complete utilization of the $\delta^{30}Si(OH)_4$ source signature of upwelled waters from the Peru-Chile Undercurrent. In contrast, the results for the $\delta^{30}Si$ of small mixed diatom fraction showed a strong control of the diatom assemblage by the seasonal diatom succession during weak or strong upwelling. Accordingly, it was shown that during strong upwelling $Si(OH)_4$ utilization continuously increases from the initial diatom succession of small opportunistic diatom species (i.e. upwelling-related, such as *Chaetoceros* spp., *Skeletonema costatum*) to the final stages of the diatom succession dominated by non-upwelling diatom species and resting spores, with a correspondingly increased the Si fractionation as recorded by the $\delta^{30}Si$ of diatoms. As the small, elongated or chain-building upwelling-related diatoms are preferentially removed during sample preparation for $\delta^{30}Si$ measurements of the 11-32 µm fraction, the resulting $\delta^{30}Si_{bSi}$ signatures may lack some of the low isotopic values formed during the early diatom succession and rather reflect the higher $\delta^{30}Si_{bSi}$ values recorded in small coastal planktonic species and in resting spores. In contrast, during weak upwelling conditions when the supply of $Si(OH)_4$ to the surface is more limited, the diatom blooms are less intense with minor contributions of upwelling-related diatom species. Given a minor initial diatom bloom and low contributions of upwelling-related species, non-upwelling coastal planktonic species occur earlier and consequently

nutrient utilization and Si isotope fractionation are lower. This results in lower $\delta^{30}Si_{bSi}$ values of the small diatom fraction in comparison to intense blooms under strong upwelling conditions. Given that $\delta^{30}Si_{bSi}$ values are dependent on the strength of upwelling and the associated diatom succession, while $\delta^{30}Si_{coscino}$ values appear constant as they reflect overall stratified conditions at the end or during interruptions of upwelling, the calculation of the difference between both values is suggested as a new proxy for upwelling intensity off Peru. Although, upwelling conditions can also be inferred by variations in the diatom assemblages, the novel application of the $\Delta^{30}Si_{coscino\text{-}bSi}$ allows to infer upwelling intensity and the degree of $Si(OH)_4$ utilization independent of a potential influence of changes in source water $\delta^{30}Si(OH)_4$ values in the past.

Furthermore, based on a paleo-reconstruction of $\delta^{30}Si_{bSi}$ signatures in comparison with the diatom assemblages in bulk sediments, the relative abundances of the dominating diatom species were used to determine the influence of species-dependent fractionation on the past $\delta^{30}Si_{bSi}$ record. Overall, this influence was shown to be insignificant in our study area, however, the approach was limited by the fact that there are only a few available estimations of ε values for subtropical diatom species.

The findings of **Chapter I** were applied to several sediment records along the Peruvian shelf in **Chapter II**. To reconstruct past primary productivity, $Si(OH)_4$ utilization and upwelling conditions along the entire Peruvian shelf since the Last Glacial Maximum the biogenic opal concentration, $\delta^{30}Si_{bSi}$ and $\delta^{30}Si_{coscino}$, $\Delta^{30}Si_{coscino\text{-}bSi}$ as well as the diatom assemblage of the 11-32 µm diatom fraction were compiled for four sediment cores between 5°S and 15°S. The results show a general decoupling of the environmental conditions on the central (5°S to 10°S) and the southern shelf (10°S to 15°S). The main upwelling cell shifted northwards from its modern position between 12°S and 15°S towards 9°S at the onset of the deglaciation, when only moderate upwelling and export productivity were recorded between 9°S and 12°S. This northward shift of the main upwelling cell was likely associated to a more northerly position of Southern Westerly Winds and the South Pacific Subtropical High. Modern conditions, with the main upwelling centre and highest productivity between 12°S and 15°S were only established at the onset of the Holocene. Moreover, the estimation of the influence of past changes in preformed $Si(OH)_4$ concentrations and $\delta^{30}Si$ signatures of subsurface waters reaching the Peruvian shelf were shown to have no significant effect on the $\delta^{30}Si$ records.

In addition to the reconstruction of $Si(OH)_4$ utilization and upwelling conditions along the past Peruvian shelf another goal of this thesis was to improve the reconstruction and distinction of past nitrate utilization and denitrification. In **Chapter III** and **IV** we compared the $\delta^{15}N_{bulk}$ records of several sediment cores covering the southern Peruvian Shelf from 11°S to 15°S over the last 600 years and from 9°S to 15°S over the last 20,000 years. The correlation of $\delta^{15}N_{bulk}$ and $\delta^{30}Si_{bSi}$ signatures was applied in both **Chapters III**

and IV to differentiate between nutrient utilization and denitrification based on the premise that $\delta^{30}Si_{bSi}$ is only influenced by the degree of nutrient utilization, while $\delta^{15}N_{bulk}$ is affected by a combination of both nutrient utilization and denitrification. It is shown that while the isotopic records at single core locations have mainly been affected by the degree nutrient utilization, the latitudinal comparison of $\delta^{30}Si_{bSi}$ versus $\delta^{15}N_{bulk}$ over different time periods (i.e. the CWP and LIA or the Holocene and the last deglaciation) allows to trace the southward increase in $\delta^{15}N_{bulk}$ values due to denitrification.

Given that it was possible to trace the southward increase in subsurface $\delta^{15}N_{NO3-}$ due to denitrification as reflected in $\delta^{15}N_{bulk}$ values over time, we further compared the strength in this southward increase in $\delta^{15}N_{bulk}$ between the last deglaciation and the Holocene (**Chapter IV**). Previously it was assumed that the high observed $\delta^{15}N_{bulk}$ values at the Peruvian Margin during the last deglaciation reflect mainly reflect an increase in local denitrification. However, while our results support ongoing denitrification during most of the last 20,000 years, the latitudinal comparison of $\delta^{15}N_{bulk}$ values does not support a significant increase in denitrification at any time. Accordingly, other processes such as a change in the preformed $\delta^{15}N_{NO3-}$ delivered to the shelf or a reduction in N_2 fixation at the time likely affected the $\delta^{15}N_{bulk}$ record.

Outlook

One of the major goals of this thesis was a better understanding of the connection of stable silicon isotope compositions of mixed diatom fractions and the influence of species-dependent isotope fractionation. While the results support a close coupling of diatom $\delta^{30}Si$ signatures with the diatom assemblages, the fact that estimations for the enrichment factor ε are mainly available for polar diatom species, the missing information for subtropical diatom species limits the possibility to evaluate potential influences by shifts in the diatom assemblage on the $\delta^{30}Si$ record of diatoms. Therefore, future studies should focus on culture or incubation experiments to gain particular insights into potential differences in the enrichment factors (ε) for silicon isotopes in tropical- and subtropical diatom species.

Furthermore, most diatom species found in the surface waters are small and fragile and are thus not transported to and preserved the sediments but dissolved in the water column. Instead larger diatom species and resting spores are more likely to reach the seafloor. As there is clearly a discrepancy between present diatoms making up the particulate biogenic opal in the water column and the diatoms recorded in the sediment, there is a clear need to obtain more the measurements of the $\delta^{30}Si$ of particulate biogenic opal in the water column in comparison with sediment trap data. A major interest in this regard further lies in the investigation of resting spores. Although it is known that diatoms form

these spores when environmental conditions are not favourable anymore, it is unclear if their formation is associated with a significant fractionation in silicon isotopes. As these spores are dominant in the sediments a better understanding of their formation would significantly improve our understanding of past $\delta^{30}Si$ records of mixed diatoms. Given that $\delta^{30}Si$ signatures of past diatoms are not only affected by the degree of nutrient utilization but also via changes in the preformed $\delta^{30}Si(OH)_4$ value, it may be interesting to measure the $\delta^{30}Si(OH)_4$ signatures of bottom-waters specifically where the remineralization of the settling bSi occurs.

Regarding investigations of past $\delta^{30}Si$ records it would be interesting to test the findings of Chapter I of the association of $\delta^{30}Si_{bSi}$ values to different upwelling conditions as well as the novel approach of using $\Delta^{30}Si$ between the large and small diatom size fractions, on samples from other upwelling regions, such as the Gulf of California or the Benguela Upwelling. Similarly, the application of combined $\delta^{30}Si$ and $\delta^{15}N$ in upwelling areas affected by N-loss processes was shown improve the understanding of past biogeochemical cycling by differentiation between nutrient utilization and denitrification. As reconstructions of past N cycling are hampered by the complexity of the processes, the combination of $\delta^{30}Si$ and $\delta^{15}N$ measurements should be further expanded to other areas.

The comparison of $\delta^{15}N_{bulk}$ and $\delta^{15}N_{db}$ in the past record indicates a constant offset between both archives, with $\delta^{15}N_{db}$ remaining generally up to 2‰. To further investigate this observation future work could measure both signatures in core-tops to evaluate if this effect is also observed in the modern sediment. Besides, diatoms also showed species-dependent fractionation factors for N, which were already shown in the Southern Ocean to potentially bias the record of the past (Horn et al., 2011). Accordingly, the investigation of species-dependent fractionation of N isotopes in Peruvian diatoms should be applied to investigate the potential variability of the observed $\delta^{15}N_{db}$ values.

Danksagung

Ich möchte mich in erster Linie bei meinen Betreuern Ralph Schneider und Martin Frank bedanken. Vielen Dank dass ihr mir die Chance für diese Arbeit gegeben habt und für eure anhaltende Unterstützung während der gesamten Zeit. Danke Martin für deinen anhaltenden Optimismus und die gute Laune die du verbreitest.

Besonders dankbar bin ich meinen Mentoren Claudia und Patricia. Vielen Dank Claudia ich hätte mir keine bessere Einarbeitung in die Silizium-Isotopen Messungen wünschen können. Danke Paddy für die unzähligen gemeinsamen Stunden im Labor und hilfreichen Diskussionen. Ohne euch beide wäre meine Doktorandenzeit sicherlich nur halb so schön gewesen.

Vielen Dank auch an Zeynep für die Zusammenarbeit innerhalb der Paläo-Projekte im SFB und die hilfreichen Diskussionen über das Peruanische Auftriebsgebiet.

I want to thank Philippe Martinez, Xavier Crosta and Sophie Fleury for their help with the bulk sedimentary nitrogen isotope measurements and diatom assemblage analyses. I really enjoyed my stay with you all in Bordeaux. I want to thank Rebecca Robinson for providing me the opportunity to visit her laboratory in Rhode Island to learn the diatom-bound nitrogen isotope measurements and supporting me with the data interpretation.

Natürlich möchte ich mich bei der gesamten Arbeitsgruppe und der Geomar Kaffeerunde bedanken. Besonderer Dank gilt Janett, Georgi und Nastya, die noch freiwillig Zeit mit mir verbracht haben auch wenn ich dauernd über die Arbeit geredet habe.

Außerdem möchte ich bei allen SFB Doktoranden bedanken, ich hatte eine schöne Zeit mit euch allen, insbesondere während der sommer schools.

Zu guter Letzt vielen Dank an meine Familie, sowie Britta und Owena, die mich immer unterstützt und motiviert haben.

References

Abrantes F., Lopes C., Mix A. and Pisias N. (2007) Diatoms in Southeast Pacific surface sediments reflect environmental properties. *Quaternary Science Reviews* **26**, 155–169. doi:10.1016/j.quascirev.2006.02.022.

Agnihotri, R., M. A. Altabet, and T. D. Herbert (2006), Influence of marine denitrification on atmospheric N_2O variability during the Holocene, *Geophys. Res. Lett.*, **33**(13), L13704, doi:10.1029/2006GL025864.

Agnihotri, R., Altabet, M.A., Herbert, T.D., Tierney, J.E., (2008) Subdecadally resolved paleoceanography of the Peru margin during the last two millennia. G*eochem. Geophys. Geosyst.* **9**, Q05013. doi:10.1029/2007GC001744

Albarède, F., P. Telouk, J. Blichert-Toft, M. Boyet, A. Agranier, and B. Nelson (2004), Precise and accurate isotopic measurements using multiple-collector ICPMS, *Geochimica et Cosmochimica Acta*, **68**(12), 2725–2744, doi:10.1016/j.gca.2003.11.024.

Altabet, M.A., Deuser, W.G., Honjo, S., Stienen, C., (1991) Seasonal and Depth-Related Changes in the Source of Sinking Particles in the North-Atlantic. *Nature* **354**, 136–139.

Altabet M. A. and François R. (1994) Sedimentary nitrogen isotopic ratio as a recorder for surface ocean nitrate utilization. *Global Biogeochem. Cycles* **8**, 103–116.

Altabet, M.A., François, R., Murray, D.W., Prell, W.L., 1995. Climate-related variations in denitrification in the Arabian Sea from sediment $^{15}N/^{14}N$ ratios. Nature 373, 506–509.

Altabet M. A. and François R. (2001) Nitrogen isotope biogeochemistry of the Antarctic Polar Frontal Zone at 170 W. **48**, 4247–4273.

Altabet, M.A., (2006). Constraints on oceanic N balance/imbalance from sedimentary ^{15}N records. *Biogeosciences Discuss*. **4,** 75-86, doi: 10.5194/bgd-3-1121-2006.

Altabet, M. A., E. Ryabenko, L. Stramma, D. W. R. Wallace, M. Frank, P. Grasse, and G. Lavik (2012), An eddy-stimulated hotspot for fixed nitrogen-loss from the Peru oxygen minimum zone, *Biogeosciences Discuss.*, *9*(12), 8013–8038, doi:10.5194/bgd-9-8013-2012.

Anderson, R. F., S. Ali, L. I. Bradtmiller, S. H. H. Nielsen, M. Q. Fleisher, B. E. Anderson, and L. H. BurckleLE (2009), Wind-Driven Upwelling in the Southern Ocean and the Deglacial Rise in Atmospheric CO_2, *Science*, *323*(5920), 1443–1448, doi:10.1126/science.1167441.

Arellano-Torres, E., L. E. Pichevin, and R. S. Ganeshram (2011), High-resolution opal records from the eastern tropical Pacific provide evidence for silicic acid leakage from HNLC regions during glacial periods, *Quaternary Science Reviews*, (30), 1112–1121.

Armbrust E. V. (2009) The life of diatoms in the world's oceans. *Nature* **459**, 185–192.

Arthur, M.A., Dean, W.E., Laarkamp, K., (1998) Organic carbon accumulation and preservation in surface sediments on the Peru margin. Chemical Geology **152**, 273–286. doi:10.1016/S0009-2541(98)00120-X

Ayón P., Criales-Hernandez M. I., Schwamborn R. and Hirche H.-J. (2008) Zooplankton research off Peru: A review. *Progress in Oceanography* **79**, 238–255.

Barber, R. T., and F. P. Chávez (1983), Biological Consequences of El Nino, *Science*, *222*(4629), 1203–1210, doi:10.1126/science.222.4629.1203.

Barber R. T. and Chávez F. P. (1991) Regulation of primary productivity rate in the equatorial Pacific. *Limnol. Oceangr.* **36**, 1803–1815.

Berger, W. H., and J. C. Herguera (1989), Reading the sedimentary record of the ocean`s productivity, edited by P. G. Falkowski and A. D. Voodhead, pp. 455–486, Primary Productivity and Biogeochemical Cycles in the Sea.

Beucher C. P., Brzezinski M. A. and Crosta X. (2007) Silicic acid dynamics in the glacial sub-Antarctic: Implications for the silicic acid leakage hypothesis. *Global Biogeochem. Cycles* **21**, 3015–3028.

Beucher, C. P., M. A. Brzezinski, and J. L. Jones (2008), Sources and biological fractionation of Silicon isotopes in the Eastern Equatorial Pacific, *Geochimica et Cosmochimica Acta*, *72*(13), 3063–3073, doi:10.1016/j.gca.2008.04.021.

Beucher, C. P., M. A. Brzezinski, and J. L. Jones (2011), Mechanisms controlling silicon isotope distribution in the Eastern Equatorial Pacific, *Geochimica et Cosmochimica Acta*, *75*(15), 4286–4294, doi:10.1016/j.gca.2011.05.024.

bin Shaari, H., M. Yamamoto, and T. Irino (2013), Enhanced upwelling in the eastern equatorial Pacific at the last five glacial terminations, *Palaeogeography, Palaeoclimatology, Palaeoecology*, *386*, 8–15.

Blaauw, M. (2010), Quaternary Geochronology, *Quaternary Geochronology*, *5*(5), 512–518, doi:10.1016/j.quageo.2010.01.002.

Blasco, D. (1971), Compsición y distribución del fitoplancton en la región del afliamientio de las costas peruanas, *Inv. Pesq.*, (1), 61–112.

Blasco D., Estrada M. and Jones B. H. (1981) Short time variability of phytoplankton populations in upwelling regions—the example of northwest Africa. *Coastal and Estuarine Sciences* **1**, 339–347.

Bopp L., Le Quéré C., Heimann M., Manning A. C. and Monfray P. (2002) Climate-induced oceanic oxygen fluxes: Implications for the contemporary carbon budget. *Global Biogeochem. Cycles* **16**, 6–1–6–13.

Bostock, H. C., B. N. Opdyke, M. K. Gagan, and L. K. Fifield (2004), Carbon isotope evidence for changes in Antarctic Intermediate Water circulation and ocean ventilation in the southwest Pacific during the last deglaciation, *Paleoceanography*, *19*(4), PA4013, doi:10.1029/2004PA001047.

Bradtmiller, L. I., R. F. Anderson, M. Q. Fleisher, and L. H. Burckle (2006), Diatom productivity in the equatorial Pacific Ocean from the last glacial period to the present: A test of the silicic acid leakage hypothesis, *Paleoceanography*, *21*(4), PA4201, doi:10.1029/2006PA001282.

Braman, R.S., Hendrix, S.A., (1989) Nanogram nitrite and nitrate determination in environmental and biological materials by vanadium (III) reduction with chemiluminescence detection. *Anal. Chem.* **61**, 2715–2718.

Brandes, J.A., Devol, A.H., (2002) A global marine-fixed nitrogen isotopic budget: Implications for Holocene nitrogen cycling. *Global Biogeochem. Cycles* 1**6**, 67–1–67–14. doi:10.1029/2001GB001856

Brandes J. A., Devol A. H. and Deutsch C. (2007) New Developments in the Marine Nitrogen Cycle. *Chem. Rev.* **107**, 577–58, doi:10.1021/cr050377t.

Brink, K. H., D. Halpern, A. Huyer, and R. L. Smith (1983), The Physical-Environment of the Peruvian Upwelling System, *Progress in Oceanography*, *12*(3), 285–305.

Brodie, I., and A. Kemp (1994), Variation in biogenic and detrital fluxes and formation of laminae in late Quaternary sediments from the Peruvian coastal upwelling zone, *Marine Geology*.

Bronk, D.A., Lomas, M.W., Glibert, P.M., Schukert, K.J., Sanderson, M.P., 2000. Total dissolved nitrogen analysis: Comparisons between the persulfate, UV and high temperature oxidation methods. Marine Chemistry 69, 163–178.

Bruland K. W., Rue E. L., Smith G. J. and DiTullio G. R. (2005) Iron, macronutrients and diatom blooms in the Peru upwelling regime: brown and blue waters of Peru. *Marine Chemistry* **93**, 81–103, doi:10.1016/j.marchem.2004.06.011.

Brunelle, B.G., Sigman, D.M., Cook, M.S., Keigwin, L.D., Haug, G.H., Plessen, B., Schettler, G., Jaccard, S.L., (2007) Evidence from diatom-bound nitrogen isotopes for subarctic Pacific stratification during the last ice age and a link to North Pacific denitrification changes. *Paleoceanography* **22**, PA1215. doi:10.1029/2005PA001205

Brunelle B. G., Sigman D. M., Jaccard S. L., Keigwin L. D., Plessen B., Schettler G., Cook M. S. and Haug G. H. (2010) Glacial/interglacial changes in nutrient supply and stratification in the western subarctic North Pacific since the penultimate glacial maximum. *Quaternary Science Reviews* **29**, 2579–2590.

Brzezinski M. A. and Nelson D. M. (1995) The annual silica cycle in the Sargasso Sea near Bermuda. *Deep Sea Research Part I: Oceanographic Research Papers* **42**, 1215–1237.

Brzezinski M. A. (2002) A switch from $Si(OH)_4$ to NO_3^- depletion in the glacial Southern Ocean. *Geophys. Res. Lett.* **29**, 1564 doi:10.1029/2001GL014349.

Brzezinski M. A., Baines S. B., Balch W. M., Beucher C. P., Chai F., Dugdale R. C., Krause J. W., Landry M. R., Marchi A., Measures C. I., Nelson D. M., Parker A. E., Poulton A. J., Selph K. E., Strutton P. G., Taylor A. G. and Twining B. S. (2011) Co-limitation of diatoms by iron and silicic acid in the equatorial Pacific. *Deep-Sea Research II.* **58**, 493–511.

Calvert, S.E., (2004) Beware intercepts: interpreting compositional ratios in multi-component sediments and sedimentary rocks. *Organic Geochemistry* **35**, 981–987. doi:10.1016/j.orggeochem.2004.03.001

Calvo, E., C. Pelejero, L. D. Pena, I. Cacho, and G. A. Logan (2011), Eastern Equatorial Pacific productivity and related-CO2 changes since the last glacial period, *Proceedings of the National Academy of Sciences*, *108*(14), 5537–5541.

Cane, M. A. (2005), The evolution of El Niño, past and future, *Earth and Planetary Science Letters* **230**, 227-240, doi: 0.1016/j.epsl.2004.12.003.

Cao Z., Frank M., Dai M., Grasse P. and Ehlert C. (2012) Silicon isotope constraints on sources and utilization of silicic acid in the northern South China Sea. *Geochimica et Cosmochimica Acta* **97**, 88–104.

Cardinal D., Alleman L. Y., Dehairs F., Savoye N., Trull T. W. and André L. (2005) Relevance of silicon isotopes to Si-nutrient utilization and Si-source assessment in Antarctic waters. *Global Biogeochem. Cycles* **19**, GB2007, doi:10.1029/2004GB002364.

Cardinal D., Savoye N., Trull T. W., Dehairs F., Kopczynska E. E., Fripiat F., Tison J.-L. and André L. (2007) Silicon isotopes in spring Southern Ocean diatoms: Large zonal changes despite homogeneity among size fractions. *Marine Chemistry* **106**, 46–62, doi:10.1016/j.marchem.2006.04.006.

Chavez, F. P. (1989), Size Distribution of phytoplankton in the central and eastern tropical Pacific, *Global Biogeochem. Cycles*, *3*(1), 27–35, doi:10.1029/GB003i001p00027.

Chavez, F. P., and R. T. Barber (1987), An estimate of new production in the equatorial Pacific, *Deep Sea Research Part A. Oceanographic Research Papers*, *34*(7), 1229–1243, doi:10.1016/0198-0149(87)90073-2.

Chazen, C. R., M. A. Altabet, and T. D. Herbert (2009), Abrupt mid-Holocene onset of centennial-scale climate variability on the Peru-Chile Margin, *Geophysical Research Letters*, *36* (18), L18704, doi:10.1029/2009GL039749.

Chávez, F. P., and M. Messié (2009), A comparison of Eastern Boundary Upwelling Ecosystems, *Progress in Oceanography*, 80–96, doi:10.1016/j.pocean.2009.07.032.

Chelton, D. B., S. K. Esbensen, M. G. Schlax, N. Thum, M. H. Freilich, F. J. Wentz, C. L. Gentemann, M. J. McPhaden, and P. S. Schopf (2001), Observations of Coupling between Surface Wind Stress and Sea Surface Temperature in the Eastern Tropical Pacific, *Journal of Climate*, *14*(7), 1–20, doi:10.1175/1520-0442(2001)014<1479:oocbsw>2.0.co;2.

Cline, J. D., and I. R. Kaplan (1975), Isotopic fractionation of dissolved nitrate during denitrification in the eastern tropical North Pacific Ocean, *Marine Chemistry*, *3*(4), 271–299.

Codispoti L. A., Brandes J. A., Christensen J. P., Devol A. H., Naqvi S., Paerl H. W. and Yoshinari T. (2001) The oceanic fixed nitrogen and nitrous oxide budgets: Moving targets as we enter the anthropocene? *Scientia Marina* **65**, 85–105.

Codispoti, L. A. (2006), An oceanic fixed nitrogen sink exceeding 400 Tg N a^{-1} vs the concept of homeostasis in the fixed-nitrogen inventory, *Biogeosciences Discuss.*, *3*(4), 1203–1246.

Crosta X. and Koç N. (2007) Diatoms: from micropaleontology to isotope geochemistry. In *Methods in Late Ceonozoic Paleoceanography* (ed. C. Hilaire-Marcel). Methods in Late Cenozoic Paleoceanography. pp. 327–369.

Czeschel R., Stramma L., Schwarzkopf F. U., Giese B. S., Funk A. and Karstensen J. (2011) Middepth circulation of the eastern tropical South Pacific and its link to the oxygen minimum zone. *J. Geophys. Res.* **116**, C01015.

Dalsgaard T., Canfield D. E., Petersen J., Thamdrup B. and Acuña-González J. (2003) N_2 production by the anammox reaction in the anoxic water column of Golfo Dulce, Costa Rica. *Nature* **422**, 606–608.

Dekaezemacker, J., Bonnet, S., Grosso, O., Moutin, T., Bressac, M., Capone, D.G., (2013). Evidence of active dinitrogen fixation in surface waters of the eastern tropical South Pacific during El Niño and La Niña events and evaluation of its potential nutrient controls. *Global Biogeochem. Cycles* **27**, 768–779. doi:10.1002/gbc.20063

De La Rocha, C. L., M. A. Brzezinski, and M. J. DeNiro (1997), Fractionation of silicon isotopes by marine diatoms during biogenic silica formation, *Geochimica et Cosmochimica Acta*, *61*(23), 5051–5056.

De La Rocha, C. L., M. A. Brzezinski, M. J. DeNiro, and A. Shemesh (1998), Silicon-isotope composition of diatoms as an indicator of past oceanic change, *Nature*, *395*(6703), 680–683.

De La Rocha De C. L., Hutchins D. A., Brzezinski M. A. and Zhang Y. (2000) Effects of iron and zinc deficiency on elemental composition and silica production by diatoms. *Mar. Ecol. Prog. Ser.* **195**, 71–79.

De La Rocha De C. L., Bescont P., Croguennoc A. and Ponzevera E. (2011) The silicon isotopic composition of surface waters in the Atlantic and Indian sectors of the Southern Ocean. *Geochimica et Cosmochimica Acta* **75**, 5283–5295.

DeMaster, D. J. (1981), The Supply and Accumulation of Silica in the Marine-Environment, *Geochimica et Cosmochimica Acta*, *45*(10), 1715–1732.

de Mendiola, B. R. (1981), Seasonal phytoplankton distribution along the Peruvian coast, in *Coastal upwelling*, vol. 1, pp. 348–356, American Geophysical Union, Washington, D. C.

De Pol-Holz, R., Ulloa, O., Dezileau, L., Kaiser, J., Lamy, F., Hebbeln, D., (2006) Melting of the Patagonian Ice Sheet and deglacial perturbations of the nitrogen cycle in the eastern South Pacific. *Geophys. Res. Lett.* **33**, L04704. doi:10.1029/2005GL024477

De Pol-Holz, R., O. Ulloa, F. Lamy, L. Dezileau, P. Sabatier, and D. Hebbeln (2007), Late Quaternary variability of sedimentary nitrogen isotopes in the eastern South Pacific Ocean, *Paleoceanography*, *22*(2), PA2207, doi:10.1029/2006PA001308.

de Souza, G. F., B. C. Reynolds, G. C. Johnson, J. L. Bullister, and B. Bourdon (2012a), Silicon stable isotope distribution traces Southern Ocean export of Si to the eastern South Pacific thermocline, *Biogeosciences*, *9*(11), 4199–4213, doi:10.5194/bg-9-4199-2012-supplement.

de Souza, G. F., B. C. Reynolds, J. Rickli, M. Frank, M. A. Saito, L. J. A. Gerringa, and B. Bourdon (2012b), Southern Ocean control of silicon stable isotope distribution in the deep Atlantic Ocean, *Global Biogeochem. Cycles*, *26*(2), 2035–2047, doi:10.1029/2011GB004141.

Deutsch, C., Sarmiento, J.L., Sigman, D.M., Gruber, N., Dunne, J.P., (2007) Spatial coupling of nitrogen inputs and losses in the ocean. *Nature* **445**, 163–167. doi:doi:10.1038/nature05392

Deutsch, C., Sigman, D.M., Thunell, R.C., Meckler, A.N., Haug, G.H., (2004 Isotopic constraints on glacial/interglacial changes in the oceanic nitrogen budget. *Global Biogeochem. Cycles* **18**, GB4012. doi:10.1029/2003GB002189

De Vries T. J. and Schrader H. (1981) Variation of upwelling/oceanic conditions during the latest Pleistocene through Holocene off the central Peruvian coast: A diatom record. *Marine Micropaleontology* **6**, 157–167.

Díaz-Ochoa, J. A., C. B. Lange, S. Pantoja, G. J. De Lange, D. Gutiérrez, P. Muñoz, and M. Salamanca (2009), Fish scales in sediments from off Callao, central Peru, *Deep Sea Research Part II: Topical Studies in Oceanography*, *56*(16), 1124–1135, doi:10.1016/j.dsr2.2008.09.015.

DiTullio G. R., Geesey M. E., Maucher J. M. and Alm M. B. (2005) Influence of iron on algal community composition and physiological status in the Peru upwelling system. *Limnol. Oceangr.* **50**, 1887–1907.

Doering, K., C. Ehlert, P. Grasse, X. Crosta, S. Fleury, M. Frank, and R. Schneider (2016), Differences between mono-generic and mixed diatom silicon isotope compositions trace present and past nutrient utilisation off Peru, *Geochimica et Cosmochimica Acta*, *177*(C), 30–47, doi:10.1016/j.gca.2015.12.029.

Doering, K., Erdem Z., Ehlert, C., Fleury S., Frank M. and Schneider R., (under review at Paleoceanography) Changes in diatom productivity and upwelling intensity off Peru since the Last Glacial Maximum: local response to basin-scale atmospheric and oceanic forcing.

Douthitt C. B. (1982) The geochemistry of the stable isotopes of silicon. *Geochimica et Cosmochimica Acta* **46**, 1449–1458.

Dubois, N., M. Kienast, S. Kienast, C. Normandeau, S. E. Calvert, T. D. Herbert, and A. Mix (2011), Millennial-scale variations in hydrography and biogeochemistry in the Eastern Equatorial Pacific over the last 100 kyr, *Quaternary Science Reviews*, **30**(1), 210–223.

Dubois, N., M. Kienast, S. Kienast, S. E. Calvert, R. François, and R. F. Anderson (2010), Sedimentary opal records in the eastern equatorial Pacific: It is not all about leakage, *Global Biogeochem. Cycles*, **24**(4), GB4020, doi:10.1029/2010GB003821.

Dubois, N., M. Kienast, S. S. Kienast, and A. Timmermann (2014), Millennial-scale

Atlantic/East Pacific sea surface temperature linkages during the last 100,000 years, *Earth and Planetary Science Letters*, **396**, 134–142, doi:10.1016/j.epsl.2014.04.008.

Dugdale, R.C., Goering, J.J., (1967). Uptake of new and regenerated forms of nitrogen in primary productivity. *Limnol. Oceangr.* **12**, 196–206. doi:10.4319/lo.1967.12.2.0196.

Dugdale R.C., Wilkerson F. P. and Minas, H. J.(1995) The role of a silicate pump in driving new production. *Deep-Sea Research I* **42**(5), 697-719.

Dugdale R. C. and Wilkerson F. P. (1998) Silicate regulation of new production in the equatorial Pacific upwelling. *Nature* **391**, 270–273.

Dugdale R. C., Wischmeyer A. G., Wilkerson F. P., Barber R. T., Chai F., Jiang M. S. and Peng T. H. (2002) Meridional asymmetry of source nutrients to the equatorial Pacific upwelling ecosystem and its potential impact on ocean-atmosphere CO_2 flux; a data and modeling approach. *Deep-Sea Research Part II* **49**, 2513–2531.

Echevin V., Aumont O., Ledesma J. and Flores G. (2008) The seasonal cycle of surface chlorophyll in the Peruvian upwelling system: A modelling study. *Progress in Oceanography* **79**, 167–176.

Egan, K.E., Rickaby, R.E.M., Leng, M.J., Hendry, K.R., Hermoso, M., Sloane, H.J., Bostock, H., Halliday, A.N., (2012). Diatom silicon isotopes as a proxy for silicic acid utilisation: A Southern Ocean core top calibration. *Geochimica et Cosmochimica Acta* **96**, 174–192.. doi:10.1016/j.gca.2012.08.002

Ehlert, C., Grasse, P., Frank, M., (2013). Changes in silicate utilisation and upwelling intensity off Peru since the Last Glacial Maximum - insights from silicon and neodymium isotopes. *Quaternary Science Reviews* **72**, 18–35. doi:10.1016/j.quascirev.2013.04.013

Ehlert, C., Grasse, P., Gutiérrez, D., Salvatteci, R., Frank, M., 2015. Nutrient utilisation and weathering inputs in the Peruvian upwelling region since the Little Ice Age. Clim. Past 11, 187–202. doi:10.5194/cp-11-187-2015-supplement

Ehlert, C., P. Grasse, E. Mollier-Vogel, T. Böschen, J. Franz, G. F. de Souza, Ben C Reynolds, L. Stramma, and M. Frank (2012), Factors controlling the silicon isotope distribution in waters and surface sediments of the Peruvian coastal upwelling, *Geochimica et Cosmochimica Acta*, *99*(C), 128–145, doi:10.1016/j.gca.2012.09.038.

Ellwood M. J., Wille M. and Maher W. (2010) Glacial Silicic Acid Concentrations in the Southern Ocean. *Science* **330**, 1088–1091.

Emmer, E., Thunell, R.C., 2000. Nitrogen isotope variations in Santa Barbara Basin sediments: Implications for denitrification in the eastern tropical North Pacific during the last 50,000 years. Paleoceanography 15, 377–387.

Erdem, Z., J. Schönfeld, N. Block and A. Eisenhauer (2016), Peruvian sediments as recorders of an evolving hiatus for the last 22 thousand years, *Quaternary Science Reviews*, *137*, 1-14, doi: 10.1016/j.quascirev.2016.01.029

Estrada, M., and D. Blasco (1985), *Phytoplankton assemblages in coastal upwelling areas*, edited by C. Bas, R. Margalef, and P. Rubies, Instituto de Investigaciones

Pesqueras, Barcelona.

Eugster, O., Gruber, N., Deutsch, C., Jaccard, S.L., Payne, M.R., 2013. The dynamics of the marine nitrogen cycle across the last deglaciation. Paleoceanography 28, 116–129. doi:10.1002/palo.20020

Fairbanks, R. G. (1989), A 17,000-year glacio-eustatic sea level record: influence of glacial melting rates on the Younger Dryas event and deep-ocean circulation, *Nature*, *342*(6250), 637–642, doi:10.1038/342637a0.

Fiedler, P. C., and L. D. Talley (2006), Hydrography of the eastern tropical Pacific: A review, *Progress in Oceanography*, *69*(2-4), 143–180, doi:10.1016/j.pocean.2006.03.008.

Fleury, S., P. Martinez, X. Crosta, K. Charlier, I. Billy, V. Hanquiez, T. Blanz, and R. R. Schneider (2015), Pervasive multidecadal variations in productivity within the Peruvian Upwelling System over the last millennium, *Quaternary Science Reviews*, *125*(C), 78–90, doi:10.1016/j.quascirev.2015.08.006.

Franz J., Krahmann G., Lavik G., Grasse P., Dittmar T. and Riebesell U. (2012) Dynamics and stoichiometry of nutrients and phytoplankton in waters influenced by the oxygen minimum zone in the eastern tropical Pacific. *Deep-Sea Research Part I* **62**, 20–31.

Freudenthal T., Wagner T., Wenzhöfer F., Zabel M. and Wefer G. (2001a) Early diagenesis of organic matter from sediments of the eastern subtropical Atlantic: evidence from stable nitrogen and carbon isotopes. *Geochimica et Cosmochimica Acta* **65**, 1795–1808.

Freudenthal, T., Neuer, S., Meggers, H., Davenport, R., Wefer, G., (2001b) Influence of lateral particle advection and organic matter degradation on sediment accumulation and stable nitrogen isotope ratios along a productivity gradient in the Canary Islands region. *Marine Geology* **177**, 93–109.

Fripiat F., Cavagna A. J., Dehairs F., Speich S., André L. and Cardinal D. (2011a) Silicon pool dynamics and biogenic silica export in the Southern Ocean inferred from Si-isotopes. *Ocean Science* **7**, 533–547.

Fripiat, F., A.-J. Cavagna, N. Savoye, F. Dehairs, L. André, and D. Cardinal (2011b), Isotopic constraints on the Si-biogeochemical cycle of the Antarctic Zone in the Kerguelen area (KEOPS), *Marine Chemistry*, **123**(1-4), 11–22, doi:10.1016/j.marchem.2010.08.005.

Fripiat F., Cavagna A. J., Dehairs F., de Brauwere A., André L. and Cardinal D. (2012) Processes controlling the Si-isotopic composition in the Southern Ocean and application for paleoceanography. *Biogeosciences* **9**, 2443–2457.

Fry B. (2006) *Stable Isotope Ecology*. Springer, New York.

Fuenzalida R., Schneider W., Garcés-Vargas J., Bravo L. and Lange C. (2009) Vertical and horizontal extension of the oxygen minimum zone in the eastern South Pacific Ocean. *Deep Sea Research Part II: Topical Studies in Oceanography* **56**, 992–1003.

Galbraith, E.D., Jaccard, S.L., 2015. Deglacial weakening of the oceanic soft tissue

pump: global constraints from sedimentary nitrogen isotopes and oxygenation proxies. Quaternary Science Reviews 109, 38–48. doi:10.1016/j.quascirev.2014.11.012

Galbraith, E.D., Kienast, M., Albuquerque, A.L., Altabet, M.A., Batista, F., Bianchi, D., Calvert, S.E., Contreras, S., Crosta, X., De Pol-Holz, R., Dubois, N., Etourneau, J., François, R., Hsu, T.C., Ivanochko, T., Jaccard, S.L., Kao, S.-J., Kiefer, T., Kienast, S., Lehmann, M.F., Martinez, P., McCarthy, M., Meckler, A.N., Mix, A., Möbius, J., Pedersen, T.F., Pichevin, L., Quan, T.M., Robinson, R.S., Ryabenko, E., Schmittner, A., Schneider, R., Schneider-Mor, A., Shigemitsu, M., Sinclair, D., Somes, C., Studer, A.S., Tesdal, J.-E., Thunell, R., Terence Yang, J.-Y., (2013) The acceleration of oceanic denitrification during deglacial warming. *Nature Geoscience* **6**, 579–584. doi:10.1038/ngeo1832

Galbraith, E.D., Kienast, M., Jaccard, S.L., Pedersen, T.F., Brunelle, B.G., Sigman, D.M., Kiefer, T., (2008) Consistent relationship between global climate and surface nitrate utilization in the western subarctic Pacific throughout the last 500 ka. *Paleoceanography* **23**, PA2212. doi:10.1029/2007PA001518

Galbraith E. D., Kienast M., Pedersen T. F. and Calvert S. E. (2004) Glacial-interglacial modulation of the marine nitrogen cycle by high-latitude O_2 supply to the global thermocline. *Paleoceanography* **19**, PA4007.

Ganeshram R. S., Pedersen T. F., Calvert S. E., McNeill G. W. and Fontugne M. R. (2000) Glacial-interglacial variability in denitrification in the World's Oceans: Causes and consequences. *Paleoceanography* **15**, 361–376.

Ganeshram, R.S., Pedersen, T.F., Calvert, S.E., Murray, J.W., (1995) Large changes in oceanic nutrient inventories from glacial to interglacial periods. *Nature* **376**, 755–758.

Garreaud, R. D., M. Vuille, R. Compagnucci, and J. Marengo (2009), Present-day South American climate, *Palaeogeography, Palaeoclimatology, Palaeoecology*, *281*(3-4), 180–195, doi:10.1016/j.palaeo.2007.10.032.

Garrison D. L. (1979) Monterey Bay phytoplankton I. Seasonal cycles of phytoplankton assemblages. *Journal of Plankton Research* **1**, 241–265.

Garrison D. L. (1981) Monterey Bay phytoplankton. II. Resting spore cycles in coastal diatom populations. *Journal of Plankton Research* **3**, 137-156.

Georg R. B., Reynolds B. C., Frank M. and Halliday A. N. (2006) New sample preparation techniques for the determination of Si isotopic compositions using MC-ICPMS. *Chemical Geology* **235**, 95–104.

Georg R. B., Zhu C., Reynolds B. C. and Halliday A. N. (2009) Stable silicon isotopes of groundwater, feldspars, and clay coatings in the Navajo Sandstone aquifer, Black Mesa, Arizona, USA. *Geochimica et Cosmochimica Acta* **73**, 2229–2241.

Gonfiantini, R., Stichler, W., Rozanski, K., (1995) Standards and intercomparison materials distributed by the International Atomic Energy Agency for stable isotope measurements.

Granger J., Sigman D. M., Needoba J. A. and Harrison P. J. (2004) Coupled nitrogen

and oxygen isotope fractionation of nitrate during assimilation by cultures of marine phytoplankton. *Limnol. Oceangr.* **49**, 1763–1773.

Granger, J., Sigman, D.M., Lehmann, M.F., Tortell, P.D., (2008) Nitrogen and oxygen isotope fractionation during dissimilatory nitrate reduction by denitrifying bacteria. *Limnol. Oceangr.* **53**, 2533.

Grasse, P., C. Ehlert, and M. Frank (2013), The influence of water mass mixing on the dissolved Si isotope composition in the Eastern Equatorial Pacific, *Earth and Planetary Science Letters*, *380*, 60–71, doi:10.1016/j.epsl.2013.07.033.

Grasshoff K., Kremling K. and Ehrhardt M. (1999) *Methods of sewater analysis*. third, John Wiley & Sons.

Gruber N. and Sarmiento J. L. (1997) Global patterns of marine nitrogen fixation and denitrification. *Global Biogeochem. Cycles* **11**, 235–266.

Gutiérrez, D., A. Sifeddine, D. B. Field, L. Ortlieb, G. Vargas Easton, F. P. Chávez, F. Velazco, V. Ferreira, P. Tapia, and R. Salvatteci (2009), Rapid reorganization in ocean biogeochemistry off Peru towards the end of the Little Ice Age, *Biogeosciences*, *6*, 835–848.

Hansen A., Ohde T. and Wasmund N. (2014) Succession of micro- and nanoplankton groups in aging upwelled waters off Namibia. *Journal of Marine Systems* **140**, 130–137.

Hasle, G.R., Fryxell, G.A., 1970. Diatoms: Cleaning and Mounting for Light and Electron Microscopy. Transactions of the American Microscopical Society 89, 469. doi:10.2307/3224555

Hayes, J.M., Popp, B.N., Takigiku, R., 1989. An isotopic study of biogeochemical relationships between carbonates and organic carbon in the Greenhorn Formation. Geochimica et Cosmochimica Acta 53, 2961–2972. doi:10.1016/0016-7037(89)90172-5

Hayes, C. T., R. F. Anderson, and M. Q. Fleisher (2011), Opal accumulation rates in the equatorial Pacific and mechanisms of deglaciation - Hayes, *Paleoceanography*, *26*(1), PA1207, doi:10.1029/2010PA002008.

Hendry, K. R., and M. A. Brzezinski (2014) Using silicon isotopes to understand the role of the Southern Ocean in modern and ancient biogeochemistry and climate, *Quaternary Science Reviews*, **89**, 13–26, doi:10.1016/j.quascirev.2014.01.019.

Hendry K. R., Georg R. B., Rickaby R. E. M., Robinson L. F. and Halliday A. N. (2010) Deep ocean nutrients during the Last Glacial Maximum deduced from sponge silicon isotopic compositions. *Earth and Planetary Science Letters* **292**, 290–300, doi:10.1016/j.epsl.2010.02.005.

Hendy, I.L., Pedersen, T.F., 2006. Oxygen minimum zone expansion in the eastern tropical North Pacific during deglaciation. Geophys. Res. Lett. 33, L20602. doi:10.1029/2006GL025975

Higginson M. J. (2004) Initial test of the silicic acid leakage hypothesis using sedimentary biomarkers. *Geophys. Res. Lett.* **31**, L18303.

Horn, M.G., Beucher, C.P., Robinson, R.S., Brzezinski, M.A., (2011a) Southern ocean nitrogen and silicon dynamics during the last deglaciation. *Earth and Planetary Science Letters* **310**, 334–339. doi:10.1016/j.epsl.2011.08.016

Horn, M.G., Robinson, R.S., Rynearson, T.A., Sigman, D.M., (2011b) Nitrogen isotopic relationship between diatom-bound and bulk organic matter of cultured polar diatoms. *Paleoceanography* **26**, PA3208. doi:10.1029/2010PA002080

Hutchins D. A. and Bruland K. W. (1998) Iron-limited diatom growth and Si: N uptake ratios in a coastal upwelling regime. *Nature* **393**, 561–564.

Hutchins D. A., Hare C. E., Weaver R. S., Zhang Y., Firme G. F., DiTullio G. R., Alm M. B., Riseman S. F., Maucher J. M., Geesey M. E., Trick C. G., Smith G. J., Rue E. L., Conn J. and Bruland K. W. (2002) Phytoplankton iron limitation in the Humboldt Current and Peru Upwelling. *Limnol. Oceangr.* **47**, 997–1011.

Huyer, A., R. L. Smith, and T. Paluszkiewicz (1987), Coastal upwelling off Peru during normal and El Niño times, 1981–1984, *Journal of Geophysical Research: Oceans*, *92*(C13), 14297–14307.

Ingalls, A.E., Anderson, R.F., Pearson, A., 2004. Radiocarbon dating of diatom-bound organic compounds. Marine Chemistry 92, 91–105. doi:10.1016/j.marchem.2004.06.019

Jaccard, S.L., Galbraith, E.D., 2011. Large climate-driven changes of oceanic oxygen concentrations during the last deglaciation. Nature Geoscience 5, 151–156. doi:10.1038/ngeo1352

Jaccard, S.L., Galbraith, E.D., Frölicher, T.L., 2014. Ocean (de) oxygenation across the last deglaciation. Oceanography 1–10.

Jacot Des Combes H., Esper O., De La Rocha C. L., Abelmann A., Gersonde R., Yam R. and Shemesh A. (2008) Diatom $\delta^{13}C$, $\delta^{15}N$, and C/N since the Last Glacial Maximum in the Southern Ocean: Potential impact of Species Composition. *Paleoceanography* **23**, PA4209, doi: 10.1029/2008PA001589.

Johnson K. S., Chavez F. P. and Friederich G. E. (1999) Continental-shelf sediment as a primary source of iron for coastal phytoplankton. *Nature* **398**, 1–4.

Jones B. H., Brink K. H., Dugdale R. C., Stuart D. W., Van Leer J. C., Blasco D. and Kelley J. C. (1983) Observations of a Persistent Upwelling Center off Point Conception, California. In *Coastal Upwelling Its Sediment Record*. Springer US, Boston, MA. pp. 37–60.

Junium, C.K., Arthur, M.A., 2007. Nitrogen cycling during the Cretaceous, Cenomanian-Turonian Oceanic Anoxic Event II - Junium - 2007 - Geochemistry, Geophysics, Geosystems - Wiley Online Library. Geochemistry. doi:10.1029/2006GC001328/pdf

Junium, C.K., Arthur, M.A., Freeman, K.H., 2015. Compound-specific ^{15}N and chlorin preservation in surface sediments of the Peru Margin with implications for ancient bulk $\delta^{15}N$ records. *Geochimica et Cosmochimica Acta* **160**, 306–318. doi:10.1016/j.gca.2014.12.018

Kalansky, J.F., Robinson, R.S., Popp, B.N., 2011. Insights into nitrogen cycling in the western Gulf of California from the nitrogen isotopic composition of diatom-bound organic matter. Geochem. Geophys. Geosyst. 12, n/a–n/a. doi:10.1029/2010GC003437

Kemp A., Pike J., Pearce R. B. and Lange C. B. (2000) The "Fall dump" — a new perspective on the role of a 'shade flora' in the annual cycle of diatom production and export flux. *Deep-Sea Research Part II*.

Kessler, W. S. (2006), The circulation of the eastern tropical Pacific: A review, *Progress in Oceanography*, **69**(2-4), 181–217, doi:10.1016/j.pocean.2006.03.009.

Kienast, M., (2000). Unchanged nitrogen isotopic composition of organic matter in the South China Sea during the last climatic cycle: Global implications. *Paleoceanography* **15**, 244–253. doi:10.1029/1999PA000407

Kienast, M., S. S. Kienast, S. E. Calvert, T. I. Eglinton, G. Mollenhauer, R. François, and A. C. Mix (2006a), Eastern Pacific cooling and Atlantic overturning circulation during the last deglaciation, *Nature*, *443*(7113), 846–849, doi:10.1038/nature05222.

Kienast, S. S., M. Kienast, S. Jaccard, S. E. Calvert, and R. Francois (2006b), Testing the silica leakage hypothesis with sedimentary opal records from the eastern equatorial Pacific over the last 150 kyrs, *Geophys. Res. Lett.*, *33*(15), L15607, doi:10.1029/2006GL026651.

Kienast, S. S., T. Friedrich, N. Dubois, P. S. Hill, A. Timmermann, A. C. Mix, and M. Kienast (2013), Near collapse of the meridional SST gradient in the eastern equatorial Pacific during Heinrich Stadial 1, *Paleoceanography*, *28*(4), 663–674, doi:doi:10.1002/2013PA002499.

Krissek, L. A., K. F. Scheidegger, and L. D. Kulm (1980), Surface sediments of the Peru-Chile continental margin and the Nazca plate, *Geol Soc America Bull*, *91*(6), 321, doi:10.1130/0016-7606(1980)91<321:SSOTPC>2.0.CO;2.

Kröger, N., Deutzmann, R., Bergsdorf, C., Sumper, M., 2000. Species-specific polyamines from diatoms control silica morphology. Proceedings of the National Academy of Sciences 97, 14133–14138.

Lam P., Lavik G., Jensen M. M., van de Vossenberg J., Schmid M., Woebken D., Gutiérrez D., Amann R., Jetten M. S. and Kuypers M. M. (2009) Revising the nitrogen cycle in the Peruvian oxygen minimum zone. *Proceedings of the National Academy of Sciences* **106**, 4752–4757.

Lisitzin A. P. (1971) Ditsribution of siliceous micro fossils in suspension and in bottom sediments. In *The Micropalaeontology of Oceans* (eds. B. M. Funnell and W. R. Riedel). Cambridge Univ.Press, New York. pp. 173–195.

Liu, K.-K., Kaplan, I.R., 1989. The eastern tropical Pacific as a source of ^{15}N-enriched nitrate in seawater off southern California. Limnol. Oceangr. 820–830.

Löscher, C.R., kopf, T.G.S., Desai, F.D., Gill, D., Schunck, H., Croot, P.L., Schlosser, C., Neulinger, S.C., Pinnow, N., Lavik, G., Kuypers, M.M.M., LaRoche, J., Schmitz, R.A., 2014. Facets of diazotrophy in the oxygen minimum zone waters off Peru 8, 2180–2192. doi:10.1038/ismej.2014.71

Löscher, C., Bourbonnais, A., Dekaezemacker, J., Charoenpong, C.N., Altabet, M.A., Bange, H.W., Czeschel, R., Hoffmann, C., Schmitz-Streit, R., 2015. N_2 fixation in eddies of the eastern tropical South Pacific Ocean. *Biogeosciences Discussions*, **12** (22). pp. 18945-18972. doi:10.5194/bgd-12-18945-2015

Loubere, P. (1999), A multiproxy reconstruction of biological productivity and oceanography in the eastern equatorial Pacific for the past 30,000 years, *Marine Micropaleontology*, *37*(2), 173–198, doi:10.1016/S0377-8398(99)00013-4.

Lourey M. J., Trull T. W. and Sigman D. M. (2003) Sensitivity of $\delta^{15}N$ of nitrate, surface suspended and deep sinking particulate nitrogen to seasonal nitrate depletion in the Southern Ocean. *Global Biogeochem. Cycles* **17**, 1081, doi: 0.1029/2002GB001973.

Lukas R. (1986) The termination of the Equatorial Undercurrent in the eastern Pacific. *Prog. Oceanogr.* **16**(2), 63-90.

MacIsaac J. J., Dugdale R. C., Barber R. T., Blasco D. and Packard T. T. (1985) Primary production cycle in an upwelling center. *Deep Sea Research Part A. Oceanographic Research Papers* **32**, 503–529, doi:10.1016/0198-0149(85)90042-1.

Macko, S.A., Estep, M.L.F., 1984. Microbial alteration of stable nitrogen and carbon isotopic compositions of organic matter. Organic Geochemistry 6, 787–790. doi:10.1016/0146-6380(84)90100-1.

McPhaden M. J., Zebiak S. E. and Glantz M. H. (2006) ENSO as an Integrating Concept in Earth Science. *Science* **314**, 1740–1745.

Maier E., Chapligin B. and Abelmann A. (2013) Combined oxygen and silicon isotope analysis of diatom silica from a deglacial subarctic Pacific record. *Journal of of Quaternay Science* **28**, 572–581.

Makou, M. C., T. I. Eglinton, D. W. Oppo, and K. A. Hughen (2010), Postglacial changes in El Nino and La Nina behavior, *Geology*, *38*(1), 43–46, doi:10.1130/G30366.1.

Margalef R. (1978) Life-forms of phytoplankton as survival alternatives in an unstable environment. *Oceanologica acta* **1**, 493–509.

Mariotti, A., J. C. Germon, P. Hubert, P. Kaiser, R. Letolle, A. Tardieux, and P. Tardieux (1981), Experimental determination of nitrogen kinetic isotope fractionation: some principles; illustration for the denitrification and nitrification processes, *Plant and soil*, *62*(3), 413–430.

Martinez, P., Lamy, F., Robinson, R.R., Pichevin, L., Billy, I., (2006) Atypical $\delta^{15}N$ variations at the southern boundary of the East Pacific oxygen minimum zone over the last 50ka. *Quaternary Science Reviews* **25**, 3017–3028. doi:10.1016/j.quascirev.2006.04.009

McGee, D., A. Donohoe, J. Marshall, and D. Ferreira (2014), Changes in ITCZ location and cross-equatorial heat transport at the Last Glacial Maximum, Heinrich Stadial 1, and the mid-Holocene, *Earth and Planetary Science Letters*, *390*, 69–79, doi:10.1016/j.epsl.2013.12.043.

Messié M. and Chavez F. (2015) Seasonal regulation of primary production in eastern boundary upwelling systems. *Progress in Oceanography* **134**, 1-18. doi:10.1016/j.pocean.2014.10.011.

Milligan A. J., Varela D. E., Brzezinski M. A. and Morel F. M. M. (2004) Dynamics of silicon metabolism and silicon isotopic discrimination in a marine diatom as a function of pCO_2. *Limnol. Oceanogr., 49 (2) 329.* **322**.

Mohtadi, M. (2004), Mechanisms and variations of the paleoproductivity off northern Chile (24°S–33°S) during the last 40,000 years, *Paleoceanography*, **19**(2), PA2023, doi:10.1029/2004PA001003.

Mollier-Vogel, E., Ryabenko, E., Martinez, P., Wallace, D., Altabet, M.A., Schneider, R., (2012). Nitrogen isotope gradients off Peru and Ecuador related to upwelling, productivity, nutrient uptake and oxygen deficiency. *Deep-Sea Research Part I* **70**, 14–25. doi:10.1016/j.dsr.2012.06.003

Mollier-Vogel E., (2012) Peruvian Oxygen Minimum Zone dynamics during the last 18 000 years. *PhD Thesis, University of Kiel.*

Mollier-Vogel, E., G. Leduc, T. Böschen, P. Martinez, and R. R. Schneider (2013), Rainfall response to orbital and millennial forcing in northern Peru over the last 18 ka, *Quaternary Science Reviews*, **76**, 29–38, doi:10.1016/j.quascirev.2013.06.021.

Montade, V., M. Kageyama, N. Combourieu-Nebout, M.-P. Ledru, E. Michel, G. Siani, and C. Kissel (2015), Teleconnection between the Intertropical Convergence Zone and southern westerly winds throughout the last deglaciation, *Geology*, G36745.1, doi:10.1130/G36745.1.

Montes, I., F. Colas, X. Capet, and W. Schneider (2010), On the pathways of the equatorial subsurface currents in the eastern equatorial Pacific and their contributions to the Peru-Chile Undercurrent, *J. Geophyss Res.*, **115**, C09003, doi:10.1029/2009JC005710.

Montes, I., W. Schneider, F. Colas, B. Blanke, and V. Echevin (2011), Subsurface connections in the eastern tropical Pacific during La Niña 1999–2001 and El Niño 2002–2003, *Journal of Geophysical Research: Oceans*, *116*(C12), C12022, doi:10.1029/2011JC007624.

Montoya J. P. and McCarthy J. J. (1995) Isotopic fractionation during nitrate uptake by phytoplankton grown in continuous culture. *Journal of Plankton Research* **17**, 439–464.

Moore J. K., Doney S. C. and Lindsay K. (2004) Upper ocean ecosystem dynamics and iron cycling in a global three-dimensional model. *Global Biogeochem. Cycles* **18**, GB4028.

Moore, C.M., Mills, M.M., Arrigo, K.R., Berman-Frank, I., Bopp, L., Boyd, P.W., Galbraith, E.D., Geider, R.J., Guieu, C., Jaccard, S.L., Jickells, T.D., La Roche, J., Lenton, T.M., Mahowald, N.M., Marañón, E., Marinov, I., Moore, J.K., Nakatsuka, T., Oschlies, A., Saito, M.A., Thingstad, T.F., Tsuda, A., Ulloa, O., (2013) Processes and patterns of oceanicnutrient limitation. *Nature Geoscience*, 1–10. doi:10.1038/ngeo1765

Morales C. E., Hormazábal S. E. and Blanco J. (1999) Interannual variability in the mesoscale distribution of the depth of the upper boundary of the oxygen minimum layer off northern Chile (18–24°S): Implications for the pelagic system and biogeochemical cycling. *Journal of Marine Research* **57**, 909–932.

Morales, L.V., Sigman, D.M., Horn, M.G., Robinson, R.S., 2013. Cleaning methods for the isotopic determination of diatom-bound nitrogen in non-fossil diatom frustules. Limnol. Oceangr. Methods 11, 101–112. doi:10.4319/lom.2013.11.101

Morel F. and Price N. M. (2003) The Biogeochemical Cycles of Trace Metals in the Oceans. *Science* **300**, 944–947.

Morley D. W., Leng M. J., Mackay A. W., Sloane H. J., Rioual P. and Battarbee R. W. (2004) Cleaning of lake sediment samples for diatom oxygen isotope analysis. *Journal of Paleolimnology* **31**, 391–401.

Mortlock R. A. and Froelich P. N. (1989) A Simple Method for the Rapid-Determination of Biogenic Opal in Pelagic Marine-Sediments. *Deep Sea Research Part A. Oceanographic Research Papers* **36**, 1415–1426.

Muratli, J. M., Z. Chase, A. C. Mix, and J. McManus (2009), Increased glacial-age ventilation of the Chilean margin by Antarctic Intermediate Water, *Nature Geoscience*, *3*(1), 23–26, doi:10.1038/ngeo715.

Müller, P. J., and R. Schneider (1993), An Automated Leaching Method for the Determination of Opal in Sediments and Particulate Matter, *Deep-Sea Research Part I*, *40*(3), 425–444.

Nelson D. M., Tréguer P., Brzezinski M. A., Leynaert A. and Queguiner B. (1995) Production and dissolution of biogenic silica in the ocean: Revised global estimates, comparison with regional data and relationship to biogenic sedimentation. *Global Biogeochem. Cycles* **9**, 359–372.

Noffke A., Hensen C., Sommer S., Scholz F., Bohlen L., Mosch T., Graco M. and Wallmann K. (2012) Benthic iron and phosphorus fluxes across the Peruvian oxygen minimum zone. *Limnol. Oceangr.* **57**, 851–867.

Nürnberg, D., T. Böschen, K. Doering, E. Mollier-Vogel, R. Schneider, and J. Raddatz (2015), Sea surface and subsurface circulation dynamics off equatorial Peru during the last ~17 kyrs, *Paleoceanography*, 30, 984–999, doi:10.1002/2014PA002706.

Ochoa, N., and O. Gomez (1981), *Variaciones del fitoplancton en el área de Chimbote durante 1977*.

Ochoa, N., M. H. Taylor, S. Purca, and E. Ramos (2010), Intra- and interannual variability of nearshore phytoplankton biovolume and community changes in the northern Humboldt Current system, *Journal of Plankton Research*, *32*(6), 843–855, doi:10.1093/plankt/fbq022.

Oku O. and Kamatani A. (1997) Resting spore formation of the marine planktonic diatom Chaetoceros anastomosans induced by high salinityand nitrogen depletion. *Marine Biology* **127**, 515–520.

Ortlieb L., Vargas G. and Saliège J.-F. (2011) Marine radiocarbon reservoir effect along

the northern Chile–southern Peru coast (14–24°S) throughout the Holocene. *Quaternary Research* **75**, 91–103, doi:10.1016/j.yqres.2010.07.018.

Pena, L. D., I. Cacho, P. Ferretti, and M. A. Hall (2008), El Niño-Southern Oscillation-like variability during glacial terminations and interlatitudinal teleconnections, *Paleoceanography*, *23*(3), PA3101, doi:10.1029/2008PA001620.

Pena, L. D., S. L. Goldstein, S. R. Hemming, K. M. Jones, E. Calvo, C. Pelejero, and I. Cacho (2013), Rapid changes in meridional advection of Southern Ocean intermediate waters to the tropical Pacific during the last 30kyr, *Earth and Planetary Science Letters*, *368*(C), 20–32, doi:10.1016/j.epsl.2013.02.028.

Pennington, J. T., K. L. Mahoney, V. S. Kuwahara, D. D. Kolber, R. Calienes, and F. P. Chavez (2006), Primary production in the eastern tropical Pacific: A review, *Progress in Oceanography*, **69**(2-4), 285–317, doi:10.1016/j.pocean.2006.03.012.

Philander S. G. (1990) *El Nino*, *La Nina*, *and the Southern Oscillation*, Academic Press, San Diego.

Pichevin, L.E., Ganeshram, R.S., Francavilla, S., 2010. Interhemispheric leakage of isotopically heavy nitrate in the eastern tropical Pacific during the last glacial period. Paleoceanography **25**, PA1204, doi:10.1029/2009PA001754.

Pichevin L. E., Ganeshram R. S., Geibert W., Thunell R. and Hinton R. (2014) Silica burial enhanced by iron limitation in oceanic upwelling margins. *Nature Geoscience* **7**, 541-546, doi:10.1038/ngeo2181.

Pichevin L. E., Reynolds B. C., Ganeshram R. S., Cacho I., Pena L., Keefe K. and Ellam R. M. (2009) Enhanced carbon pump inferred from relaxation of nutrient limitation in the glacial ocean. *Nature* **459**, 1114–1117, doi:10.1038/nature08101.

Poulsen, N., Sumper, M., Kroger, N., 2003. Biosilica formation in diatoms: Characterization of native silaffin-2 and its role in silica morphogenesis. Proceedings of the National Academy of Sciences 100, 12075–12080. doi:10.1073/pnas.2035131100

Rafter, P. A., D. M. Sigman, C. D. Charles, J. Kaiser, and G. H. Haug (2012), Subsurface tropical Pacific nitrogen isotopic composition of nitrate: Biogeochemical signals and their transport, *Global Biogeochem. Cycles*, *26*(1), GB1003, doi:10.1029/2010GB003979.

Ragueneau O., Tréguer P., Leynaert A., Anderson R. F., Brzezinski M. A., DeMaster D. J., Dugdale R. C., Dymond J., Fischer G. and Francois R. (2000) A review of the Si cycle in the modern ocean: recent progress and missing gaps in the application of biogenic opal as a paleoproductivity proxy. *Global and Planetary Change* **26**, 317–365.

Rathburn A. E., Pichon J. J. and Ayress M. A. (1997) Microfossil and stable-isotope evidence for changes in Late Holocene palaeoproductivity and palaeoceanographic conditions in the Prydz Bay region of Antarctica. *Palaeogeography. Palaeoclimatology, Paleaoecology* **131**, 485-510.

Reimer P. J. and Bard E. (2013) IntCal13 and Marine13 radiocarbon age calibration curves 0-50,000 years cal BP. *Radiocarbon* **55**, 1869–1887.

Rein, B. (2004), A major Holocene ENSO anomaly during the Medieval period, *Geophys. Res. Lett.*, *31*(17), L17211, doi:10.1029/2004GL020161.

Rein, B., Lückge, A., Reinhardt, L., Sirocko, F., Wolf, A., Dullo, W.-C., 2005. El Niño variability off Peru during the last 20,000 years. Paleoceanography 20, PA4003. doi:10.1029/2004PA001099

Revesz, K., Böhlke, J.K., Yoshinari, T., 1997. Determination of $\delta^{18}O$ and $\delta^{15}N$ in Nitrate. Anal. Chem. 69, 4375–4380.

Reynolds B. C., Frank M. and Halliday A. N. (2006) Silicon isotope fractionation during nutrient utilization in the North Pacific. *Earth and Planetary Science Letters* **244**, 431–443.

Reynolds B. C., Aggarwal J., Andr L., Baxter D., Beucher C., Brzezinski M. A., Engstr m E., Georg R. B., Land M., Leng M. J., Opfergelt S., Rodushkin I., Sloane H. J., van den Boorn S. H. J. M., Vroon P. Z. and Cardinal D. (2007) An inter-laboratory comparison of Si isotope reference materials. *J. Anal. At. Spectrom.* **22**, 561.

Reynolds, B. C., M. Frank, and A. N. Halliday (2008), Evidence for a major change in silicon cycling in the subarctic North Pacific at 2.73 Ma, *Paleoceanography*, *23*(4), PA4219, doi:10.1029/2007PA001563.

Robinson R. S., Brunelle B. G. and Sigman D. M. (2004) Revisiting nutrient utilization in the glacial Antarctic: Evidence from a new method for diatom-bound N isotopic analysis. *Paleoceanography* **19**, PA3001.

Robinson, R.S., Martinez, P., Pena, L.D., Cacho, I., (2009) Nitrogen isotopic evidence for deglacial changes in nutrient supply in the eastern equatorial Pacific. *Paleoceanography* **24**, PA4213. doi:10.1029/2008PA001702

Robinson, R.S., Mix, A., Martinez, P., (2007) Southern Ocean control on the extent of denitrification in the southeast Pacific over the last 70ka. *Quaternary Science Reviews* **26**, 201-212, doi: 10.1016/j.quascirev.2006.08.005.

Robinson, R.S., Sigman, D.M., (2008) Nitrogen isotopic evidence for a poleward decrease in surface nitrate within the ice age Antarctic. *Quaternary Science Reviews* **27**, 1076–1090. doi:10.1016/j.quascirev.2008.02.005

Robinson R. S., Kienast M., Luiza Albuquerque A., Altabet M., Contreras S., De Pol-Holz R., Dubois N., François R., Galbraith E., Hsu T. C., Ivanochko T., Jaccard S., Kao S.-J., Kiefer T., Kienast S., Lehmann M., Martinez P., McCarthy M., Möbius J., Pedersen T., Quan T. M., Ryabenko E., Schmittner A., Schneider R., Schneider-Mor A., Shigemitsu M., Sinclair D., Somes C., Studer A., Thunell R. and Yang J.-Y. (2012) A review of nitrogen isotopic alteration in marine sediments. *Paleoceanography* **27**, PA4203.

Robinson R. S., Sigman D. M., DiFiore P. J., Rohde M. M., Mashiotta T. A. and Lea D. W. (2005) Diatom-bound $^{15}N/^{14}N$: New support for enhanced nutrient consumption in the ice age subantarctic. *Paleoceanography* **20**, PA3003.

Robinson, R.S., Brzezinski, M.A., Beucher, C.P., Horn, M.G.S., Bedsole, P., (2014) The changing roles of iron and vertical mixing in regulating nitrogen and silicon cycling in the Southern Ocean over the last glacial cycle. Paleoceanography **29**, 1–

17. doi:10.1002/(ISSN)1944-9186

Rojas de Mendiola B. (1981) Seasonal phytoplankton distribution along the Peruvian coast. In *Coastal upwelling* Coastal and Estuarine Sciences. American Geophysical Union, Washington, D. C. pp. 348–356.

Romero O. and Hebbeln D. (2003) Biogenic silica and diatom thanatocoenosis in surface sediments below the Peru–Chile Current: controlling mechanisms and relationship with productivity of surface waters. *Marine Micropaleontology* **48**, 71–90.

Romero O., Mollenhauer G., Schneider R. R. and Wefer G. (2003) Oscillations of the siliceous imprint in the central Benguela Upwelling System from MIS 3 through to the early Holocene: the influence of the Southern Ocean. *Journal of Quaternary Science*. **18**, 733–743.

Romero, O. E., J.-H. Kim, and D. Hebbeln (2006), Paleoproductivity evolution off central Chile from the Last Glacial Maximum to the Early Holocene, *Quaternary Research*, *65*(3), 519–525, doi:10.1016/j.yqres.2005.07.003.

Rousseau, J., M. J. Ellwood, H. Bostock, and H. Neil (2016), Estimates of late Quaternary mode and intermediate water silicic acid concentration in the Pacific Southern Ocean, *Earth and Planetary Science Letters*, *439*(C), 101–108, doi:10.1016/j.epsl.2016.01.023

Sachs, J. P., D. Sachse, R. H. Smittenberg, Z. Zhang, D. S. Battisti, and S. Golubic (2009), Southward movement of the Pacific intertropical convergence zone AD 1400–1850, *Nature Geoscience*, *2*(7), 519–525, doi:10.1038/ngeo554.

Salvatteci, R. et al. (2014a), Cross-stratigraphies from a seismically active mud lens off Peru indicate horizontal extensions of laminae, missing sequences, and a need for multiple cores for high resolution records, *Marine Geology*, doi:10.1016/j.margeo.2014.07.008.

Salvatteci, R., D. Gutiérrez, D. Field, A. Sifeddine, L. Ortlieb, I. Bouloubassi, M. Boussafir, H. Boucher, and F. Cetin (2014b), The response of the Peruvian Upwelling Ecosystem to centennial-scale global change during the last two millennia, *Clim. Past*, *10*(2), 715–731, doi:10.5194/cp-10-715-2014.

Salvatteci, R., Gutiérrez, D., Sifeddine, A., Ortlieb, L., Druffel, E., Boussafir, M., Schneider, R., 2016. Centennial to millennial-scale changes in oxygenation and productivity in the Eastern Tropical South Pacific during the last 25,000 years. Quaternary Science Reviews 131, 102–117. doi:10.1016/j.quascirev.2015.10.044

Sanchez, G., R. Calienes, and S. Zuta (2000), The 1997-98 El Niño and its effects on the coastal marine ecosystem off Peru, *Reports of California Cooperative Oceanic Fisheries Investigations*, *41*, 62–86.

Sarmiento, J.L., Gruber, N., Brzezinski, M.A., Dunne, J.P., 2004. High-latitude controls of thermocline nutrients and low latitude biological productivity. Nature 427, 53–56. doi:10.1038/nature02204

Sarthou G., Timmermans K. R., Blain S. and Tréguer P. (2005) Growth physiology and fate of diatoms in the ocean: a review. *Journal of Sea Research* **53**, 25–42.

Schönfeld, J., W. Kuhnt, Z. Erdem, S. Flögel, N. Glock, M. Aquit, M. Frank, and A. Holbourn (2015), Records of past mid-depth ventilation: Cretaceous ocean anoxic event 2 vs. Recent oxygen minimum zones, *Biogeosciences*, *12*(4), 1169–1189, doi:10.5194/bg-12-1169-2015-supplement.

Scholz F., McManus J., Mix A. C., Hensen C. and Schneider R. R. (2014) The impact of ocean deoxygenation on iron release from continental margin sediments. *Nature Geoscience* **7**, 433-437.

Schrader H. (1992) Coastal upwelling and atmospheric CO_2 changes over the last 400,000 years: Peru. *Marine Geology* **107**, 239–248.

Schrader, H. (1992), Comparison of Quaternary coastal upwelling proxies off central Peru, *Marine Micropaleontology*.

Schrader H. J. and Gersonde R. (1978) Diatoms and Silicoflagellates. In: Utrecht Micropaleontological Bulletins. pp. 129–176.

Schrader, H., and R. Sorknes (1991), Peruvian Coastal Upwelling - Late Quaternary Productivity Changes Revealed by Diatoms, *Marine Geology*, *97*(3-4), 233–249.

Schubert, C.J., Calvert, S.E., 2001. Nitrogen and carbon isotopic composition of marine and terrestrial organic matter in Arctic Ocean sediments:. Deep Sea Research Part I: Oceanographic Research Papers 48, 789–810. doi:10.1016/S0967-0637(00)00069-8

Schuette G. (1980) Recent marine diatom taphoceoenoses off Peru and off southwet Africa: Reflection of coastal upwelling. 1–125 pp. Oregon State University.

Schuette G. and Schrader H. (1981) Diatoms in surface sediments: a reflection of coastal upwelling. *Coastal and Estuarine Sciences* **1**, 372–380.

Schuette, G., and H. Schrader (1981), Diatom taphocoenoses in the coastal upwelling area off South West Africa, *Marine Micropaleontology*, *6*(2), 131–155, doi:10.1016/0377-8398(81)90002-5.

Shemesh A., Macko S. A., Charles C. D. and Rau G. H. (1993) Isotopic evidence for reduced productivity in the glacial Southern Ocean. *Science* **262**, 407–410.

Sifeddine, A. et al. (2008), Laminated sediments from the central Peruvian continental slope: A 500 year record of upwelling system productivity, terrestrial runoff and redox conditions, *Progress in Oceanography*, *79*(2-4), 190–197, doi:10.1016/j.pocean.2008.10.024.

Sigman, D.M., Altabet, M.A., François, R., McCorkle, D.C., Gaillard, J.-F., (1999a) The isotopic composition of diatom-bound nitrogen in Southern Ocean sediments. *Paleoceanography* **14**, 118–134. doi:10.1029/1998PA900018

Sigman, D.M., Altabet, M.A., McCorkle, D.C., Francois, R., Fischer, G., (2000) The $\delta^{15}N$ of nitrate in the Southern Ocean: Nitrogen cycling and circulation in the ocean interior. J. *Geophys. Res.* **105**, 19599–19614. doi:10.1029/2000JC000265

Sigman D. M., Altabet M. A., McCorkle D. C., Francois R. and Fischer G. (1999b) The $\delta^{15}N$ of Nitrate in the Southern Ocean: Consumption of Nitrate in Surface Waters.

Global Biogeochem. Cycles **13**, 1149–1166.

Sigman D. M., Casciotti K. L., Andreani M., Barford C., Galanter M. and Böhlke J. K. (2001) A Bacterial Method for the Nitrogen Isotopic Analysis of Nitrate in Seawater and Freshwater. *Anal. Chem.* **73**, 4145–4153, doi:10.1021/ac010088e

Sigman, D.M., DiFiore, P.J., Hain, M.P., Deutsch, C., Karl, D.M., 2009. Sinking organic matter spreads the nitrogen isotope signal of pelagic denitrification in the North Pacific. Geophys. Res. Lett. 36, L08605. doi:10.1029/2008GL035784.

Spero, H. J. (2002), The Cause of Carbon Isotope Minimum Events on Glacial Terminations, *Science*, *296*(5567), 522–525, doi:10.1126/science.1069401.

Stramma L., Johnson G. C., Sprintall J. and Mohrholz V. (2008) Expanding Oxygen-Minimum Zones in the Tropical Oceans. *Science* **320**, 655–658.

Stramma, L., H. W. Bange, R. Czeschel, A. Lorenzo, and M. Frank (2013), On the role of mesoscale eddies for the biological productivity and biogeochemistry in the eastern tropical Pacific Ocean off Peru, *Biogeosciences Discuss.*, *10*(6), 9179–9211, doi:10.5194/bgd-10-9179-2013.

Strub, P. T., J. M. Mesias, V. Montecino, J. Rutllant, and S. Salinas (1998), Coastal Ocean Circulation off Western South America, in *The Sea*, vol. 11, edited by A. R. Robinson and K. H. Brink, pp. 273–313, John Wiley & Sons.

Studer A. S., Martínez-Garcia A., Jaccard S. L., Girault F. E., Sigman D. M. and Haug G. H. (2012) Enhanced stratification and seasonality in the Subarctic Pacific upon Northern Hemisphere Glaciation–New evidence from diatom-bound nitrogen isotopes, alkenones and archaeal tetraethers. *Earth and Planetary Science Letters* **351-352**, 84–94.

Suess, E., L. D. Kulm, and J. S. Killingley (1987), Coastal upwelling and a history of organic-rich mudstone deposition off Peru, in *Marine Petroleum Source Rocks*, edited by J. Brooks and F. A. J, pp. 181–197, Geological Society Special Publication.

Sumper M. and Kröger N. (2004) Silica formation in diatoms: the function of long-chain polyamines and silaffins. *J. Mater. Chem.* **14**, 2059.

Sutton J. N., Varela D. E., Brzezinski M. A. and Beucher C. P. (2013) Species-dependent silicon isotope fractionation by marine diatoms. *Geochimica et Cosmochimica Acta* **104**, 300–309.

Takeda S. (1998) Influence of iron availability on nutrient consumption ratio of diatoms in oceanic waters. *Nature* **393**, 774–777.

Thamdrup B. (2012) New Pathways and Processes in the Global Nitrogen Cycle. *Annual Review of Ecology, Evolution, and Systematics* **43**, 407–428.

Tarazona J. and Arntz W. (2001) The Peruvian Coastal Upwelling System. In *Coastal Marine Ecosystems of Latin America* Ecological Studies. Springer Berlin Heidelberg, Berlin, Heidelberg. pp. 229–244.

Tarazona J., Gutiérrez D., Paredes C. and Indacochea A. (2003) Overview and challenges of marine biodiversity research in Peru. *Gayana* **67**, 206–231.

Tesdal, J.E., Galbraith, E.D., Kienast, M., (2013) Nitrogen isotopes in bulk marine sediment: linking seafloor observations with subseafloor records. *Biogeosciences* **10**, 101–118. doi:10.5194/bg-10-101-2013

Thunell, R.C., Kepple, A.B., (2004) Glacial-Holocene $\delta^{15}N$ record from the Gulf of Tehuantepec, Mexico: Implications for denitrification in the eastern equatorial Pacific and changes in atmospheric N_2O. *Global Biogeochem. Cycles* 18, GB1001, doi:10.1029/2002GB002028

Timmermann, A., S. J. Lorenz, S.-I. An, A. Clement, and S.-P. Xie (2007), The Effect of Orbital Forcing on the Mean Climate and Variability of the Tropical Pacific, *J. Climate*, *20*(16), 4147–4159, doi:10.1175/JCLI4240.1

Toggweiler J. R., Dixon K. and Broecker W. S. (1991) The Peru Upwelling and the Ventilation of the South-Pacific Thermocline. *J. Geophys. Res.* **96**, 20467–20497.

Toggweiler, J. R., J. L. Russell, and S. R. Carson (2006), Midlatitude westerlies, atmospheric CO_2, and climate change during the ice ages, *Paleoceanography*.

Tréguer P. J. and La Rocha De C. L. (2013) The World Ocean Silica Cycle. *Annu. Rev. Marine. Sci.* **5**, 477–501.

Tréguer P., Nelson D. M., Van Bennekom A. J., DeMaster D. J., Leynaert A. and Quéguiner B. (1995) The Silica Balance in the World Ocean: A Reestimate. *Science* **268**, 375–379.

Van Bennekom A. J., Berger G. W., Vandergaast S. J. and DeVries R. (1988) Primary Productivity and the Silica Cycle in the Southern-Ocean (Atlantic Sector). *Palaeogeography*, *Palaeoclimatology*, *Palaeoecology* **67**, 19–30.

Varela D. E., Pride C. J. and Brzezinski M. A. (2004) Biological fractionation of silicon isotopes in Southern Ocean surface waters. *Global Biogeochem. Cycles* **18**, 1047–1054.

Verleye, T.J., Martinez, P., Robinson, R.S., Louwye, S., (2013) Changes in the source of nutrients associated with oceanographic dynamics offshore southern Chile (41°S) over the last 25,000years. *Quaternary Research* **80** (3), 495-501, doi:10.1016/j.yqres.2013.07.002.

Wada, E., Hattori, A., (1978) Nitrogen isotope effects in the assimilation of inorganic nitrogenous compounds by marine diatoms. *Geomicrobiology Journal* **1**, 85–101. doi:10.1080/01490457809377725.

Waliser D. E. and Gautier C. (1993) A Satellite-derived Climatology of the ITCZ. J*ournal of Climate* **6** (11), 2162-2174.

Wang C. and Fiedler P. C. (2006) ENSO variability and the eastern tropical Pacific: A review. *Progress in Oceanography* **69**, 239–266.

Waser N., Harrison P. J., Nielsen B., Calvert S. E. and Turpin D. H. (1998) Nitrogen isotope fractionation during the uptake and assimilation of nitrate, nitrite, ammonium, and urea by a marine diatom. *Limnol. Oceangr.* **43**, 215–224.

Wu J. P., Calvert S. E. and Wong C. S. (1997) Nitrogen isotope variations in the subarctic northeast Pacific: Relationships to nitrate utilization and trophic structure.

Deep-Sea Research Part I **44**, 287–314.

Wyrtki, K. (1975), Fluctuations of the dynamic topography in the Pacific Ocean, *J. Phys. Oceanogr.*

Wyrtki, K. (1981), An Estimate of Equatorial Upwelling in the Pacific, *J. Phys. Oceanogr.*, *11*(9), 1205–1214.

Xie, R. C., and F. Marcantonio (2012), Deglacial dust provenance changes in the Eastern Equatorial Pacific and implications for ITCZ movement, *Earth and Planetary Science Letters*.

Xiong Z., Li T., Algeo T., Doering K., Frank M., Brzezinski M. A., Chang F., Opfergelt S., Crosta X., Jiang F., Wan S. and Zhai B. (2015) The silicon isotope composition of *Ethmodiscus rex* laminated diatom mats from the tropical West Pacific: implications for silicate cycling during the Last Glacial Maximum. *Palaeoceanography* **30**(7), 803–823.

Zuta, S., and O. Guillén (1970), Oceanografía de las aguas costeras del Perú, *Bo. Inst. Mar. Perú*, *2*(5), 157–324.

Supplementary Material

Chapter II

Table II: S1: Age model core M77/2-052-2 based on Erdem et al., (2016).

Depth (cm)	C^{14} age (yrs BP)	error (years)	correlation with core	depth (m)	C^{14} age (yrs BP)	calibrated age (cal BP)	calibrated age (cal ka BP)	Dated Material
90			059-1	1.48	3490	3130	3.13	N.dutertrei
229			059-1	4.03	7815	8097	8.097	N.dutertrei
319			059-1	6.58	10470	11277	11.277	N.dutertrei
370	12290	50				13641	13.641	N.dutertrei
550	19320	80				22678	22.678	N.dutertrei
630	24470	130				28011	28.011	N.dutertrei
770			ice core EDML	1181.75		30562	30.562	
880	31880	270				35249	35.249	N.dutertrei
952			ice core EDML	1334.25		38886	38.886	
1100	41740	770				44697	44.697	N.dutertrei
Calib 7.0								
delta R:	102 +/- 175		**EPICA Community Members (2010):** Stable oxygen isotopes of ice core EDML. doi:10.1594/PANGAEA.754444					

Table II. S2 Radiocarbon dates (^{14}C AMS) and calibrated ages used for the age model of core M77/2-029.

Depth (cm)	^{14}C age (yrs BP)	error (yrs)	2σ (yrs BP)	Calibrated (cal BP)
38	4250	±35	4085-4335	4210
48	7605	±30	7872-8020	7946
113	10325	±40	11112-11296	11204
203	11715	±45	12932-13228	13080
333	12775	±50	13986-14441	14214
361	13085	±60	14503-15162	14833
381	13105	±60	14601-15197	14899
423	13095	±55	14587-15173	14880
484	13415	±60	15192-15650	15421
517	13610	±60	15422-15949	15686
583	13600	±50	15769-16184	15977
743	14005	±50	16154-16601	16378
823	14245	±50	16339-16829	16584
938	14515	±55	16731-17222	16977
948	14770	±70	17124-17572	17348
1080	15100	±70	17566-17962	17764
1103	14750	±50	17135-17517	17326
1113	14990	±80	17427-17896	17662
1125	15040	±70	17501-17916	17709
1263	15335	55	17853-18207	18030

Table II.S3: Accumulation rates of biogenic opal (bSi) and organic carbon (C_{org}) concentrations and corresponding for core M77/2-029.

Age (ka BP)	bSi (%)	AR_{bSi} (g cm^{-2} ka^{-1})	Age (ka BP)	C_{org} (%)	AR_{Corg} (g cm^{-2} ka^{-1})
2.94	3.23	0.22	2.94	8.6	0.58
4.71	5.92	0.40	3.83	7.39	0.50
6.49	1.96	0.13	4.71	7.96	0.53
8.13	4.61	0.37	5.60	7.14	0.48
9.51	4.30	0.41	6.49	2.01	0.14
10.63	6.43	0.63	7.34	3.91	0.29
11.51	8.28	1.14	8.13	4.01	0.32
12.16	15.36	2.88	8.85	5.22	0.45
12.64	12.74	3.34	9.51	5.35	0.51
12.99	17.84	5.46	10.10	7.23	0.77
13.26	26.32	10.59	10.63	6.48	0.64
13.48	11.11	5.22	11.10	7.69	0.87
13.67	16.93	8.30	11.51	7.01	0.97
13.84	13.13	7.09	11.86	5.29	0.85
14.00	17.94	11.61	12.16	7.15	1.34
14.15	15.43	8.10	12.42	6.18	1.36
14.32	22.83	8.88	12.64	5.12	1.34
14.49	19.99	7.18	12.83	5.28	1.40
14.67	28.59	11.14	12.99	3.78	1.16
14.82	30.36	21.11	13.13	4.9	1.71
14.92	15.92	12.42	13.26	5.27	2.12
15.04	19.04	15.86	13.37	3.8	1.66
15.16	32.12	28.02	13.48	3.91	1.84
15.31	26.59	22.53	13.58	4.77	2.41
15.44	21.23	17.85	13.67	4.76	2.34
15.57	20.44	13.16	13.76	5.53	2.86
15.68	22.69	14.61	13.84	3.97	2.14
15.79	23.79	19.32	13.92	4.24	2.36
15.89	28.51	26.35	14.00	4.42	2.86
15.97	46.30	60.05	14.08	5.14	3.33
16.04	39.05	59.37	14.15	4.22	2.22
16.10	27.03	33.55	14.23	4.68	2.39
16.15	36.24	75.66	14.32	5.18	2.02
16.20	32.37	74.90	14.40	6.13	2.27
16.24	33.14	81.83	14.49	5.4	1.94
16.28	27.35	68.53	14.58	4.09	1.49
16.33	37.09	77.81	14.67	4.59	1.79
16.37	20.61	37.88	14.75	5.12	2.17
16.42	27.29	44.91	14.82	4	2.78
16.47	39.29	66.27	14.89	5.04	3.81
16.53	27.25	36.94	14.95	4.46	3.57
16.60	29.74	35.55	15.07	3.22	2.66
16.68	31.38	33.63	15.19	3.69	3.19
16.77	14.51	13.82	15.31	3.41	2.89
16.86	21.45	15.94	15.44	3.1	2.61
16.96	26.73	20.33	15.57	3.15	2.03
17.06	28.03	20.98	15.79	2.61	2.12
17.16	42.55	38.64	15.97	2.93	3.80
17.25	21.23	22.93	16.10	3.01	3.74
17.33	21.81	27.26	16.20	2.98	6.89
17.40	15.15	20.30	16.28	2.89	7.24
17.46	34.20	57.48	16.37	2.85	5.24
17.51	24.05	50.06	16.47	2.47	4.17
17.54	17.68	47.73	16.60	2.73	3.26

Table II.S3 (part 2): Accumulation rates of biogenic opal (bSi) and organic carbon (C_{org}) concentrations and corresponding for core M77/2-029.

Age (ka BP)	bSi (%)	AR_{bSi} (g cm^{-2} ka^{-1})	Age (ka BP)	C_{org} (%)	AR_{Corg} (g cm^{-2} ka^{-1})
17.57	15.61	70.39	16.77	2.23	2.12
17.60	22.51	72.46	16.96	2.29	1.74
17.64	16.66	39.00	17.16	1.94	1.76
17.69	14.94	32.45	17.33	2.3	2.87
17.74	27.31	44.05	17.46	2.4	4.03
17.79	24.96	38.51	17.54	2.15	5.80
17.85	16.95	25.23	17.60	2.57	8.27
17.91	21.86	31.78	17.69	1.88	4.08
17.97	15.70	22.52	17.79	1.99	3.07
18.03	21.55	58.55	17.91	1.77	2.57
18.09	18.14	37.41	18.03	1.95	5.30
18.15	25.30	40.58			
18.21	20.76	33.30			
18.27	25.82	61.65			

Table II. S4a: Downcore records of the diatom assemblage counts from the small-mixed diatom fraction (11-32 µm) for cores M77/2-052 and M77/2-029.

M772-52-2

Age (ka BP)	Upwelling (%)	CP (%)	CF (%)	Others (%)
0.37	2.85	17.23	63.36	16.55
1.11	2.53	10.91	67.47	19.09
1.86	6.88	12	67.75	13.37
5.57	2.08	10.59	75.35	11.98
11.51	4.34	8.77	76.4	10.5
13	11.17	10.64	68.59	9.59
13.74	1.22	4.97	86.51	7.3
15.68	3.68	11.17	64.59	20.56
18.59	1.53	7.15	59.87	31.46
20.53	1.13	7.23	75.4	16.24

M772-29-3

Age (ka BP)	Upwelling (%)	CP (%)	CF (%)	Others (%)	Sponges (%)
0.62	1.61	23.92	52.01	22.47	-
2.59	1.52	15.15	49.24	27.27	6.82
10.92	2.21	23.16	46.97	14.89	12.78
12.18	2.01	23.18	40.33	22.72	11.77
12.6	3.4	40.12	40.33	14.3	1.85
13.39	6.88	29.88	53.29	8.52	1.44
13.78	2.64	53.08	33.58	10.41	0.29
14.26	4.78	33.43	36.72	23.58	1.49
14.9	6.48	32.41	51.85	8.33	0.93
15.62	5.78	39.6	38.44	14.74	1.45
15.87	5.99	38.8	32.55	21.88	0.78
15.98	15.96	25.27	45.48	12.77	0.53
16.21	9.54	42.77	33.98	13.71	0
16.28	8.79	49.78	30.7	10.28	0.45
16.39	6.63	38.22	39.11	14.75	1.29
16.63	7.69	25	44.51	21.7	1.1
16.8	5.97	31.76	28.3	33.02	0.94
17.76	8.93	25.36	51.01	13.54	1.15
18.6	1.22	21.63	42.7	33.33	1.12

Table II. S4b: Downcore records of the diatom assemblage counts from the small-mixed diatom fraction (11-32 µm) for cores M77/2-003 and SO147-106KL.

M77/2-003-2

Age (ka BP)	Upwelling (%)	CP (%)	CF (%)	Others (%)	Sponges (%)
0.95	5.98	11.97	60.24	21.68	0.13
1.31	17.7	18.91	49.17	13.77	0.45
1.97	4.23	10.66	13.14	71.97	0
2.72	14.6	22.11	46.53	16.04	0.72
4.19	13.32	21.82	37.77	25.62	1.46
4.83	24.71	9.48	24.57	41.09	0.14
5.89	8.2	26.33	33.24	31.37	0.86
6.79	8.96	27.74	36.7	26.32	0.28
8.16	6.13	4.99	8.13	80.74	0
8.54	11.84	36.49	26.04	25.35	0.28
9.39	20.44	14.12	52.65	12.65	0.15
10.43	16.87	24.04	31.34	27.36	0.4
11.62	5.03	33.85	31.47	29.09	0.56
12.36	4.6	38.42	45.47	10.65	0.86
13.53	6.76	29.86	46.48	12.11	4.79
15.05	6.04	34.02	42.42	15.61	1.91
16.23	6.31	24.52	46.55	20.12	2.5
17.62	10.68	31.35	31.35	24.55	2.08

SO147-106KL

Age (ka BP)	Upwelling (%)	CP (%)	CF (%)	Others (%)	Sponges (%)
1.18	20.43	23.97	36.88	18.58	0.14
1.33	41.66	14.4	32.54	11.21	0.18
1.39	46.91	9.55	32.68	10.3	0.56
1.86	24.9	6.35	12.3	56.25	0.2
2.45	13.89	17.77	50.15	17.16	1.02
3.47	13.95	23.29	47.14	13.53	2.09
4.83	31.47	20.88	31.47	15.44	0.74
8.37	8.84	21.81	45.63	22.96	0.77
9.11	27.24	17.21	43.5	11.38	0.68
9.28	14.91	18.33	51.66	14.38	0.72
9.73	28.51	21.7	32.41	16.13	1.25
10.32	11.68	21.29	45.25	18.91	2.87
12.41	12.61	22.43	47.48	15.68	1.8
14.01	26.13	15.87	45.07	12.13	0.8
14.93	11.4	19.9	47.44	19.61	1.64
16.03	17.8	13.63	45.88	21.67	1.02
18.8	67.99	7.85	17.64	5.5	1.02

Chapter III

Table III.S1: Downcore records of bSi concentrations (%) of single laminations in core M77/2-003-2TC.

Depth (mm)	Age (yrs BP)	bSi (%)	Depth (mm)	Age (yrs BP)	bSi (%)	Depth (mm)	Age (yrs BP)	bSi (%)
0	-36	33	296	343	19	571	694	42
9	-24	31	304	353	21	578	703	36
17	-14	24	311	362	17	614	749	50
24	-5	26	317	370	20	619	756	45
31	4	26	321	375	18	621	758	49
48	26	23	326	381	19	626	765	43
55	35	23	334	391	17	632	772	37
61	42	23	342	402	21	640	782	36
68	51	22	355	418	47	656	803	39
74	59	21	368	435	29	672	823	53
86	74	43	369	436	30	676	828	47
97	88	36	378	448	28	688	844	36
107	101	45	385	457	23	704	864	41
128	128	36	390	463	26	708	869	33
134	136	33	396	471	25	713	876	28
140	143	35	403	480	30	717	881	33
144	148	38	410	488	29	719	883	29
148	154	34	418	499	27	725	891	24
154	161	32	421	503	32	729	896	33
159	168	28	425	508	27	737	906	29
164	174	40	430	514	26	742	913	29
174	187	50	437	523	28	745	917	38
185	201	44	445	533	31	752	926	25
188	205	33	455	546	25	759	935	22
190	207	33	459	551	28	762	938	31
192	210	23	465	559	24	767	945	19
198	218	21	473	569	29	774	954	31
208	230	22	480	578	25	781	963	23
216	241	17	489	589	32	784	967	37
224	251	20	492	593	23	787	970	43
228	256	22	502	606	25	790	974	38
231	260	26	512	619	28	796	982	42
239	270	23	519	628	35			
241	272	27	526	637	32			
247	280	20	533	646	31			
252	287	24	537	651	44			
262	299	24	541	656	34			
271	311	24	548	665	32			
276	317	25	554	673	41			
281	324	30	557	676	38			
284	327	49	564	685	35			

Chapter IV

Table IV.S1: Bulk sedimentary nitrogen isotopes ($\delta^{15}N_{bulk}$) of core SO147-106KL.

Age (ka BP)	$\delta^{15}N_{bulk}$ (‰)	Age (ka BP)	$\delta^{15}N_{bulk}$ (‰)
1.17	5.06	9.73	7.63
1.29	6.77	9.75	6.69
1.34	5.51	9.83	7.70
1.39	5.72	9.90	6.15
1.44	4.91	10.16	8.11
1.49	5.97	10.19	8.14
1.53	5.78	10.32	6.68
1.58	5.86	10.47	8.66
1.65	5.68	10.58	7.71
1.70	5.35	10.70	9.06
1.77	5.90	10.80	8.55
1.86	6.62	10.94	8.88
1.90	5.72	11.06	9.91
2.06	4.86	11.18	8.79
2.22	5.58	11.27	8.11
2.38	6.03	11.42	8.32
2.45	5.53	11.54	10.73
2.55	4.55	11.66	6.62
2.71	3.94	11.82	6.79
2.89	4.44	12.02	6.19
3.09	4.71	12.23	7.17
3.31	5.09	12.40	10.25
3.47	5.35	12.66	7.63
3.63	5.07	12.87	9.12
3.78	5.59	13.09	7.91
3.99	5.69	13.26	7.97
4.27	5.11	13.51	8.59
4.50	5.20	13.73	8.61
4.83	5.97	13.89	8.23
5.83	6.06	14.01	8.66
7.84	5.55	14.18	8.38
8.37	5.93	14.33	9.46
8.91	7.40	14.44	9.44
8.95	7.62	14.61	9.82
8.99	5.95	14.93	9.11
9.03	6.85	15.07	8.44
9.08	7.37	15.23	7.94
9.11	7.97	15.38	7.92
9.21	7.79	15.51	8.43
9.28	7.13	15.72	8.38
9.45	6.53	15.89	7.51
9.48	7.22	16.03	8.38
9.50	8.19	16.73	8.60
9.53	6.54	17.45	8.79
9.59	5.07	18.80	7.23

Table IV. S2: Diatom-bound nitrogen isotope measurements of core M77/2-003-2. The 1σ gives the error for replicate measurements.

Age (ka BP)	$\delta^{15}N_{db}$ (‰)	1σ (‰)
1.97	8.30	-
2.72	9.90	0.86
3.58	6.60	0.28
3.95	4.93	-
4.19	7.40	0.87
5.27	8.03	0.65
5.44	5.44	0.21
5.58	4.75	0.91
5.89	6.63	0.16
6.79	7.09	-
8.54	6.89	0.99
9.39	8.77	0.02
9.93	8.81	1.10
10.43	9.77	0.40
12.36	9.43	1.03
14.43	10.96	0.29
15.05	9.01	-
17.62	11.04	0.39